New tariquidar-like ABCB1 modulators in cancer chemotherapy:

Preclinical pharmacokinetic / pharmacodynamic investigations and computational studies

Dissertation

zur Erlangung des Doktorgrades der Naturwissenschaften (Dr. rer. nat.) der
Naturwissenschaftlichen Fakultät IV – Chemie und Pharmazie –
der Universität Regensburg

vorgelegt von

Peter Höcherl

aus Cham

2010

Die vorliegende Arbeit entstand in der Zeit von Januar 2007 bis Mai 2010 unter der Anleitung von Herrn Prof. Dr. Armin Buschauer und Herrn Prof. Dr. Günther Bernhardt am Institut für Pharmazie der Naturwissenschaftlichen Fakultät IV – Chemie und Pharmazie – der Universität Regensburg.

Das Promotionsgesuch wurde eingereicht im Mai 2010.

Tag der mündlichen Prüfung: 02. Juni 2010

Prüfungsausschuss:	Prof. Dr. J. Wegener	(Vorsitzender)
	Prof. Dr. A. Buschauer	(Erstgutachter)
	Prof. Dr. G. Bernhardt	(Zweitgutachter)
	Prof. Dr. J. Heilmann	(Prüfer)
	Prof. Dr. A. Göpferich	(Ersatzprüfer)

Für
meine wunderbare
Frau Julia

Experience is the name we give to our mistakes
Oscar Wilde (1854 - 1900)

Danksagung

An dieser Stelle bedanke ich mich bei:

Herrn Prof. Dr. Armin Buschauer, dass er mir die Möglichkeit gegeben hat, an diesem spannenden und vielschichtigen Projekt arbeiten zu dürfen, seine wissenschaftlichen Anregungen sowie seine konstruktive Kritik bei der Durchsicht dieser Arbeit.

Herrn Prof. Dr. Günther Bernhardt für seine wissenschaftliche Anleitung, sein Interesse am Fortgang der Experimente, seine stete Unterstützung beim Lösen experimenteller Probleme und die kritische Durchsicht der Arbeit.

Herrn Prof. Dr. Stefan Dove für seine fachliche Anleitung, insbesondere im Bereich des Molecular Modelling sowie die konstruktive Kritik bei der Durchsicht von Kapitel 7.

Herrn Dr. Thilo Spruß für die umfassende Betreuung bei der Durchführung der tierexperimentellen Arbeiten sowie der histologischen Untersuchungen.

Herrn Franz Wiesenmayer und Herrn Oskar Baumann für ihre stete Hilfsbereitschaft und die hervorragende Zusammenarbeit bei den tierexperimentellen Arbeiten.

Herrn Prof. Dr. Burkhard König, Herrn Dr. Michael Egger, Frau Alexandra Bila und Frau Carolin Fischer für die Synthese der Tariquidar Derivate und die gute Zusammenarbeit.

Herrn Dr. Otto Gleich und Herrn Dr. Dietmar Gross für die Anleitung bei der Durchführung der immuncyto- und immunhistochemischen Experimente.

Frau Petra Pistor für die Anfertigung der unzähligen histologischen Präparate sowie deren Färbung.

Frau Brigitte Wenzl und Frau Elvira Schreiber für die Unterstützung bei den Arbeiten mit der Zellkultur, der Praktikumsvorbereitung und den Chromosomenuntersuchungen.

Herrn Prof. Dr. Frieder Kees für seine Hilfe bei der Berechnung der pharmakokinetischen Kenngrößen.

Herrn Prof. Dr. Jörg Heilmann und Herrn Prof. Dr. Achim Göpferich für die Möglichkeit zur Nutzung der Fluoreszenzmikroskope und des Konfokalmikroskops.

Der Elektronik- und Feinmechanikerwerkstatt der Universität Regensburg für die fachkundige und schnelle Anfertigung benötigter Spezialkonstruktionen.

Frau Sabine Stempfhuber für die Recherche in der Cambridge Structural Database.

Meinem langjährigen Laborkollegen Dr. Matthias Kühnle für seine Hilfsbereitschaft, die anregenden fachlichen Diskussionen, die ausgezeichnete Zusammenarbeit und seine Untersuchungen zur Modulation des ABCG2 Transporters.

Meinen Kollegen Tobias Birnkammer, Irena Brunskole, Kira Bürger, Daniela Erdmann, Miriam Ertel, Dr. Christine Ertelt, Roland Geyer, Janina Hamberger, Tobias Holzammer, Dr. Patrick Igel, Melanie Kaske, Dr. Max Keller, Miroslaw Lopuch, Dr. Johannes Mosandl, Uwe Nordemann, Senthil-Kumar Palaniappan, Nikola Plym, Nathalie Pop und Christian Textor für die schöne Zeit mit Ihnen in Regensburg.

Allen meinen studentischen Hilfskräften, Praktikanten und Forschungspraktikanten, insbesondere E. Raab, S. Gunaratman, P. Kos, V. Thalhammer, S. Samei und S. Bauer für Ihre engagierte Mitarbeit im Labor,

sowie allen weiteren Mitgliedern des Lehrstuhls für ihre Kollegialität und Hilfsbereitschaft.

Des Weiteren geht mein besonderer Dank an:

Meine Kolleginnen in der Abensapotheke, mit deren Unterstützung die Arbeitssamstage wie im Fluge vergingen.

Alle Freunde außerhalb der Universität, insbesondere an Tine und Benny für die schönen gemeinsamen Unternehmungen und Abende.

Meine wunderbare Familie, meine Geschwister Johanna und Stefan und meine Schwiegereltern Bärbel und Stephan, für ihre Unterstützung und Liebe. Allen voran jedoch an meine Eltern, die mich von Anfang an selbstlos getragen haben und deren Hilfe ich mir zu jeder Zeit sicher sein konnte.

Meine geliebte Frau Julia, dass Sie ein steter Quell des Glücks in meinem Leben ist.

Abstracts and publications

Prior to submission of this thesis, results were published in part.

Publication:

Hubensack, M.; Müller, C.; Höcherl, P.; Fellner, S.; Spruss, T.; Bernhardt, G., et al. (2008); *Effect of the ABCB1 modulators elacridar and tariquidar on the distribution of paclitaxel in nude mice.* J. Cancer Res. Clin. Oncol. 134, 597-607.

Poster presentations:

Frontiers in Medicinal Chemistry (2008), Regensburg, March 2 - 5:
Höcherl, P.; Müller, C.; Egger, M.; König, B.; Bernhardt, G.; Buschauer, A.
Species dependent differences in P-glycoprotein 170 inhibition: in vitro investigations on the human and the murine transporter

4th Summer School Medicinal Chemistry (2008), Regensburg, September 29 – October 1:
Höcherl, P.; Egger, M.; König, B.; Bernhardt, G.; Buschauer, A.
Analytical procedures and tumor models for pharmacokinetic and pharmacodynamic studies on new ABCB1 modulators

Frontiers in Medicinal Chemistry (2009), Heidelberg, March 15 - 18:
Höcherl, P.; Egger, M.; König, B.; Bernhardt, G.; Buschauer, A.
New tariquidar-like ABCB1 modulators: quantification by HPLC and impact on the distribution of paclitaxel in NMRI mice

DPhG Doktorandentagung (2009), Pichlarn (Austria), November 18 – 21:
Höcherl, P.; Egger, M.; König, B.; Spruss, T.; Bernhardt, G.; Buschauer, A.
Refined in vivo tumor models for the investigation of new ABCB1 modulators in cancer chemotherapy

Short lecture:

Treffen der Blut-Hirn Schranke Experten und CaCo2-Anwender (2008), Bad Herrenalb, May 19 - 21:
Speziesabhängige Modulation von P-Glycoprotein 170

Contents

1 GENERAL INTRODUCTION 1

1.1 TRANSPORT ACROSS CELL MEMBRANES 1
1.2 ATP-BINDING CASSETTE (ABC) TRANSPORTERS 2
1.3 THE BLOOD-BRAIN BARRIER AND MALIGNANT BRAIN TUMORS 4
1.4 IN VITRO SCREENING ASSAYS TO DETERMINE ABC TRANSPORTER INTERACTIONS 5
1.4.1 ATPase activity assays 6
1.4.2 Photoaffinity labeling assays 7
1.4.3 Chemosensitivity assays 7
1.4.4 Transcellular transport assays 8
1.4.5 Cellular accumulation assays 9
1.4.6 Isolated organ preparations 10
1.5 REFERENCES 11

2 SCOPE AND OBJECTIVES 15

2.1 REFERENCES 17

3 THE ABCB1 TRANSPORTER: MODULATION, SPECIES DIFFERENCES AND IN VITRO CHARACTERIZATION OF TARIQUIDAR-LIKE COMPOUNDS 19

3.1 INTRODUCTION 19
3.2 MATERIALS AND METHODS 20
3.2.1 Drugs and chemicals 20
3.2.2 Cell lines and culture conditions 21
3.2.3 Calcein-AM efflux assay 21
3.2.3.1 Flow cytometry 22
3.2.3.1.1 Kb-V1 cells 22
3.2.3.1.2 P388D$_1$Doxo cells 22
3.2.3.2 Microtiter plate format 23
3.2.4 Plasma albumin binding 23
3.2.5 Chemosensitivity assay 24

3.2.6 Determination of cell membrane integrity 24
3.2.7 Immunocytochemistry and confocal laser-scanning microscopy 25
3.2.8 Inhibition of cytochrome P450 isoenzymes 26
3.2.8.1 Preparation of rat liver microsomes 26
3.2.8.2 CYP3A4 and CYP2C8 inhibition assay using bioluminescence based methods 26
3.3 RESULTS AND DISCUSSION 27
3.3.1 Species dependent differences in P-glycoprotein inhibition 27
3.3.1.1 Induction of P-gp overexpression in murine P388D$_1$ cells and optimization of assay parameters 27
3.3.1.2 Inhibitory activity of ABCB1 modulators on the murine transporter 28
3.3.2 In vitro characterization of tariquidar-like ABCB1 modulators 30
3.3.2.1 Binding to serum albumin 30
3.3.2.2 Effect on the proliferation of U-118 MG and Kb-V1 cells 31
3.3.2.3 Effect of ME27-4 and tariquidar on the integrity of the cell membrane 33
3.3.2.4 Effect of tariquidar on the tubulin architecture 33
3.3.2.5 Interaction of the modulators with cytochrome P450 isoenzymes 34
3.3.3 Adaptation of the calcein-AM efflux assay to the microtiter plate format 37
3.3.3.1 Establishment of assay parameters 37
3.3.3.1.1 Impact of cell number and calcein-AM concentration 37
3.3.3.1.2 Co-incubation of calcein-AM with the ABCB1 modulator 39
3.3.3.1.3 Normalization of fluorescence intensity by cell mass 39
3.3.3.2 Comparison of microplate assay with flow cytometry 40
3.4 SUMMARY AND CONCLUSIONS 42
3.5 REFERENCES 43

4 TARIQUIDAR ANALOGS: QUANTIFICATION BY HPLC AND IMPACT ON THE DISTRIBUTION OF CO-ADMINISTERED PACLITAXEL IN NMRI MICE 47

4.1 INTRODUCTION 47
4.2 MATERIALS AND METHODS 48
4.2.1 Drugs and chemicals 48
4.2.2 Sample preparation 49
4.2.3 HPLC analysis of ME27-4, ME30-1, ME33-1 and paclitaxel 49
4.2.4 Recovery of tariquidar-like modulators 50
4.2.5 Pharmacokinetic studies in NMRI mice 50

4.3 RESULTS AND DISCUSSION 51
4.3.1 Elaboration of the analytical method 51
4.3.2 Specificity of the separation method 53
4.3.3 Linearity and quantification range 54
4.3.4 Limit of quantification 54
4.3.5 Stability of the analytes in murine plasma and in mobile phase 55
4.3.6 Recoveries 56
4.3.7 Accuracy and precision of the established method 58
4.3.8 Distribution of tariquidar-like modulators in NMRI mice 58
4.3.9 Effect of tariquidar-like modulators on the distribution of paclitaxel 60
4.4 SUMMARY AND CONCLUSIONS 63
4.5 REFERENCES 65

5 REVERSAL OF CLASSICAL MULTIDRUG RESISTANCE BY CO-ADMINISTRATION OF ABCB1 MODULATORS AND PACLITAXEL IN A SUBCUTANEOUS XENOGRAFT MODEL 69

5.1 INTRODUCTION 69
5.2 MATERIALS AND METHODS 70
5.2.1 Drugs and chemicals 70
5.2.2 Cell line and culture conditions 71
5.2.3 Determination of chemosensitivity, growth and doubling times in vitro 71
5.2.4 Cytological staining 71
5.2.5 Karyology 71
5.2.6 Immunocytochemical staining 72
5.2.7 Immunohistochemical investigations 72
5.2.8 Flow cytometric determination of functional ABCB1 transporters 73
5.2.9 Subcutaneous injection Kb-V1 cells and serial transplantation of solid tumor fragments 74
5.2.10 Histology 74
5.2.11 Therapeutic in vivo studies 75
5.3 RESULTS AND DISCUSSION 75
5.3.1 In vitro characterization of Kb-V1 cells 75
5.3.1.1 Morphology 75
5.3.1.2 In vitro growth of Kb-V1 cells 76
5.3.1.3 Chromosomal number 77

5.3.1.4 Immunocytochemical detection of the ABCB1 transporter 80
5.3.1.5 Chemosensitivity against selected cytostatic drugs 80
5.3.1.6 Reversal of P-gp mediated classical multidrug resistance 83
5.3.1.7 Maintenance of the transporter status after discontinued vinblastine exposure 84
5.3.2 In vivo characterization of solid Kb-V1 tumors 85
5.3.2.1 Tumorigenicity and in vivo growth characteristics 85
5.3.2.2 Histology 86
5.3.2.3 Maintenance of the ABCB1 transporter status in vivo 87
5.3.3 Effect of paclitaxel and co-administered ABCB1 modulators on subcutaneous multidrug resistant xenografts 88
5.3.3.1 Morpholino analog of tariquidar (ME30-1) 89
5.3.3.2 Ethoxyethyloxy analog of tariquidar (ME33-1) 91
5.3.3.3 The parent compound tariquidar 91
5.4 SUMMARY AND CONCLUSIONS 92
5.5 REFERENCES 94

6 STUDIES ON THE EFFICACY OF ABCB1 MODULATORS BY OPTICAL IMAGING OF INTRACEREBRAL TUMOR XENOGRAFTS IN NUDE MICE 97

6.1 INTRODUCTION 97
6.1.1 Fluorescence imaging 97
6.1.2 Bioluminescence imaging 98
6.2 MATERIALS AND METHODS 99
6.2.1 Drugs and chemicals 99
6.2.2 Stable transfection of human U-118 MG glioblastoma cells 99
6.2.3 Cell lines and culture conditions 100
6.2.4 Determination of chemosensitivity and in vitro growth characteristics 100
6.2.5 Intracerebral and subcutaneous implantation of glioblastoma cells into nude mice 100
6.2.6 Detection of Katushka- and DsRed2-mediated fluorescence 101
6.2.6.1 Fluorescence microscopy 101
6.2.6.2 Maestro™ imaging system 101
6.2.7 Fluorescence imaging of subcutaneous glioblastoma in nude mice 101
6.2.8 Determination of luciferase2 activity 101
6.2.8.1 In cell lysates 101

6.2.8.2 In whole cells 102
6.2.9 Bioluminescence imaging of subcutaneous and intracerebral glioblastoma in nude mice 102
6.2.10 Histology 103
6.2.11 Therapeutic in vivo studies 103
6.3 RESULTS AND DISCUSSION 104
6.3.1 In vivo imaging using fluorescent and bioluminescent U-118 MG glioblastoma cells 104
6.3.1.1 DsRed2-mediated fluorescence of U-118 transfectants 104
6.3.1.2 Luciferase2-mediated bioluminescence of U-118 transfectants 105
6.3.1.3 Chemosensitivity and in vitro growth characteristics of luciferase2 and luciferase2/DsRed2 transfected glioblastoma cells 108
6.3.1.4 Tumorigenicity and bioluminescence of subcutaneously implanted transfectants 110
6.3.1.5 Tumorigenicity and bioluminescence of intracerebrally implanted transfectants 114
6.3.2 In vivo imaging of Katushka-mediated fluorescent U-118 MG glioblastoma cells 116
6.3.2.1 Katushka-mediated fluorescence of U-118 transfectants in vitro 116
6.3.2.2 In vivo imaging of subcutaneous tumors 117
6.3.3 Effect of concomitant application of paclitaxel and ABCB1 modulators on the growth of intracerebral human glioblastoma 119
6.3.3.1 Chemosensitivity of luciferase2 expressing human U-87 MG glioblastoma cells 119
6.3.3.2 Confirmation of tumorigenicity by bioluminescence imaging 121
6.3.3.3 Observation of tumor growth by bioluminescence imaging 121
6.3.3.4 Comparison of bioluminescence signals with histological serial sections 126
6.4 SUMMARY AND CONCLUSIONS 128
6.5 REFERENCES 129

7 IDENTIFICATION OF PUTATIVE BINDING MODES OF TARIQUIDAR-LIKE MODULATORS AT P-GLYCOPROTEIN 133

7.1 INTRODUCTION 133
7.1.1 Mechanism of transport 135

7.1.2 Location of the binding region 136
7.1.3 Genetic docking algorithm of FlexiDock™ 138
7.2 MATERIALS AND METHODS 139
7.2.1 Selected ABCB1 modulators 139
7.2.2 Determination of IC_{50}- and log D-values 140
7.2.3 Conformational analysis 141
7.2.4 Preparation of the transporter 141
7.2.5 Docking of ABCB1 modulators 142
7.2.6 Sequence alignment 142
7.3 RESULTS AND DISCUSSION 142
7.3.1 Correlation between lipophilicity and inhibitory activity 142
7.3.2 Conformational analysis of compound ME30-1 143
7.3.3 Analysis of binding modes of ABCB1 modulators 145
7.3.3.1 Binding modes of tariquidar and ME30-1 146
7.3.3.2 Binding modes of ME25-3 and ME5-7 148
7.3.3.3 Binding mode of elacridar 149
7.4 SUMMARY AND CONCLUSIONS 150
7.5 REFERENCES 154

8 SUMMARY 157

A APPENDIX 1: IN VITRO ACTIVITY OF EPOTHILONES AGAINST HUMAN GLIOBLASTOMA CELLS AND INTERACTION WITH ABC TRANSPORTERS 159

A.1 INTRODUCTION 159
A.2 MATERIALS AND METHODS 161
A.2.1 Drugs and chemicals 161
A.2.2 Cell lines and culture conditions 161
A.2.3 Chemosensitivity assay 161
A.2.4 Calcein-AM efflux assay 161
A.2.5 Confocal laser-scanning microscopy 161
A.3 RESULTS AND DISCUSSION 162
A.3.1 Antiproliferative activity against human glioblastoma cells 162
A.3.1.1 Effect of permanent exposure 162
A.3.1.2 Effect of short-term exposure 163

A.3.2 Influence of murine serum on stability and activity of epothilones 164
A.3.3 Effect on quiescent U-373 MG cells 165
A.3.4 Interactions with the ABCB1 transporter 166
A.3.5 Interactions with the ABCG2 transporter 168
A.3.6 Effect of epothilones on the tubulin architecture of Kb-V1 cells 169
A.4 SUMMARY 170
A.5 REFERENCES 170

B APPENDIX 2: DEVELOPMENT OF AN AUTOMATED CRYO-PRESERVATION PROCEDURE FOR SOLID TUMORS 173

B.1 INTRODUCTION 173
B.2 MATERIALS AND METHODS 173
B.2.1 Chemicals, culture media and technical devices 173
B.2.2 Freezing and procedure 173
B.2.3 Thawing procedure and subcutaneous xenograft implantation 175
B.3 RESULTS AND DISCUSSION 175
B.3.1 Effect of freezing and thawing on tumorigenicity and growth kinetics of Kb-V1 tumors 175

Abbreviations

AB	antibody
ABCB1	ATP-binding cassette transporter, subfamily B, member 1
ABCC1	ATP-binding cassette transporter, subfamily C, member 1
ABCG2	ATP-binding cassette transporter, subfamily G, member 2
ADP	adenosine diphosphate
AM	acetoxymethylester
aq.	aqueous
ATCC	American Type Culture Collection
ATP	adenosine triphosphate
AUC	area under the concentration-time curve
BBB	blood-brain barrier
BCNU	carmustine
BCRP	Breast Cancer Resistance Protein (= ABCG2-transporter)
BLI	bioluminescence in vivo imaging
BSA	bovine serum albumin
C	C-terminal end of a protein
CCD	charge coupled device
CNS	central nervous system
CPD	citrate-phosphate-dextrose
CT	computer tomography
CV	coefficient of variation
Da	Dalton
DAPI	4',6-diamidino-2-phenylindole
DMEM	Dulbecco's Modified Eagle Medium
DMSO	dimethyl sulfoxide
DNA	desoxyribonucleic acid
Doxo	doxorubicin
DsRed2	enhanced version of the *Discosoma* species red fluorescent protein
DTT	dithiotreitol
EGFP	enhanced green fluorescent protein
EGTA	ethylene glycol tetraacetic acid
EM	electron multiplying
EMEM	Eagles Minimum Essential Medium
Epo A	epothilone A
Epo B	epothilone B
Epo D	epothilone D
FACS	Fluorescence Activated Cell Sorter
FCS	fetal calf serum
FFF	free filtratable fraction
FLI	fluorescence in vivo imaging
FSC	forward scatter
G418	geneticin
GeoMean	geometric mean value

GFP	green fluorescent protein
HE	haematoxylin-eosin staining
HPLC	high performance (pressure) liquid chromatography
i.p.	intraperitoneal
IC_{50}	concentration of inhibitor required to give 50 % inhibition of activity
IgG	immunoglobulin G
IS	internal standard
IVI	in vivo imaging
log D	logarithm of the distribution coefficient of a given solvent between octanol and water
Luc2	luciferase2 enzyme
MDR	multidrug resistance
MeCN	acetonitril
MG	Masson-Goldner staining
MRI	magnetic resonance imaging
MRP1	Multidrug Resistance Associated Protein 1 (= ABCC1-transporter)
MTS	methanethiosulfonate
MTT	[3-(4,5-dimethylthiazol-2-yl)-2,5-diphenyltetrazolium bromide]
N	N-terminal end of a protein
NBD	nucleotide binding domain
Pac	paclitaxel
PBS	phosphate buffered saline
PBS-T	PBS supplemented with 0.1 % triton X-100
PDB	Protein Data Bank
PET	positron emission tomography
PFA	paraformaldehyde
P-gp	P-glycoprotein (= ABCB1-transporter)
pH	negative logarithm of the hydrogen ion concentration
r	coefficient of correlation
RFI	relative fluorescence intensity
RFU	relative fluorescence unit
RLU	relative light unit
RMS	root mean square
RP	reversed phase
RPM	revolutions per minute
s	standard error of estimate
s.c.	subcutaneous
SDS	sodium dodecyl sulfate
SEM	standard error of the mean
SSC	sideward scatter
TFA	trifluoroacetic acid
TM	transmembranal helix
TMD	transmembrane domain
Topo	topotecan

Tris	tris(hydroxymethyl)aminomethane
UV	ultraviolet
VBL	vinblastine
V_i	inorganic vanadate
WHO	World Health Organization
x-ray	X-radiation (crystallography)

Chapter 1

1 General introduction

1.1 Transport across cell membranes

Every cell is enclosed by a selectively permeable membrane to guarantee the homeostasis of essential cellular constituents depending on the requirements and functions of the respective cell type. In addition to its physiological function, biological membranes are an effective barrier for xenobiotics. Consequently, the ability to pass these membranes is essential for the efficacy of administered therapeutic agents (Rees et al., 2009). The majority of drugs are small, lipophilic and often planar molecules that predominantly enter cells via passive diffusion (Higgins, 2007). In order to estimate the passive permeability (and solubility) of a given compound considering its physico-chemical properties, empirical guidelines have been established (Lipinski et al., 2001).

Despite the indisputable significance of passive diffusion for the absorption and distribution of orally administered drugs, it must not be forgotten that there is a vast number of alternative routes (Mehdipour and Hamidi, 2009). Endogenous macromolecules such as peptides and proteins are shuttled via absorptive-mediated transcytosis (e.g. albumin, histones) and receptor-mediated transport (e.g. transferrin, insulin) across cell membranes. Inorganic ions as well as charged (e.g. amino acids) and uncharged (e.g. sugars) polar compounds rely on selective membrane transport proteins to enter and leave cells. In *E. coli*, approximately 10 % of the total genome encodes for membrane proteins like ion channels, carriers and ATP-powered pumps (Blattner et al., 1997). These proteins enable cells to maintain the exact conditions needed to fulfill diverse functions such as the generation of energy, the processing of information or the storage of nutrients. It has been suggested that the uptake (and the excretion) of drugs by membrane transport proteins is a common rule rather than an exception (Dobson and Kell, 2008). Indeed, for a substantial number of drugs, the ability to cross cell membranes cannot satisfactorily be explained by

passive diffusion. Whereas solute carriers (SLC) enhance uptake, efflux is mediated by members of the ABC transporter superfamily.

1.2 ATP-binding cassette (ABC) transporters

ABC transporters belong to one of the four classes of ATP-powered transport proteins that use the energy of ATP hydrolysis to translocate various compounds against their concentration gradients across cell membranes (Lodish et al., 2003). Substrates of representatives of the other classes (V-, F- and P-class (e.g. the Na^+/K^+ ATPase, the H^+/K^+ ATPase and the Ca^{2+} ATPase) pumps) are invariably inorganic ions. In contrast, members of the ABC transporter superfamily are capable to transport structurally diverse substrates such as amino acids, lipids, polypeptides and small hydrophobic molecules (Higgins, 2007). They are named after their characteristic, highly conserved intracellular ATP-binding cassette domains and are distributed ubiquitously over all species (and cells). The human genome encodes 48 different ABC transporters. Depending on their sequence, they were categorized by the HUGO Gene Nomenclature Committee into seven subfamilies termed A - G. The functional unit consists of four distinctive domains: two transmembrane domains (TMDs), containing 6 alpha helices each, and two intracellular nucleotide binding domains (NBDs). Detailed information regarding the structural organization and the mechanism of transport is presented in chapter 7. While individual members of the various subfamilies are specific for a certain substrate (e.g. ABCB4 for phosphatidyl choline), some expel a broad variety of hydrophobic compounds (see below). Furthermore, dysfunctions of particular transporters are associated with diseases such as cystic fibrosis, Dubin-Johnson syndrome, adrenoleukodystrophy et cetera (Higgins and Linton, 2001).

More important with regard to pharmacological aspects are a number of multispecific efflux pumps. These ABC transporters greatly influence the absorption, distribution (e.g. across the blood-brain barrier, BBB), excretion and the toxicity of many commonly prescribed drugs (Ecker et al., 2008; Szakacs et al., 2008). Additionally, approximately one third of all malignancies in the periphery develop resistance against various chemotherapeutic agents (MDR, multidrug resistance) due to the (over)expression of ABC transporters (Gillet and Gottesman, 2010; Mellor and Callaghan, 2008). The significance of multidrug transporters in this field as well as the therapeutic approach to improve cancer chemotherapy by inhibition of these efflux pumps is discussed in chapter 5.

Beyond the three most important transporters listed in **Table 1.1**, ABCB11 and ABCC2-5 (MRP2-5) also influence drug distribution and resistance. The role in protecting the

organism against xenobiotics is underlined by the fact that these transporters are preferentially expressed in excretory organs as liver (Chandra and Brouwer, 2004) or kidney (Thiebaut et al., 1987) and at important pharmacological barriers. The presence of ABCB1/ABCG2 at the brush border membrane of intestinal cells limits the oral bio-availability of drugs that are substrates of the respective transporters. This has been shown for paclitaxel and topotecan in experiments with Abcb1a/b double knockout mice or by concomitant application of the ABCB1/ABCG2 modulator elacridar (Breedveld et al., 2006; Koolen et al., 2010). During lactation, in particular BCRP plays an important role in the excretion of xenobiotics into the milk (Jonker et al., 2005). In contrast, due to its high expression at the placenta, BCRP protects the fetus against potential harmful compounds present in the general circulation (Maliepaard et al., 2001; van Herwaarden and Schinkel, 2006).

Table 1.1: Overview of the most important ABC transporters at the blood-brain barrier and with regard to multidrug resistance in cancer[a]

Gene term	Protein name (abbreviations; synonyms)	Substrates	Modulators / inhibitors
ABCB1	Multidrug Resistance Protein 1 (MDR1; P-gp; P-glycoprotein)	taxanes, epi-podophyllotoxines vinca alkaloids, anthracyclines	verapamil, cyclosporin, valspodar, elacridar, tariquidar
ABCC1	Multidrug Resistance Associated Protein 1 (MRP1)	doxorubicin, folic acid	quinidine, tricyclic isooxazoles
ABCG2	Breast Cancer Resistance Protein (BCRP; Mitoxantrone Resistance Protein, MXR)	mitoxantrone, methotrexate, topotecan	fumitremorgin C, Ko143, elacridar, ME22-1

[a] Common synonyms are listed in parentheses. With modifications according to Szakacs et al. (2006)

Since many substrates are toxic natural products from plants and microorganisms (or derivatives thereof), the presence of such transporters is an essential evolutionary advantage that could explain the above mentioned ubiquitous distribution (Higgins, 2007).
Due to its morphological properties, the high level of P-glycoprotein expression and the presence of multiple other efflux transporters, the blood-brain barrier is presumably the most important pharmacological barrier (Cooray et al., 2002; Dombrowski et al., 2001).

1.3 The blood-brain barrier and malignant brain tumors

The BBB is formed by the endothelial cells of brain capillary microvessels. These vessels are estimated to have the substantial length of 600 km (and a surface area of approximately 20 m^2) to meet the immense demand of the brain with regard to oxygen, glucose and other nutrients (Pardridge, 2003).

By contrast, the CNS has to be protected from immunological risks (bacteria, viruses), endogenous constituents (that may disturb neuronal signal transmission; e.g. epinephrine, potassium) and potential harmful xenobiotics present in the general circulation. In order to fulfill this function, brain capillaries show, opposite to vessels of the periphery, some distinct characteristics such as low pinocytic activity, an additional basal membrane as well as a 90 % coverage with astrocyte end feet (Deeken and Löscher, 2007). While all these factors limit transcellular permeation, the lacking fenestration and, especially the formation of tight junctions, restrict paracellular transport (Rubin and Staddon, 1999).

Additionally, the entry of pharmacologically active compounds into brain tissue is severely limited due to the expression of ABC transporters. The main subject of the present work, P-glycoprotein, is the most prominent member of these efflux pumps. The high transport capacity and the broad substrate specifity make it the major obstacle for drug delivery into the brain (Miller et al., 2008).

Due to their physico-chemical properties, highly hydrophobic agents should be able to cross the BBB. However, the recognition by P-gp is responsible for the efflux back into the blood circulation. This problem severely limits the treatment options of CNS disorders. Since many substrates of P-glycoprotein are integral parts of most chemotherapeutic regimens (Szakacs et al., 2006), in particular the treatment of CNS malignancies is affected.

Malignancies of the brain can be categorized into primary and secondary tumors. While secondary tumors are metastases originating from malignant tumors outside the CNS, primary tumors descend from brain tissue. The majority (approximately 80 % in adult patients) of the latter arises from the supportive tissue of the brain (the glial cells) and is subsumed under the term gliomas. Within this heterogeneous group of neoplasm, 80 % are astrocytomas (malignant forms of astrocytes). According to histological characteristics of malignancy, the World Health Organization (WHO) categorizes astrocytomas into four grades (Louis et al., 2007).

High-grade gliomas (WHO grades III/IV) and especially glioblastomas have an unfavorable prognosis due to the high risk of tumor recurrence (Hou et al., 2006). The median survival time of patients under maximal treatment is estimated to be between 12 and 18 month. A

multidisciplinary treatment approach is recommended comprising maximal feasible tumor resection, postoperative external-beam radiotherapy and multimodal chemotherapy (Mason et al., 2007). In particular, alkylating agents (see **Figure 1.1**) that are no substrates of P-glycoprotein and therefore reach adequate concentrations in brain tissue are in use (Fadul et al., 2008). Combination of the p.o. bioavailable temozolomide with radiotherapy is the best treatment currently available (Stupp et al., 2005). Nevertheless, the median survival time of 14.6 month after prognosis is still disillusioning.

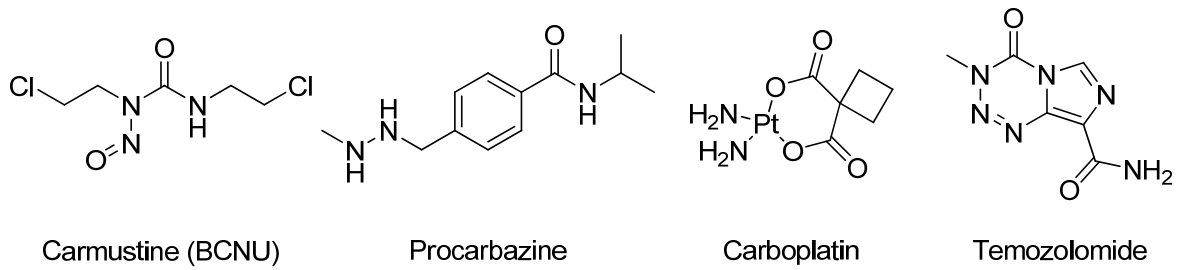

Figure 1.1: Chemical structures of chemotherapeutic agents used in the therapy of malignant (or high-grade) gliomas.

As discussed above, the efficacy of many otherwise active anticancer agents (e.g. paclitaxel) is severely restricted because they are substrates of the ABCB1 transporter. Consequently, the inhibition of P-glycoprotein by selective modulators is an attractive strategy to improve the limited therapeutic options in both, the treatment of malignant gliomas and multidrug resistant tumors in the periphery. Intense research efforts over the past decades yielded potent ABCB1 modulators such as tariquidar (cf. Figure 2.1) with superior characteristics compared to previous generations of inhibitors (Lee, 2010). The investigation of the therapeutic potential of new tariquidar-like modulators in preclinical in vivo tumor models is the central part of this thesis.

1.4 In vitro screening assays to determine ABC transporter interactions

Considering the enormous impact of ABC transporters on the items discussed in the previous sections, reliable in vitro test systems for the screening of potential substrates and inhibitors are indispensable. Beside the identification of potent inhibitors of ABC transporters, such assays are of general interest for the evaluation of new lead structures at early stages of the drug development process since ABC transporters can be considered as off-targets (anti-targets).

The in vitro models can be categorized into two main classes, cell based and membrane/protein-based test systems. Assays of the first class use cells (preferentially mammalian, but also bacterial, insect cells etc.) expressing the respective transporter due to the exposure to cytostatic agents or the transfection with the gene(s) of interest. Protein-based test systems normally utilize membranes prepared from that kind of cells. Additionally, models using isolated organs are described.

As measuring vesicular transport (Szakacs et al., 2008) and micro-pH (Landwojtowicz et al., 2002) are of no or of minor relevance for P-glycoprotein, these methods are only mentioned and not considered in detail. The subsequent discussion of the most important assays to examine drug interactions with ABC transporters is essentially based on the following literature: Szakacs et al. (2008), Varma et al. (2003) and Xia et al. (2007).

1.4.1 ATPase activity assays

According to Callaghan et al. (2006), the complex translocation process of P-glycoprotein (and other ABC transporters) comprises four distinct stages: the loading of P-gp with substrate and nucleotide (1), reorientation of TMDs combined with the transition of the binding site from the high to the low affinity state (2), release of substrate followed by the hydrolysis of ATP (3) and the resetting of TMDs (4). The energy to power the vast conformational changes required for substrate transport (cf. chapter 7) is provided by the hydrolysis of the nucleotide. The correlation between ATPase activity and transport function allows the characterization of substrates or modulators by quantifying the release of phosphate/ADP or the amount of ATP. The liberation of inorganic phosphate can easily be monitored by a simple colorimetric reaction using ammonium molybdate (Polli et al., 2001). In contrast, the quantification of nucleotides requires more elaborate methods such as luciferase-mediated bioluminescence, ion-exchange HPLC or ion-pairing reverse phase HPLC (Meyer et al., 1999; Varma et al., 2003).

The assay is usually performed with membranes prepared from cells expressing the respective transporter (cultured cells are also suitable). In order to eliminate the effect of mitochondrial and Ca^{2+} ATPases, sodium azide and ethylene glycol tetraacetic acid (EGTA) are included in the assay systems. After one cycle of ATP-hydrolysis, released phosphate is replaced by inorganic vanadate (V_i) and the resulting complex traps the investigated ABC transporter in an intermediate state. Consequently, the difference in the amount of ATP consumed (or phosphate released) in the presence or absence of V_i represents ABC transporter-mediated ATPase activity (Xia et al., 2007).

Normally, the addition of substrates increases the extent of ATP hydrolysis, whereas modulators (inhibitors or slowly transported compounds) decrease substrate stimulated

ATPase activity. Constitutive ATPase activity, most likely caused by the transportation of endogenous substrates (e.g. membrane lipids), is characteristic for most ABC transporters. Consequently, false negative results are possible for substrates (e.g. reported for vincristine, colchicine or digoxin) that do not further stimulate ATP hydrolysis (Litman et al., 1997; Schwab et al., 2003). Additionally, the basal ATPase activity can be influenced by the composition of the utilized membrane and the experimental set-up (Telbisz et al., 2007). A further limitation is the low reproducibility (high inter-day variability). In contrast, the utilized membranes are easily prepared and maintained (or even commercially available). Combined with a compound independent, practicable colorimetric quantification, the assay is suitable for high throughput screening.

1.4.2 Photoaffinity labeling assays

This technique requires photolabeling agents (substrates/inhibitors of the respective transport) e.g. [^{125}I]iodoaryl-azidoprazosin (Pouliot et al., 1997) or [^{3}H]azidopine (Safa et al., 1987). These agents are incubated with transporter enriched membranes at various concentrations of the test compound. After UV-irradiation, the transporter is isolated by SDS gel electrophoresis. Test compounds that interact with the protein should significantly reduce the amount of labeled transporter (quantified by autoradiography). Moderate reliability due to low labeling efficacy is the major limitation of this time consuming procedure. Additionally, different (or only partially overlapping) binding sites of test compound and photolabeling agents (cf. chapter 7) as well as the indefinite mechanism of transport have to be considered.

1.4.3 Chemosensitivity assays

In this assay type, the chemosensitivity of cells is a surrogate parameter for the cellular accumulation of cytostatic agents. In order to identify substrates, cells expressing the respective transporter and the parental (transporter negative) cell line are incubated in the presence of increasing concentrations of the test compound. After a certain incubation period (or after various incubation times; cf. the kinetic crystal violet assay described in section 3.2.5) the amount of viable cells is determined and IC_{50}-values are calculated.

Methods to quantify the number of surviving cells are manifold. Commonly used colorimetric techniques are to measure the activity of reductive enzymes (e.g. the conversion of [3-(4,5-dimethylthiazol-2-yl)-2,5-diphenyltetrazolium bromide]; MTT) (Mosmann, 1983) or the mass of viable cells with special dyes (Bernhardt et al., 1992). More recent approaches also utilize the detection of luciferase-mediated light signals

(Niles et al., 2007). Significant differences in the obtained IC_{50}-values (i.e. unequal chemosensitivity) are observed if the drug is extruded by the transporter-expressing cells. Limitations are a mandatory antiproliferative activity of the test compound as well as a restricted comparability of data obtained with different cell lines (depending on the expression level and/or pattern of ABC transporter(s)).

With a modified approach, it is also feasible to identify non-toxic modulators/inhibitors. The combination of a known (cytostatic) substrate of the transporter of interest with the test compound should reverse the efflux transporter-mediated multidrug resistance. Virtually all first and second generation P-gp modulators (Gottesman and Ling, 2006) as well the fumitremorgin C analog and selective BCRP inhibitor Ko143 were identified using this type of assay (Allen et al., 2002).

1.4.4 Transcellular transport assays

Before drugs can exert a pharmacological action by interacting with the respective cellular targets, they have to overcome various epithelial barriers (e.g. in the intestine, the liver and at the BBB). Transcellular transport assays simulate the physiological situation and allow the direct determination of the permeability as well as the evaluation of the interaction with transport proteins. Normally, cells expressing the transporter of interest are cultured on porous membranes that are mounted on multi-well plates (cf. **Figure 1.2**). Having reached confluency, the test compound is added either to the apical or the basolateral reservoir. After different periods of incubation, the concentration of the test compound in the receiving compartment is quantified by sensitive analytical methods (see below). The apparent permeability is calculated (flux rate corrected to the surface area and the initial concentration) separately for the basolateral-to-apical direction ($P_{app\ B\text{-}A}$) and the apical-to-basolateral direction ($P_{app\ A\text{-}B}$). If the test compound is not a substrate of the present transporter (or the efflux transporter is inhibited by a modulator), the ratio of both values equals unity. In contrast, if the compound is recognized by P-gp or BCRP (expressed in the apical membrane), $P_{app\ B\text{-}A}$ will significantly exceed $P_{app\ A\text{-}B}$. Additionally, active transport (saturable) can be discriminated from passive diffusion (linear increase) if the apparent permeability is determined at varying concentrations of the test compound. In an indirect setting, inhibitory properties can be identified by comparing the permeability ratios of know substrates in the presence and the absence of the test compound.

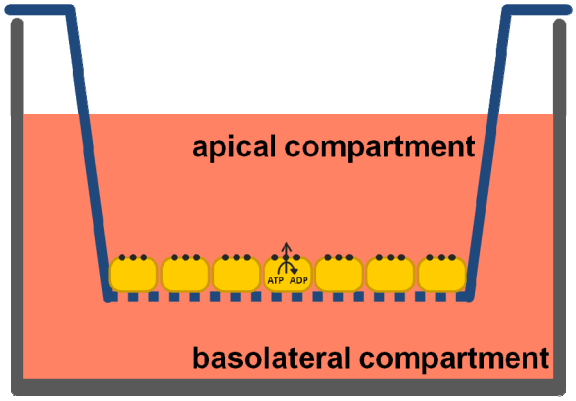

Figure 1.2: Schematic illustration of the experimental set-up of a characteristic trans-cellular transport assay to evaluate the activity of efflux transporter. The ABC transporters are represented by black circles. Illustration adapted from the Corning® HTS Transwell® - 96 Tissue Culture System.

Suitable cells must be polarized, i. e. express the transporter of interest at a defined side of the membrane and form tight junctions. Commonly used cell lines are Caco-2 (human colonic adenocarcinoma; simulation of the absorption process in the intestine), LLC-PK1 (epithelial porcine kidney cells) and MDCK (Madin-Darby canine kidney cells). In contrast to LLC-PK1 and MDCK cells (3 - 4 days), Caco-2 cells have to be cultured 3 weeks on the filter membranes until the studies can be initiated. Additionally, it has to be taken into consideration that numerous different transporters are expressed in this cell type.

Further general problems are varying levels of transporter expression as well as the possibility of misinterpretations due to membrane leakage (toxicity of the substrate or insufficient confluence). False negative results (with regard to the identification of substrates) are caused if the investigated compound shows a high passive permeability (Doppenschmitt et al., 1999). In this case it is assumed that the high intrinsic permeability levels the ABC transporter mediated efflux (Lentz et al., 2000). Moreover, the substrates have to be available radioactively labeled or show fluorescent properties. If a high number of compounds has to be screened, the quantification necessitates elaborate analytical methods such as liquid chromatography with tandem mass spectrometry (Polli et al., 2001).

1.4.5 Cellular accumulation assays

In contrast to chemosensitivity investigations, the accumulation of transporter substrates in ABC transporter expressing cells is measured directly. If the test compound shows inherent fluorescence or is radioactively labeled, substrate properties as well as characteristic pharmacological parameters (e.g. K_m or V_{max}) can be determined straightforward. Since the majority of agents lacks these properties, mostly indirect methods utilizing fluorescent indicators are applied. In this set-up, the concentration dependent inhibition of the respective transporter can be quantified by the successively increased cellular fluorescence. As becomes obvious, the method is especially suitable for

the identification of modulators. Nevertheless, due to the competitive inhibition of dye efflux in higher concentrations, the assay is not able to discriminate between substrates and inhibitors.

Commonly used fluorescent indicators are rhodamine 123 (P-gp) (Eytan et al., 1997), pheophorbide a (BCRP) (Henrich et al., 2006), Hoechst 33342 (P-gp and BCRP) (Seigel and Campbell, 2004) and calcein-AM (P-gp and MRP1) (Homolya et al., 1993). The latter has become the preferred fluorescent dye for the evaluation of ABCB1 mediated efflux due to its unique activation mechanism (cf. section 3.2.3). Nevertheless, a suitable fluorescent probe has to be selected with regard to the ABC transporter expression pattern of the used cell line and the protein of interest. Alternatively, selectivity for an individual protein can be achieved by utilizing cells that express solely (genetically engineered) or preferentially the respective ABC transporter.

In the indirect set-up, the fluorescent indicator assays are suitable for the screening of large compound libraries and were recommended for investigations in early stages of drug discovery (Rautio et al., 2006; Schwab et al., 2003). Despite a generally high reliability, false negative results are possible due to an inherent toxicity or lacking completion of the test compound and the fluorescent probe. For example, colchicine inhibited Hoechst 33342 transport whereas rhodamine 123 transport was stimulated (Shapiro and Ling, 1998). Responsible for this and similar observations are most likely different interaction sites for the various substrates and modulators (Martin et al., 2000). A combination with ATPase and/or transcellular transport assays circumvents these problems and facilitates the differentiation of substrates and inhibitors (Polli et al., 2001).

1.4.6 Isolated organ preparations

The perfusion technique stands at the interface between in vitro assays and more time consuming and cost intensive in vivo investigations. Isolated organs are perfused with solutions containing the test compound (ABC transporter substrate) at a certain concentration. Determination of the substrate concentrations in the perfusate and the organ enables the estimation of transporter activity in the respective tissue. This technique has been successfully applied for the evaluation of the significance of ABC transporters in liver (Lau et al., 2004), kidney (Hori et al., 1993) or intestine (Adachi et al., 2003). With regard to the role of P-gp at the BBB, perfusion studies showed that the uptake of colchicine and vinblastine into the brain of mdr1a deficient mice was three times higher compared to wild type animals. Pre-administration of the P-glycoprotein modulators valspodar or elacridar increased the apparent brain transport of the respective compounds to the level observed with P-gp deficient animals (Cisternino et al., 2001). Due to the intact

organ structure, these models may provide data of high predictive value and contribute to reduce the number of animal experiments. Nevertheless, compared to the assays discussed above, the organ preparations are elaborate and time consuming. Additionally, handling errors due to the complex methodology as well as tissue injuries may cause misleading results.

1.5 References

Adachi, Y.; Suzuki, H.; Sugiyama, Y. Quantitative evaluation of the function of small intestinal P-glycoprotein: comparative studies between in situ and in vitro. *Pharm. Res.* **2003,** 20, 1163-1169.

Allen, J. D.; van Loevezijn, A.; Lakhai, J. M.; van der Valk, M.; van Tellingen, O.; Reid, G., et al. Potent and specific inhibition of the breast cancer resistance protein multidrug transporter in vitro and in mouse intestine by a novel analogue of fumitremorgin C. *Mol. Cancer Ther.* **2002,** 1, 417-425.

Bernhardt, G.; Reile, H.; Birnbock, H.; Spruss, T.; Schonenberger, H. Standardized kinetic microassay to quantify differential chemosensitivity on the basis of proliferative activity. *J. Cancer Res. Clin. Oncol.* **1992,** 118, 35-43.

Blattner, F. R.; Plunkett, G., 3rd; Bloch, C. A.; Perna, N. T.; Burland, V.; Riley, M., et al. The complete genome sequence of Escherichia coli K-12. *Science* **1997,** 277, 1453-1462.

Breedveld, P.; Beijnen, J. H.; Schellens, J. H. Use of P-glycoprotein and BCRP inhibitors to improve oral bioavailability and CNS penetration of anticancer drugs. *Trends Pharmacol. Sci.* **2006,** 27, 17-24.

Callaghan, R.; Ford, R. C.; Kerr, I. D. The translocation mechanism of P-glycoprotein. *FEBS Lett.* **2006,** 580, 1056-1063.

Chandra, P.; Brouwer, K. L. The complexities of hepatic drug transport: current knowledge and emerging concepts. *Pharm. Res.* **2004,** 21, 719-735.

Cisternino, S.; Rousselle, C.; Dagenais, C.; Scherrmann, J. M. Screening of multidrug-resistance sensitive drugs by in situ brain perfusion in P-glycoprotein-deficient mice. *Pharm. Res.* **2001,** 18, 183-190.

Cooray, H. C.; Blackmore, C. G.; Maskell, L.; Barrand, M. A. Localisation of breast cancer resistance protein in microvessel endothelium of human brain. *Neuroreport* **2002,** 13, 2059-2063.

Deeken, J. F.; Löscher, W. The blood-brain barrier and cancer: transporters, treatment, and Trojan horses. *Clin. Cancer Res.* **2007,** 13, 1663-1674.

Dobson, P. D.; Kell, D. B. Carrier-mediated cellular uptake of pharmaceutical drugs: an exception or the rule? *Nat. Rev. Drug Discov.* **2008,** 7, 205-220.

Dombrowski, S. M.; Desai, S. Y.; Marroni, M.; Cucullo, L.; Goodrich, K.; Bingaman, W., et al. Overexpression of multiple drug resistance genes in endothelial cells from patients with refractory epilepsy. *Epilepsia* **2001,** 42, 1501-1506.

Doppenschmitt, S.; Spahn-Langguth, H.; Regardh, C. G.; Langguth, P. Role of P-glycoprotein-mediated secretion in absorptive drug permeability: An approach using passive membrane permeability and affinity to P-glycoprotein. *J. Pharm. Sci.* **1999,** 88, 1067-1072.

Ecker, G. F.; Stockner, T.; Chiba, P. Computational models for prediction of interactions with ABC-transporters. *Drug Discov. Today* **2008,** 13, 311-317.

Eytan, G. D.; Regev, R.; Oren, G.; Hurwitz, C. D.; Assaraf, Y. G. Efficiency of P-glycoprotein-mediated exclusion of rhodamine dyes from multidrug-resistant cells is determined by their passive transmembrane movement rate. *Eur. J. Biochem.* **1997,** 248, 104-112.

Fadul, C. E.; Wen, P. Y.; Kim, L.; Olson, J. J. Cytotoxic chemotherapeutic management of newly diagnosed glioblastoma multiforme. *J. Neurooncol.* **2008,** 89, 339-357.

Gillet, J. P.; Gottesman, M. M. Mechanisms of multidrug resistance in cancer. In *Multi-drug resistance in cancer*, Zhou, J., Ed. Humana Press: New York, 2010; pp 47-76.

Gottesman, M. M.; Ling, V. The molecular basis of multidrug resistance in cancer: the early years of P-glycoprotein research. *FEBS Lett.* **2006,** 580, 998-1009.

Henrich, C. J.; Bokesch, H. R.; Dean, M.; Bates, S. E.; Robey, R. W.; Goncharova, E. I., et al. A high-throughput cell-based assay for inhibitors of ABCG2 activity. *J. Biomol. Screen* **2006,** 11, 176-183.

Higgins, C. F. Multiple molecular mechanisms for multidrug resistance transporters. *Nature* **2007,** 446, 749-757.

Higgins, C. F.; Linton, K. J. Structural biology. The xyz of ABC transporters. *Science* **2001,** 293, 1782-1784.

Homolya, L.; Hollo, Z.; Germann, U. A.; Pastan, I.; Gottesman, M. M.; Sarkadi, B. Fluorescent cellular indicators are extruded by the multidrug resistance protein. *J. Biol. Chem.* **1993,** 268, 21493-21496.

Hori, R.; Okamura, N.; Aiba, T.; Tanigawara, Y. Role of P-glycoprotein in renal tubular secretion of digoxin in the isolated perfused rat kidney. *J. Pharmacol. Exp. Ther.* **1993,** 266, 1620-1625.

Hou, L. C.; Veeravagu, A.; Hsu, A. R.; Tse, V. C. Recurrent glioblastoma multiforme: a review of natural history and management options. *Neurosurg. Focus* **2006,** 20, E5.

Jonker, J. W.; Merino, G.; Musters, S.; van Herwaarden, A. E.; Bolscher, E.; Wagenaar, E., et al. The breast cancer resistance protein BCRP (ABCG2) concentrates drugs and carcinogenic xenotoxins into milk. *Nat. Med.* **2005,** 11, 127-129.

Koolen, S. L.; Beijnen, J. H.; Schellens, J. H. Intravenous-to-oral switch in anticancer chemotherapy: a focus on docetaxel and paclitaxel. *Clin. Pharmacol. Ther.* **2010,** 87, 126-129.

Landwojtowicz, E.; Nervi, P.; Seelig, A. Real-time monitoring of P-glycoprotein activation in living cells. *Biochemistry* **2002,** 41, 8050-8057.

Lau, Y. Y.; Wu, C. Y.; Okochi, H.; Benet, L. Z. Ex situ inhibition of hepatic uptake and efflux significantly changes metabolism: hepatic enzyme-transporter interplay. *J. Pharmacol. Exp. Ther.* **2004,** 308, 1040-1045.

Lee, C. H. Reversing agents for ATP-binding cassette drug transporters. In *Multi-Drug Resistance in Cancer*, Zhou, J., Ed. Humana Press: New York, 2010; pp 325-340.

Lentz, K. A.; Polli, J. W.; Wring, S. A.; Humphreys, J. E.; Polli, J. E. Influence of passive permeability on apparent P-glycoprotein kinetics. *Pharm. Res.* **2000,** 17, 1456-1460.

Lipinski, C. A.; Lombardo, F.; Dominy, B. W.; Feeney, P. J. Experimental and computational approaches to estimate solubility and permeability in drug discovery and development settings. *Adv Drug Deliv Rev* **2001,** 46, 3-26.

Litman, T.; Zeuthen, T.; Skovsgaard, T.; Stein, W. D. Structure-activity relationships of P-glycoprotein interacting drugs: kinetic characterization of their effects on ATPase activity. *Biochim. Biophys. Acta* **1997,** 1361, 159-168.

Lodish, H.; Berk, A.; Masudaira, P.; Kaiser, C. A.; Krieger, M.; Scott, M. P., et al. *Molecular cell biology*. 5th ed.; W.H. Freeman and Company: New York, 2003.

Louis, D. N.; Ohgaki, H.; Wiestler, O. D.; Cavenee, W. K.; Burger, P. C.; Jouvet, A., et al. The 2007 WHO classification of tumours of the central nervous system. *Acta Neuropathol.* **2007,** 114, 97-109.

Maliepaard, M.; Scheffer, G. L.; Faneyte, I. F.; van Gastelen, M. A.; Pijnenborg, A. C.; Schinkel, A. H., et al. Subcellular localization and distribution of the breast cancer resistance protein transporter in normal human tissues. *Cancer Res.* **2001,** 61, 3458-3464.

Martin, C.; Berridge, G.; Higgins, C. F.; Mistry, P.; Charlton, P.; Callaghan, R. Communication between multiple drug binding sites on P-glycoprotein. *Mol. Pharmacol.* **2000,** 58, 624-632.

Mason, W. P.; Maestro, R. D.; Eisenstat, D.; Forsyth, P.; Fulton, D.; Laperriere, N., et al. Canadian recommendations for the treatment of glioblastoma multiforme. *Current Oncology* **2007,** 14, 110-117.

Mehdipour, A. R.; Hamidi, M. Brain drug targeting: a computational approach for overcoming blood-brain barrier. *Drug Discov. Today* **2009,** 14, 1030-1036.

Mellor, H. R.; Callaghan, R. Resistance to chemotherapy in cancer: a complex and integrated cellular response. *Pharmacology* **2008,** 81, 275-300.

Meyer, S.; Noisommit-Rizzi, N.; Reuss, M.; Neubauer, P. Optimized analysis of intracellular adenosine and guanosine phosphates in Escherichia coli. *Anal. Biochem.* **1999,** 271, 43-52.

Miller, D. S.; Bauer, B.; Hartz, A. M. Modulation of P-glycoprotein at the blood-brain barrier: opportunities to improve central nervous system pharmacotherapy. *Pharmacol. Rev.* **2008,** 60, 196-209.

Mosmann, T. Rapid colorimetric assay for cellular growth and survival: application to proliferation and cytotoxicity assays. *J. Immunol. Methods* **1983,** 65, 55-63.

Niles, A. L.; Moravec, R. A.; Eric Hesselberth, P.; Scurria, M. A.; Daily, W. J.; Riss, T. L. A homogeneous assay to measure live and dead cells in the same sample by detecting different protease markers. *Anal. Biochem.* **2007,** 366, 197-206.

Pardridge, W. M. Blood-brain barrier drug targeting: The future of brain drug development. *Mol. Interv.* **2003,** 3, 90-105.

Polli, J. W.; Wring, S. A.; Humphreys, J. E.; Huang, L.; Morgan, J. B.; Webster, L. O., et al. Rational use of in vitro P-glycoprotein assays in drug discovery. *J. Pharmacol. Exp. Ther.* **2001,** 299, 620-628.

Pouliot, J. F.; L'Heureux, F.; Liu, Z.; Prichard, R. K.; Georges, E. Reversal of P-glycoprotein-associated multidrug resistance by ivermectin. *Biochem. Pharmacol.* **1997,** 53, 17-25.

Rautio, J.; Humphreys, J. E.; Webster, L. O.; Balakrishnan, A.; Keogh, J. P.; Kunta, J. R., et al. In vitro p-glycoprotein inhibition assays for assessment of clinical drug interaction potential of new drug candidates: a recommendation for probe substrates. *Drug Metab. Dispos.* **2006,** 34, 786-792.

Rees, D. C.; Johnson, E.; Lewinson, O. ABC transporters: the power to change. *Nat. Rev. Mol. Cell Biol.* **2009,** 10, 218-227.

Rubin, L. L.; Staddon, J. M. The cell biology of the blood-brain barrier. *Annu. Rev. Neurosci.* **1999,** 22, 11-28.

Safa, A. R.; Glover, C. J.; Sewell, J. L.; Meyers, M. B.; Biedler, J. L.; Felsted, R. L. Identification of the multidrug resistance-related membrane glycoprotein as an acceptor for calcium channel blockers. *J. Biol. Chem.* **1987,** 262, 7884-7888.

Schwab, D.; Fischer, H.; Tabatabaei, A.; Poli, S.; Huwyler, J. Comparison of in vitro P-glycoprotein screening assays: recommendations for their use in drug discovery. *J. Med. Chem.* **2003,** 46, 1716-1725.

Seigel, G. M.; Campbell, L. M. High-throughput microtiter assay for Hoechst 33342 dye uptake. *Cytotechnology* **2004,** 45, 155-160.

Shapiro, A. B.; Ling, V. The mechanism of ATP-dependent multidrug transport by P-glycoprotein. *Acta Physiol. Scand. Suppl.* **1998,** 643, 227-234.

Stupp, R.; Mason, W. P.; van den Bent, M. J.; Weller, M.; Fisher, B.; Taphoorn, M. J., et al. Radiotherapy plus concomitant and adjuvant temozolomide for glioblastoma. *N. Engl. J. Med.* **2005,** 352, 987-996.

Szakacs, G.; Paterson, J. K.; Ludwig, J. A.; Booth-Genthe, C.; Gottesman, M. M. Targeting multidrug resistance in cancer. *Nat. Rev. Drug Discov.* **2006,** 5, 219-234.

Szakacs, G.; Varadi, A.; Ozvegy-Laczka, C.; Sarkadi, B. The role of ABC transporters in drug absorption, distribution, metabolism, excretion and toxicity (ADME-Tox). *Drug Discov. Today* **2008,** 13, 379-393.

Telbisz, A.; Muller, M.; Ozvegy-Laczka, C.; Homolya, L.; Szente, L.; Varadi, A., et al. Membrane cholesterol selectively modulates the activity of the human ABCG2 multidrug transporter. *Biochim. Biophys. Acta* **2007,** 1768, 2698-2713.

Thiebaut, F.; Tsuruo, T.; Hamada, H.; Gottesman, M. M.; Pastan, I.; Willingham, M. C. Cellular localization of the multidrug-resistance gene product P-glycoprotein in normal human tissues. *Proc. Natl. Acad. Sci. U. S. A.* **1987,** 84, 7735-7738.

van Herwaarden, A. E.; Schinkel, A. H. The function of breast cancer resistance protein in epithelial barriers, stem cells and milk secretion of drugs and xenotoxins. *Trends Pharmacol. Sci.* **2006,** 27, 10-16.

Varma, M. V.; Ashokraj, Y.; Dey, C. S.; Panchagnula, R. P-glycoprotein inhibitors and their screening: a perspective from bioavailability enhancement. *Pharmacol. Res.* **2003,** 48, 347-359.

Xia, C. Q.; Milton, M. N.; Gan, L. S. Evaluation of drug-transporter interactions using in vitro and in vivo models. *Curr. Drug Metab.* **2007,** 8, 341-363.

Chapter 2

2 Scope and objectives

ABCB1 transporter mediated efflux is the most important cause of multidrug resistance (MDR) in cancer (Szakacs et al., 2006). Furthermore, as an essential component of the blood-brain barrier, P-glycoprotein compromises the efficacy of many otherwise potent drugs in the central nervous system (Deeken and Löscher, 2007). Within the plethora of drugs (antidepressants, hormones, antibiotics etc.), in particular many clinically used anti-cancer agents (taxanes, anthracyclines, vinca alkaloids etc.) are transported by P-glycoprotein. This results in low concentrations of the cytostatics in the CNS and is arguably the main cause for the disillusioning prognosis of malignant brain tumors.

In previous studies with nude mice bearing intracerebral human U-118 MG glioblastomas, the brain levels of paclitaxel were significantly increased when the cytostatic was combined with the second generation modulator valspodar (Fellner et al., 2002). While the elevated brain concentration of paclitaxel resulted in a reduction of tumor volume by 90 %, valspodar also increased the concentration (and hence the toxicity) of the cytostatic agent in the periphery. By contrast, studies performed with the (in vitro even more potent) third generation modulator tariquidar, showed no influence on the plasma concentration of paclitaxel (Hubensack et al., 2008). Compared to co-administered valspodar, tariquidar significantly elevated the paclitaxel brain levels as well, but to a lesser extent than expected. Considering the high in vitro potency of tariquidar, the discrepancy to the in vivo results was attributed to poor drug-like properties, for instance high lipophilicity (accumulation in adipose tissue) and low solubility. Consequently, it was hypothesized that more hydrophilic tariquidar-like modulators will be more effective in vivo.

In order to investigate this hypothesis, a series of tariquidar-like modulators with pronounced differences in lipophilicity was synthesized in the group of Prof. Dr. Burkhard König (Egger et al., 2007). With substantial different octanol-water partition coefficients (covering the range of two orders of magnitude), the three derivatives ME27-4, ME30-1 and ME33-1 were identified as potent inhibitors of P-glycoprotein (cf. **Figure 2.1**).

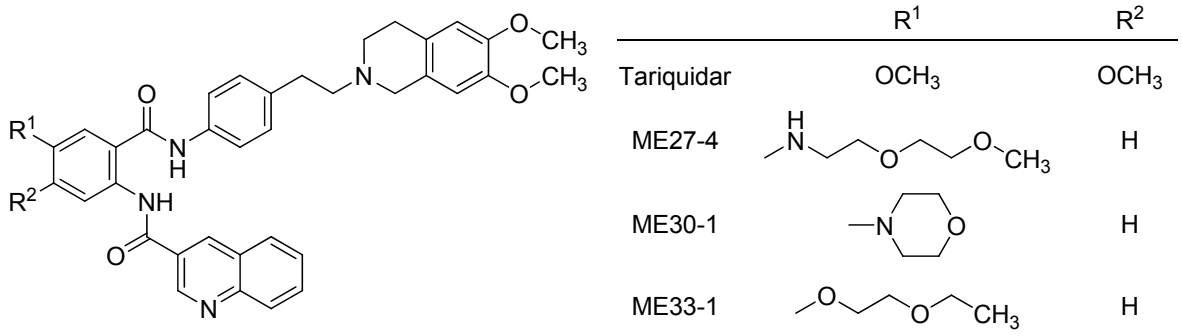

Figure 2.1: Chemical structures of tariquidar and the three new ABCB1 modulators selected for in vitro and in vivo studies

Accordingly, these compounds were considered suitable to test the aforementioned hypothesis by the tumor pharmacological and bio-analytical investigations described in this thesis. The objectives of this work are summarized in the following.

- Firstly, a series of experiments aimed at the in vitro characterization of the selected modulators to assess their suitability for further in vivo studies. Especially bio-pharmaceutical issues such as stability, toxicity, plasma albumin binding properties etc. should be addressed. To assure inhibition of the murine ABCB1 transporter subtypes, a cellular model with predictive value for the intended experiments in nude mice had to be established. Moreover, to facilitate the rapid screening of test compounds with putative activity at the ABCB1 transporter, there was a need for a fluorescence-based inhibition assay in the microtiter plate format.

- Subsequently, bio-distribution studies in NMRI mice should confirm sufficient bioavailability and metabolic stability of the modulators prior to pharmacodynamic in vivo studies. Hence, a reliable method to determine the concentration in brain and plasma samples had to be installed. Quantification of co-administered paclitaxel should assure the desired increase of the cytostatic drug in the brain. With regard to the increased toxicity observed in previous studies with valspodar, the new tariquidar-like modulators should not affect paclitaxel plasma levels.

- To elucidate, if the putative increase in the CNS concentration of paclitaxel is of clinical significance for the treatment of malignant gliomas, a third approach was intended. Previous studies (using intracerebral tumor xenografts) were limited to a single endpoint evaluation of tumor load by time consuming histological serial sections of the brain. Fluorescence- and luminescence-based in vivo imaging methods were considered appropriate to facilitate the non-invasive determination of tumor burden at the beginning as well as during the therapy. For this purpose, U-118 MG glioblastoma

cells had to be transfected with genes encoding for various fluorescent proteins or the luciferase2 enzyme. Following the in vitro characterization, the transfectants should be used to optimize the existing orthotopic brain tumor model. Ultimately, the refined model should be utilized to study the therapeutic value of the most promising ABCB1 modulators in combination with paclitaxel.

- In an analogous therapeutic approach, the effect on MDR tumors in the periphery should be assessed. Consequently, an ABCB1 transporter expressing subcutaneous tumor model had to be established in nude mice. Therefore, P-glycoprotein expressing Kb-V1 cells as well as the resulting xenografts should be characterized concerning malignancy, growth kinetics and maintenance of transporter expression.

- Work in a different subject of this thesis was inspired by the recent publication of the first high resolution x-ray structure of a mammalian ABC transporter (Aller et al., 2009). Based on experimental data from the literature, docking experiments should localize the binding region of the tariquidar-like modulators at P-glycoprotein and identify important interacting residues. The obtained results could in turn contribute to the structure based design of improved ABCB1 modulators in the future.

2.1 References

Aller, S. G.; Yu, J.; Ward, A.; Weng, Y.; Chittaboina, S.; Zhuo, R., et al. Structure of P-glycoprotein reveals a molecular basis for poly-specific drug binding. *Science* **2009,** 323, 1718-1722.

Deeken, J. F.; Löscher, W. The blood-brain barrier and cancer: transporters, treatment, and Trojan horses. *Clin. Cancer Res.* **2007,** 13, 1663-1674.

Egger, M.; Li, X. Q.; Müller, C.; Bernhardt, G.; Buschauer, A.; König, B. Tariquidar analogues: Synthesis by Cu-^{I}-catlyzed N/O-aryl coupling and inhibitory activity against the ABCB1 transporter. *Eur. J. Org. Chem.* **2007**, 2643-2649.

Fellner, S.; Bauer, B.; Miller, D. S.; Schaffrik, M.; Fankhänel, M.; Spruss, T., et al. Transport of paclitaxel (Taxol) across the blood-brain barrier in vitro and in vivo. *J. Clin. Invest.* **2002,** 110, 1309-1318.

Hubensack, M.; Müller, C.; Höcherl, P.; Fellner, S.; Spruss, T.; Bernhardt, G., et al. Effect of the ABCB1 modulators elacridar and tariquidar on the distribution of paclitaxel in nude mice. *J. Cancer Res. Clin. Oncol.* **2008,** 134, 597-607.

Szakacs, G.; Paterson, J. K.; Ludwig, J. A.; Booth-Genthe, C.; Gottesman, M. M. Targeting multidrug resistance in cancer. *Nat. Rev. Drug Discov.* **2006,** 5, 219-234.

Chapter 3

3 The ABCB1 transporter: modulation, species differences and in vitro characterization of tariquidar-like compounds

3.1 Introduction

The (over)expression of ABCB1 transporters in MDR tumors and at the blood-brain barrier has prompted the search for potent inhibitors over the past decades (Lee, 2010). The first modulators identified (e.g. verapamil or quinidine) were approved drugs already used for other indications (the so called first generation modulators). The low affinity of these compounds required high therapeutic doses that resulted in toxic side effects due to lacking specificity. Second generation modulators such as the cyclosporine D analogue valspodar showed higher affinity for P-glycoprotein at per se nontoxic doses (Fox and Bates, 2007). However, pharmacokinetic interactions increased the concentration and hence the toxicity of the administered cytostatic drug (cf. chapter 4).

Intense research efforts have yielded potent and specific third generation ABCB1 modulators (e.g. tariquidar) lacking the aforementioned shortcomings. Indeed, tariquidar was well tolerated in clinical studies with healthy volunteers at a dosage of 2 mg/kg i.v. (or 750 mg p.o.) (Stewart et al., 2000) as well as in combination with the cytotoxic drug vinorelbine (Abraham et al., 2009). By contrast, whereas tariquidar was considerably more potent than valspodar on human ABCB1 transporters in vitro, both compounds were approximately equipotent in inhibiting P-gp at the blood-brain barrier in vivo (Fellner et al., 2002; Hubensack et al., 2008). These discrepancies could result from species dependent peculiarities of the nude mouse model as well as poor drug-like properties (as low solubility and high lipophilicity) of tariquidar. Accordingly, the first objective of this study was to

establish a cellular model to compare the activities of selected P-glycoprotein modulators at both, the human and the murine transporter.

Additionally, it was speculated that less hydrophobic and better water soluble tariquidar-like modulators may be more suitable for in vivo studies. Consequently, a series of more hydrophilic tariquidar-like ABCB1 modulators was synthesized (Egger et al., 2007). The most promising modulators ME27-4, ME30-1 and ME33-1 (cf. Figure 2.1) were selected for further in vitro characterization. During these biopharmaceutical studies, issues regarding stability (see section 4.3.5), drug-like properties, toxicity, antiproliferative activity against MDR Kb-V1 cells and human glioblastoma cells (cf. sections 5.3.1.6 / 6.3.3.1) as well as potential pharmacokinetic interactions should be investigated. The studies should also help to assess the suitability of the modulators for the intended in vivo studies.

A third series of experiments aimed at the adaptation of the established flow cytometric assay to the microtiter plate format. Though calcein-AM proved to be the supreme reference substrate for ABCB1 mediated transport (Szakacs et al., 2008), the flow cytometric assay has disadvantages with regard to cost-intensity and moderate throughput. Moreover, another series of tariquidar analogs (with the hetarylcarboxamide moiety in meta position to the benzamide core, cf. chapter 7) turned out to be among the most potent and selective inhibitors of ABCG2 mediated efflux (Kühnle et al., 2009). To evaluate the selectivity of future modulators for the ABCG2 transporter, a fast and reliable assay would be of additional advantage.

3.2 Materials and methods

3.2.1 Drugs and chemicals

Elacridar (GF 120918) and valspodar (SDZ PSC 833) were kindly provided by GSK (Research Triangle Park, NC) and Novartis (Nürnberg, Germany), respectively. The tariquidar-like modulators were synthesized (Egger et al., 2007) in the workgroup of Prof. König (Institute of Organic Chemistry, University of Regensburg, Germany). Tariquidar was synthesized in our laboratory according to the literature (Dodic et al., 1995; Roe et al., 1999) with slight modifications (Hubensack, 2005). Vinblastine, doxorubicin and paclitaxel were purchased from Sigma (Munich, Germany). Calcein-AM (4 mM in anhydrous DMSO) as well as pluronic F127 were obtained from Biotium (Hayward, CA). All stock solutions (made in DMSO or 70 % ethanol depending on the solubility of the compounds) as well as the solid substances were stored at -20 °C.

Phosphate buffered saline (PBS) contained 8.0 g/L NaCl, 1.0 g/L $Na_2HPO_4 \cdot 2\ H_2O$, 0.20 g/L KCl, 0.20 g/L KH_2PO_4 and 0.15 g/L $NaH_2PO_4 \cdot H_2O$ and was adjusted to pH 7.4 with

1 M NaOH. If not otherwise stated, chemicals (p.a. quality) were obtained from Merck (Darmstadt, Germany). Purified water (Milli-Q system, Millipore, Eschborn, Germany) was used throughout.

3.2.2 Cell lines and culture conditions

Human Kb-V1 cells were cultured in DMEM containing 10 % FCS (Biochrom, Berlin, Germany) and 330 nM vinblastine to maintain ABCB1 transporter expression.

Murine $P388D_1$ cells (CCL-46, murine lymphoid neoplasm with macrophage-like morphology) were maintained as suspension culture in DMEM supplemented with 10 % FCS (Biochrom). The ABCB1 transporter expressing subclone $P388D_1$Doxo was obtained by subculturing of wild type cells with increasing concentrations of doxorubicin. The characterization of modulators was performed with cells propagated in the presence of 1.25 µM doxorubicin.

The human glioblastoma cell line U-118 MG (HTB-15) was maintained in DMEM containing 5 % FCS (Biochrom).

Wild type cells were obtained from the American Type Culture Collection (Rockville, MD) and were cultured in water-saturated atmosphere (95 % air/5 % CO_2) at 37 °C in cell culture flasks purchased from Nunc (Wiesbaden, Germany). Dulbecco´s Minimum Essential Medium (DMEM; Sigma, Munich, Germany) was supplemented with 3.7 g/L sodium hydrogen carbonate and 110 mg/L sodium pyruvate. Subculturing of adherently growing cells was performed after trypsinization (0.05 % trypsin/0.02 % EDTA, Roche Diagnostics, Mannheim, Germany). Cell were routinely monitored for *mycoplasma* contamination by PCR (Venor® GeM, Minerva Biolabs GmbH, Berlin) and only *mycoplasma* negative cultures were used.

3.2.3 Calcein-AM efflux assay

Since calcein-AM (cf. **Figure 3.1**) is a substrate of P-glycoprotein, ABCB1 transporter expressing cells show lower intracellular levels of the compound compared to P-gp negative cells. Inside the cell, endogenous esterases cleave the ester bonds and the fluorescent calcein is formed. Consequently, inhibition of ABCB1 transporters can be quantified by the determination of calcein-mediated fluorescence (Homolya et al., 1993).

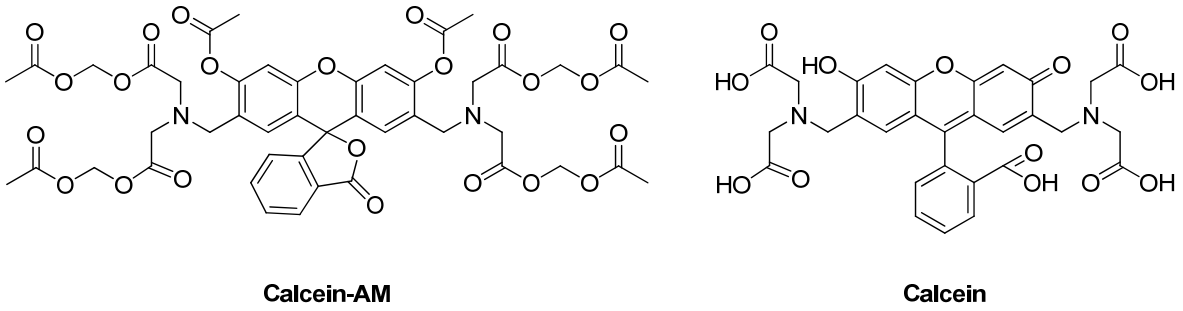

Figure 3.1: Chemical structures of the P-gp substrate calcein-AM and the intracellularly generated fluorescent calcein

In all assays, tariquidar served as positive control at a final concentration of 1 µM corresponding to 100 % inhibition of calcein-AM efflux. IC_{50}-values were calculated with SigmaPlot 9.0 using the Hill equation.

3.2.3.1 Flow cytometry

3.2.3.1.1 Kb-V1 cells

The assays were performed as described previously (Müller et al., 2007).

3.2.3.1.2 P388D$_1$Doxo cells

The protocol was adopted from the flow cytometric assay using Kb-V1 cells (Müller et al., 2007). In brief: having reached a sufficient density, P388D$_1$Doxo cells were harvested and washed with PBS. After centrifugation, the supernatant was discarded, and the cell density was adjusted to $1 \cdot 10^6$ cells per 0.75 mL with loading buffer (120 mM NaCl, 5 mM KCl, 2 mM $MgCl_2 \cdot 6\ H_2O$, 1.5 mM $CaCl_2 \cdot 2\ H_2O$, 25 mM HEPES, 10 mM glucose, pH 7.4). Additionally, 0.25 mL loading suspension (loading buffer, 20 mg/mL BSA, 5 µL/mL pluronic F127 (20 % in DMSO)) were added to reach a final density of $1 \cdot 10^6$ cells/mL. Subsequent to a pre-incubation period with various concentrations of test compounds for 15 min at 37 °C/5 % CO_2, calcein-AM solution was added to achieve a final concentration of 0.75 µM and samples were incubated for 10 min at 37 °C/5 % CO_2. After centrifugation the supernatant was discarded, cells were washed once with ice cold PBS and re-suspended in 0.5 mL loading buffer per sample. Calcein fluorescence was determined with a FACS Calibur™ flow cytometer (Becton Dickinson, Heidelberg, Germany) in the FL1-H channel. In each measurement 20,000 gated events were evaluated. The geometric means were calculated from the fluorescence intensity histograms, related to the controls and plotted against the various concentrations of test compounds. The photomultiplier settings were as follows: E-1 for FSC, 270 for SSC and 345 for FL1-H. Data analysis was performed by the WinMDI 2.9 software.

3.2.3.2 Microtiter plate format

Human Kb-V1 cells were seeded into flat-bottomed 96-well plates (Greiner, Frickenhausen, Germany) at a density of 20,000 cells per well. On the following day, cells were washed with loading buffer (120 mM NaCl, 5 mM KCl, 2 mM $MgCl_2 \cdot 6\ H_2O$, 1.5 mM $CaCl_2 \cdot 2\ H_2O$, 25 mM HEPES, 10 mM glucose, pH 7.4) in order to remove unspecific serum esterases. Afterwards, cells were incubated with loading suspension (loading buffer, 5 mg/mL BSA, 1.25 µL/mL pluronic F127 (20 % in DMSO)) containing 0.5 µM calcein-AM and the test compound at increasing concentrations for 10 min (37 °C/5 % CO_2). In general, test compounds were investigated as triplicates, controls as sextets, respectively. Subsequently, the loading suspension was discarded and cells were fixed with 4 % paraformaldehyde (PFA) solution in PBS for 20 min. After three washing circles (loading buffer), fixed cells were overlaid with loading buffer and relative fluorescence intensities were determined at 535/25 nm at a GENios Pro microplate reader (Tecan Deutschland GmbH, Crailsheim, Germany) after excitation at 485/20 nm. The obtained mean fluorescence intensities were related to the controls and plotted against the various concentrations of test compounds.

The validation of the relevant assay parameters was performed according to the published literature (Bauer et al., 2003; Bubik et al., 2006; Polli et al., 2001) and is presented in section 3.3.3.1.

3.2.4 Plasma albumin binding

10 µM solutions of tariquidar and the tariquidar-like modulators were prepared in PBS containing 40 mg/mL bovine serum albumin (BSA, Serva, Heidelberg, Germany). In order to reach equilibrium between bound and unbound ligand, the respective solutions were incubated for 30 min at 37 °C. Subsequently, the samples were ultra-filtrated by an Microcon centrifugal filter device with a nominal molecular weight limit of 10,000 Da (Millipore, Eschborn, Germany) at 10,700 g for 16 min (15 °C). Aliquots of the filtrates were combined with two parts of ice-cold acetonitrile and stored at 4 °C for 1 h. Afterwards, samples were centrifuged at 10,700 g for 8 min and the supernatant was transferred to glass vials and an equal volume of 0.05 % TFA (aq.) was added.

The subsequent RP-HPLC analysis was performed as described in section 4.2.3 (cf. conditions of the recovery analysis) immediately, or after a storage period ≤ 24 h at -78 °C. The free filtratable fractions were determined by comparison of peak areas to the respective areas of not ultra-filtrated samples prepared in PBS without BSA by an otherwise identical procedure.

3.2.5 Chemosensitivity assay

The assay was performed as described previously (Bernhardt et al., 1992). In brief: tumor cells were seeded into flat-bottomed 96-well plates (Greiner) at a density of 10 - 15 cells per microscopic field (magnification: 320-fold). After an incubation period of 48 - 72 h at 37 °C/5 % CO_2, the medium was replaced by fresh culture medium containing the test compounds at various concentrations. Growth of untreated cells (respective solvent of the test compound in a dilution of 1:1000) served as control. After different incubation periods, growth was stopped by fixation with glutardialdehyde. The mass of viable cells was determined by simultaneous staining of all plates with 0.02 % aqueous crystal violet (Serva, Heidelberg, Germany) solution. After removal of excess dye with water, cell-bound crystal violet was re-dissolved with 70 % ethanol under agitation for 2 - 3 h. Absorbance was measured at 578 nm (BioTek 309 Autoreader, Tecnomara, Fernwald, Germany) or at 580 nm (GENios Pro microplate reader, Tecan Deutschland GmbH, Crailsheim, Germany), respectively.

The effects of test compounds on the investigated cells were expressed as corrected T/C values according to

$$\frac{T}{C}corr\ (\%) = \frac{T - C_0}{C - C_0} \cdot 100 \qquad \text{(equation 1)}$$

where T is the mean absorbance of treated cells, C the mean absorbance of controls and C_0 the mean absorbance at the time when test compounds were added (t = 0).

If the absorbance of treated cells T was less than the absorbance at t = 0 (cytocidal drug effect), the extent of killed cells was calculated as

$$cytocidal\ effect\ (\%) = \frac{C_0 - T}{C_0} \cdot 100 \qquad \text{(equation 2)}$$

3.2.6 Determination of cell membrane integrity

HEL cells were transferred into 8 chamber BD Falcon Culture Slides (BD Biosciences, Heidelberg, Germany) and test compounds were added to the cell culture medium at various concentrations. After different exposure times a mixture of ethidium bromide and acridine orange (50 mg of ethidium bromide and 15 mg of acridine orange dissolved in 50 mL of Millipore water containing 2 % ethanol) was added as 400-fold concentrated

stock solutions to each chamber. Digitonin at a concentration of 0.25 mg/mL served as positive control.

Microscopic images were acquired with a Carl Zeiss Axiovert 200M LSM510 confocal laser-scanning microscope equipped with a Carl Zeiss AxioCam HR. At every investigated concentration, 200 cells were evaluated concerning to their viability (see section 3.3.2.3).

3.2.7 Immunocytochemistry and confocal laser-scanning microscopy

Labeling of α-tubulin was essentially performed as described elsewhere (Gross, 2006). Briefly: Kb-V1 cells were seeded into 8 chamber BD Falcon Culture Slides (BD Biosciences, Heidelberg, Germany). 48 h later, the medium was replaced with culture medium containing the test compounds at various concentrations (prepared by dilution of the 1000-fold concentrated DMSO stock solution).

After an incubation period of 3 h at 37 °C/5 % CO_2, paraformaldehyde solution in PBS was added to achieve a final concentration of 4 % PFA and cells were fixed for 20 min at room temperature. Subsequently, cells were washed three times with 0.5 % BSA in PBS. Permeabilisation of cells was achieved by incubation with PBS containing 0.5 % BSA and 1 % Triton X-100 (Sigma, Munich, Germany) for 10 min, followed by three washing steps with 0.5 % BSA in PBS.

Microtubules were labeled by incubation with the mouse anti-human α-tubulin primary antibody DLN-09992 (Dianova, Hamburg, Germany) for 1 hour followed by 3 washing steps with 0.5 % BSA in PBS. Subsequently, cells were simultaneously treated with Cy5™-conjugated anti-mouse secondary antibody (Dianova) and 1 µM of the nucleic acid staining dye SYTOXGreen® (Molecular Probes, Eugene, OR) for 40 min. The primary and secondary antibodies were used as a 1:200 dilution in PBS, containing 0.5 % BSA. After three washing steps, object slides where dried and embedded in Konfokal-matrix® (Micro Tec Lab, Graz, Austria).

Picture acquisition was performed with a Carl Zeiss Axiovert 200M LSM510 confocal laser-scanning microscope equipped with a Carl Zeiss AxioCam HR. Multifluorescence images were acquired in the multitrack acquisition mode and the following instrument settings: SYTOXGreen®, 488 nm Argon laser, 505 nm longpass filter; Cy5™-conjugated secondary antibody, 633 nm HeNe laser, 650 nm longpass filter.

3.2.8 Inhibition of cytochrome P450 isoenzymes

3.2.8.1 Preparation of rat liver microsomes

In order to isolate rodent microsomes, male CD rats were killed by cervical dislocation, livers were excised and immediately placed on ice. After dissection with scissors, tissue was transferred to a Potter-Elvehjem homogenizer tube. Homogenization was performed in 0.15 M phosphate buffer (pH 7.4) under ice cooling by 25 heaves at 100 RPM. After 5 heaves, a break of 30 seconds allowed the tube to cool down. Subsequently, a first centrifugation was performed for 30 min at 9000 g (4 °C). The supernatant was removed and centrifuged for 1 hour at 105,000 g (4 °C). The resulting microsome pellet was suspended in 83 mM phosphate buffer (pH 7.4) containing 17 mM KCl and stored at -78 °C.

The amount of microsomal protein in the respective samples was determined according to the method of Bradford (1976). 95 µL of Millipore water were added to 5 µL of the various dilutions of the microsome suspension (in 0.1 M Tris buffer, pH 7.4) and incubated with 1000 µL of Bradford´s dye reagent (Bio Rad Laboratories, Munich, Germany) for 10 min. Subsequently, the absorbance at 595 nm was measured with an Uvikon 930 spectrophotometer (Kontron, Düsseldorf, Germany). The protein concentrations were calculated from a standard calibration curve of bovine serum albumin (Serva, Heidelberg, Germany) in the range of 1 - 12 µg protein per sample.

3.2.8.2 CYP3A4 and CYP2C8 inhibition assay using bioluminescence based methods

10 µL of the respective inhibitor (1:100 dilution in Millipore filtered water) or Millipore water containing 1 % DMSO (for the background control) were pipetted into white Lumitrac 200 96-well plates (Greiner Bio-One, Frickenhausen, Germany). As positive controls for CYP3A4 inhibition, 25 µM terfenadine (Decker et al., 1998), for CYP2C8 inhibition 25 µM trimethoprim (Wen et al., 2002), respectively, were used. Afterwards, 10 µL of ice-cold 0.1 mM Tris buffer (pH 7.4) containing 6.7 µg microsomal protein (or 1 pM CYP2C8) and 100 µM luciferin-PPXE (CYP3A4) or 600 µM luciferin-ME (CYP2C8) were added (mixture prepared immediately prior to use). In the respective background control wells, heat inactivated (10 min at 100 °C) microsomal protein was used. After careful vortexing, the plate was pre-incubated for 10 min at 37 °C. Subsequently, 20 µL of the two-fold concentrated NADPH regeneration system (Promega, Mannheim, Germany) was added and the plate was incubated at 37 °C for 15 min (luciferin-PPXE) or 35 min (luciferin-ME), respectively. Afterwards, addition of 40 µL of the reconstituted Luciferin Detection Reagent (Promega, Mannheim, Germany) started the luciferase-mediated light emission. After a

stabilization period (20 min in assays using microsomes and 10 min when CYP2C8 bactosomes were utilized), luminescence was determined with a GENios Pro microplate reader (Tecan Deutschland GmbH, Crailsheim, Germany) at 25 °C (1000 ms integration time, no attenuation).

3.3 Results and discussion

3.3.1 Species dependent differences in P-glycoprotein inhibition

3.3.1.1 Induction of P-gp overexpression in murine P388D$_1$ cells and optimization of assay parameters

By analogy with the method used to generate ABCB1 transporter expressing human Kb-V1 cells, murine P388D$_1$ cells were subcultured with increasing concentrations of doxorubicin over a period of approximately 4 months. The increase in functional P-glycoprotein was monitored after different periods of time by means of the calcein-AM efflux assay (see **Figure 3.2**). Total inhibition of transporter function was achieved by addition of tariquidar at a final concentration of 1 µM. The difference between the geometrical mean values of the fluorescence intensities (GeoMean) of untreated (100 % function) versus tariquidar treated cells corresponds to the amount of functional efflux transporter (cf. also section 5.3.1.7 and Figure 5.10 A).

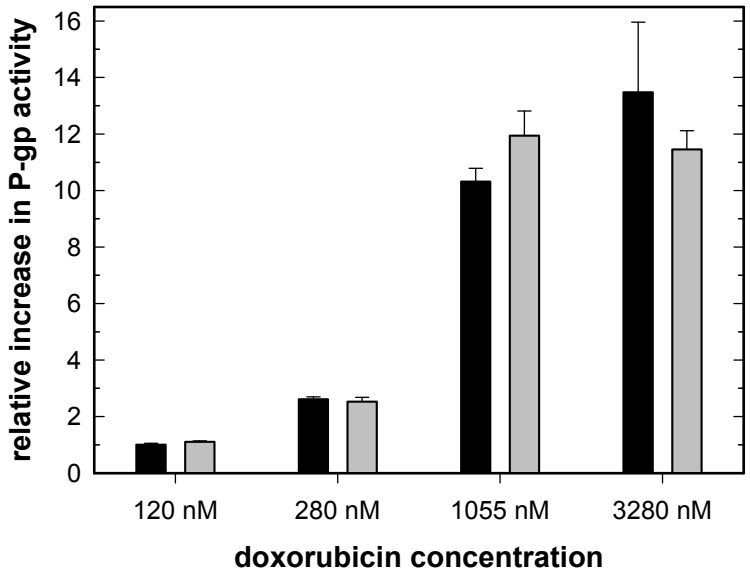

Figure 3.2: Relative increase in P-glycoprotein activity in murine P388D$_1$ cells depending on doxorubicin exposure. The calcein-AM incubation time had no significant influence on the relative activity: 10 min *(black bars)* and 20 min *(grey bars)*. At a concentration of 120 nM doxorubicin, the GeoMean value of the wild type was compared to that of doxorubicin induced cells (mean values ± SEM, n = 2 - 4).

The activity of P-glycoprotein did not increase significantly at concentrations higher than 1 µM. Additionally, an approximately 11-fold increase (at a doxorubicin concentration of

1,055 nM) in the signal ratio of positive control and background is by far sufficient for the performance of inhibition studies. Consequently, the characterization of modulators was performed with cells propagated in the presence of 1.25 µM doxorubicin.

Since a different cell line was utilized, it was investigated if assay parameters such as incubation time or temperature of calcein-AM had to be adopted. Fortunately, this was unnecessary (data not shown). Nevertheless, the calcein-AM concentration was slightly reduced to 0.75 µM (1 µM with Kb-V1 cells), since at this concentration the observed shift of the GeoMean value was also sufficient for the planned investigations. Additionally, the number of gated events in each measurement was reduced to 20,000 (30,000 with Kb-V1 cells) to increase the throughput of the assay. All other factors that could influence the results of the assay were kept constant for reasons of comparability.

3.3.1.2 Inhibitory activity of ABCB1 modulators on the murine transporter

The inhibitory activity of selected modulators on the murine transporter was determined with the newly established calcein-AM efflux assay at the flow cytometer. Determination of calcein-mediated cellular fluorescence revealed that P388D$_1$Doxo cells responded in a concentration-dependent manner. This allowed the construction of sigmoidal concentration response curves (see **Figure 3.3**) and the calculation of IC_{50}-values. All investigated modulators, except for ME27-4 (IC_{50}: 199 nM), were active in the double-digit nanomolar range at the murine transporter.

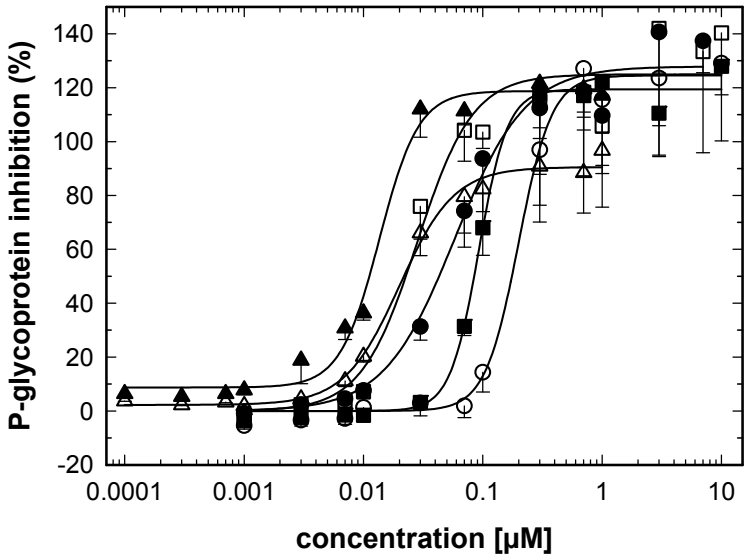

Figure 3.3: Concentration response curves for P-glycoprotein inhibition by the investigated modulators in the calcein-AM assay on P388D$_1$Doxo cells: elacridar *(open triangles)*, tariquidar *(filled triangles)*, ME33-1 *(open squares)*, ME30-1 *(filled squares)*, ME27-4 *(open circles)* and valspodar *(filled circles)*; mean values ± SEM, n = 3

The obtained data were compared with results of the calcein-AM efflux assay performed with human Kb-V1 cells (see **Table 3.1** and **Figure 3.4**). At the murine cells, all investigated compounds were more potent compared to human Kb-V1 cells. Whereas the

ratio of IC_{50}-values ranged from 8 to 16 in the case of elacridar and the tariquidar (analogs), valspodar was 46 times more active on the murine transporter.

Table 3.1: Comparison of P-glycoprotein inhibition (IC_{50}-values and maximal effects) of the selected modulators in the calcein-AM assay on human Kb-V1 and murine $P388D_1$Doxo cells

P-gp modulator	Human Kb-V1 cells		Murine $P388D_1$Doxo cells		IC_{50}-ratio[a]
	IC_{50} [nM][a]	E_{max} (%)[a]	IC_{50} [nM][a]	E_{max} (%)[a]	Kb-V1/ $P388D_1$Doxo
Elacridar	193 ± 24	106 ± 6	20 ± 2	91 ± 2	9.7 ± 2.2
Tariquidar	223 ± 8	103 ± 2	14 ± 1	119 ± 3	15.9 ± 1.7
ME33-1	256 ± 14	121 ± 3	28 ± 6	125 ± 5	9.1 ± 2.5
ME30-1	798 ± 42	120 ± 4	93 ± 4	119 ± 2	8.6 ± 0.8
ME27-4	1775 ± 155	120 ± 6	199 ± 15	125 ± 3	8.9 ± 1.0
Valspodar	2648 ± 331	113 ± 9	58 ± 9	128 ± 5	45.7 ± 13.0

[a] Mean values ± SEM, n = 3

Figure 3.4 visualizes the higher relative activity of valspodar at the murine transporter compared to the third generation modulators. These compounds (all with a similar chemical structure; cf. Figures 2.1 and 7.4) showed nearly the same increase in affinity at the murine compared to the human transporter. This can be explained with the experimental set-up using a different cell type or by species differences in the affinity of P-glycoprotein. In particular the significantly higher relative activity of valspodar is most plausible explained by the latter. It can be speculated that valspodar occupies a binding site different from that of the structurally very similar tariquidar analogs (cf. section 7.4).

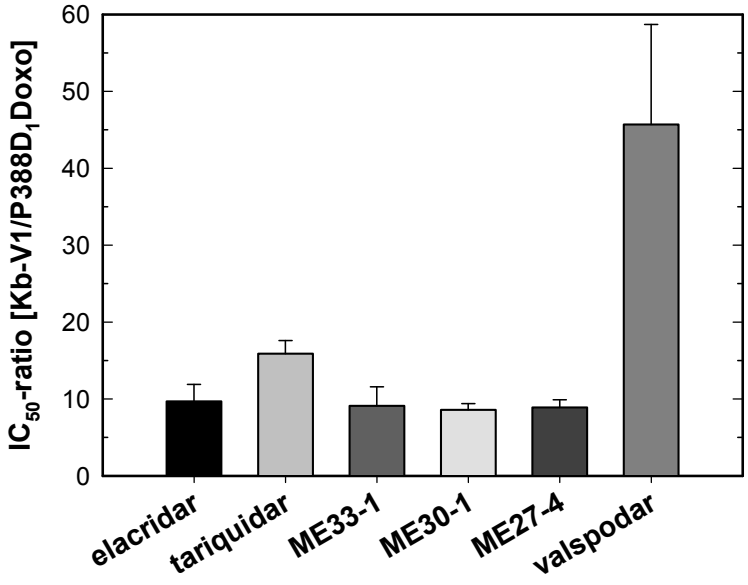

Figure 3.4: Ratios of IC_{50}-values obtained with human Kb-V1 cells versus murine $P388D_1$Doxo cells are depicted (mean values ± SEM, n = 3).

The cell line dependent shift in the concentration response curves of valspodar is shown in **Figure 3.5**. The higher activity in P388D$_1$Doxo cells becomes obvious.

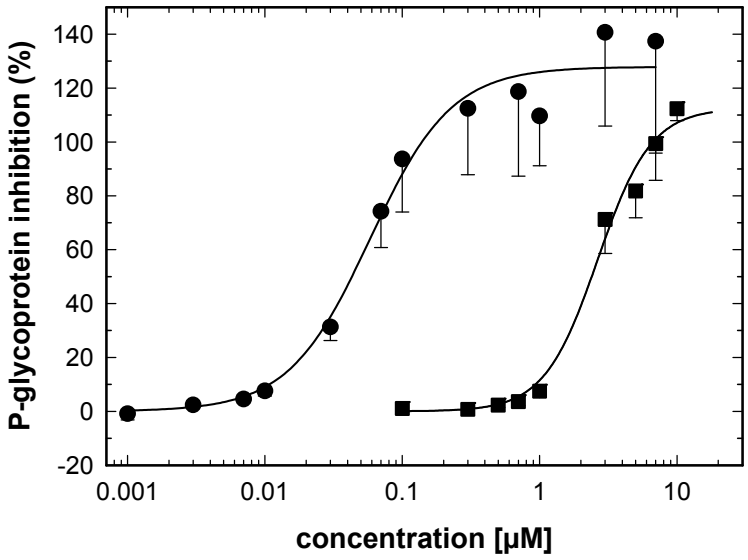

Figure 3.5: Concentration response curves for P-glycoprotein inhibition by valspodar in the calcein-AM assay on human Kb-V1 *(squares)* and murine P388D$_1$Doxo cells *(circles)*; at the murine transporter, valspodar was 46 times more potent (mean values ± SEM, n = 3).

The results suggest that the previously reported (Fellner et al., 2002; Hubensack et al., 2008) discrepancies between the in vitro potency and the activity in nude mice reflect, at least in part, species differences in the affinities of modulators to P-gp. Consequently, the cellular models presented in this work should be of predictive value for the activity of P-glycoprotein modulators in further preclinical in vivo studies (see chapters 4, 5 and 6).

3.3.2 In vitro characterization of tariquidar-like ABCB1 modulators

With regard to future in vivo studies, the most promising new tariquidar-like ABCB1 modulators ME27-4, ME30-1 and ME33-1 (see Figure 2.1) were selected and further characterized in vitro.

3.3.2.1 Binding to serum albumin

In order to estimate the fraction of modulators bound to serum albumin, ME27-4, ME30-1, ME33-1 and tariquidar were incubated with PBS containing 40 mg/mL BSA. Subsequently, the amounts of modulators found after ultra-filtration (free filtratable fraction, FFF) were determined (see **Figure 3.6**).

As expected, the adsorption to albumin correlated with the lipophilicity of the compounds. Nevertheless, it has to be kept in mind that the lipophilicity also influences the adsorption to boundary surfaces such as the filter membrane. When the ultra-filtrate of compounds incubated in BSA-free PBS was investigated, the determined FFF of the various modulators was ≤ 35 % (data not shown). Since the presence of BSA (in the previously

described experiment) could in turn have reduced the adsorption to the filter membrane (and vessel material) it is complicated to discriminate between adsorption to albumin and boundary surfaces.

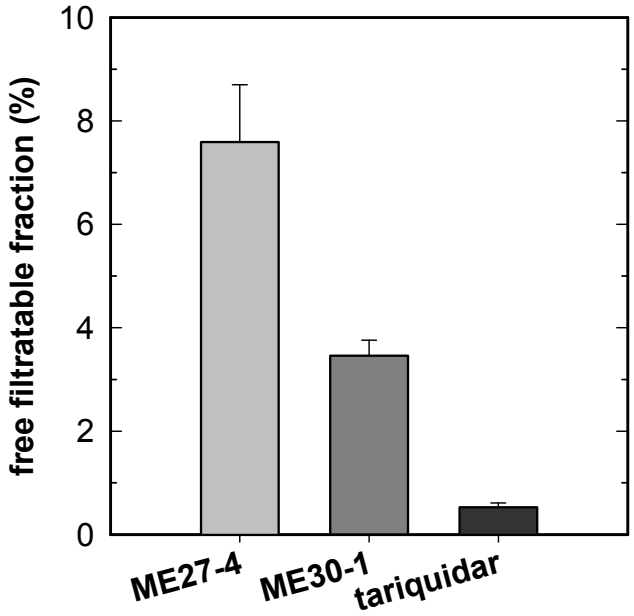

Figure 3.6: Percental amounts of the various modulators found in the ultra-filtrate; the FFF of ME33-1 could not be determined due to an interfering peak (a compound most likely eluted from the filter membrane). Mean values ± SEM, n = 3

Nevertheless, the percental amount of ABCB1 modulators not bound to serum albumin has to be considerably higher than the determined FFF. Therefore, the serum albumin binding is lower than that observed for many clinically established drugs.

3.3.2.2 Effect on the proliferation of U-118 MG and Kb-V1 cells

Prior to in vivo studies, the toxicity of ME27-4, ME30-1 and ME33-1 on two different cell lines was investigated by means of the crystal violet chemosensitivity assay (see **Figure 3.7** and **Figure 3.8**).

On proliferating human U-118 MG glioblastoma cells solely ME27-4 showed a strong cytocidal effect at a concentration of 10 µM. At a concentration of 20 µM, the respective compound exerted also a cytocidal effect on quiescent U-373 MG cells (Müller, 2007).

When proliferating Kb-V1 cells were incubated with the new ABCB1 modulators, the three compounds showed a cytotoxic drug action at a concentration of 5 µM. The sensitivity at this high concentration decreased according to the following order: ME27-4 > ME33-1 > ME30-1. The observed effect on cell growth resulted from long-term exposure of the cells to the modulators for several days, whereas the residence time is significantly shorter under in vivo conditions (see chapter 4). Despite this, the suitability of ME27-4 is compromised with respect to therapeutic in vivo studies.

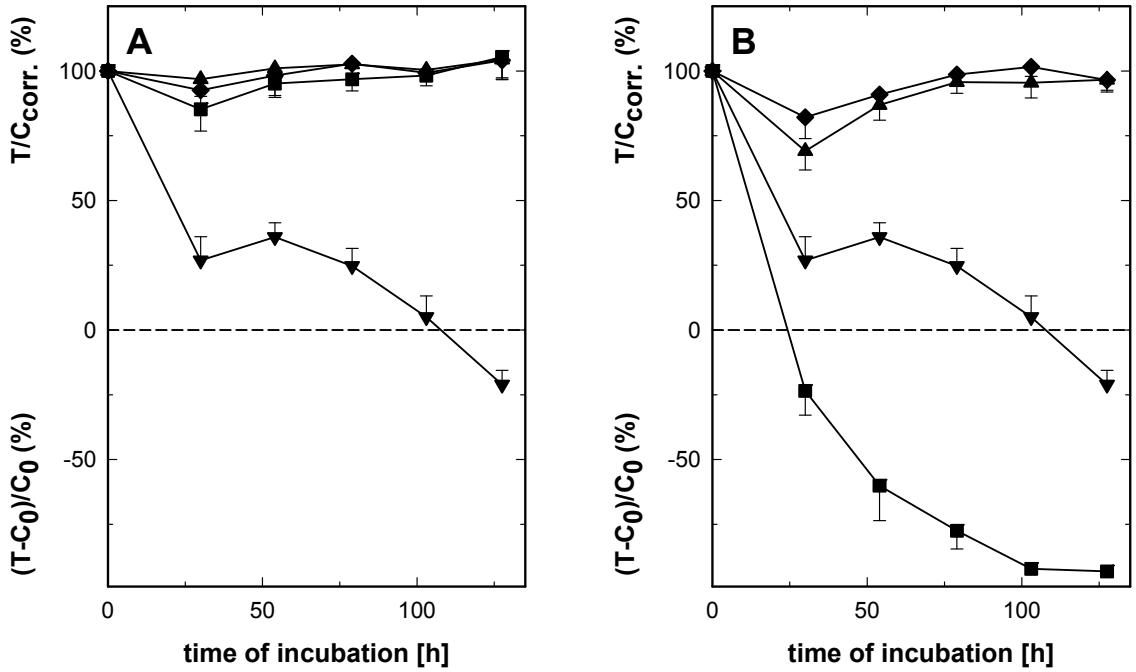

Figure 3.7: Effect of ME27-4 *(squares)*, ME30-1 *(triangles)* and ME33-1 *(diamonds)* on proliferating U-118 MG cells (passage 481) upon long-term exposure; positive control: 30 nM paclitaxel *(inverted triangles)*; investigated concentrations of the ABCB1 modulators: **A)** 1 µM, **B)** 10 µM

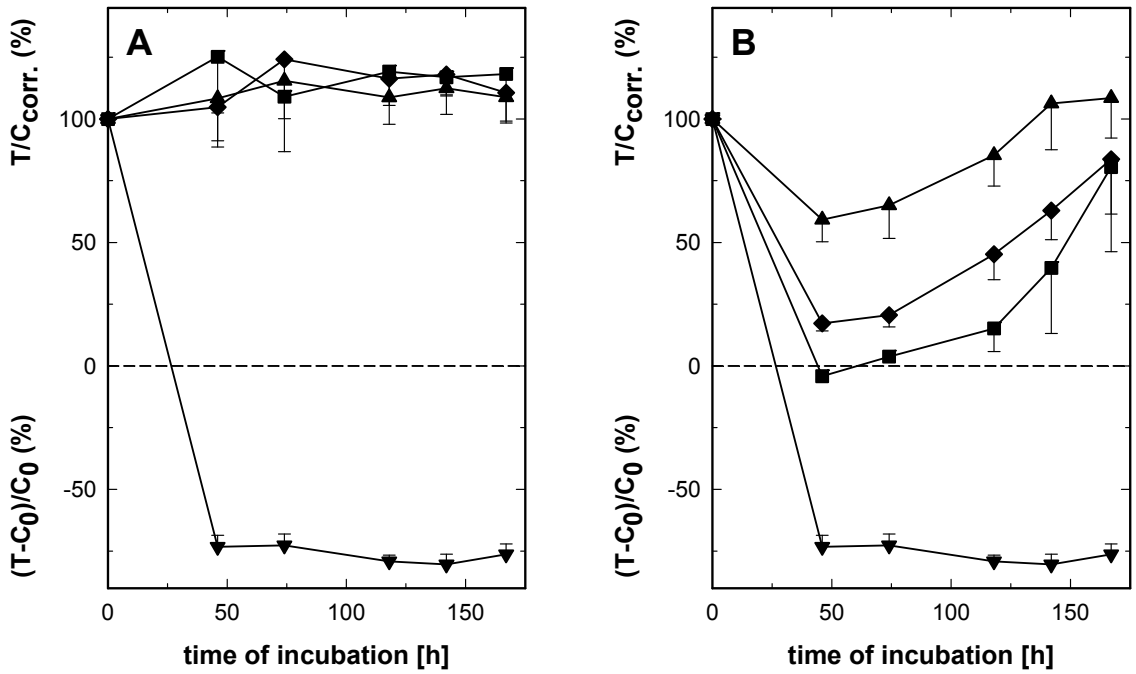

Figure 3.8: Effect of ME27-4 *(squares)*, ME30-1 *(triangles)* and ME33-1 *(diamonds)* on proliferating Kb-V1 cells (passage 49) upon long-term exposure; positive control: 1 µM vinblastine *(inverted triangles)*; investigated concentrations of the ABCB1 modulators: **A)** 1 µM **B)** 5 µM

3.3.2.3 Effect of ME27-4 and tariquidar on the integrity of the cell membrane

A potentially harmful effect of the ABCB1 modulators on the integrity of the cell membrane is detectable by this method, since the used fluorescent dyes differ with regard to their membrane permeability. In contrast to ethidium bromide, acridine orange is cell-permeable and viable cells with normal membrane function show a green color. If compounds increase permeability or damage the cell membrane, ethidium bromide is able to penetrate into the cell, resulting in a yellow to orange color (of the nuclei) of dead cells.

At a concentration of 20 µM, ME27-4 showed a cytocidal effect on quiescent U-373 MG glioblastoma cells (Müller, 2007). Since this is an indication of unspecific toxicity, ME27-4 and tariquidar (for comparison) were investigated concerning an unspecific effect on the permeability of the cell membrane (see **Table 3.2**). As becomes obvious, the cytotoxicity of ME27-4 is probably not caused by membrane damage, whereas tariquidar showed a pronounced effect on the viability of HEL cells, especially upon long-term incubation at a concentration of 10 µM.

Concentration [µM]	Percentage of dead cells			
	ME27-4		Tariquidar	
	4.5 h	20 h	4.5 h	20 h
0.1	n.d.	1.0	n.d.	3.5
1.0	n.d.	1.5	n.d.	8.5
10	2.5	1.5	11.0	38.0

Table 3.2: Fraction of dead HEL cells after different periods of incubation with ME27-4 or tariquidar[a]

[a] Treatment of cells with 0.25 mg/mL of digitonin resulted in 100 % cell death, whereas the fraction of harmed cells was ≤ 2.5 % upon incubation with the respective solvents.

3.3.2.4 Effect of tariquidar on the tubulin architecture

In order to investigate if a synergistic cytostatic effect of epothilones in combination with the ABCB1 modulators (cf. appendix A) resulted from alteration in microtubule organization, α-tubulin was visualized by immunodetection. These investigations revealed an impact of tariquidar (100 nM) on the cytoskeleton of Kb-V1 cells (see **Figure 3.9**). Since tariquidar alone did not affect the growth of Kb-V1 cells even during long-term incubation and at concentrations up to 500 nM (Hubensack, 2005), the effect on tubulin seems not to correlate with cytotoxicity.

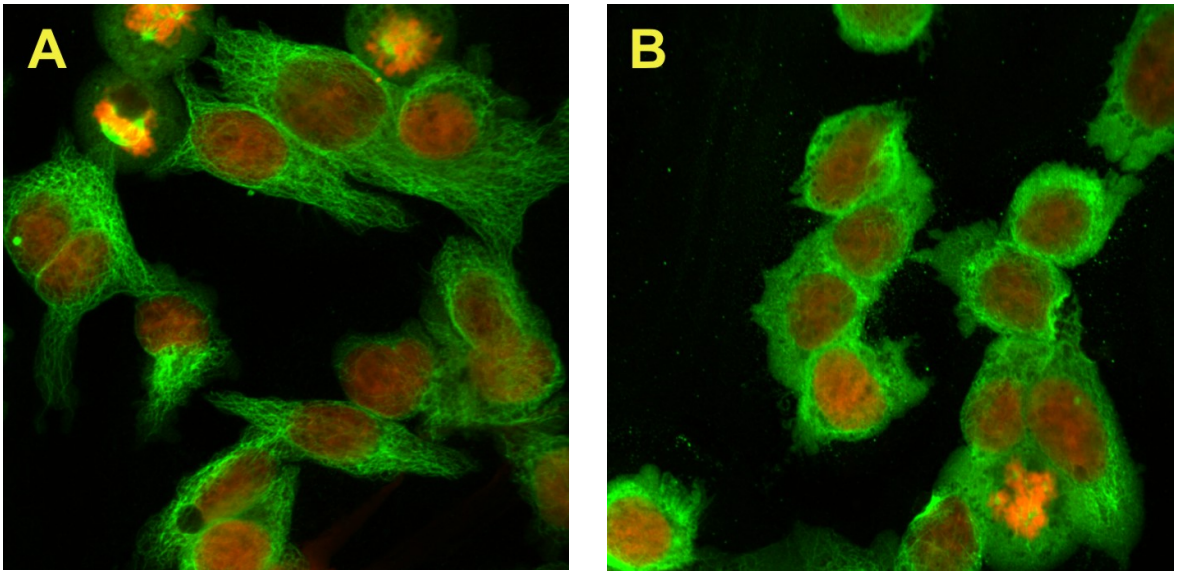

Figure 3.9: Impact of tariquidar on the tubulin architecture of Kb-V1 cells (passage 59); **A)** Untreated cells; **B)** After incubation with 100 nM tariquidar for 3 h; primary AB: mouse anti-human α-tubulin AB (dilution 1:200); secondary AB: Cy5™-conjugated anti mouse AB (dilution 1:200); nuclei were stained with SYTOXGreen®. Microscopic images were acquired with a Carl Zeiss Axiovert 200M LSMM510 confocal laser-scanning microscope.

3.3.2.5 Interaction of the modulators with cytochrome P450 isoenzymes

A further objective was to exclude interactions of the new tariquidar-like modulators with the metabolism of paclitaxel. Since paclitaxel is preferentially metabolized by CYP3A4 and CYP2C8 (Fischer et al., 1998; Jamis-Dow et al., 1995), the investigation of the inhibitory properties of the modulators concentrated on these isoenzymes. For comparison, elacridar and valspodar were included into these investigations.

Figure 3.10 shows the chemical structures of the utilized proluciferin substrates. Whereas luciferin-PPXE is solely metabolized by CYP3A4, -3A5 and -3A7, luciferin-ME is converted by a number of isoenzymes (CYP2C8, CYP1A2, CYP2C9, CYP2J2, CYP4A11, CYP4F3 and CYP19) to luciferin. After addition of luciferase, the emission of light can be measured and correlates with the amount of produced luciferin.

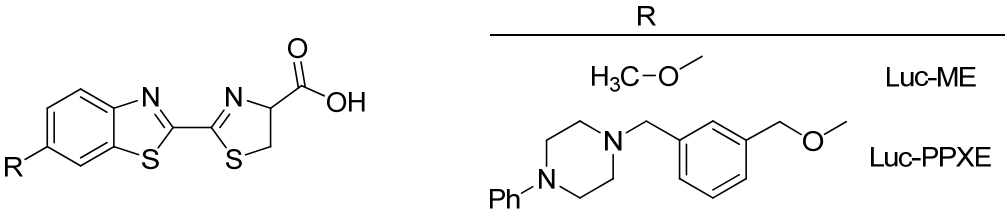

Figure 3.10: Chemical structures of used proluciferin substrates. Selectivity for certain cytochrome P450 isoenzymes is mediated by the residue R.

As part of the assay validation, among other things, the linearity and the stability of the light signal was investigated (see **Figure 3.11**).

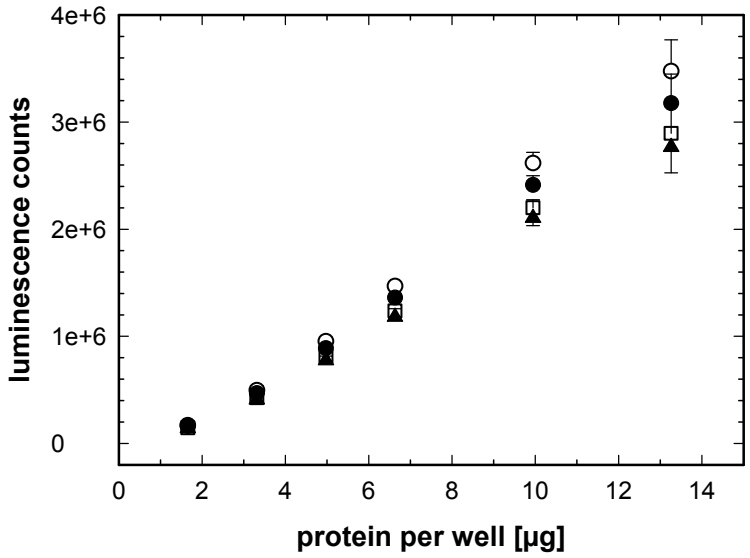

Figure 3.11: Direct correlation of the luminescence signal with the amount of microsomal protein. Time after addition of the enzyme: 14 *(open circles)*, 20 *(filled circles)*, 30 *(open squares)* and 40 min *(filled triangles)*; mean values ± SEM, n = 3

In the following experiments, 6.7 µg protein per well and a stabilization time of 20 min after addition of luciferase enzyme was used.

Figure 3.12 illustrates the impact of the modulators on the activity of CYP3A4, CYP3A5 and CYP3A7. Due to the lacking specificity of the substrate, it cannot be differentiated between effects on individual isoenzymes. At a concentration of 2.5 µM, no investigated modulator significantly inhibited the aforementioned cytochromes. In contrast, at 12.5 µM the various compounds reduced cytochrome P450 mediated generation of luciferin in the range between 20 and 50 %. Due to the comparatively high concentrations and the fact that protein binding is not considered (see section 3.3.2.1), the observed effect should presumably be irrelevant under clinical conditions (cf. also chapter 4).

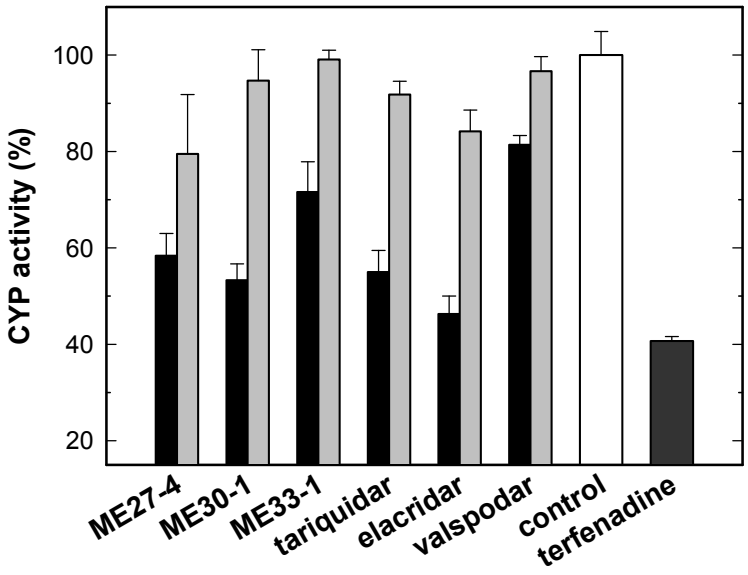

Figure 3.12: Impact of the various compounds at 2.5 µM *(light grey bars)* and 12.5 µM *(black bars)* on the activity of CYP3A4, CYP3A5 and CYP3A7. Luciferin-PPXE mediated luminescence was measured 20 min after addition of the enzyme. The CYP3A4 inhibitor terfenadine (25 µM) served as positive control (mean values ± SEM, n = 3).

Interestingly, in this assay the inhibition of CYP3A4 by valspodar reported in the literature (Fischer et al., 1998) was not observed. Since CYP3A4 is involved in the metabolism of paclitaxel (Jamis-Dow et al., 1995), higher toxicity of the cytostatic (Fellner et al., 2002; Kemper et al., 2003) after co-administration with valspodar is commonly attributed to increased systemic exposure due to the inhibition of cytochrome P450 enzymes (Fox and Bates, 2007). A possible explanation why no CYP3A4 inhibition was observed in the present investigation could be that Luciferin-PPXE is also metabolized by CYP3A5 and CYP3A7. Consequently, selective inhibition of CYP3A4 can hardly be detected, when microsomes are utilized (see below for CYP2C8). Furthermore, it is conceivable that valspodar accumulates in the liver at concentrations above those investigated in this study. In the corresponding assay using luciferin-ME and rat liver microsomes, the generation of luciferin could not be suppressed by 25 µM of the CYP2C8 inhibitor trimethoprim (data not shown). This was attributed to the vast number of isoenzymes capable to convert luciferin-ME. If a compound selectively modulates CYP3A4, the educt is metabolized by other isoenzymes present in the rat liver microsomes and the light intensity is comparable to the untreated control. To circumvent that problem, human CYP3A4 bactosomes were utilized for further investigations. Since preliminary experiments revealed a limited stability of the luminescent signal (data not shown), the stabilization period was reduced to 10 min.

Figure 3.13 shows the effect of the modulators on the activity of human CYP2C8 bactosomes. As becomes obvious, even at a concentration of 2.5 µM all compounds moderately inhibit CYP2C8 activity. Nevertheless, it is important to emphasize the higher significance of CYP3A4 for the metabolism of paclitaxel.

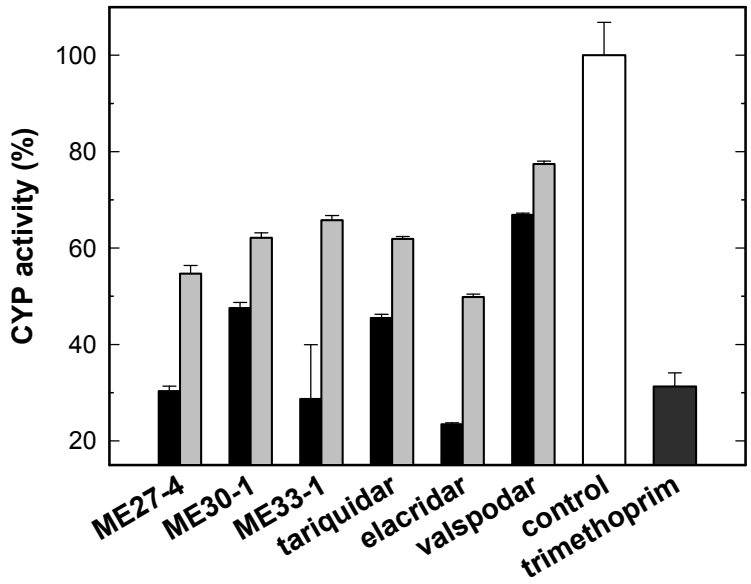

Figure 3.13: Impact of the various compounds at 2.5 µM *(light grey bars)* and 12.5 µM *(black bars)* on the activity of CYP2C8 bactosomes; Luciferin-ME mediated luminescence was measured 10 min after addition of the enzyme. The CYP2C8 inhibitor trimethoprim (25 µM) served as positive control (mean values ± SEM, n = 3).

Investigations on the relevance of the observed modulation of CYP2C8 with respect to pharmacokinetics and toxicity are described in chapter 4 and chapter 5, respectively.

3.3.3 Adaptation of the calcein-AM efflux assay to the microtiter plate format

3.3.3.1 Establishment of assay parameters

3.3.3.1.1 Impact of cell number and calcein-AM concentration

In order to determine the linearity of calcein-AM uptake and to optimize the number of cells per well, Kb-V1 cells were investigated (cf. section 3.2.3.2) at various cell densities (see **Figure 3.14**) in 96-well plates. A first attempt revealed a nonlinear relationship between the number of seeded cells and the relative fluorescence intensity (RFI) especially at higher cell densities.

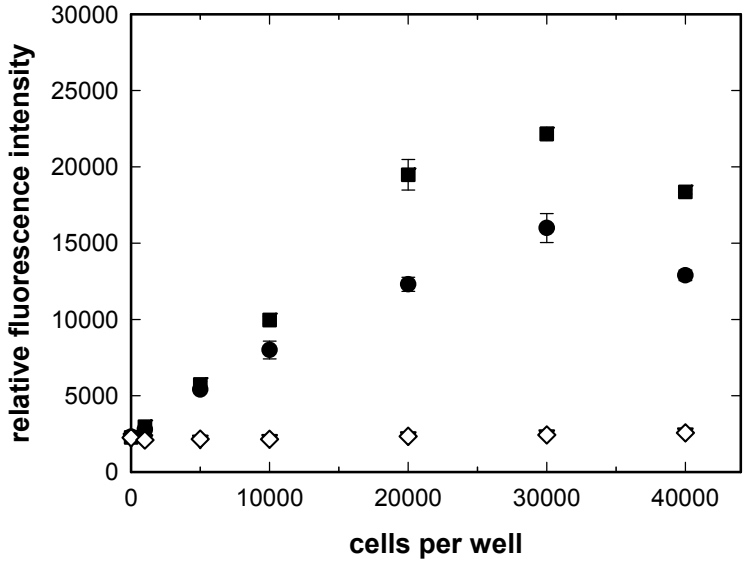

Figure 3.14: Calcein fluorescence without fixation after pre-incubation of Kb-V1 cells with various concentrations of calcein-AM and 1.0 µM tariquidar; calcein-AM combined with tariquidar: 0.5 µM *(filled circles)* and 1.0 µM *(filled squares)*; the fluorescent dye without tariquidar: 0.5 µM *(open inverted triangles) and* 1.0 µM *(open diamonds)*; mean values ± SEM, n = 3

Since the lacking correlation between cell number and RFI was attributed to a loss of cells during the various incubation and washing cycles, a fixation step (4 % PFA in PBS for 20 min) was implemented after the 10 min incubation period with calcein-AM (see **Figure 3.15**). This modification resulted in a linear dye uptake up to 40,000 cells/well. Due to the high activity of ABCB1 transporters in Kb-V1 cells, even a dye concentration of 1.5 µM produced only a slight increase in RFI at higher cell densities. When cells were pre-incubated with the ABCB1 modulator tariquidar, a linear and concentration dependent increase of fluorescence was observed.

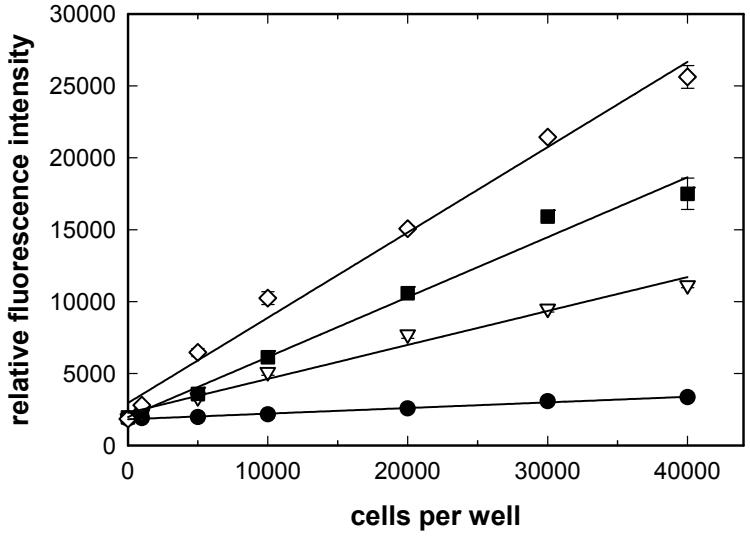

Figure 3.15: Correlation of cell number with fluorescence after fixation of cells with 4 % PFA; combination of tariquidar (1 µM) with calcein-AM at various concentrations: 1.5 µM *(open diamonds)*, 1.0 µM *(filled squares)* and 0.5 µM *(open inverted triangles)*; negative control: 1.5 µM calcein-AM without tariquidar *(filled circles)*; mean values ± SEM, n = 3

3.3.3.1.2 Co-incubation of calcein-AM with the ABCB1 modulator

All previous experiments were carried out with a pre-incubation period (with the modulator) of 15 min as in the calcein-AM assay at the flow cytometer. **Figure 3.16** shows the results of a second approach, in which the modulators were added in combination with calcein-AM. Though the linear increase in the RFI was smaller, the signal-to-noise ratio was by far sufficient for quantitative measurement even at a concentration of 0.5 µM calcein-AM.

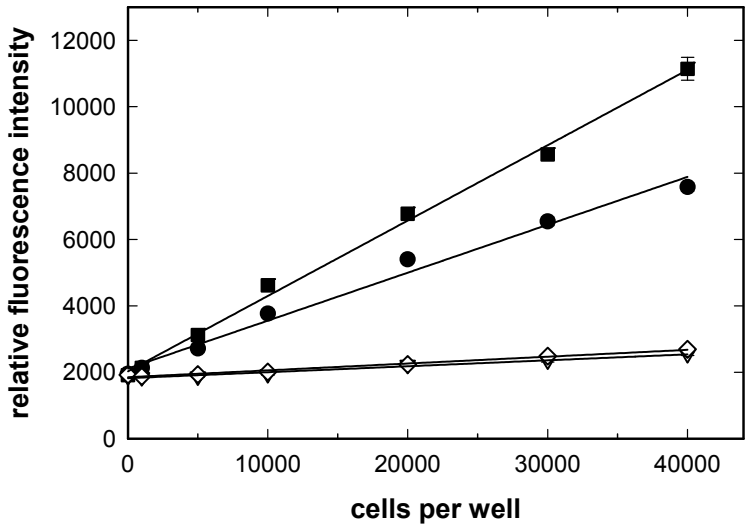

Figure 3.16: Correlation of cell number with fluorescence after co-incubation of Kb-V1 cells with tariquidar (1 µM) and calcein-AM at various concentrations: 1.0 µM *(filled squares) and* 0.5 µM *(filled circles)*; negative controls: 1.0 µM *(open diamonds)* and 0.5 µM *(open inverted triangles)* of calcein-AM without tariquidar (mean values ± SEM, n = 3)

3.3.3.1.3 Normalization of fluorescence intensity by cell mass

Additionally, aiming at further optimization of the calcein assay, fluorescence was normalized by cell mass. For this purpose, the cells in 96-well plates were fixed with glutardialdehyde and stained with 0.02 % crystal violet solution (as described in detail in section 3.2.5) after measurement of calcein fluorescence. **Figure 3.17 A** shows the correlation of cell mass with the measured RFI. Compared to Figure 3.16, there is no distinct advantage of counter-staining with crystal violet. This is also true for the constructed concentration response curves (see **Figure 3.17 B** for tariquidar). The calculated IC_{50}-values differed by less than 12 %.

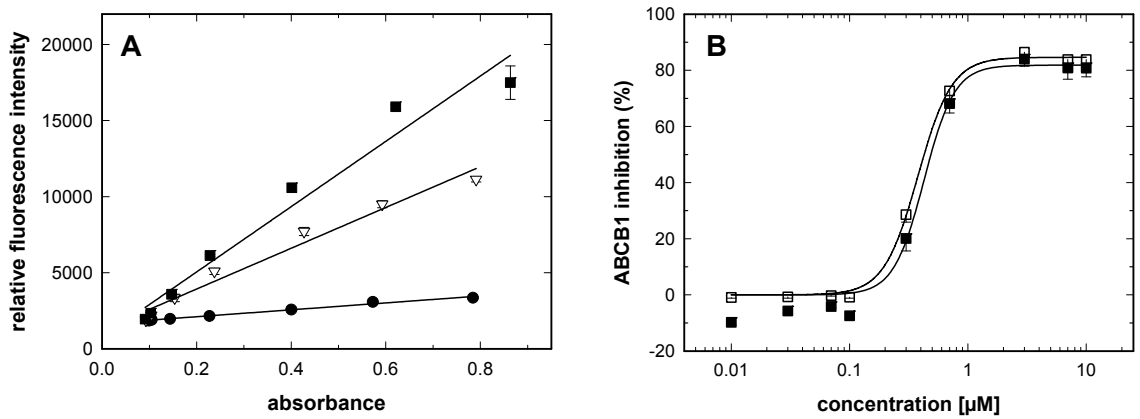

Figure 3.17: A) Correlation of absorbance (cell mass) with fluorescence intensity. 1 µM tariquidar combined with calcein-AM at various concentrations: 1.0 µM *(filled squares)* and 0.5 µM *(open inverted triangles)*; calcein-AM at a concentration of 1.5 µM without tariquidar *(filled circles)*; **B)** Concentration response curve of tariquidar with (filled squares) and without (open squares) normalization (mean values ± SEM, n = 3)

In consideration of the aforementioned results, the assay was performed after seeding of 20,000 cells/well. Modulators were investigated by co-incubation with 0.5 µM calcein-AM and after cell fixation with 4 % PFA solution (as described in section 3.2.3.2).

Compared to the flow cytometric characterization of a test compound (in triplicates), the required number of cells could be lowered from 48 to approximately 1 million. Moreover, the amount of test compounds, calcein-AM and the expenditure of time were reduced by a factor 8, 16 and 6, respectively.

3.3.3.2 Comparison of microplate assay with flow cytometry

Investigation of ABCB1 modulators with the established assay protocol at the microplate reader allowed the construction of sigmoidal concentration response curves (cf. **Figure 3.18**) and the calculation of IC_{50}-values.

It is important to note that the control samples should be placed in the middle of the plate and the solutions of inhibitor/calcein-AM have to be added immediately to avoid any delay critically affecting the results (E_{max}- and IC_{50}-values). This is due to the comparatively short co-incubation period of 10 min and the fact that the intensity of calcein fluorescence correlates with the incubation period which must be carefully kept constant.

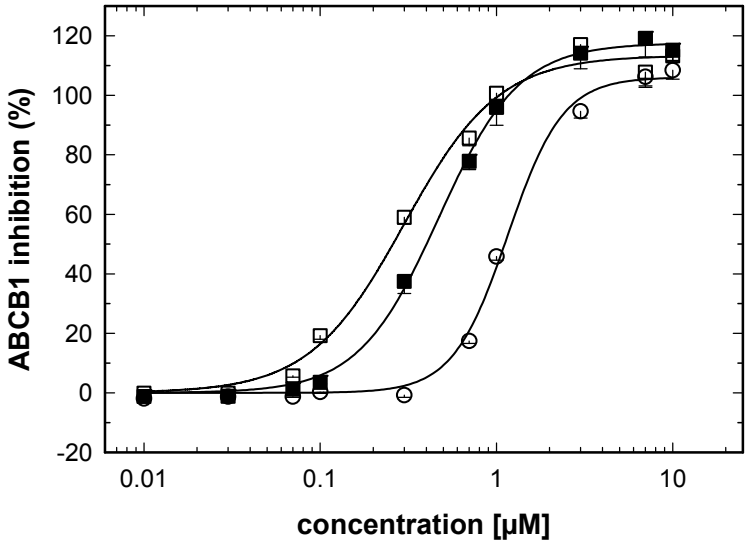

Figure 3.18: Concentration response curves for ABCB1 inhibition determined according to the optimized standard protocol described in section 3.2.3.2; ME27-4 *(open circles)*, ME30-1 *(filled squares)* and ME33-1 *(open squares)*; mean values ± SEM, n = 3

Subsequently, the inhibitory activities of 11 modulators with IC_{50}-values ranging from 0.20 to 12.6 µM as determined at the flow cytometer were investigated in the microplate format. In addition to the most potent inhibitors described in section 3.3.1.2, the previously characterized (Müller, 2007) modulators ME1-2, ME1-3, ME27-2; ME27-3 and ME32 were included in this study. In **Figure 3.19** the results are compared with those from the flow cytometric calcein-AM efflux assay. A strong correlation between data from the two assay types is obvious.

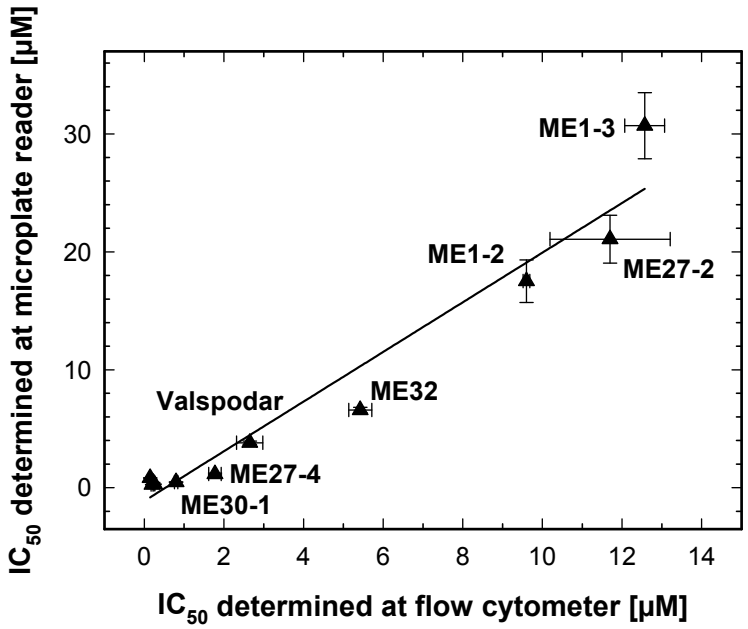

Figure 3.19: Comparison of the two variants of the calcein-AM efflux assay; IC_{50}-values obtained at the flow cytometer are correlated with IC_{50}-values determined at the microplate reader; ME27-3, ME33-1, tariquidar and elacridar show approximately the same affinity and are in the lower left corner (not individually labeled). Mean values ± SEM, n = 3

On average, the IC_{50}-values determined at the microplate reader were 1.82-fold (SEM: ± 0.42) higher. The seemingly lower potency in this assay is attributed to the lack of the

pre-incubation period which allows modulators to accumulate in the membrane bilayer (see chapter 7). By a modified experimental procedure (15 min pre-incubation of the cells with test compounds followed by a 30 min calcein-AM incubation period) at the microplate reader, valspodar, tariquidar and elacridar were investigated (data not shown). Under these conditions, the obtained IC_{50}-values were on the average 4.40-fold (range: 2.81 - 4.55, SEM: ± 0.88) lower compared to the standard assay at the microplate reader. Consequently, the incubation period is a critical parameter that has to be carefully controlled.

3.4 Summary and conclusions

In the present study, the ABCB1 transporter expressing murine P388D$_1$Doxo cells were utilized to establish a cellular model with predictive value for the administration of P-glycoprotein modulators in preclinical in vivo studies. Subsequently, the inhibitory activity of selected modulators at murine P-gp was determined and compared with data from the calcein-AM efflux assay performed with human Kb-V1 cells. These investigations revealed that the ratio of IC_{50}-values ranged from 8 to 16 in the case of elacridar and the tariquidar-type compounds, whereas valspodar was 46 times more active on the murine transporter. Species differences in the affinities to rodent and human (and/or porcine) P-gp were also described for other substrates and modulators such as vinblastine, itraconazole and verapamil (Schwab et al., 2003; Tang-Wai et al., 1995). It has to be considered that there are two different isoforms of P-glycoprotein in mice (Abcb1a and Abcb1b) that have distinct and in part complementary substrate specificities. Since it is unknown which one is prevalent (or if both are expressed) in P388D$_1$Doxo cells, it remains unclear if the observed higher inhibitory activity of valspodar has to be attributed to one distinct subtype. Nevertheless, the significantly higher relative activity of valspodar is in agreement with previously reported discrepancies between the potencies of P-glycoprotein modulators in vitro (human Kb-V1 cells) and in nude mice (Fellner et al., 2002; Hubensack et al., 2008).

In another approach, the established flow cytometric calcein-AM efflux assay was successfully adapted to the microtiter plate format. The newly established assay enormously reduced the amount of materials (e.g. number of cells, test compounds and fluorescent dye) while throughput was substantially increased. Additionally, the assay led to comparable and reliable data when compared to the flow cytometric procedure. Due to the influence of the incubation period on E_{max}- and IC_{50}-values (discussed in section 3.3.3.2), it is recommended to prolong this period to 30 min for the investigation of

future compound libraries. In general, there are further issues that may enormously effect the determination of P-gp modulatory activity. Beside plasma protein binding (presence of BSA) and species-dependent differences (as discussed above), the utilized substrate may affect the inhibition data (Schwab et al., 2003). Such interdependencies have also been reported for other promiscuous macromolecular targets such as the cytochrome P450 enzymes (Korzekwa et al., 1998). Consequently, all above mentioned issues should be kept in mind, when comparing data of modulators from different laboratories.

With respect to intended in vivo studies, in a third series of experiments, the biopharmaceutical properties of the most promising new tariquidar-like modulators ME27-4, ME30-1 and ME33-1 were investigated. During these studies, the compounds were characterized with regard to cytotoxicity, potential pharmacokinetic interactions and drug-like properties. In summary, the results of these investigations identified the new ABCB1 modulators as candidates for further in vivo experiments which are presented in the following chapters.

3.5 References

Abraham, J.; Edgerly, M.; Wilson, R.; Chen, C.; Rutt, A.; Bakke, S., et al. A phase I study of the P-glycoprotein antagonist tariquidar in combination with vinorelbine. *Clin. Cancer Res.* **2009,** 15, 3574-3582.

Bauer, B.; Miller, D. S.; Fricker, G. Compound profiling for P-glycoprotein at the blood-brain barrier using a microplate screening system. *Pharm. Res.* **2003,** 20, 1170-1176.

Bernhardt, G.; Reile, H.; Birnbock, H.; Spruss, T.; Schonenberger, H. Standardized kinetic microassay to quantify differential chemosensitivity on the basis of proliferative activity. *J. Cancer Res. Clin. Oncol.* **1992,** 118, 35-43.

Bradford, M. M. A rapid and sensitive method for the quantitation of microgram quantities of protein utilizing the principle of protein-dye binding. *Anal. Biochem.* **1976,** 72, 248-254.

Bubik, M.; Ott, M.; Mahringer, A.; Fricker, G. Rapid assessment of p-glycoprotein-drug interactions at the blood-brain barrier. *Anal. Biochem.* **2006,** 358, 51-58.

Decker, C. J.; Laitinen, L. M.; Bridson, G. W.; Raybuck, S. A.; Tung, R. D.; Chaturvedi, P. R. Metabolism of amprenavir in liver microsomes: role of CYP3A4 inhibition for drug interactions. *J. Pharm. Sci.* **1998,** 87, 803-807.

Dodic, N.; Dumaitre, B.; Daugan, A.; Pianetti, P. Synthesis and activity against multidrug resistance in Chinese hamster ovary cells of new acridone-4-carboxamides. *J. Med. Chem.* **1995,** 38, 2418-2426.

Egger, M.; Li, X. Q.; Müller, C.; Bernhardt, G.; Buschauer, A.; König, B. Tariquidar analogues: Synthesis by Cu-^{I}-catlyzed N/O-aryl coupling and inhibitory activity against the ABCB1 transporter. *Eur. J. Org. Chem.* **2007**, 2643-2649.

Fellner, S.; Bauer, B.; Miller, D. S.; Schaffrik, M.; Fankhänel, M.; Spruss, T., et al. Transport of paclitaxel (Taxol) across the blood-brain barrier in vitro and in vivo. *J. Clin. Invest.* **2002,** 110, 1309-1318.

Fischer, V.; Rodriguez-Gascon, A.; Heitz, F.; Tynes, R.; Hauck, C.; Cohen, D., et al. The Multidrug Resistance Modulator Valspodar (PSC 833) Is Metabolized by Human Cytochrome P450 3A. Implications for Drug-Drug Interactions and Pharmacological Activity of the Main Metabolite. *Drug Metab. Dispos.* **1998,** 26, 802-811.

Fox, E.; Bates, S. E. Tariquidar (XR9576): a P-glycoprotein drug efflux pump inhibitor. *Expert Rev. Anticancer Ther.* **2007,** 7, 447-459.

Gross, D. New Approaches to the Chemotherapy of Glioblastoma: investigations on doxorubicin nanoparticles, inhibition of PDGF receptors and kinesin Eg5, with emphasis on confocal laser-scanning microscopy. PhD thesis, University of Regensburg, Regensburg, Germany, 2006.

Homolya, L.; Hollo, Z.; Germann, U. A.; Pastan, I.; Gottesman, M. M.; Sarkadi, B. Fluorescent cellular indicators are extruded by the multidrug resistance protein. *J. Biol. Chem.* **1993,** 268, 21493-21496.

Hubensack, M. Approaches to overcome the blood brain barrier in the chemotherapy of primary and secondary brain tumors: modulation of P-glycoprotein 170 and targeting of the transferrin receptor. PhD thesis, University of Regensburg, Regensburg, Germany, 2005.

Hubensack, M.; Müller, C.; Höcherl, P.; Fellner, S.; Spruss, T.; Bernhardt, G., et al. Effect of the ABCB1 modulators elacridar and tariquidar on the distribution of paclitaxel in nude mice. *J. Cancer Res. Clin. Oncol.* **2008,** 134, 597-607.

Jamis-Dow, C. A.; Klecker, R. W.; Katki, A. G.; Collins, J. M. Metabolism of taxol by human and rat liver in vitro: a screen for drug interactions and interspecies differences. *Cancer Chemother. Pharmacol.* **1995,** 36, 107-114.

Kemper, E. M.; van Zandbergen, A. E.; Cleypool, C.; Mos, H. A.; Boogerd, W.; Beijnen, J. H., et al. Increased penetration of paclitaxel into the brain by inhibition of P-Glycoprotein. *Clin. Cancer Res.* **2003,** 9, 2849-2855.

Korzekwa, K. R.; Krishnamachary, N.; Shou, M.; Ogai, A.; Parise, R. A.; Rettie, A. E., et al. Evaluation of atypical cytochrome P450 kinetics with two-substrate models: evidence that multiple substrates can simultaneously bind to cytochrome P450 active sites. *Biochemistry* **1998,** 37, 4137-4147.

Kühnle, M.; Egger, M.; Müller, C.; Mahringer, A.; Bernhardt, G.; Fricker, G., et al. Potent and selective inhibitors of breast cancer resistance protein (ABCG2) derived from the p-glycoprotein (ABCB1) modulator tariquidar. *J. Med. Chem.* **2009,** 52, 1190-1197.

Lee, C. H. Reversing agents for ATP-binding cassette drug transporters. In *Multi-Drug Resistance in Cancer*, Zhou, J., Ed. Humana Press: New York, 2010; pp 325-340.

Müller, C. New approaches to the therapy of glioblastoma: investigations on RNA interference, kinesin Eg5 and ABCB1/ABCG2 inhibition. PhD thesis, University of Regensburg, Regensburg, Germany, 2007.

Müller, C.; Gross, D.; Sarli, V.; Gartner, M.; Giannis, A.; Bernhardt, G., et al. Inhibitors of kinesin Eg5: antiproliferative activity of monastrol analogues against human glioblastoma cells. *Cancer Chemother. Pharmacol.* **2007,** 59, 157-164.

Polli, J. W.; Wring, S. A.; Humphreys, J. E.; Huang, L.; Morgan, J. B.; Webster, L. O., et al. Rational use of in vitro P-glycoprotein assays in drug discovery. *J. Pharmacol. Exp. Ther.* **2001,** 299, 620-628.

Roe, M.; Folkes, A.; Ashworth, P.; Brumwell, J.; Chima, L.; Hunjan, S., et al. Reversal of P-glycoprotein mediated multidrug resistance by novel anthranilamide derivatives. *Bioorg. Med. Chem. Lett.* **1999,** 9, 595-600.

Schwab, D.; Fischer, H.; Tabatabaei, A.; Poli, S.; Huwyler, J. Comparison of in vitro P-glycoprotein screening assays: recommendations for their use in drug discovery. *J. Med. Chem.* **2003,** 46, 1716-1725.

Stewart, A.; Steiner, J.; Mellows, G.; Laguda, B.; Norris, D.; Bevan, P. Phase I Trial of XR9576 in Healthy Volunteers Demonstrates Modulation of P-glycoprotein in CD56+ Lymphocytes after Oral and Intravenous Administration. *Clin. Cancer. Res.* **2000,** 6, 4186-4191.

Szakacs, G.; Varadi, A.; Ozvegy-Laczka, C.; Sarkadi, B. The role of ABC transporters in drug absorption, distribution, metabolism, excretion and toxicity (ADME-Tox). *Drug Discov. Today* **2008,** 13, 379-393.

Tang-Wai, D. F.; Kajiji, S.; DiCapua, F.; de Graaf, D.; Roninson, I. B.; Gros, P. Human (MDR1) and mouse (mdr1, mdr3) P-glycoproteins can be distinguished by their respective drug resistance profiles and sensitivity to modulators. *Biochemistry* **1995,** 34, 32-39.

Wen, X.; Wang, J. S.; Backman, J. T.; Laitila, J.; Neuvonen, P. J. Trimethoprim and sulfamethoxazole are selective inhibitors of CYP2C8 and CYP2C9, respectively. *Drug Metab. Dispos.* **2002,** 30, 631-635.

Chapter 4

4 Tariquidar analogs: quantification by HPLC and impact on the distribution of co-administered paclitaxel in NMRI mice

4.1 Introduction

Paclitaxel (Taxol®) is active against a broad variety of clinically relevant malignancies. According to the guidelines of the National Institute for Health and Clinical Excellence[1] this cytostatic drug is recommended for the first and second line therapy of ovarian cancer, non-small cell lung cancer and advanced breast cancer. In contrast to the indisputable benefit in the treatment of peripheral neoplasms, in the clinics taxol is ineffective against primary and secondary brain tumors (Brandes et al., 2000; Glantz et al., 1999) regardless of the chemosensitivity of such malignant cells in vitro. This is mainly caused by the special location of the tumors in the CNS "behind" the blood-brain barrier (Debinski, 2008). Indeed, 98 % of small molecular drugs (Pardridge, 2007) are not able to cross the BBB due to its special architecture (see section 1.3) and the presence of ATP-driven drug efflux transporters (Glantz et al., 1999; Miller et al., 2000). Among these transporters, P-glycoprotein is the major obstacle for drug delivery to the brain due to the high expression level, the eminent transport capacity and the broad substrate specificity (Miller et al., 2008).

In previous studies with nude mice bearing intracerebral human glioblastomas, the brain levels of paclitaxel, an ABCB1 substrate, were significantly increased when the drug was co-administered with the second generation modulator valspodar (Fellner et al., 2002). Furthermore, the elevated concentration of paclitaxel in the brain caused a reduction of the

[1] www.nice.org.uk

tumor volume by 90 %. However, concomitant administration of valspodar resulted in elevated plasma levels and thereby increased toxic side effects of the cytostatic drug (cf. chapter 2). A plausible explanation for this observation is that paclitaxel is metabolized by the enzymes CYP3A4 and CYP2C8 (Fachinformation Taxol®, (Jamis-Dow et al., 1995)) which are inhibited by valspodar (Fischer et al., 1998). On the other hand, elevated plasma levels could result from impaired drug clearance as P-glycoprotein is also present in the membranes of epithelia lining excretory organs. However, the latter can be ruled out as Kemper et al. (2003) showed that in contrast to valspodar and cyclosporin A, the third generation modulator elacridar did not increase brain or plasma AUCs of paclitaxel in both wild type and Abcb1a/b double-knockout mice. Moreover, experiments with other intravenously administered P-gp substrates and modulators (e.g. digoxin, verapamil, vinblastine etc.) in Abcb1a/b double-knockout mice showed no substantial increase in plasma levels compared to wild type animals (Mizuno et al., 2003).

Subsequent pharmacokinetic studies using the third generation inhibitor tariquidar confirmed these findings and revealed that the plasma levels of co-adminestered paclitaxel were comparable to those achieved by mono-therapy (Hubensack et al., 2008). By contrast, the brain levels of paclitaxel, albeit lower than after co-administration of valspodar, were significantly elevated. The discrepancy between high in vitro potency of tariquidar (by far superior to valspodar) and the in vivo results was attributed to poor drug-like properties such as high lipophilicity (accumulation in adipose tissue) and poor solubility. Consequently, it was hypothesized that more hydrophilic tariquidar-like modulators should have improved pharmacokinetic and pharmacodynamic properties.

In order to investigate this hypothesis, a series of tariquidar like modulators was synthesized (Egger et al., 2007). The three most potent compounds were characterized in vitro (see chapter 3) and, based on these results, selected for in vivo investigations.

One objective of this study was to investigate the bioavailability and distribution of these new modulators. The second objective was to elucidate the potential to increase the concentration of paclitaxel in the CNS to improve brain cancer chemotherapy. Special attention was dedicated to answer the question if these new modulators may be superior to valspodar with respect to systemic toxicity.

4.2 Materials and methods

4.2.1 Drugs and chemicals

The tariquidar-like modulators ME27-4, Me30-1 and ME33-1 were synthesized (Egger et al., 2007) by the workgroup of Prof. König (Institute of Organic Chemistry, University of

Regensburg, Germany). Tariquidar was synthesized in our laboratory according to the literature (Dodic et al., 1995; Roe et al., 1999) with slight modifications (Hubensack, 2005). In order to improve solubility with respect to the in vivo experiments, the modulators were transferred to the TFA salt in a mixture of acetonitril/water (80:20), and the respective solution was freeze-dried subsequently. Drug formulations for in vivo administration (ketamine (Ketanest®, WVD, Garbsen, Germany), xylazine (Rompun®, Bayer, Leverkusen, Germany) and paclitaxel (6 mg/mL; Bristol-Meyers Squibb; Wien, Austria)) as well as pure material (paclitaxel and docetaxel) for HPLC standardization were obtained from the Regensburg University Hospital´s pharmacy. Bovine serum albumin was purchased from Serva (Heidelberg, Germany), CPD (citrate-phosphate-dextrose) plasma from the Bavarian Red Cross (BRK, Regensburg, Germany), respectively. If not stated otherwise, chemicals (p.a. quality) were obtained from Merck (Darmstadt, Germany). Millipore filtered water was used throughout.

4.2.2 Sample preparation

Sample preparation by liquid-liquid and solid-phase extraction was performed according to the method established by Sparreboom et al. (1995) with modifications described in detail previously (Fellner, 2001; Hubensack, 2005). After the elution of paclitaxel and docetaxel, the ABCB1 modulators ME27-4, ME30-1, ME33-1 and tariquidar (internal standard) were rinsed from the SPE columns with 0.8 mL of tetrahydrofuran and processed as described for paclitaxel (Fellner, 2001; Hubensack, 2005). This modification allowed the selective detection of the taxanes and the tariquidar-like modulators extracted according to one sample preparation protocol. The method yielded very clear extracts, containing no interfering substances (see sections 4.3.1 and 4.3.4).

4.2.3 HPLC analysis of ME27-4, ME30-1, ME33-1 and paclitaxel

The samples obtained after SPE were analyzed immediately (paclitaxel brain extracts) or after storage at -78 °C. Subsequent RP-HPLC analysis was performed with a Waters (Eschborn, Germany) system composed of a 600S controller and pump, a Waters degasser, a temperature control module, a 717 plus autosampler and a 2487 UV-detector. A Luna RP-18 (Phenomenex, Aschaffenburg, Germany) analytical column (3 µm, 150 mm x 4.6 mm) thermostatted to 30 °C with a flow rate of 0.8 mL/min was used. 100 µL of the sample were injected while UV-detection was performed at 227 nm for paclitaxel and at 210 nm for the analyzed ABCB1 modulators, respectively. During recovery analysis, the applied gradient was as following: MeCN/0.05 % TFA (aq.): 0 min: 15/85, 19 min: 60/40,

20 min: 95/5, 24.5 min: 95/5, 25 min: 15/85, 38 min: 15/85. For the subsequent in vivo investigations the gradient was slightly modified (0 min: 15/85, 21.1 min: 65/45, 22.5 min: 95/5, 26.5 min: 95/5, 27 min: 15/85, 40 min: 15/85) to optimize paclitaxel analysis without affecting the retention time of tariquidar-like modulators.

For the quantification of plasma and brain samples, at the day of analysis calibration curves were constructed by dilution of the respective stock solutions (paclitaxel and docetaxel in absolute ethanol; tariquidar and its analogs in anhydrous DMSO; stored at -20 °C) with mobile phase (1:100). Depending on the type of tissue, 5 to 6 different concentrations between 50 nM and 10 µM were analyzed. Coefficients of determination for the various analytes and sample types were higher than 0.995 throughout.

The method for paclitaxel analysis was validated previously (Fellner, 2001). Recoveries for paclitaxel ranged from 69 to 85 % (plasma samples) and 50 to 59 % (brain samples), respectively. In the concentration range from 0.13 to 6.67 nmol/g, the method´s accuracy[2] was better than 8 % while precision[3] was not more than 9 % CV.

4.2.4 Recovery of tariquidar-like modulators

By analogy with the protocol for the analysis of paclitaxel, a quantification method for ME27-4, ME30-1 and ME33-1 in plasma and brain samples was set up and validated. To determine the recoveries, human CPD plasma and porcine brain was used instead of the murine tissues. Prior to the extraction routine, 10 µL of the IS (tariquidar, [50 µM]) and the respective analyte ([50 µM], [125 µM] and [250 µM]) were added to 250 µL plasma or 134 mg brain tissue, respectively.

The density of murine plasma was averaged by exact weighting of 1000 µL (n = 5) murine plasma to be 1.048 g/mL. The amount of tissue in the homogenates was 134 mg/mL (determined by Fellner (2001)). Quantification was carried out by calibration curves as described in section 4.2.3.

4.2.5 Pharmacokinetic studies in NMRI mice

The in vivo experiments were performed with slight modifications by analogy with previous studies (Fellner et al., 2002; Hubensack et al., 2008) and are summarized in **Figure 4.1**. In brief: 24 female six- to eight-week-old NMRI mice were used per treatment group providing 4 replicates (n = 4) per time point. All modulators were dissolved in a vehicle composed of

[2] Percental difference between the determined value and the true value (Shah, et al., 1991)
[3] Closeness of replicate determinations of an analyte by an assay expressed as coefficient of variation (CV) (Shah, et al., 1991)

52.5 g cremophor RH40 (Caelo, Hilden, Germany), 15 g Labrafil M2125CS (Gatefosse, Weil am Rhein, Germany), 15 g absolute ethanol, 7.5 g propylene glycol and 0.1 g of D,L-α-tocopherol (Sigma, Munich, Germany) by sonication at 37 °C. A volume of 5 µL per gram of body weight (concentration: 10 mg/mL) was administered by gavage into the stomach. Control animals received the respective amount of vehicle.

After a lag time of 2.5 hours, animals were anesthetized with 30 - 50 µL (depending on the body weight) of a mixture of ketamine/xylazine (3:1) and received 8 mg/kg (5 µL per gram of body weight) paclitaxel by injection via the retrobulbar plexus. Prior to paclitaxel administration, drug solution (6 mg/mL) was diluted with 0.9 % NaCl solution to a concentration of 1.6 mg/mL.

10, 30, 60, 120, 240 and 420 minutes after paclitaxel injection, ketamine/xylazine-anesthetized mice were killed by cardiac puncture, and heparin-plasma as well as brain samples were collected. All samples were immediately stored on ice, and brain tissue was subsequently homogenized in 4 % BSA solution with a Potter-Elvehjem homogenizer. Within 15 minutes after sampling, plasma and brain homogenates were shock-frozen in liquid nitrogen and stored at -78 °C until SPE and RP-HPLC analysis.

Pharmacokinetic parameters were determined by standard non-compartmental analysis. The area under the concentration-time curve (AUC) after intravenous paclitaxel administration was calculated by linear trapezoidal rule from t = 0 min (t_0) to the last quantified concentration. The paclitaxel concentration at t_0 was extrapolated by linear regression (plasma) or designated to be zero (brain), respectively.

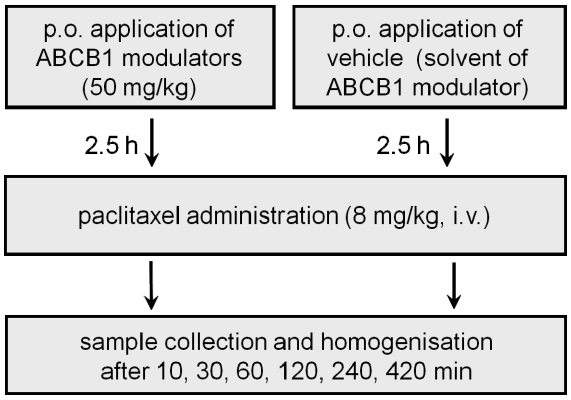

Figure 4.1: Application scheme of the tariquidar-like modulators and paclitaxel to NMRI mice; the treatment experiments with subcutaneously (chapter 5) and intra-cerebrally (chapter 6) growing tumors in nude mice were carried out by analogy (with different concentrations of the modulator and the cytostatic drug; quod vide).

4.3 Results and discussion

4.3.1 Elaboration of the analytical method

By means of the modified extraction procedure it became possible to quantitate paclitaxel and the tariquidar-like modulators using a single extraction routine, followed by a single,

standardized HPLC method. As becomes obvious from **Figure 4.2**, SPE yielded very pure extracts, containing no interfering substances.

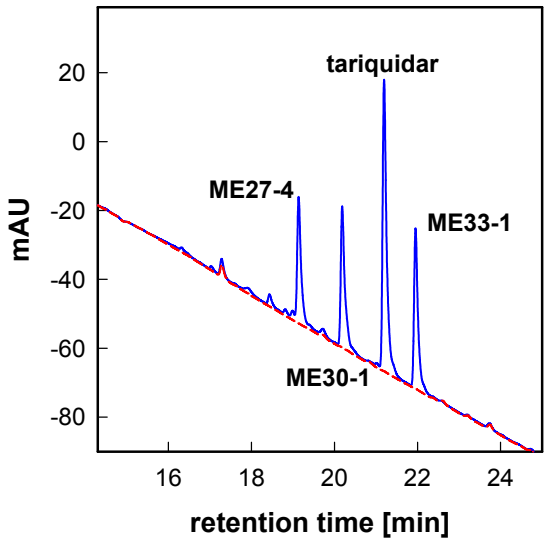

Figure 4.2: Chromatogram of a CPD plasma sample spiked with the tariquidar analogs [1 nmol/mL] obtained after sample preparation with the modified SPE procedure *(blue solid line)*; the respective chromatogram of a blank plasma sample *(red dotted line)* processed by the same method shows no interfering peaks originating from plasma constituents. HPLC conditions: Luna RP-18 (3 µm, 150 mm x 4.6 mm); gradient mode: MeCN/0.05 % TFA (aq.): 0 min: 15/85, 19 min: 60/40, 20 min: 95/5, 24.5 min: 95/5, 25 min: 15/85, 38 min: 15/85; flow: 0.8 mL/min; UV-detection at 210 nm; 30 °C

A major problem of the tariquidar-like compounds was the high affinity to boundary surfaces. This property was responsible for low recoveries at the beginning of the investigations and impeded precise quantification. **Figure 4.3** shows that the adsorption to vessel material could be effectively prevented by siliconization. Consequently, for subsequent analysis, solely siliconized glass vials were used for the construction of calibration curves.

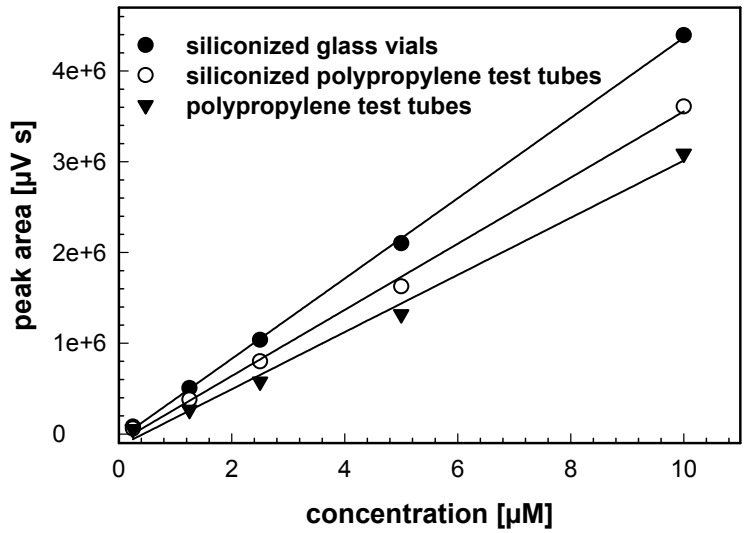

Figure 4.3: Influence of vessel material on the slope of a calibration curve for ME33-1; adsorption of the analyte to the surface is responsible for the outcome. The same effect was observed for tariquidar and the other modulators (data not shown).

4.3.2 Specificity of the separation method

A specific detection of the various analytes is fundamental for accurate quantification. To guarantee sufficient separation of the internal standard from the respective analyte, resolution[4] was determined at different concentrations of the modulators (see **Figure 4.4**). In general, baseline separation is defined as a resolution ≥ 1.5 (provided that peaks are symmetrical and areas comparable) (Rücker et al., 2008). The obtained data demonstrate that the established HPLC method is by far sufficient for specific analyte detection in the investigated concentration range.

Table 4.1: Resolution of internal standard [2.5 µM] and the different analytes at various concentrations[a]

Concentration [µM]	Resolution		
	ME27-4	ME30-1	ME33-1
0.25	13.47	6.10	4.91
2.5	13.28	6.46	4.79
10.0	13.22	7.20	5.51

[a] HPLC conditions as described in section 4.2.3

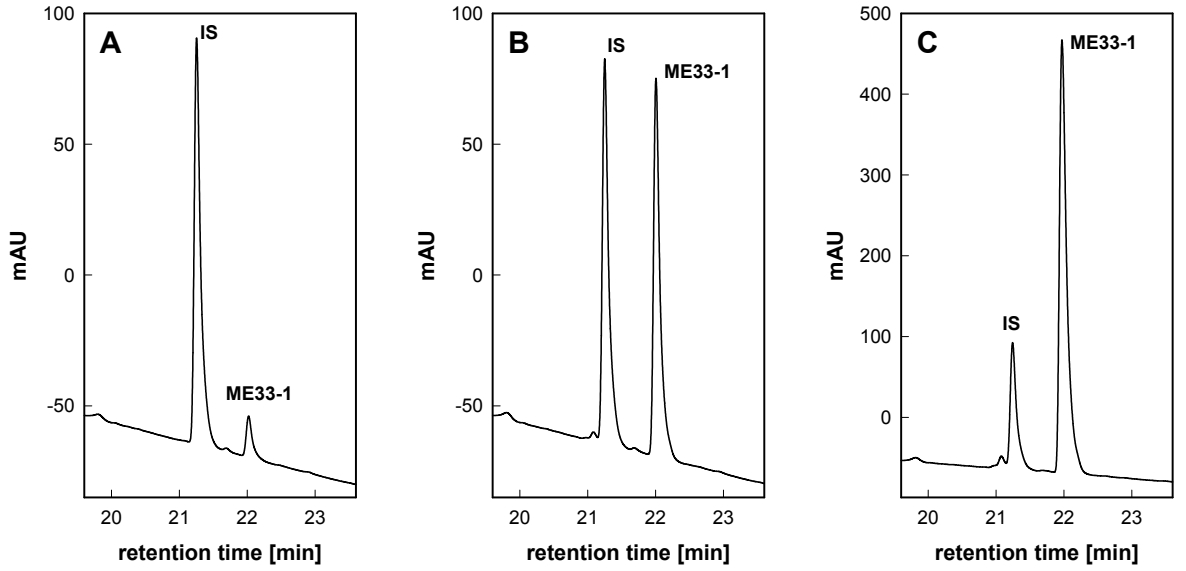

Figure 4.4: Chromatograms of the internal standard (IS) [2.5 µM] and ME33-1 (analyte with the lowest resolution to the IS at various concentrations: **A)** 0.25 µM, **B)** 2.5 µM and **C)** 10 µM; HPLC conditions as described in section 4.2.3 for the in vivo investigations

To exclude undesired matrix effects, samples obtained by SPE of CPD plasma spiked with ME27-4, ME30-1 and ME33-1 were also analyzed (cf. **Table 4.2**). Since the extraction

[4] The resolution as well as the modified signal-to-noise ratio (see section 4.3.4) was determined according to European Pharmacopoeia (Ph. Eur., 6th Edition, 2008), section 2.2.46.

routine had no influence on the quality of resolution, only a medium concentration of every modulator was investigated.

Modulator	Resolution	CV (%)
ME27-4	13.51	0.96
ME30-1	6.55	0.53
ME33-1	4.79	1.57

Table 4.2: Resolution of the IS [2 µM] and the different analytes [5 µM] after SPE[a]

[a] HPLC conditions as described in section 4.2.3 for the in vivo investigations, n = 3

4.3.3 Linearity and quantification range

The linearity of the detector signal was verified for all analytes in the concentration range between 30 nM and 10 µM. **Figure 4.5** shows the result for ME30-1 and illustrates that the instrumental setup is adequate to determine the anticipated very low concentrations in the brain as well as high peak plasma levels.

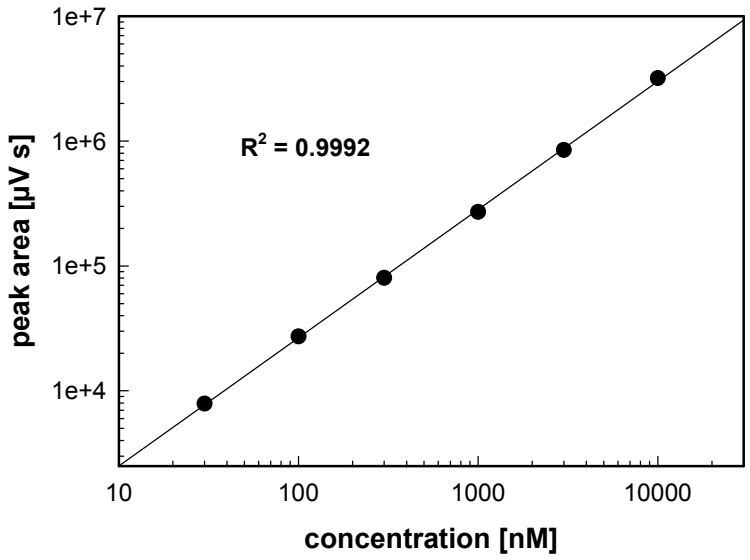

Figure 4.5: Linearity of the detector signal for ME30-1 in the concentration range between 30 nM and 10 µM (injection volume 100 µL); for all other analytes the coefficient of determination was > 0.9999 (data not shown). HPLC conditions as described in section 4.2.3

4.3.4 Limit of quantification

To estimate the lowest concentration to be reliably quantified, ME27-4, ME30-1 and ME33-1 were analyzed at various concentrations. Since the “noise” of the given analytical procedure mainly results from interfering peaks from components of the biological matrix, signal intensities were compared to background signals obtained by SPE of the respective blank tissue (see **Table 4.3** and **Figure 4.6**).

Table 4.3: Ratio of analyte to background signals at various concentrations[a]

Concen -tration [nM]	ME27-4		ME30-1		ME33-1	
	Plasma	Brain	Plasma	Brain	Plasma	Brain
30	-	-	-	-	3.3	3.5
50	11.5	2.8	3.6	2.2	5.3	5.7
100	17.0	5.2	6.9	4.2	10.7	11.3
300	53.0	16.3	19.3	12.0	33.8	35.8
1000	178.0	54.8	63.6	38.9	-	-

[a] HPLC conditions as described in section 4.2.3 for the in vivo investigations

Even at the lowest examined concentrations, peak heights of the modulators exceeded impurity peaks several times. Additionally, for none of the compounds, background signals did interfere (different retention times) with the analyte peaks.

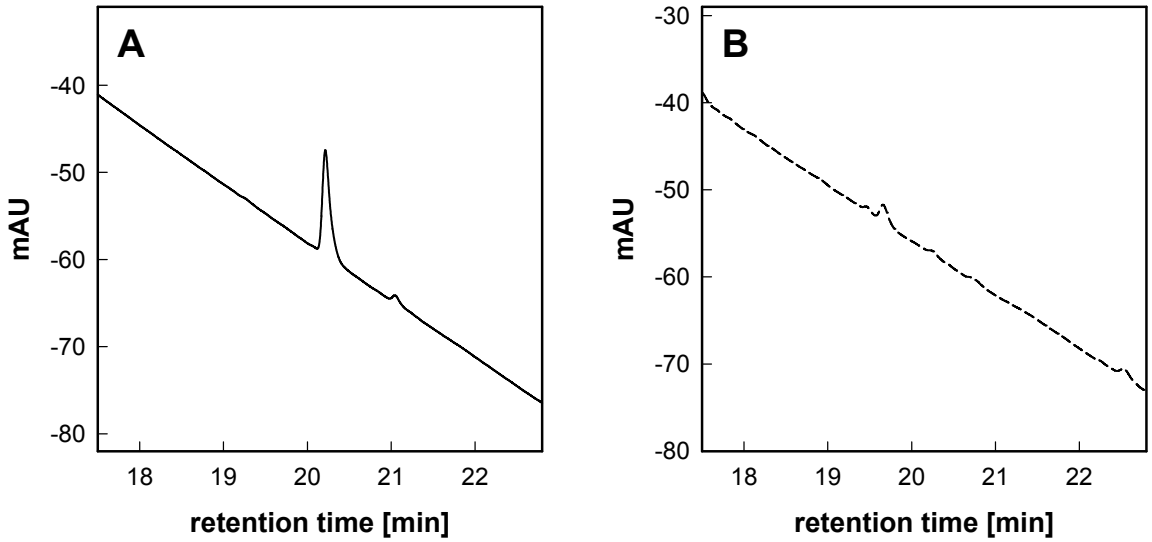

Figure 4.6: Chromatogram of ME30-1 at a concentration of 300 nM **(A)** and the corresponding blank brain sample **(B)**; the analyte to background signal ratio for the selected example is 12. HPLC conditions as described in section 4.2.3 for the in vivo investigations

Taken together, the purity of the SPE samples allows a quantification of the various analytes in the two-digit nanomolar range.

4.3.5 Stability of the analytes in murine plasma and in mobile phase

Due to reasons of feasibility, tissue samples were stored at -78 °C (maximum storage period 14 days) until subsequent SPE. Owing to the same reason, the extracts obtained by SPE were stored under identical conditions for less than 14 days (paclitaxel brain samples

were analyzed immediately after the extraction routine). In order to investigate the influence of the storage on the concentration of the various modulators, spiked plasma samples and analytes in mobile phase were quantified immediately and after a storage period of 14 days. **Table 4.4** summarizes the obtained results.

Modulator	Δ concentration during storage (%)	
	Spiked plasma sample	Analytes in mobile phase
ME27-4	-5.2	+6.5
ME30-1	-7.6	-5.7
ME33-1	-14.0	-15.1

Table 4.4: Mean change of the concentration of the analytes [5 µM] after storage[a]

[a] storage conditions: 14 days at -78 °C, n = 4

The observed concentration differences are tolerable and most likely not caused by degradation of the analytes (no additional peaks in the respective chromatograms). Arguably, the decrease in concentration is caused by adsorption to vessel walls (difference increases with the lipophilicity of the modulators). Moreover, the overall accuracy of the established method has to be considered (see section 4.3.7).

4.3.6 Recoveries

The recoveries of ME27-4, ME30-1 and ME33-1 from plasma and brain samples were determined at various concentrations (see **Table 4.5** for plasma and **Table 4.6** for brain samples, respectively). The same amount of the internal standard (10 µL of a [50 µM] tariquidar solution in DMSO) was added to every sample prior to the extraction procedure.

Table 4.5: Plasma recoveries of ME27-4, ME30-1 and ME33-1 at various concentrations[a]

Modulator	Concentration [µM][b]	Recovery (%)	CV (%)	Recovery ratio (modulator/IS)	CV (%)
ME27-4	1	68.8	6.5	0.974	1.5
	5	81.6	3.2	0.935	3.4
	10	84.6	1.7	0.981	1.2
ME30-1	1	79.8	2.6	1.122	2.8
	5	79.4	2.8	0.925	2.9
	10	75.0	5.2	0.964	1.6
ME33-1	1	79.4	5.4	1.069	2.3
	5	75.1	1.5	0.976	1.3
	10	72.7	2.2	0.932	1.9

[a] Prior to sample preparation 10 µL of the respective analyte (25-fold concentrated stock solution) and 10 µL of tariquidar stock solution (always 50 µM) were added.
[b] For each concentration 5 - 6 samples were analyzed.

The extraction procedure yielded consistently high recoveries in the range of 69 to 85 % for all analytes at the examined concentrations. Even at low concentrations, constant recovery ratios around unity were obtained. That indicates that the modulators as well as tariquidar are extracted to the same extent, enabling a reliable calculation in the subsequent in vivo investigations. Additionally, the precision of the determined recoveries and recovery ratios was considerably high (1.5 to 6.5 % and 1.2 to 3.4 %, respectively).

Table 4.6: Brain recoveries of ME27-4, ME30-1 and ME33-1 at various concentrations[a]

Modulator	Concentration [nM/g][b]	Recovery (%)	CV (%)	Recovery ratio (modulator/IS)	CV (%)
ME27-4	1.87	40.0	14.3	1.018	5.2
	9.24	20.7	19.7	1.007	4.9
	18.66	28.9	14.3	1.142	2.8
ME30-1	1.87	30.2	19.9	1.105	2.9
	9.24	42.7	15.2	1.214	4.3
	18.66	37.0	12.2	1.020	0.7
ME33-1	1.87	54.9	13.3	1.156	3.6
	9.24	50.2	15.8	1.093	2.3
	18.66	47.1	12.5	1.128	9.0

[a] Prior to sample preparation 10 µL of the respective analyte (25-fold concentrated stock solution) and 10 µL of tariquidar stock solution (always 50 µM) were added.
[b] For each concentration 5 - 6 samples were analyzed.

Compared to the results obtained with plasma, the recoveries from brain samples are consistently lower (most probably due to additional (insufficient) diethyl ether extraction). However, the recovery ratios converged to unity and showed high precision between 0.7 and 5.2 %.

4.3.7 Accuracy and precision of the established method

The reliability of the modified SPE method was determined exemplarily for plasma samples spiked with ME30-1. **Table 4.7** shows that the accuracy ranged between 1.5 and 7.0 % while precision was not more than 3.1 % CV.

Table 4.7: Determination of known ME30-1[a] concentrations in plasma samples to revise accuracy and precision[b]

Reference concentration [µM]	Determined concentration [µM]	Accuracy (%)	Precision (%)[c]
1.0	0.93	-7.0	3.1
5.0	4.93	-1.5	1.5
10.0	9.55	-4.5	1.6

[a] Modulator with medium lipophilicity; [b] For each concentration 5 - 6 samples were analyzed.
[c] Precision is expressed as coefficient of variation (CV).

The accuracy of spiked brain samples (ME30-1, 18.7 nmol/g, n = 5) was better than 16.7 %. In general, an accuracy better than 20 % is demanded for quantitative determinations (Shah et al., 1991). The precision (2.5 %) was excellent.

4.3.8 Distribution of tariquidar-like modulators in NMRI mice

Adequate bioavailability and stability of the ABCB1 modulators is a prerequisite for successful tumor pharmacological studies (cf. chapters 5 and 6) on the efficacy of combined cancer chemotherapy. Additionally, the modulators should be devoid of inherent toxicity and should not increase the toxicity of the co-administered anticancer drug (see section 4.3.9). The established and validated method for the quantification of ME27-4, ME30-1 and ME33-1 was utilized to assess the bioavailability and stability of these compounds. The study design as well as the application scheme is described in section 4.2.5.

Figure 4.7 shows the plasma concentration time curves of tariquidar-like modulators. Within the considered period of time, the determined concentrations of the various modulators ranged from approximately 4 to 12 µM and were far above the limit of quantification. The plasma levels of ME30-1 and ME33-1 were 10 to 285 times higher than

the IC_{50}-values obtained in vitro (depending on assay type and used cell line, cf. chapter 3). In the case of ME27-4 this ratio (4 to 35 times) was considerably lower. ME33-1 was the only modulator that showed an increase in plasma levels over the investigation period, possibly due to redistribution from adipose tissue or retarded absorption from the gastro-intestinal tract.

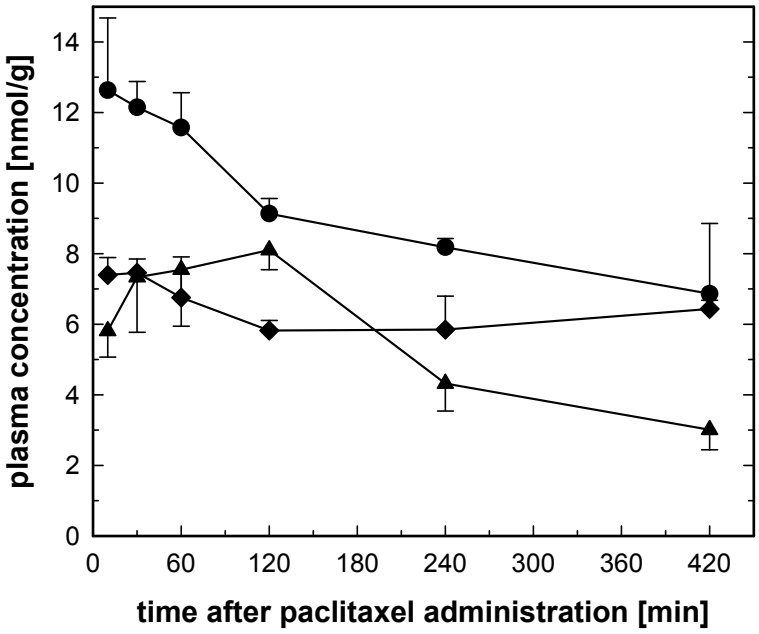

Figure 4.7: Plasma concentrations of the ABCB1 modulators ME27-4 *(circles)*, ME30-1 *(diamonds)* and ME33-1 *(triangles)* in NMRI mice (mean values ± SEM, n = 3 - 4)

The brain concentrations of ME27-4 and ME30-1 (**Figure 4.8**) ranged in the low micromolar level and were remarkably lower than those determined in plasma. By contrast, the brain concentrations of the most lipophilic compound (ME33-1) were significantly higher and with approximately 2.5 to 8.0 µM comparable to those in plasma (**Figure 4.8**).

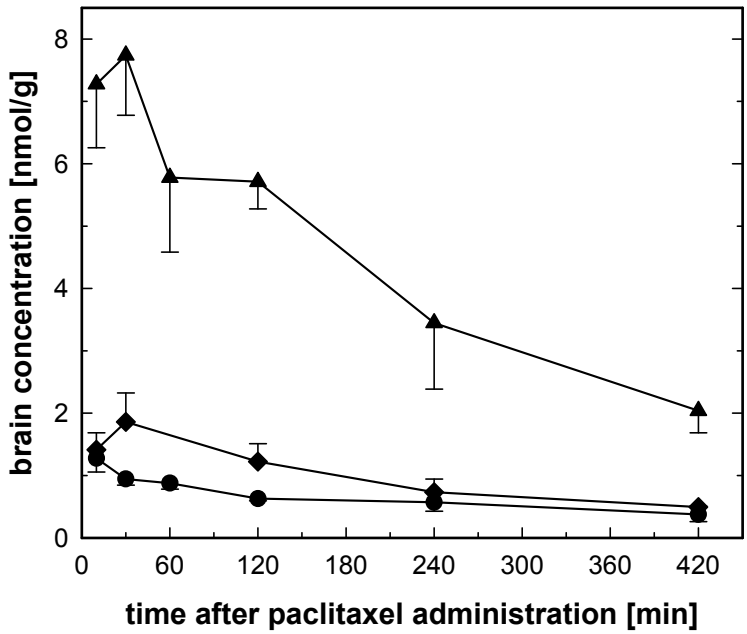

Figure 4.8: Brain concentrations of the ABCB1 modulators ME27-4 *(circles)*, ME30-1 *(diamonds)* and ME33-1 *(triangles)* in NMRI mice (mean values ± SEM, n = 3 - 4)

Taken together, all investigated modulators showed adequate bioavailability and high metabolic stability obvious from the only moderate decrease in concentration over the investigation period. Additionally, no acute intrinsic toxicity of the modulators was observed. Taking the determined concentrations and the differing in vitro potency of the modulators into account, ME30-1 and ME33-1 should be superior to ME27-4.

4.3.9 Effect of tariquidar-like modulators on the distribution of paclitaxel

The second prerequisite for the efficacy of adjuvant brain cancer chemotherapy is the potential of the individual ABCB1 inhibitor to increase the concentration of the cytostatic drug (in our study paclitaxel) in the CNS. In addition, with respect to systemic toxicity, the modulator should not increase the paclitaxel plasma levels. The latter is also an important issue to conclude that elevated CNS levels result exclusively from the inhibition of ABC transporters at the BBB.

The effect of tariquidar-like modulators on the brain levels of co-administered paclitaxel is summarized in **Figure 4.9**. The results correlate with the previously determined in vitro potency. With nearly constant paclitaxel levels of approximately 400 nM over 7 hours, ME33-1 produced the most pronounced effect. ME30-1 induced brain levels between 400 and 150 nM, especially in the first two hours. Unless ME27-4 had the lowest effect on the brain concentration of paclitaxel, the levels were still about 100 % higher than in the control

experiments. It is important to note that against the glioblastoma cells selected for in vivo investigations (U-118 MG and U-87 Luc2 clone 3, cf. chapter 6) a cytocidal effect of paclitaxel was observed at concentrations of 50 nM and 100 nM, respectively (long-term drug exposure). This means that the extent of the increase in brain levels of the anticancer drug was sufficient to achieve the therapeutically relevant concentration.

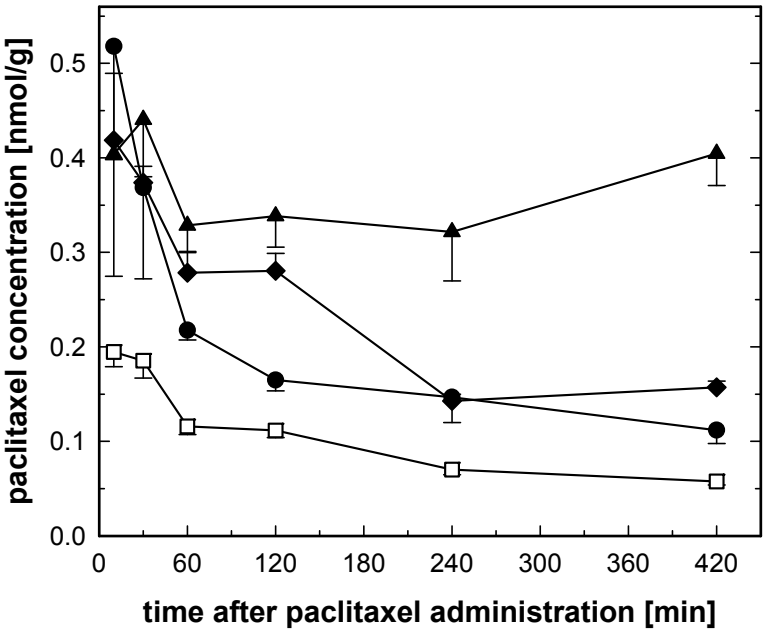

Figure 4.9: Effect of ABCB1 modulator co-administration on paclitaxel levels in the brain of NMRI mice (mean values ± SEM, n = 3 - 4); ME27-4 *(filled circles)*, ME30-1 *(filled diamonds)* and ME33-1 *(filled triangles)* were used as ABCB1 modulators. Untreated mice served as control *(open squares)*.

The determined paclitaxel plasma concentration time curves presented in **Figure 4.10** are typical for intravenous drug administration. The concentrations ranged from 5.5 to 7.0 µM after 10 minutes and decreased to 2.5 µM within one hour. Four hours and seven hours after paclitaxel administration, the concentration decreased to 590 and 270 nM, respectively. It is important to emphasize that none of the modulators affected the paclitaxel plasma concentration significantly.

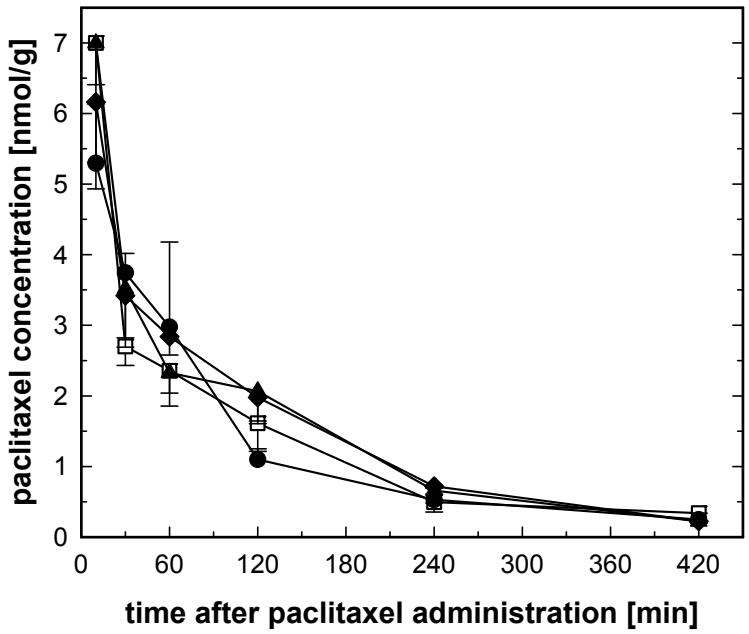

Figure 4.10: Effect of ABCB1 modulator co-administration on paclitaxel levels in the plasma of NMRI mice (mean values ± SEM, n = 3 - 4); ME27-4 *(filled circles)*, ME30-1 *(filled diamonds)* and ME33-1 *(filled triangles)* were used as ABCB1 modulators. Untreated mice served as control *(open squares)*.

In **Figure 4.11** the area under the paclitaxel concentration-time curves obtained by co-administration of the respective modulator are compared with the AUC of paclitaxel mono-therapy (control). Depending on the substance, the brain AUCs were increased to 190, 230 or 380 %. By contrast, the paclitaxel plasma AUCs remained unchanged, irrespective of the concomitant modulator. Therefore, the systemic paclitaxel toxicity should be lower compared to previous studies using valspodar as modulator of P-glycoprotein (Fellner et al., 2002). Additionally, the data confirm that the enhanced penetration of paclitaxel into the brain is not a consequence of an increased plasma/brain concentration gradient of the cytostatic drug.

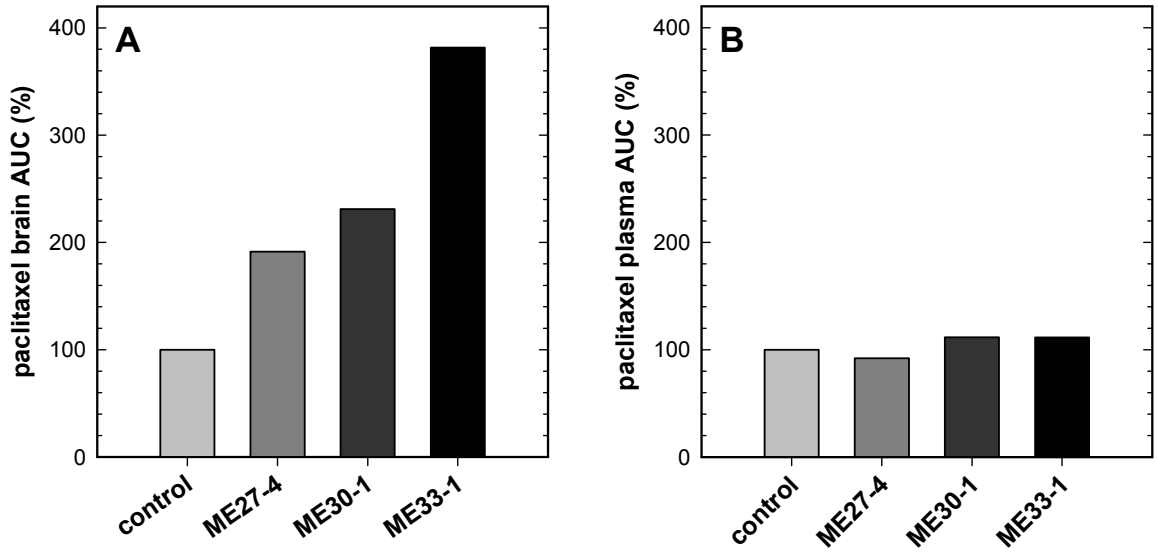

Figure 4.11: Effect of ABCB1 modulator co-administration on the AUC of paclitaxel in brain **(A)** and plasma **(B)** of NMRI mice; the AUC of the control (paclitaxel + vehicle) was defined as 100 %. As becomes obvious, every compound had the potency to elevate the brain AUC of paclitaxel. The extent of the increase is in agreement with the determined in vitro activity of the ABCB1 modulators. In contrast, none of the tariquidar-like modulators has a significant impact on the paclitaxel plasma AUC.

4.4 Summary and conclusions

The P-glycoprotein modulators ME27-4, ME30-1 and ME33-1 were investigated in vivo due to encouraging results in vitro (see chapter 3). Furthermore, the hypothesis that more hydrophilic ABCB1 inhibitors are superior to tariquidar in terms of pharmacokinetics and pharmacodynamics should be evaluated.

The modified SPE routine yielded very clear extracts, containing no interfering substances. Additionally, it became possible to quantitate the modulators and paclitaxel with one extraction routine, followed by one consistent RP-HPLC procedure. Validation revealed high specificity, reproducibility, accuracy, precision and a low limit of quantification for the various modulators.

Subsequent biodistribution studies in NMRI mice revealed the absence of acute inherent toxicity, favorable bioavailability and high metabolic stability of the tariquidar-like compounds. Moreover, it should be stressed that all investigated modulators selectively elevated the brain paclitaxel levels in accordance with the determined in vitro potency. The increase in the paclitaxel brain AUCs by approximately 100 to 300 % was less pronounced than that observed previously with co-administered valspodar (Fellner et al., 2002). Nevertheless, it has to be taken into consideration that most likely cytochrome P450

related pharmacokinetic interactions of valspodar (Fischer et al., 1998; Jamis-Dow et al., 1995) contributed to the increased penetration of paclitaxel into the brain. This is confirmed by experiments done with Abcb1a/b double knockout mice in which valspodar increased the plasma as well as the brain levels of paclitaxel (Kemper et al., 2003). Plasma levels were elevated 1.6 to 4.4-fold, and brain concentrations 1.4 to 1.8-fold, respectively. In contrast to the absorption of orally administered drugs, P-glycoprotein seems not to reduce the excretion of substrates. Studies with P-gp knockout mice showed no elevated plasma levels of intravenously administered vinblastine, digoxin et cetera (Mizuno et al., 2003), whereas the bioavailability of per orally dosed paclitaxel and docetaxel was significantly increased (Bardelmeijer et al., 2002; Koolen et al., 2010; Sparreboom et al., 1997).

Another important finding from the performed in vivo studies is that none of the new modulators influenced the paclitaxel plasma AUC. This observation is in agreement with data from the literature for the close structural analog tariquidar. In a phase I study using tariquidar in patients with a broad variety of tumors (renal cell carcinoma, breast cancer, adrenocortical cancer, ovarial cancer etc.), Abraham et al. (2009) found no influence on the pharmacokinetics and the toxicity of the P-gp substrate vinorelbin. Moreover, tariquidar did also not alter the plasma levels of paclitaxel in NMRI (nu/nu) mice (Hubensack et al., 2008) or CD rats (Mistry et al., 2001). The absence of effects on the plasma level of paclitaxel should result in lower systemic toxicity. As a consequence, the investigated modulators are more suitable for co-administration in cancer chemotherapy compared to second generation modulators. Indeed, due to toxic side effects in combination with valspodar, the paclitaxel dose had to be reduced to 2 mg/kg body weight in the subsequent treatment experiments (Fellner et al., 2002). Due to the lacking effect on the AUC of paclitaxel in plasma, a dose reduction of the cytostatic agent is not necessary when combined with the new modulators in therapeutic studies.

The discrepancy between the high in vitro potency of tariquidar (and elacridar) and the in vivo results led to the assumption that the modulators reach the target at suboptimal concentrations due to low solubility, high lipophilicity and, possibly, accumulation in adipose tissue (Hubensack et al., 2008). Consequently, it was hypothesized that more hydrophilic modulators should show a higher in vivo potency. The investigated tariquidar-like modulators show pronounced differences (approximately two orders of magnitude) in lipophilicity and were suitable to investigate the working hypothesis. However, a decrease in lipophilicity was not associated with increased paclitaxel levels in the brain. On the contrary, the effect directly correlated with lipophilicity: the most lipophilic inhibitor (ME33-1) was most potent, followed by the compound with the medium lipophilicity (ME30-1) and the most hydrophilic ABCB1 modulator (ME27-4). A certain degree of

hydrophobicity seems to be required for the accumulation in the membrane and to reach the binding site of the transporter (see chapter 7, in particular section 7.3.1). It has to be taken into consideration that the more hydrophilic modulators had also higher IC_{50}-values in vitro. Nevertheless, even the compound with the highest IC_{50}-value investigated in this study had a higher in vitro potency than valspodar.

On the basis of the results of the pharmacokinetic studies, the two modulators with the most pronounced effect on the paclitaxel brain AUC were chosen for more detailed tumor pharmacological experiments in nude mice. In chapter 5 the effect of concomitant paclitaxel administration on subcutaneously growing, ABCB1 transporter over-expressing human Kb-V1 tumors (ME30-1 and ME33-1) is evaluated. In chapter 6 an analogous approach is used to study the impact of combination treatment on intracerebral human glioblastomas (ME33-1).

4.5 References

Abraham, J.; Edgerly, M.; Wilson, R.; Chen, C.; Rutt, A.; Bakke, S., et al. A phase I study of the P-glycoprotein antagonist tariquidar in combination with vinorelbine. *Clin. Cancer Res.* **2009,** 15, 3574-3582.

Bardelmeijer, H. A.; Ouwehand, M.; Buckle, T.; Huisman, M. T.; Schellens, J. H.; Beijnen, J. H., et al. Low systemic exposure of oral docetaxel in mice resulting from extensive first-pass metabolism is boosted by ritonavir. *Cancer Res.* **2002,** 62, 6158-6164.

Brandes, A. A.; Pasetto, L. M.; Monfardini, S. New drugs in recurrent high grade gliomas. *Anticancer Res.* **2000,** 20, 1913-1920.

Debinski, W. Drug cocktails for effective treatment of glioblastoma multiforme. *Expert. Rev. Neurother.* **2008,** 8, 515-517.

Dodic, N.; Dumaitre, B.; Daugan, A.; Pianetti, P. Synthesis and activity against multidrug resistance in Chinese hamster ovary cells of new acridone-4-carboxamides. *J. Med. Chem.* **1995,** 38, 2418-2426.

Egger, M.; Li, X. Q.; Müller, C.; Bernhardt, G.; Buschauer, A.; König, B. Tariquidar analogues: Synthesis by Cu^{I}-catlyzed N/O-aryl coupling and inhibitory activity against the ABCB1 transporter. *Eur. J. Org. Chem.* **2007**, 2643-2649.

Fellner, S. Pharmakokinetische und pharmakodynamische Untersuchungen zur Koapplikation von MDR-Modulatoren (SDZ PSC 833) und Hyaluronidase bei der Chemotherapie maligner Gliome. Doctoral thesis, University of Regensburg, Regensburg, Germany, 2001.

Fellner, S.; Bauer, B.; Miller, D. S.; Schaffrik, M.; Fankhänel, M.; Spruss, T., et al. Transport of paclitaxel (Taxol) across the blood-brain barrier in vitro and in vivo. *J. Clin. Invest.* **2002,** 110, 1309-1318.

Fischer, V.; Rodriguez-Gascon, A.; Heitz, F.; Tynes, R.; Hauck, C.; Cohen, D., et al. The Multidrug Resistance Modulator Valspodar (PSC 833) Is Metabolized by Human Cytochrome P450 3A. Implications for Drug-Drug Interactions and Pharmacological Activity of the Main Metabolite. *Drug Metab. Dispos.* **1998,** 26, 802-811.

Glantz, M. J.; Chamberlain, M. C.; Chang, S. M.; Prados, M. D.; Cole, B. F. The role of paclitaxel in the treatment of primary and metastatic brain tumors. *Semin. Radiat. Oncol.* **1999,** 9, 27-33.

Hubensack, M. Approaches to overcome the blood brain barrier in the chemotherapy of primary and secondary brain tumors: modulation of P-glycoprotein 170 and targeting of the transferrin receptor. PhD thesis, University of Regensburg, Regensburg, Germany, 2005.

Hubensack, M.; Müller, C.; Höcherl, P.; Fellner, S.; Spruss, T.; Bernhardt, G., et al. Effect of the ABCB1 modulators elacridar and tariquidar on the distribution of paclitaxel in nude mice. *J. Cancer Res. Clin. Oncol.* **2008,** 134, 597-607.

Jamis-Dow, C. A.; Klecker, R. W.; Katki, A. G.; Collins, J. M. Metabolism of taxol by human and rat liver in vitro: a screen for drug interactions and interspecies differences. *Cancer Chemother. Pharmacol.* **1995,** 36, 107-114.

Kemper, E. M.; van Zandbergen, A. E.; Cleypool, C.; Mos, H. A.; Boogerd, W.; Beijnen, J. H., et al. Increased penetration of paclitaxel into the brain by inhibition of P-Glycoprotein. *Clin. Cancer Res.* **2003,** 9, 2849-2855.

Koolen, S. L.; Beijnen, J. H.; Schellens, J. H. Intravenous-to-oral switch in anticancer chemotherapy: a focus on docetaxel and paclitaxel. *Clin. Pharmacol. Ther.* **2010,** 87, 126-129.

Miller, D. S.; Bauer, B.; Hartz, A. M. Modulation of P-glycoprotein at the blood-brain barrier: opportunities to improve central nervous system pharmacotherapy. *Pharmacol. Rev.* **2008,** 60, 196-209.

Miller, D. S.; Nobmann, S. N.; Gutmann, H.; Toeroek, M.; Drewe, J.; Fricker, G. Xenobiotic transport across isolated brain microvessels studied by confocal microscopy. *Mol. Pharmacol.* **2000,** 58, 1357-1367.

Mistry, P.; Stewart, A. J.; Dangerfield, W.; Okiji, S.; Liddle, C.; Bootle, D., et al. In vitro and in vivo reversal of P-glycoprotein-mediated multidrug resistance by a novel potent modulator, XR9576. *Cancer Res.* **2001,** 61, 749-758.

Mizuno, N.; Niwa, T.; Yotsumoto, Y.; Sugiyama, Y. Impact of drug transporter studies on drug discovery and development. *Pharmacol. Rev.* **2003,** 55, 425-461.

Pardridge, W. M. Blood-brain barrier delivery. *Drug Discov. Today* **2007,** 12, 54-61.

Roe, M.; Folkes, A.; Ashworth, P.; Brumwell, J.; Chima, L.; Hunjan, S., et al. Reversal of P-glycoprotein mediated multidrug resistance by novel anthranilamide derivatives. *Bioorg. Med. Chem. Lett.* **1999,** 9, 595-600.

Rücker, G.; Neugebauer, M.; Willems, G. G. Validierung und Kalibrierung. In *Instumentelle Pharmazeutische Analytik*, 4th ed.; Wissenschaftliche Verlagsgesellschaft Stuttgart: Stuttgart, Germany, 2008.

Shah, V. P.; Midha, K. K.; Dighe, S.; McGilveray, I. J.; Skelly, J. P.; Yacobi, A., et al. Analytical methods validation: bioavailability, bioequivalence and pharmacokinetic studies. Conference report. *Eur. J. Drug Metab. Pharmacokinet.* **1991,** 16, 249-255.

Sparreboom, A.; van Asperen, J.; Mayer, U.; Schinkel, A. H.; Smit, J. W.; Meijer, D. K., et al. Limited oral bioavailability and active epithelial excretion of paclitaxel (Taxol) caused by P-glycoprotein in the intestine. *Proc. Natl. Acad. Sci. U. S. A.* **1997,** 94, 2031-2035.

Sparreboom, A.; van Tellingen, O.; Nooijen, W. J.; Beijnen, J. H. Determination of paclitaxel and metabolites in mouse plasma, tissues, urine and faeces by semi-automated reversed-phase high-performance liquid chromatography. *J. Chromatogr. B. Biomed. Appl.* **1995,** 664, 383-391.

Chapter 5

5 Reversal of classical multidrug resistance by co-administration of ABCB1 modulators and paclitaxel in a subcutaneous xenograft model

5.1 Introduction

In the previous 50 years considerable research effort has been devoted to the design and the clinical use of innovative chemotherapeutic agents (Mellor and Callaghan, 2008). Additionally, substantial advances have been achieved in the fields of molecular biology, genetics, tumor biology and immunology. This information has ameliorated our understanding of carcinogenesis, development and progression of malignant tumors at a molecular level.

Despite this indisputable progress, the translation of this knowledge into a clinically relevant improvement of therapy is still lacking for many tumor types (Gillet and Gottesman, 2010). In particular this is true for neoplasms with a special location that impedes dissection and/or drug therapy (e.g. in the CNS; cf. chapters 4 and 6) and after dissemination. Moreover, a vast number of malignancies in the periphery is also affected, since these tumors show inherent and/or developed (approximately 40 % of all cancer types) resistance against chemotherapy (Higgins, 2007). Characteristic of the latter is that many of the affected patients previously underwent chemotherapy and showed initial response followed by relapse (Mellor and Callaghan, 2008). In most cases relapse is accompanied by the insensitivity to a broad spectrum of cytostatic agents (including drugs, which in the patient initially reduced the tumor size). This phenotype was subsumed under the designation multidrug resistance (MDR). Consequently, it is important to consider that MDR is a multifactorial phenomenon (see **Table 5.1**). Although multiple mechanisms play

a role, ABC transporter mediated efflux (particular by ABCB1) is the most important and the best characterized cause for MDR.

Table 5.1: Main mechanisms of multidrug resistance observed in tumor cell lines[a]

Mechanism	Effect / Examples
Altered membrane transport	Decreased uptake of water soluble drugs via carrier systems (e.g. folate antagonists, nucleoside analogs, cisplatin)
	Increased export of mainly lipophilic drugs via efflux transporter (most important are ABCB1, ABCG2 and ABCC1)
Increased detoxification by metabolic enzymes	Cytochrome P450 enzymes (e.g. cyclophosphamide)
	Glutathion S-transferase (e.g. carmustine, cyclophosphamide)
	UDP-glucoronyltransferase (e.g. etoposide, tamoxifen)
Alterations in target molecules	Increased transcription of the target (e.g. taxanes)
	Mutation of the binding site (e.g. epothilones)
Alterations in genes regulation	Enhanced DNA repair (alkylating agents)
	Reduced apoptosis (Bcl2 pathway, p53 protein; e.g. vinorelbine)
	Pertubation of cell cycle (p53 protein; e.g. fluorouracil, paclitaxel)

[a] Modified from Meijerman et al. (2008) and complemented according to Gillet and Gottesman (2010), Luqmani (2005) and Szakacs et al. (2006)

The significance of P-gp, both at the BBB and in classical MDR, as well as the encouraging in vitro results of the investigated modulators (see chapter 3 and section 5.3.1.6), prompted the development of a predictive in vivo model to investigate the therapeutic value of the new ABCB1 modulators in multidrug resistant tumor xenografts.

5.2 Materials and methods

5.2.1 Drugs and chemicals

Vinblastine, doxorubicin and cisplatin were purchased from Sigma (Munich, Germany). Mitoxantrone and topotecan stock solutions were obtained by diluting Novantron® (Wyeth Pharma, Münster, Germany) and Hycamtin® (GlaxoSmithKline, Munich, Germany) with 70 % ethanol. For tariquidar, ME30-1 and ME33-1 see section 3.2.1. Paclitaxel (6 mg/mL, Bristol-Meyers Squibb, Wien, Austria) was obtained from the pharmacy of the University Hospital Regensburg. Bovine serum albumin and fetal calf serum were acquired from Serva (Heidelberg, Germany) and Biochrom (Berlin, Germany), respectively. Detection of P-gp was performed with Mdr C19 purified polyclonal primary antibody raised in goat (Santa Cruz Biotechnology, Heidelberg, Germany). The secondary antibody (texas red conjugated donkey anti-goat IgG (H+L)) as well as the ImmunoSelect antifading Mounting

Medium with DAPI were purchased from Dianova (Hamburg, Germany). If not otherwise stated, chemicals (p.a. quality) were obtained from Merck (Darmstadt, Germany). Water was purified by a Milli-Q system (Millipore, Eschborn, Germany)

5.2.2 Cell line and culture conditions

Kb-V1 cells were cultured at 37 °C/5 % CO_2 in DMEM (supplemented with 3.7 g/L sodium hydrogen carbonate, 110 mg/L sodium pyruvate and 10 % FCS (Biochrom, Berlin, Germany)) containing 330 nM vinblastine to maintain ABCB1 transporter expression (cf. section 3.2.2). For further general details cf. section 3.2.2.

5.2.3 Determination of chemosensitivity, growth and doubling times in vitro

Chemosensitivity was investigated by means of the kinetic crystal violet assay that was performed as described in section 3.2.5. In vitro growth was determined by a similar approach. After various periods of incubation (37 °C/5 % CO_2) cells were fixed with glutardialdehyde, stained with crystal violet and the absorbance (A_{580nm}) was plotted against the cultivation time. Doubling times were calculated using a computer analysis program (Reile et al., 1990).

5.2.4 Cytological staining

Two days after seeding on specially prepared microscopic slides (cf. section 5.2.5), cells were fixed for 1 hour with Carnoy´s solution (ethanol/chloroform/glacial acetic acid 6:3:1) and stored in PBS containing 0.1 % NaN_3. Subsequent staining with Harris` haematoxylin, orange G6 and eosin azure 50 was performed by the method of Papanicolaou (Takahashi, 1987). The stained sections were evaluated with a BH-2 microscope (Olympus, Hamburg, Germany) with 40x and 100x Planapo oil immersion objectives (Zeiss, Jena, Germany).

5.2.5 Karyology

The assay was essentially performed as described previously (Jarzyna, 2007). In brief: microscopic slides were prepared (immersion in ethanol/hydrochloric acid (6 mL of concentrated hydrochloric acid in 200 mL 70 % ethanol for 24 hours)) according to the procedure of Rooney and Czepulkowski (1986). After cells had reached a confluency of approximately 15 % on the prepared slides (in Quadriperm lux-multiplates, Greiner Bio-One, Frickenhausen, Germany), cell culture medium was replaced with medium

containing 0.5 µg/mL of colcemide. After an incubation period of 2.5 hours (37 °C/5 % CO_2), culture medium was removed and hypotonic potassium chloride solution (75 mM, 37 °C) was added carefully. After 30 minutes, an equal volume of fixative (ice-cold methanol/glacial acetic acid 3:1) was added and removed (by careful suction) immediately. The fixation step was repeated twice (last step: 10 minutes fixation period). Subsequently, the dried slides were stained with Giemsa dye solution for 8 minutes. (10 mL filtered Giemsa solution, 90 mL of 0.025 M KH_2PO_4, pH 6.8) and mounted with DePeX (EMS, Hatfield, PA). Chromosome numbers were determined with a BH-2 microscope (Olympus, Hamburg, Germany) using a 100x Planapo oil immersion objective (Zeiss, Jena, Germany). For each passage of Kb-V1 cells 50 metaphases were counted.

5.2.6 Immunocytochemical staining

Kb-V1 cells were seeded into 8 chamber BD Falcon Culture Slides (BD Biosciences, Heidelberg, Germany). 24 h later (at approximately 50 % confluency), culture medium was replaced with 4 % paraformaldehyde in PBS and cells were fixed for 30 minutes. After a washing step (0.5 % BSA in PBS) and two subsequent permeabilisation steps with 0.1% Triton X-100 (Sigma, Munich, Germany) in PBS (PBS-T), an additional washing step followed. Unspecific binding of the primary AB was blocked by incubation with BSA solution (10 % in PBS-T) for 30 minutes. Afterwards, slides were incubated with various concentrations of the primary AB (Mdr C19) in PBS (containing 0.5 % BSA) over night at 4 °C. To the controls, 0.5 % BSA in PBS without primary AB was added. Subsequent to three washing steps, samples were incubated with the secondary AB (texas red conjugated donkey anti-goat IgG (H+L), 1:200) in the dark for 1.5 hours. Then, the secondary AB was removed in 3 washing steps and by rinsing with Millipore water (2 seconds) afterwards. Counterstaining of the nuclei was achieved by mounting the slides with ImmunoSelect antifading Mounting Medium containing DAPI. Picture acquisition was performed as described in section 5.2.7.

5.2.7 Immunohistochemical investigations

Fixation, cryosectioning, staining and image acquisition were essentially performed according to the literature (Gleich and Pina, 2008; Gleich and Strutz, 2002; Gleich et al., 2004) with some modifications. In brief: a nude mouse, bearing a subcutaneous human Kb-V1 tumor (passage 1) was killed by an overdose of narcotic (200 mg/kg ketamine, 50 mg/kg xylazine; i.p.). To remove the blood and enlarge the vascular system the animal was transcardially perfused with 50 mg/L $NaNO_3$ in common salt solution for 1 minute

(flow : 8 mL/min). Subsequently, tissue was fixed by perfusion with 0.1 M phosphate buffer (pH 7.4) containing 4 % paraformaldehyde/0.1 % glutardialdehyde for 30 minutes. After tumor dissection, tissue was cryoprotected with 30 % saccharose in 0.1 M phosphate buffer at 4 °C for 24 hours under agitation.

Subsequently, the tumor was embedded in Tissue Freezing Medium (Jung, Leica Instruments GmbH, Nussloch, Germany) and sections of 50 µm were cut by a Leica CM 1900 cryostat (Leica Mikrosysteme, Bensheim, Germany). Sections were immediately transferred into 24 well plates (Nunc, Wiesbaden, Germany) containing phosphate buffer. All further washing and staining steps were performed in these 24 well plates under agitation at room temperature (unless otherwise noted).

Sections were washed three times (10 minutes) with PBS-T. Unspecific binding of the primary AB was blocked by incubation with 10 % BSA in PBS-T for 1 hour. Thereafter, tissue samples were incubated with various concentrations of the primary AB (Mdr C19) in PBS-T (containing 0.5 % BSA) for 24 hours at 4 °C. In controls, the respective solution without primary AB was added. After three washing steps (10 minutes) with PBS-T, secondary AB (texas red conjugated donkey anti-goat IgG (H+L), 1:400) was added and samples were stored for 2 hours in the dark. After additional three washing steps with PBS-T, sections were transferred to SuperFrost plus microscope slides. Nuclei were counterstained by mounting the samples with ImmunoSelect antifading Mounting Medium containing DAPI.

Stained tissue samples were analyzed with a Leica DM RBE microscope (Leica Mikrosysteme, Bensheim, Germany). Image acquisition was conducted by using the digital high resolution Spot 2000 camera (Diagnostic Instruments, Stirling Heights, MI) under software control (Metamorph, Universal Imaging Corporation, West Chester, NY). Optimal exposure time for the red channel was determined empirically and kept constant in the following. Picture processing was performed with Adobe Photoshop in the same manner for all samples.

5.2.8 Flow cytometric determination of functional ABCB1 transporters

In order to determine the amount of functional P-gp, Kb-V1 cells were split into two subgroups. A control group (CG) was propagated with medium containing 330 nM vinblastine as before. The test group (TG) was subcultured without vinblastine. After various periods of time (with both subgroups) the calcein-AM efflux assay was performed at the flow cytometer with slight modifications according to Müller et al. (2007). 100 % inhibition of P-gp function was achieved by addition of 1 µM of tariquidar. The difference between the geometrical mean values in fluorescence intensity (GeoMean) of untreated

(100 % function) versus tariquidar treated cells corresponds to P-gp function. The percental amount of functional transporter in the TG in relation to the CG was calculated according to the following equation:

$$functional\ P-gp\ (\%) = \frac{GeoMean\_TG(+) - GeoMean\_TG(-)}{GeoMean\_CG(+) - GeoMean\_CG(-)} \cdot 100 \qquad \text{(equation 3)}$$

where (+) indicates treatment with 1 µM tariquidar and (-) addition of the respective volume of DMSO.

5.2.9 Subcutaneous injection Kb-V1 cells and serial transplantation of solid tumor fragments

Nude mice, housed under specified pathogen free (SPF) conditions in the central animal facility of the University of Regensburg, were used to establish and characterize subcutaneous Kb-V1 tumors for subsequent treatment experiments. The mice were kept in type III cages from Tecniplast™ (Hohenpeißenberg, Germany) at a 12 hours light/dark cycle, 26 °C and 70 % relative humidity. Animals took food (Ssniff, Soest, Germany) and water (autoclaved tap water) ad libitum.

For subcutaneous tumor cell implantation, cells were detached from the culture flask with trypsin/EDTA and FCS-free DMEM. After a subsequent washing step, cells were re-suspended with serum-free DMEM and $1 \cdot 10^7$ cells (100 - 150 µL cell suspension) were injected under the thoracic dermis of nude mice. Tumor progression as well as body weight was monitored once weekly (all animals were individually identifiable due to tattooed pads). In order to maintain tumor growth over various passages a solid tumor was excised, pieces of approximately 2 mm^3 were prepared in sterile PBS and serially transplanted.

5.2.10 Histology

Excised tumor tissue and organs were fixed for at least three days in Bouin´s solution (300 mL aqueous saturated picric acid, 100 mL formaldehyde and 20 mL glacial acetic acid) and embedded in paraffin by a standard procedure (cf. section 2.3.9.1 in Müller (2007)). Sections of 6 µm were cut by a Leica RM2255 microtome (Leica, Bensheim, Germany), transferred to SuperFrost plus microscope slides followed by deparaffinization using xylene and rehydration in a descending alcohol series. Subsequently, the samples

were stained by the procedure of Masson-Goldner or with haematoxylin-eosin (HE) as described elsewhere (Romeis, 1989).

5.2.11 Therapeutic in vivo studies

Compound preparation and administration was essentially performed as described in section 4.2.5. The modulators were dissolved in the vehicle and administered by gavage into the stomach (30 mg/kg, 7.5 mg/mL, 4 µL per gram of body weight) 2.5 hours before i.v. injection of paclitaxel (concentration range 2.5 - 4.5 mg/kg, 4 µL per gram of body weight). For the exact concentration and time regime of the various modulators see sections 5.3.3.1, 5.3.3.2 and 5.3.3.3. In the following, the treatment arm receiving this dose regime is designated as Pac/Mod-group.

Animals in the control group received vehicle and 0.9 % common salt solution, whereas mice in the modulator group were dosed with the respective modulator alone. In order to exclude an impact of components of the vehicle on tumor growth, the lipid carrier was administered 2.5 hour prior to injection of the cytostatic agent to animals in the paclitaxel group. During and after therapy, tumor progression as well as body weight was monitored twice weekly.

5.3 Results and discussion

5.3.1 In vitro characterization of Kb-V1 cells

The HeLa derived (cervical carcinoma) human Kb cells were obtained from the American Type Culture Collection (ATCC, Rockville, MD). In order to obtain the ABCB1 transporter (over)expressing subclone Kb-V1, cells were maintained in the presence of the P-gp substrate vinblastine at increasing concentrations (Hubensack, 2005). At a final vinblastine concentration of 330 nM, the expression level of the efflux transporter was sufficiently high for in vitro investigations on ABCB1 modulators (cf. chapter 3). With respect to the use of this subclone for the generation of an ABCB1 transporter expressing subcutaneous tumor model in nude mice, the obtained cells had to be characterized in vitro first.

5.3.1.1 Morphology

In general, Kb-V1 cells grew tightly adherent to cell culture flasks in monolayers. **Figure 5.1** shows cells stained by the method of Papanicolaou that stains plasma turquoise, nuclei blue and nucleoli deep blue. Distinctive features of malignancy as anisomorphic cells, an increased nucleocytoplasmic ratio and multiple prominent nucleoli are visible.

Further characteristics of the irregularly formed cells are numerous polynucleated cells (cf. Figure 5.1 B).

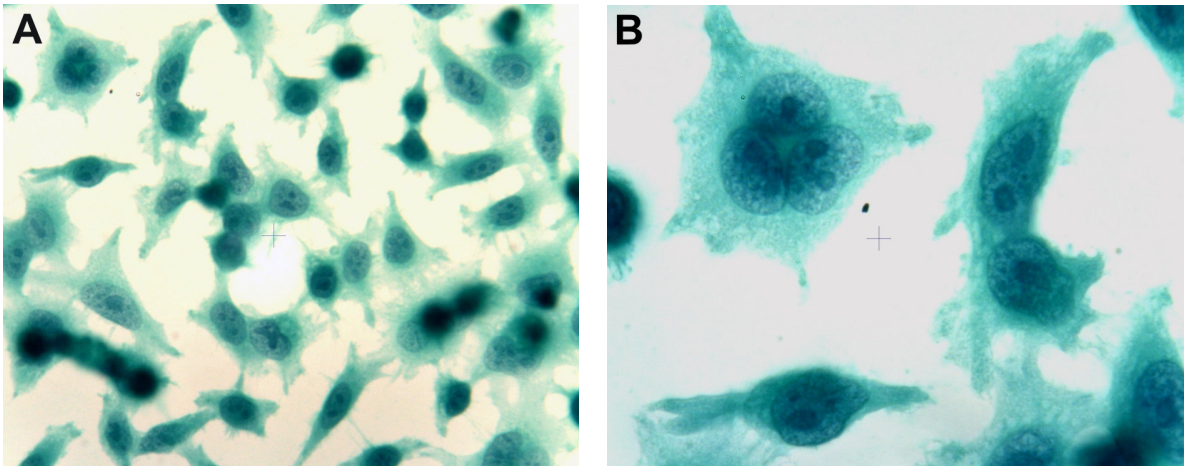

Figure 5.1: Morphology of human Kb-V1 cells (passage 46, Papanicolaou staining); **A)** The anisomorphic cells show mitotic activity, an increased nucleocytoplasmic ratio as well as multiple prominent nucleoli (objective: 40x). **B)** Detail (objective: 100x) of the upper left corner of (A) showing a highly malignant tri-nucleated cell.

No or only minor morphological changes were recognized over the various passages (data not shown).

5.3.1.2 In vitro growth of Kb-V1 cells

Due to the fact that cancer cell lines are usually polyclonal and genetically instable (cf. section 5.3.1.3), long-term culture can result in significantly altered growth parameters. Modified growth kinetics can in turn affect the antiproliferative effect of cytostatic drugs as well as the in vivo growth of resulting solid tumors. Consequently, to exclude the above mentioned issues, the growth kinetics of Kb-V1 cells in various in vitro passages were investigated.

Figure 5.2 compares the growth rates of Kb-V1 cells in the passages 25, 41 and 64. As becomes obvious, there were no significant alterations so that doubling times were comparable (data not shown).

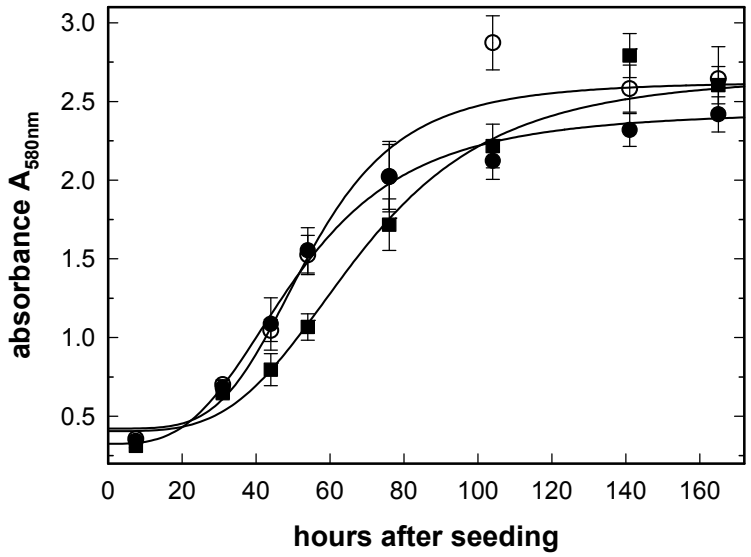

Figure 5.2: Growth kinetics of Kb-V1 cells over various passages: 25th *(open circles)*, 41th *(filled squares)* and 64th passage *(filled circles)*; mean values ± SEM

A minimal doubling time of 20 hours was reached 15 - 20 hours after seeding. Within the next 50 hours doubling times slowly (and almost linearly) increased to 40 hours followed by a steep ascent afterwards.

Taken together, growth kinetics did not vary significantly, indicating that chemosensitivity and growth rates of resulting solid tumors should not depend on the utilized in vitro passage of Kb-V1 cells.

5.3.1.3 Chromosomal number

An aneuploidy (abnormal number of chromosomes per cell) is a well known characteristic of tumor cells. Additionally, extensiveness and alteration over time can be used to estimate malignancy as well as genetic stability. Consequently, various passages of the newly generated, ABCB1 transporter expressing Kb-V1 cell line were examined with respect to their chromosome distribution.

Figure 5.3 shows characteristic images (obtained after cell preparation and Giemsa staining) used to determine the number of chromosomes in individual cells.

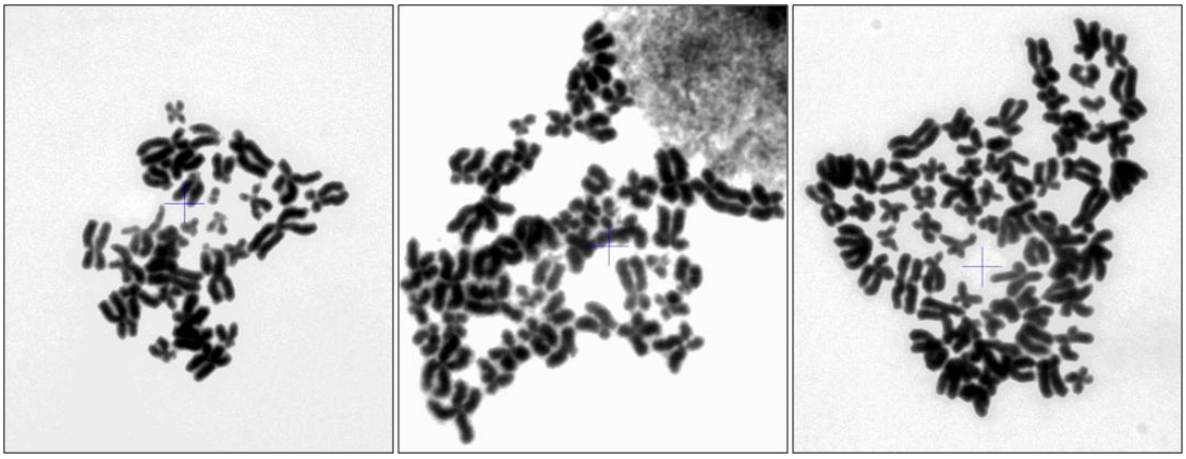

Figure 5.3: Representative metaphase chromosomes of Kb-V1 cells (46th passage) stained with Giemsa solution; the micrographs demonstrate the broad variety of chromosome numbers from 30 *(cell on the left)* over a normal diploid chromosome set *(middle)* to the prevalent triploid one *(right)*.

In **Figure 5.4** the number of chromosomes is plotted against the frequency in which the respective number was observed. In all investigated passages the modal number was 69 corresponding to the prevalent triploid karyotype. With regard to other tumor cell lines, the chromosomal distribution was quite uniform over a comparatively narrow range.

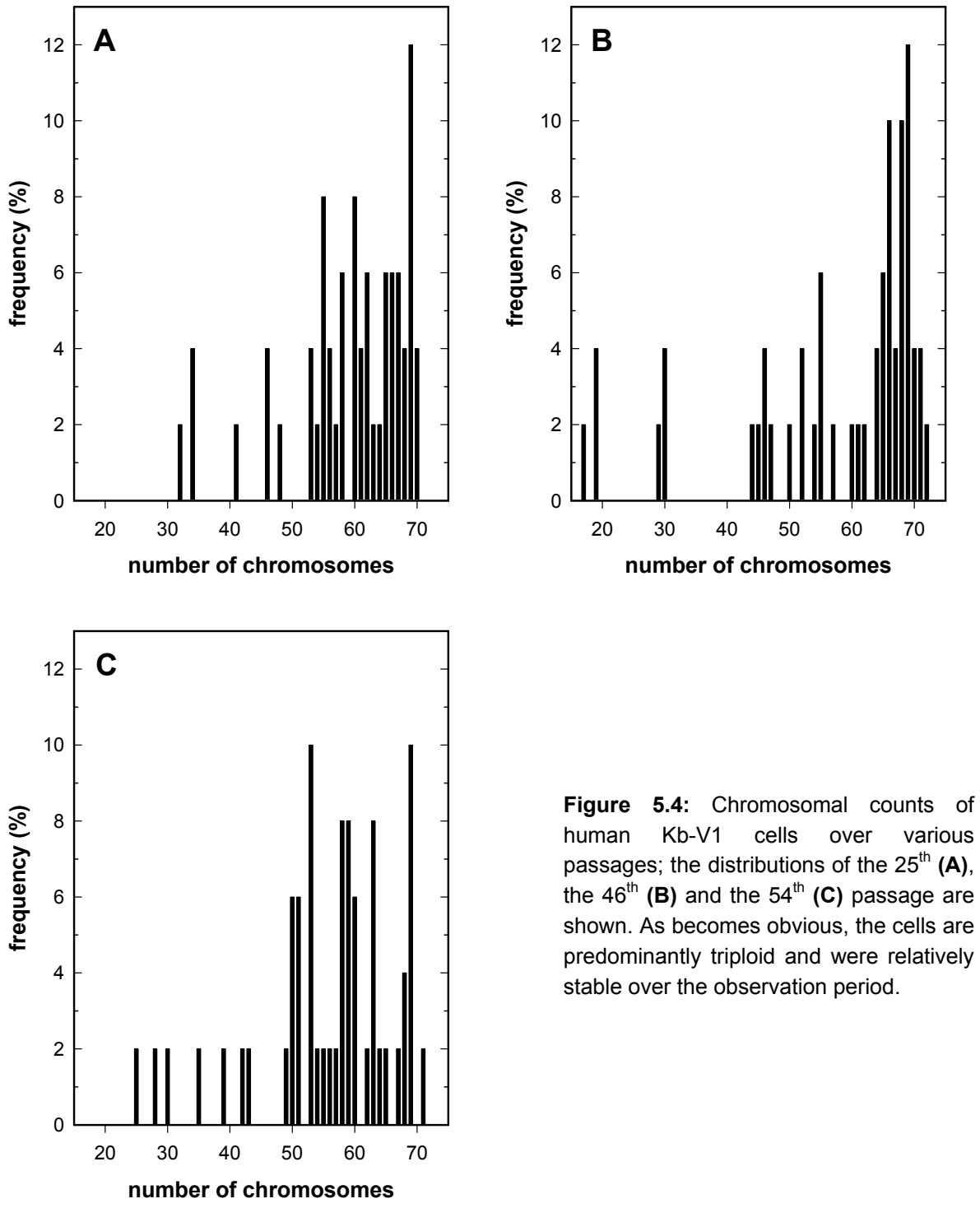

Figure 5.4: Chromosomal counts of human Kb-V1 cells over various passages; the distributions of the 25th **(A)**, the 46th **(B)** and the 54th **(C)** passage are shown. As becomes obvious, the cells are predominantly triploid and were relatively stable over the observation period.

Due to their growth characteristics and the observed genetic stability, Kb-V1 cells were considered suitable to establish a multidrug resistant tumor model in nude mice.

5.3.1.4 Immunocytochemical detection of the ABCB1 transporter

Over-expression of ABCB1 transporters (especially important after discontinuing vinblastine exposure) was examined by flow cytometry (cf. section 5.3.1.7) and immunocytochemical methods.

Figure 5.5 shows the detection of P-glycoprotein in Kb-V1 cells with a primary antibody directed against an intracellular amino acid sequence of P-gp. It can be seen from the control sample that the staining procedure could not completely eliminate unspecific AB binding. Nevertheless, the expression of the relevant efflux transporter is obvious.

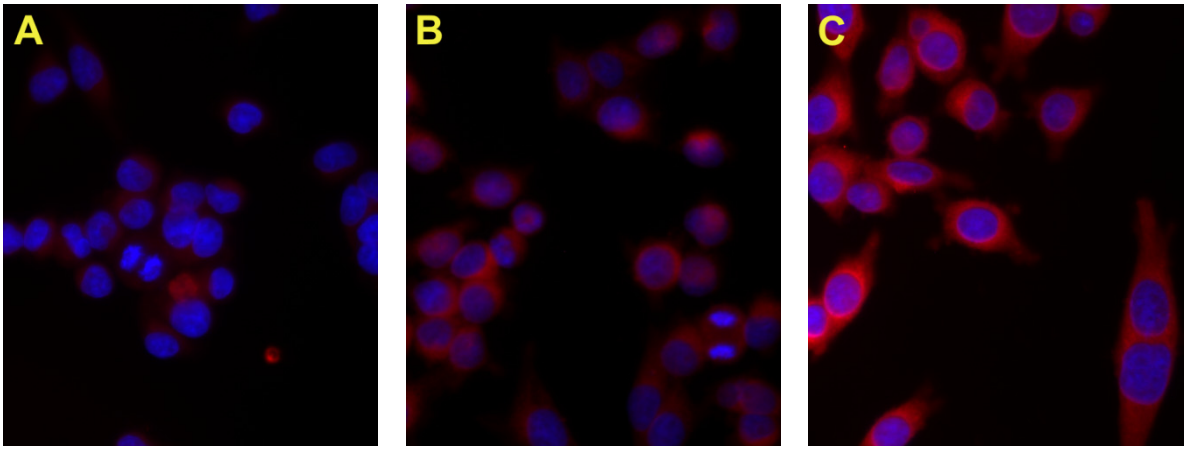

Figure 5.5: Immunocytochemical detection of ABCB1 transporter in Kb-V1 cells (passage 63; primary AB: Mdr C19 (raised in goat); secondary AB: texas red conjugated donkey anti-goat AB, 1:200; nuclei were stained with DAPI); **A)** Identically treated control cells without primary AB; **B)** Primary AB in a dilution of 1:500; **C)** Primary AB in a dilution of 1:50

5.3.1.5 Chemosensitivity against selected cytostatic drugs

Expression of ATP dependent efflux transporters is the most common cause for acquired resistance of tumor cells to a broad variety of anticancer drugs (Gottesman, 2002). Therefore, the effect of the known ABC transporter substrates (Szakacs et al., 2008) paclitaxel, doxorubicin, topotecan and mitoxantrone (see **Figure 5.6**) on proliferating Kb-V1 cells was investigated. Additionally, for reasons of comparison and control, cisplatin (no ABC transporter substrate) was included in the investigations.

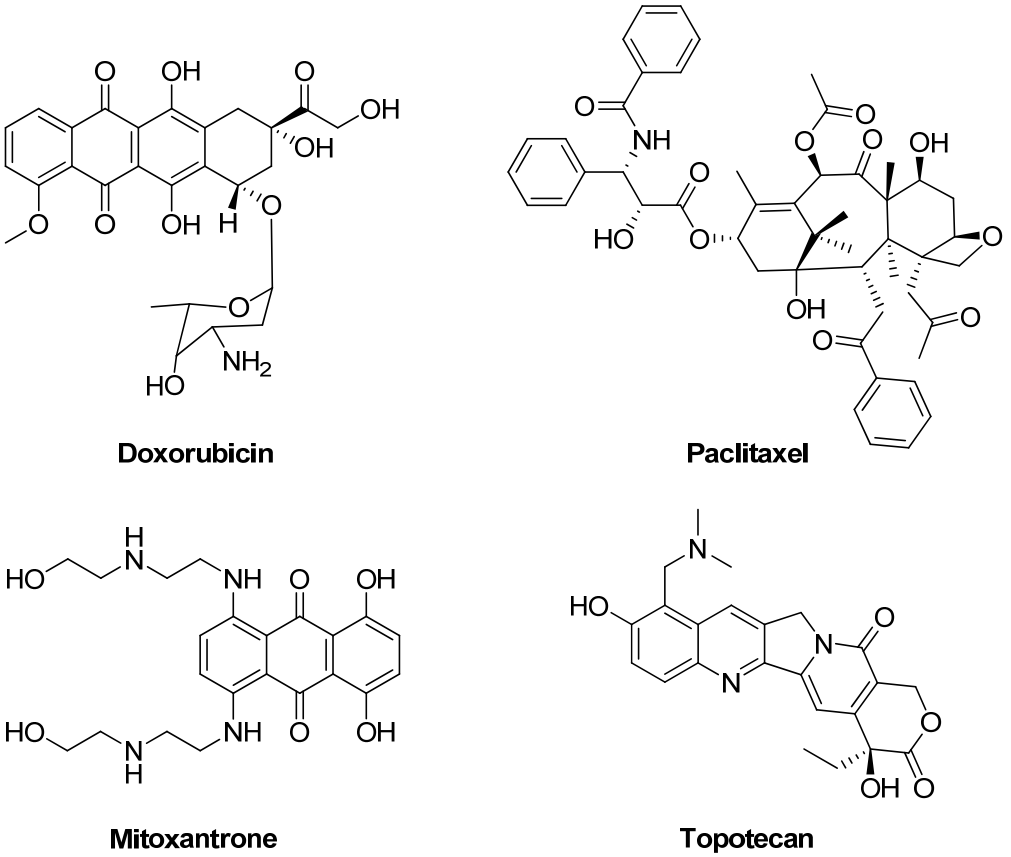

Figure 5.6: Chemical structures of cytotoxic drugs in clinical use that are substrates of ABC transporters

Cisplatin was cytocidal at a concentration of 1 µM (data not shown), demonstrating that the Kb-V1 cells had not developed resistance against this cytostatic. On the contrary, the substantial tolerance against anticancer drugs, which are P-gp substrates, becomes obvious from **Figure 5.7** and **Figure 5.8**. In the case of doxorubicin and paclitaxel, concentrations up to 5 µM and 500 nM, respectively, were tolerated without any effect on cell growth. The anthracycline analog mitoxantrone showed a cytostatic effect at concentrations of 500 nM and 1 µM. Also the topoisomerase inhibitor topotecan was able to exert a cytostatic to cytocidal drug effect at a concentration of 1 µM.

The fact that such enormous concentrations of anticancer drugs are tolerated indicates the presence of ABC transporters. Even after administration of paclitaxel to nude mice at a dosage as high as 8 mg/kg (see section 4.3.9), the paclitaxel plasma levels decrease to less than 500 nM approximately 4 hours after injection (the levels in tumor tissue are most likely lower). Therefore, a clinical relevant effect of paclitaxel mono-therapy on Kb-V1 tumors should be highly implausible.

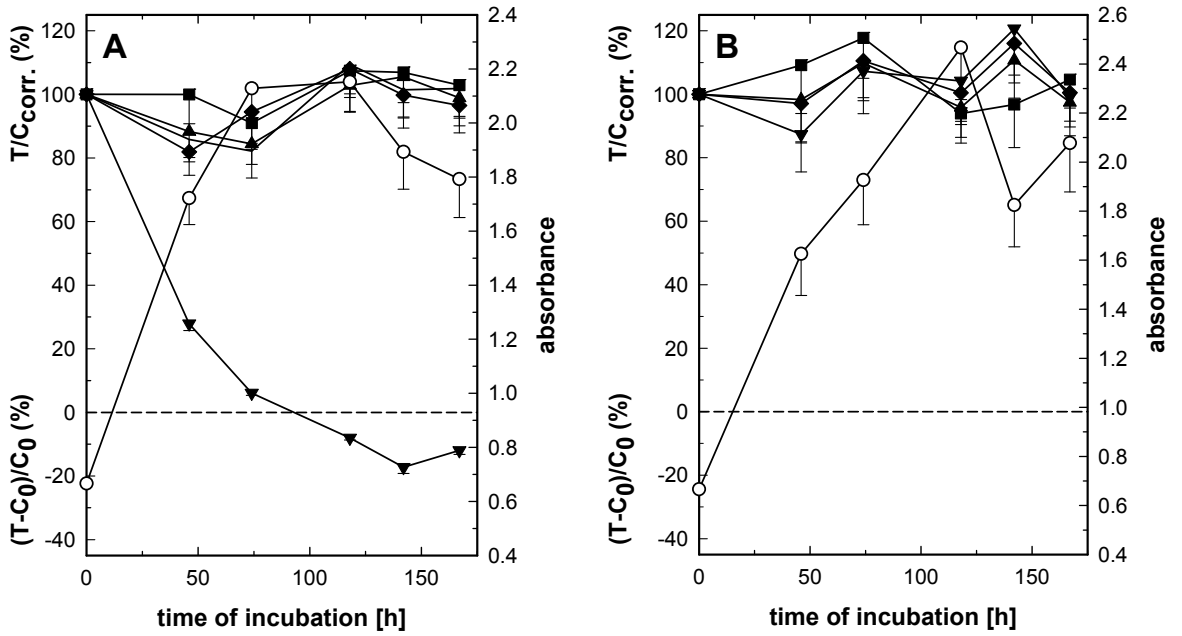

Figure 5.7: Resistance of Kb-V1 cells (passage 49) against doxorubicin and paclitaxel; vehicle *(open circles)*; **A)** Doxorubicin at various concentrations: 500 nM *(filled squares)*, 1 µM *(filled triangles)*, 5 µM *(filled diamonds)* and 10 µM *(filled inverted triangles)*; **B)** Paclitaxel at various concentrations: 10 nM *(filled squares)*, 50 nM *(filled triangles)*, 100 nM *(filled diamonds)* and 500 nM *(filled inverted triangles)*

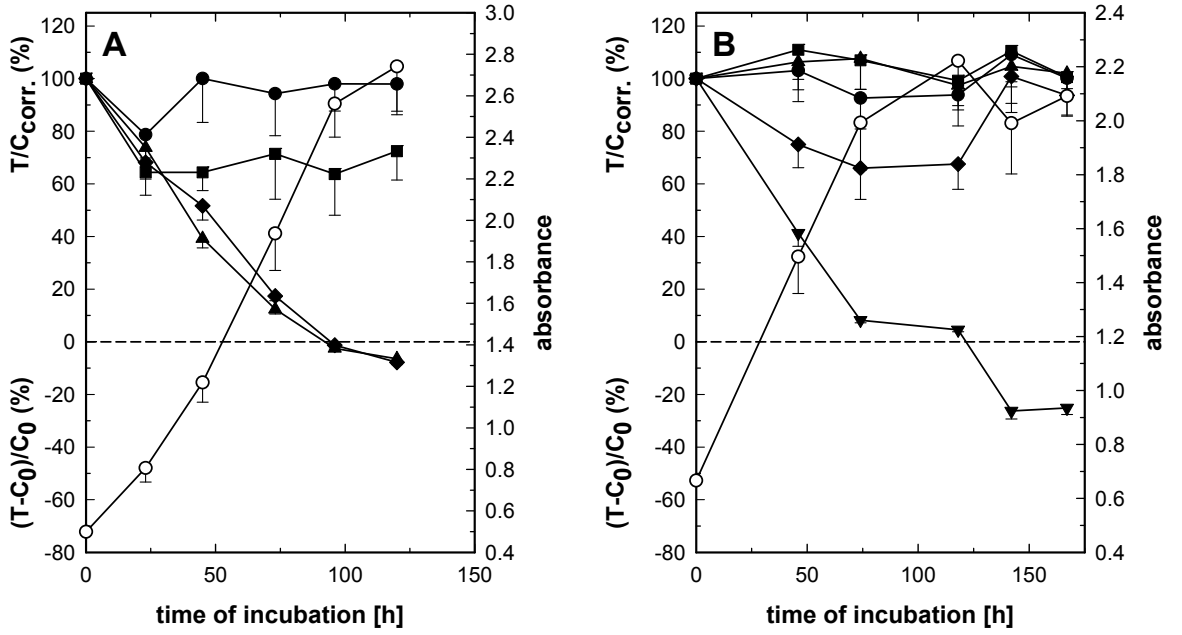

Figure 5.8: Resistance of Kb-V1 cells (passage 64 (A) and 49 (B)) against mitoxantrone and topotecan; vehicle *(open circles)*; **A)** Mitoxantrone at various concentrations: 50 nM *(filled circles)* 100 nM *(filled squares)*, 500 nM *(filled triangles)* and 1 µM *(filled diamonds)*; **B)** Topotecan at various concentrations: 10 nM *(filled circles)*, 50 nM *(filled squares)*, 100 nM *(filled triangles)*, 500 nM *(filled diamonds)* and 1 µM *(filled inverted triangles)*

5.3.1.6 Reversal of P-gp mediated classical multidrug resistance

Prior to treatment studies in nude mice, it was crucial to assure that P-glycoprotein mediated multidrug resistance can be reversed by the combination with ABCB1 modulators in vitro.

In **Figure 5.9** the cytotoxicities of high concentrations of doxorubicin (or paclitaxel) alone are compared to the effect of the respective anticancer drug at lower concentrations in combination with a low amount of different ABCB1 modulators. Furthermore, the impact of the modulators alone (at a high concentration of 1 µM) was determined to exclude inherent toxicity.

Addition of 100 nM ME30-1 results in a strong cytocidal effect of 500 nM doxorubicin (compared to inefficacy of doxorubicin alone at a concentration of 5 µM). When combined with ME33-1 (identical doxorubicin concentration), 50 nM of the inhibitor were sufficient to produce a cytocidal effect (data not shown). In the case of paclitaxel, even 30 nM were sufficient to exert a full cytocidal effect on Kb-V1 cells when 30 nM of ME33-1 were added to the culture medium (compared to inefficacy of paclitaxel alone at a concentration of 500 nM). Both modulators alone had no impact on cell growth up to a concentration of 1 µM.

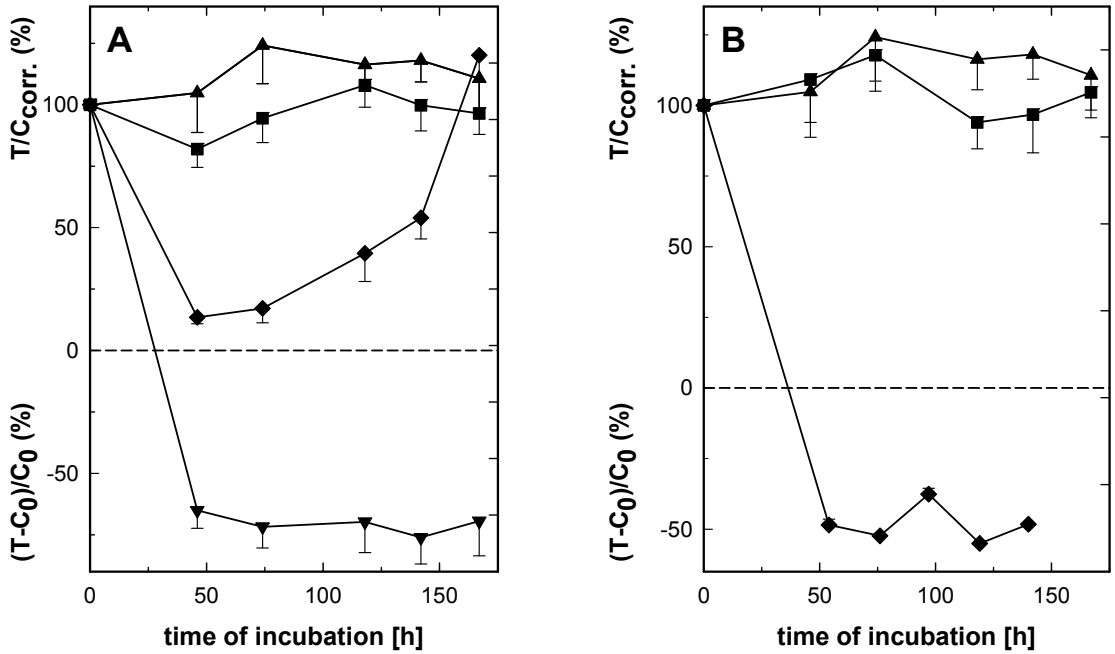

Figure 5.9: Reversal of P-gp mediated drug resistance of Kb-V1 cells by combination with an ABCB1 modulator; **A)** Doxorubicin [5 µM] *(filled squares)*, ME30-1 [1 µM] *(filled triangles)*, doxorubicin [500 nM] + ME30-1 [50 nM] *(filled diamonds)* and doxorubicin [500 nM] + ME30-1 [100 nM] *(filled inverted triangles)*; **B)** Paclitaxel [500 nM] *(filled squares)*, ME33-1 [1 µM] *(filled triangles)* and paclitaxel [30 nM] + ME33-1 [30 nM] *(filled diamonds)*

Nevertheless, incubation with 5 µM of both modulators revealed a modest cytotoxic effect on cell growth, indicating inherent toxicity, albeit at very high concentrations (see section 3.3.2.2).

As expected, the combination of 100 nM ME33-1 and cisplatin (investigated in the concentration range between 50 nM and 10 µM) showed no increase in toxicity of the anticancer agent (data not shown).

5.3.1.7 Maintenance of the transporter status after discontinued vinblastine exposure

Under in vitro conditions a selection pressure in terms of persistent efflux transporter expression is mediated by the P-gp substrate and cytotoxic agent vinblastine. Since selection pressure cannot be sustained in vivo, the following approach (see also section 5.2.8) was used to investigate if a drastic reduction of ABCB1 transporter function has to be expected after discontinuation of vinblastine treatment. Therefore, a corresponding reference group was subcultured without vinblastine. After various periods of time, the P-gp activity was compared with that of the cells which had been permanently exposed to the cytostatic using the flow cytometric calcein-AM efflux assay.

Figure 5.10 A illustrates the underlying principle. 100 % inhibition of P-gp function was achieved by addition of 1 µM of tariquidar. The difference between the geometrical means (GeoMeans) in fluorescence intensity of untreated (100 % function) versus tariquidar treated cells corresponds to the amount of functional P-glycoprotein. **Figure 5.10 B** reveals that P-gp transport activity was reduced by 35 % within 7 days after discontinuation of vinblastine treatment. More important, after that initial reduction, ABCB1 mediated transport activity did not decrease further during the remaining observation period.

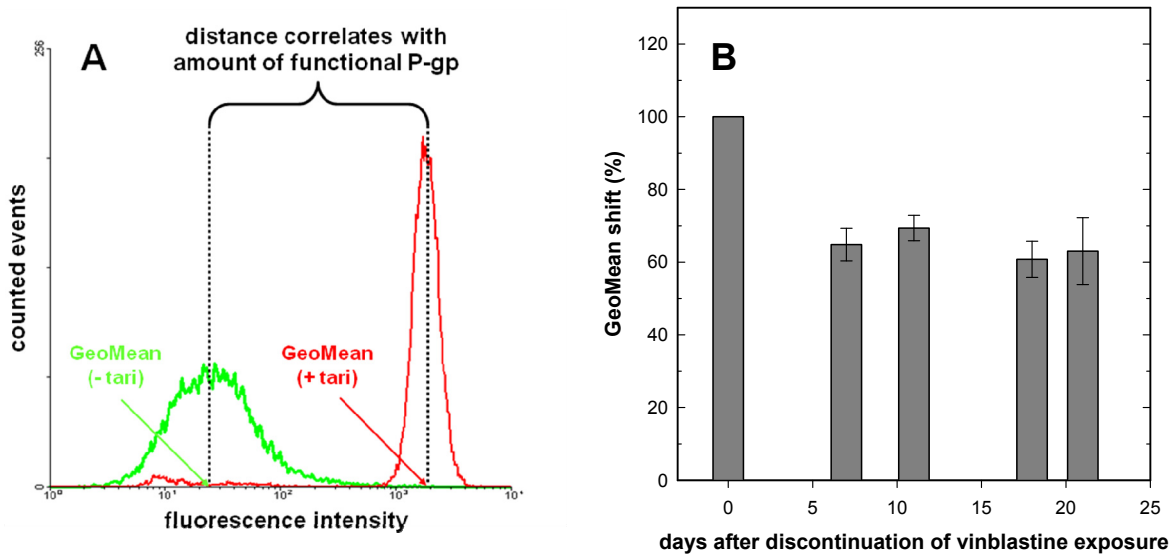

Figure 5.10: Verification of maintained transporter status after discontinuing vinblastine exposure to Kb-V1 cells; **A)** Schematic illustration of the principle; **B)** The difference at the beginning of the experiment is defined as 100 %. After an initial reduction to approximately 65 %, ABCB1 transport activity remains constant over time (mean values ± SEM, n = 5).

Taken together, the detailed in vitro characterization revealed the suitability of Kb-V1 cells to establish an ABCB1 transporter expressing subcutaneous tumor model in nude mice. Consequently, further in vivo experiments were initiated and are described in the following.

5.3.2 In vivo characterization of solid Kb-V1 tumors

5.3.2.1 Tumorigenicity and in vivo growth characteristics

In order to assure tumorigenicity as well as reproducible growth characteristics in vivo, Kb-V1 cells were implanted and resulting tumors were serially transplanted as described in section 5.2.9.

Figure 5.11 shows the in vivo growth kinetics of Kb-V1 xenografts over various passages. Tumors in the passages zero, one and two exhibited stable and reproducible growth rates, especially within the first 50 days after cell (or tumor tissue) implantation. This is of special importance, since the characteristic observation phase during treatment experiments coincides with that period. In contrast, in vivo passage 3 shows a pronounced retardation of tumor growth.

Within the first three in vivo passages, tumorigenicity was sufficiently high (above 70 %) to provide s.c. xenografts for therapeutic studies in nude mice. Additionally, tumor growth did not affect the animals´ general state of health.

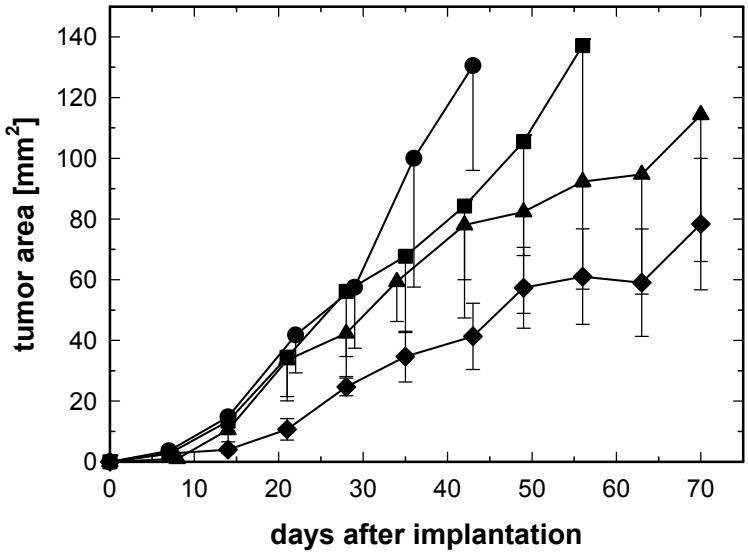

Figure 5.11: Growth curves of subcutaneous human Kb-V1 xenografts over the in vivo passages 0 *(circles)*, 1 *(squares)*, 2 *(triangles)* and 3 *(diamonds)*; a retardation of tumor growth in higher passages is obvious (mean values ± SEM).

Subsequent treatment studies were performed using tumors in the first in vivo passage.

5.3.2.2 Histology

In order to confirm the malignant nature of the xenografts, tissue samples were collected and histologically characterized over the various passages (for passage 0 see **Figure 5.12**). Criteria of malignancy such as an increased nucleocytoplasmic ratio, largely undifferentiated tissue, anisomorphic cells, multiple prominent nucleoli and a hyperchromatic cell membrane, are obvious. The mitotic activity is moderate (cf. section 5.3.1.1).

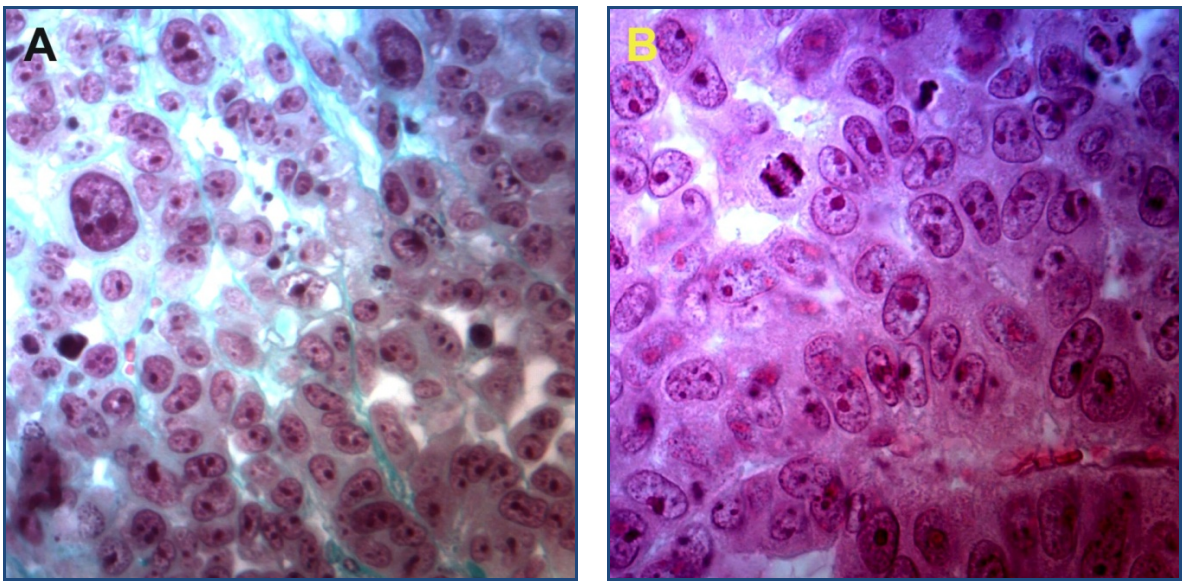

Figure 5.12: Histological staining of a subcutaneous Kb-V1 tumor (passage 0); **A)** Masson-Goldner staining (objective 40x) and **B)** Haematoxylin-eosin staining (objective 63x)

5.3.2.3 Maintenance of the ABCB1 transporter status in vivo

Due to the lack of vinblastine-induced selection pressure in vivo, expression of the ABCB1 transporter in subcutaneously growing Kb-V1 tumors had to be controlled. A staining protocol using paraffin embedded sections of tumor tissue fixed with Bouin´s solution was inadequate. Most likely, the harsh fixation and embedding procedure did alter the relevant antigenic determinant and/or impeded the AB from reaching its intracellular target (see below). A more sophisticated approach (detailed described in section 5.2.7) using an in vivo fixation method followed by cryosectioning of tumor tissue and subsequent staining of free floating sections was successful.

Figure 5.13 shows the immunohistochemical detection of P-glycoprotein in a Kb-V1 tumor (first passage). Since the primary antibody is directed against an intracellular peptide sequence (at the C-terminus of P-gp), permeabilisation of cells prior to AB staining is crucial. Due to the staining procedure (free floating sections) and the moderate fixation, the highly vulnerable tissue was cut into 50 µm thick sections, which is reflected by the diffuse fluorescence of AB-labeled P-glycoprotein.

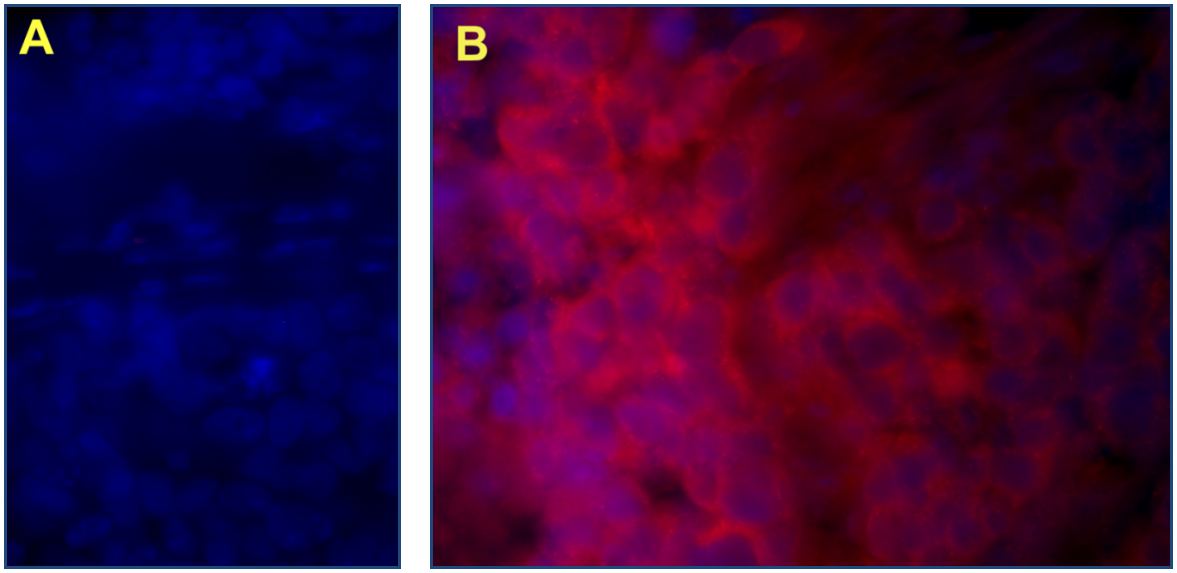

Figure 5.13: Immunohistochemical detection of ABCB1 transporters in a solid Kb-V1 tumor in the 1st in vivo passage (primary AB: Mdr C19 (raised in goat) directed against an intracellular peptide sequence of P-gp; secondary AB: texas red conjugated donkey anti goat-AB; nuclei were stained with DAPI); **A)** Identically treated control section without primary AB; **B)** Primary AB in a dilution of 1:25

Despite the aforementioned problems, the expression of the ABCB1 protein in solid tumors was confirmed. Thus, a major requirement was fulfilled with respect to therapeutic studies.

5.3.3 Effect of paclitaxel and co-administered ABCB1 modulators on subcutaneous multidrug resistant xenografts

Due to the encouraging in vitro (see chapter 3 and section 5.3.1.6) and in vivo (cf. chapter 4) results, the effect of ME30-1, ME33-1 and tariquidar (efficacy was confirmed in previous studies (Hubensack et al., 2008)) in combination with paclitaxel was investigated on multidrug resistant Kb-V1 tumors.

Table 5.2 summarizes the major characteristics of the various treatment groups. The animals were assigned to groups considering a homogeneous distribution of body weight and especially tumor area to avoid inherent bias. Compounds were administered weekly, because this treatment regimen has been reported as at least equieffective and less hematotoxic, when compared with the licensed 2- or 3-weekly schedule (Green et al., 2005; Mauri et al., 2010). As the achieved in vivo concentrations were up to 285 times higher than the IC_{50}-values obtained in vitro (see chapter 4) and due to limited availability of the test compounds, the dosage of the modulator was reduced to 30 mg/kg.

Table 5.2: Biometric parameters at the day of randomization

	Study parameter	Control group	Modulator group	Paclitaxel group	Paclitaxel + Modulator group
ME30-1	n[a]	8	7	10	10
	Body weight[b]	34.4 ± 0.9	35.3 ± 0.8	36.0 ± 0.9	35.5 ± 1.0
	Tumor area[c]	9.5 ± 2.2	8.1 ± 2.2	8.5 ± 2.5	9.0 ± 3.3
ME33-1	n[a]	9	9	11	11
	Body weight[b]	30.9 ± 1.2	30.3 ± 1.3	31.8 ± 1.2	30.7 ± 0.9
	Tumor area[c]	9.6 ± 2.1	10.4 ± 2.1	8.9 ± 2.1	9.5 ± 2.9
Tariquidar	n[a]	9	8	11	11
	Body weight[b]	30.9 ± 1.2	28.8 ± 1.1	31.8 ± 1.2	30.1 ± 0.6
	Tumor area[c]	9.6 ± 2.1	8.4 ± 3.1	8.9 ± 2.1	9.3 ± 2.8

[a] Number of animals per treatment group; [b] body weight in [g] ± SEM; [c] tumor area in [mm^2] ± SEM

In order to exclude gender related impact on tumor growth, solely male nude mice at an age between 8 and 12 weeks were included in all studies. A group receiving only the respective modulator was implemented to detect a possible inherent cytotoxic effect of the tariquidar-like compounds.

5.3.3.1 Morpholino analog of tariquidar (ME30-1)

ME30-1 was the first tariquidar-like modulator investigated in therapeutic in vivo studies. Consequently, the cytostatic agent was co-administered at a relatively low dosage initially.

Figure 5.14 shows the effect on tumor progression and body weight of nude mice. While paclitaxel mono-therapy had no impact on tumor growth, the combination of ME30-1 and paclitaxel resulted in a retardation of the mean tumor area **(A)**. This effect becomes more obvious when the median tumor area (less sensitive to outliers) is plotted **(B)**. Additionally, no increase in paclitaxel related toxicity (emaciation of the animals) was observed in the Pac/Mod-group (most probably because the new modulators do not increase the paclitaxel plasma levels) **(C)**. Administration of the modulator alone (also true for ME33-1 and tariquidar, see below) did not significantly retard tumor progression.

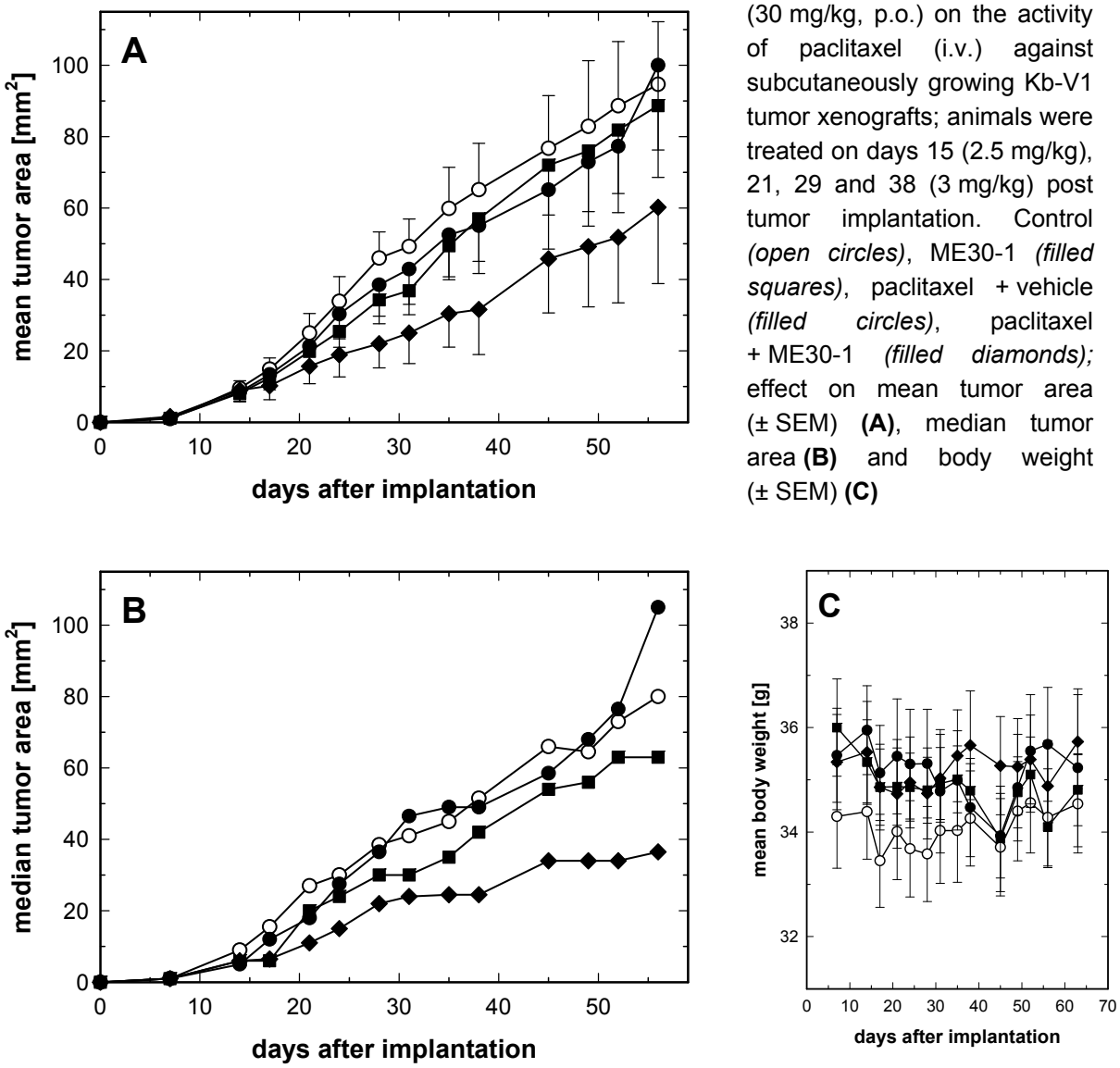

Figure 5.14: Effect of ME30-1 (30 mg/kg, p.o.) on the activity of paclitaxel (i.v.) against subcutaneously growing Kb-V1 tumor xenografts; animals were treated on days 15 (2.5 mg/kg), 21, 29 and 38 (3 mg/kg) post tumor implantation. Control *(open circles)*, ME30-1 *(filled squares)*, paclitaxel + vehicle *(filled circles)*, paclitaxel + ME30-1 *(filled diamonds);* effect on mean tumor area (± SEM) **(A)**, median tumor area **(B)** and body weight (± SEM) **(C)**

Figure 5.15 compares the individual tumor growth curves of animals in the group receiving the combination therapy **(A)** with animals treated with paclitaxel alone **(B)**. Combined administration of the modulator led to moderate retardation of tumor progression in the Pac/Mod-group, while there was a pronounced effect in five out of ten animals (tumor area ≤ 20 mm^2 after 52 days). In the paclitaxel group only two tumors were ≤ 20 mm^2. In the control group the three smallest neoplasms had tumor areas of 35, 40 and 56 mm^2. In the experiments with the modulators ME33-1 and tariquidar, the tumor areas of the three smallest neoplasms in the paclitaxel group (51 days after tumor transplantation) were determined to be 35, 36 and 40 mm^2.

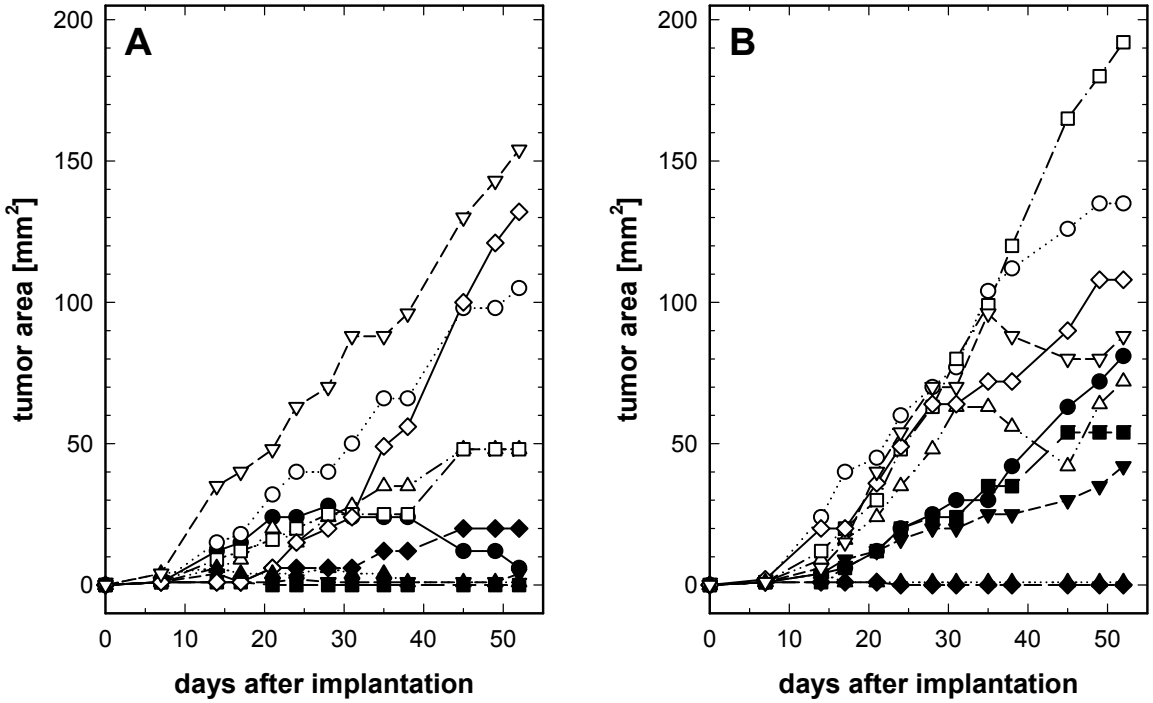

Figure 5.15: Growth curves of individual tumors (n = 10) in the treatment groups of paclitaxel + ME30-1 **(A)** and paclitaxel + vehicle **(B)**; the five tumors of the respective treatment group showing slowest growth are represented by filled symbols. As becomes obvious, half of the animals (especially those with small tumors at the beginning of the study) show a pronounced retardation of tumor growth (or even remission).

It may be speculated why only a subpopulation of animals benefits substantially from the combination therapy. Additional resistance mechanisms (independent of ABCB1 transporter expression, confer section 5.4) as well as inconsistencies in the vascularization of in the individual tumors could play a role in the therapy-refractory animals.

Additionally, tumors, liver and kidneys of 3 to 4 randomly selected animals per treatment group were harvested and histologically investigated for potential (toxic) effects of the therapy. None of the investigated tissue samples showed histologically recognizable abnormalities (data not shown).

5.3.3.2 Ethoxyethyloxy analog of tariquidar (ME33-1)

The results of the treatment experiments performed with ME33-1 are shown in **Figure 5.16**. Though the paclitaxel dose was increased to 4.5 mg/kg (due to the good tolerance of the combination with ME30-1) co-administration of ME33-1 resulted only in a slight (probably irrelevant) retardation of tumor growth. Also when the median tumor areas were compared, no significant differences were detectable (data not shown). Additionally, no individual animals in the Pac/Mod-group did benefit above-average (data not shown). Interestingly, the comparatively high paclitaxel dosage did not cause toxic side effects.

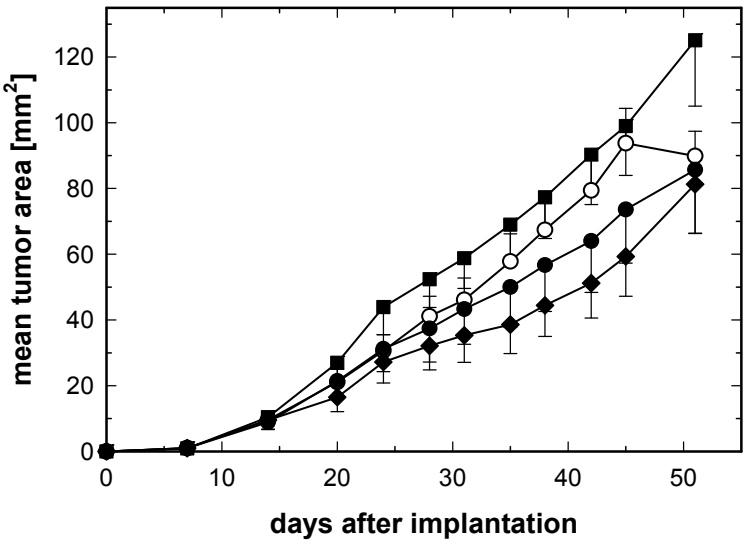

Figure 5.16: Effect of ME33-1 (30 mg/kg, p.o.) on the activity of paclitaxel (4.5 mg/kg, i.v.) against subcutaneously growing Kb-V1 tumor xenografts (mean tumor area ± SEM); animals were treated on days 14, 20, 28 and 35 post tumor implantation. Control *(open circles)*, ME33-1 *(filled squares)*, paclitaxel + vehicle *(filled circles)* and paclitaxel + ME331 *(filled diamonds)*

5.3.3.3 The parent compound tariquidar

As becomes obvious from **Figure 5.17**, concomitant application of tariquidar did not result in a significant retardation of mean tumor progression or in that of individual animals (data not shown). As described for the other modulators, the combination therapy was well tolerated by the animals (data not shown).

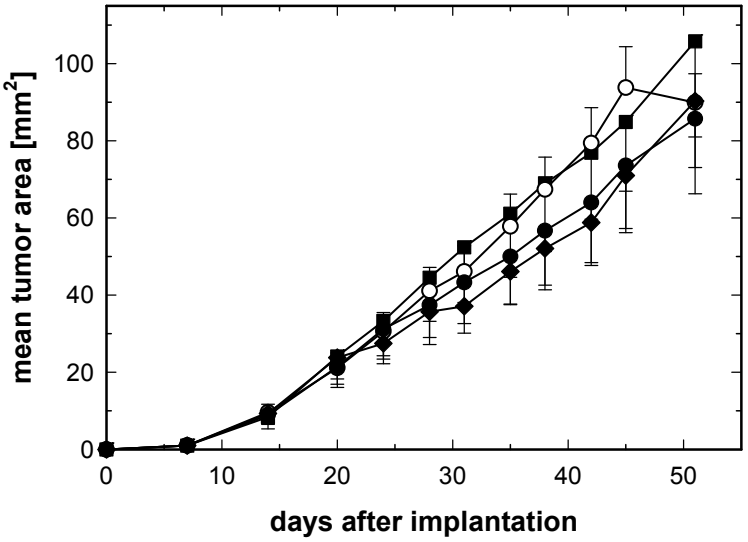

Figure 5.17: Effect of tariquidar (30 mg/kg, p.o.) on the activity of paclitaxel (4.5 mg/kg, i.v.) against subcutaneously growing Kb-V1 tumor xenografts (mean tumor area ± SEM); animals were treated on days 14, 20, 28 and 35 post tumor implantation. Control *(open circles)*, tariquidar *(filled squares)*, paclitaxel + vehicle *(filled circles)* and paclitaxel + tariquidar *(filled diamonds)*

5.4 Summary and conclusions

In order to study the suitability of human Kb-V1 cells for a multidrug resistant subcutaneous tumor model in nude mice, the cells were characterized in vitro first. Therefore, the cells were (among other things) investigated with respect to morphology, growth kinetics, chromosome distribution, chemosensitivity and expression of the relevant efflux transporter.

Growth kinetics as well as the number of chromosomes (indicator for genetic stability) did not vary significantly over various in vitro passages. As expected, the cells were highly resistant against anticancer agents that are known substrates of P-gp such as doxorubicin, topotecan and paclitaxel. The ABCB1-mediated multidrug resistance was reversed by addition of ABCB1 modulators in vitro. For instance, 30 nM of ME33-1 were sufficient to fully restore the sensitivity of Kb-V1 cells against paclitaxel (used at the same concentration as the modulator). Additionally, expression of P-gp remained (after a slight initial reduction) constant after discontinuation of vinblastine exposure. Taken together, the in vitro characterization revealed the suitability of Kb-V1 cells for further in vivo experiments.

The resulting tumors showed stable and reproducible growth rates over multiple passages, sufficiently high tumorigenicity (above 70 %) and were well tolerated by the animals. Additionally, the expression of ABCB1 transporters at the protein level was confirmed in the solid tumors.

In subsequent treatment experiments, the effect of concomitant administration of paclitaxel and various modulators was investigated. Solely the combination of ME30-1 with paclitaxel resulted in a significant retardation of tumor progression. However, only a subgroup of

tumors responded to combined application of ME30-1 and paclitaxel. The other modulators (despite a higher in vitro potency) showed no significant effect in vivo. It may be speculated that varying penetration of the modulators in the tumor tissue is responsible for that outcome. Another possible explanation is that additional mechanism(s) of resistance (independent of ABCB1 transporter expression) could have evolved. It is well know that the majority of clinical tumors exhibit intrinsic or acquired resistance to paclitaxel (McGrogan et al., 2008; Schmidt et al., 2003). Beside the most important cause of resistance, the expression of the ABCB1 transporter, a number of other mechanisms of paclitaxel resistance are described. For instance, over-expression of the HER-*2/neu* protein (Ueno et al., 2000; Yu et al., 1996), of β-tubulin (Kavallaris et al., 1997; Mozzetti et al., 2005) and of the microtubule function regulating tau proteins (Rouzier et al., 2005). On the other hand also deficiencies in the function of the tumor suppressor protein p53 (Giannakakou et al., 2000; Nielsen et al., 1998) and spindle checkpoint proteins such as MAD2 (Kienitz et al., 2005) were reported to confer resistance. Additional mechanisms as the expression of other efflux transporters from the ABCC family (Longley and Johnston, 2005) and the mutation of the target (Berrieman et al., 2004) should also be taken into consideration. If only one of the described mechanisms of paclitaxel resistance has evolved prior or during therapy, even an effective ABCB1 modulator is unable to positively influence tumor growth. The findings are in agreement with a clinical phase I study on tariquidar in combination with the ABCB1 substrate vinorelbine in which 26 patients with various tumors (renal cell carcinoma, breast cancer, adrenocortical cancer, ovarial cancer etc.) were enrolled (Abraham et al., 2009). Although tariquidar increased ^{99m}Tc-sestamibi retention in most tumors and mediated a long-lasting inhibition of P-gp mediated rhodamine efflux from CD56+ cells, only one partial remission (renal carcinoma) was reported.

Another important conclusion can be drawn from experiments with multidrug resistant human 2780AD ovarian carcinoma xenografts in nude mice (Mistry et al., 2001). In this study, mice tolerated 3 cycles (at a 2-day interval!) of a combination of tariquidar (10 mg/kg, i.v.) and 15 mg/kg paclitaxel. That means a higher dosage of paclitaxel should be administered in future studies. Moreover, treatment experiments could be more successful with tumors in the in vivo passage zero (instead of one) due to lower probability of tumors to lose the MDR phenotype or to develop other mechanisms of resistance. Considering the fact that cytostatics are generally more active against small tumors, therapy could be started 7 to 10 days after cell implantation (without a randomization according to tumor area).

5.5 References

Abraham, J.; Edgerly, M.; Wilson, R.; Chen, C.; Rutt, A.; Bakke, S., et al. A phase I study of the P-glycoprotein antagonist tariquidar in combination with vinorelbine. *Clin. Cancer Res.* **2009,** 15, 3574-3582.

Berrieman, H. K.; Lind, M. J.; Cawkwell, L. Do beta-tubulin mutations have a role in resistance to chemotherapy? *Lancet Oncol.* **2004,** 5, 158-164.

Giannakakou, P.; Poy, G.; Zhan, Z.; Knutsen, T.; Blagosklonny, M. V.; Fojo, T. Paclitaxel selects for mutant or pseudo-null p53 in drug resistance associated with tubulin mutations in human cancer. *Oncogene* **2000,** 19, 3078-3085.

Gillet, J. P.; Gottesman, M. M. Mechanisms of multidrug resistance in cancer. In *Multi-drug resistance in cancer*, Zhou, J., Ed. Humana Press: New York, 2010; pp 47-76.

Gleich, O.; Pina, A. L. Protein expression of pigment-epithelium-derived factor in rat cochlea. *Cell Tissue Res.* **2008,** 332, 565-571.

Gleich, O.; Strutz, J. Age dependent changes in the medial nucleus of the trapezoid body in gerbils. *Hear. Res.* **2002,** 164, 166-178.

Gleich, O.; Weiss, M.; Strutz, J. Age-dependent changes in the lateral superior olive of the gerbil (Meriones unguiculatus). *Hear. Res.* **2004,** 194, 47-59.

Gottesman, M. M. Mechanisms of cancer drug resistance. *Annu. Rev. Med.* **2002,** 53, 615-627.

Green, M. C.; Buzdar, A. U.; Smith, T.; Ibrahim, N. K.; Valero, V.; Rosales, M. F., et al. Weekly paclitaxel improves pathologic complete remission in operable breast cancer when compared with paclitaxel once every 3 weeks. *J. Clin. Oncol.* **2005,** 23, 5983-5992.

Higgins, C. F. Multiple molecular mechanisms for multidrug resistance transporters. *Nature* **2007,** 446, 749-757.

Hubensack, M. Approaches to overcome the blood brain barrier in the chemotherapy of primary and secondary brain tumors: modulation of P-glycoprotein 170 and targeting of the transferrin receptor. PhD thesis, University of Regensburg, Regensburg, Germany, 2005.

Hubensack, M.; Müller, C.; Höcherl, P.; Fellner, S.; Spruss, T.; Bernhardt, G., et al. Effect of the ABCB1 modulators elacridar and tariquidar on the distribution of paclitaxel in nude mice. *J. Cancer Res. Clin. Oncol.* **2008,** 134, 597-607.

Jarzyna, P. Preclinical investigations on the effect of the human hyaluronidase Hyal-1 on growth and metastasis of human colon carcinoma. PhD thesis, University of Regensburg, Regensburg, Germany, 2007.

Kavallaris, M.; Kuo, D. Y.; Burkhart, C. A.; Regl, D. L.; Norris, M. D.; Haber, M., et al. Taxol-resistant epithelial ovarian tumors are associated with altered expression of specific beta-tubulin isotypes. *J. Clin. Invest.* **1997,** 100, 1282-1293.

Kienitz, A.; Vogel, C.; Morales, I.; Muller, R.; Bastians, H. Partial downregulation of MAD1 causes spindle checkpoint inactivation and aneuploidy, but does not confer resistance towards taxol. *Oncogene* **2005,** 24, 4301-4310.

Longley, D. B.; Johnston, P. G. Molecular mechanisms of drug resistance. *J. Pathol.* **2005,** 205, 275-292.

Luqmani, Y. A. Mechanisms of drug resistance in cancer chemotherapy. *Med. Princ. Pract.* **2005,** 14 Suppl 1, 35-48.

Mauri, D.; Kamposioras, K.; Tsali, L.; Bristianou, M.; Valachis, A.; Karathanasi, I., et al. Overall survival benefit for weekly vs. three-weekly taxanes regimens in advanced breast cancer: A meta-analysis. *Cancer Treat. Rev.* **2010,** 36, 69-74.

McGrogan, B. T.; Gilmartin, B.; Carney, D. N.; McCann, A. Taxanes, microtubules and chemoresistant breast cancer. *Biochim. Biophys. Acta* **2008,** 1785, 96-132.

Meijerman, I.; Beijnen, J. H.; Schellens, J. H. Combined action and regulation of phase II enzymes and multidrug resistance proteins in multidrug resistance in cancer. *Cancer Treat. Rev.* **2008,** 34, 505-520.

Mellor, H. R.; Callaghan, R. Resistance to chemotherapy in cancer: a complex and integrated cellular response. *Pharmacology* **2008,** 81, 275-300.

Mistry, P.; Stewart, A. J.; Dangerfield, W.; Okiji, S.; Liddle, C.; Bootle, D., et al. In vitro and in vivo reversal of P-glycoprotein-mediated multidrug resistance by a novel potent modulator, XR9576. *Cancer Res.* **2001,** 61, 749-758.

Mozzetti, S.; Ferlini, C.; Concolino, P.; Filippetti, F.; Raspaglio, G.; Prislei, S., et al. Class III beta-tubulin overexpression is a prominent mechanism of paclitaxel resistance in ovarian cancer patients. *Clin. Cancer. Res.* **2005,** 11, 298-305.

Müller, C. New approaches to the therapy of glioblastoma: investigations on RNA interference, kinesin Eg5 and ABCB1/ABCG2 inhibition. PhD thesis, University of Regensburg, Regensburg, Germany, 2007.

Müller, C.; Gross, D.; Sarli, V.; Gartner, M.; Giannis, A.; Bernhardt, G., et al. Inhibitors of kinesin Eg5: antiproliferative activity of monastrol analogues against human glioblastoma cells. *Cancer Chemother. Pharmacol.* **2007,** 59, 157-164.

Nielsen, L. L.; Lipari, P.; Dell, J.; Gurnani, M.; Hajian, G. Adenovirus-mediated p53 gene therapy and paclitaxel have synergistic efficacy in models of human head and neck, ovarian, prostate, and breast cancer. *Clin. Cancer. Res.* **1998,** 4, 835-846.

Reile, H.; Birnböck, H.; Bernhardt, G.; Spruß, T.; Schönenberger, H. Computerized determination of growth kinetic curves and doubling times from cells in microculture. *Anal. Biochem.* **1990,** 187, 262-267.

Romeis, B. *Mikroskopische Technik*. Urban & Schwarzenberg: Munich, Germany, 1989.

Rooney, D.; Czepulkowski, B. *Human cytogenesis: a practical approach.* IRL Press: 1986.

Rouzier, R.; Rajan, R.; Wagner, P.; Hess, K. R.; Gold, D. L.; Stec, J., et al. Microtubule-associated protein tau: a marker of paclitaxel sensitivity in breast cancer. *Proc. Natl. Acad. Sci. U. S. A.* **2005,** 102, 8315-8320.

Schmidt, M.; Bachhuber, A.; Victor, A.; Steiner, E.; Mahlke, M.; Lehr, H. A., et al. p53 expression and resistance against paclitaxel in patients with metastatic breast cancer. *J. Cancer Res. Clin. Oncol.* **2003,** 129, 295-302.

Szakacs, G.; Paterson, J. K.; Ludwig, J. A.; Booth-Genthe, C.; Gottesman, M. M. Targeting multidrug resistance in cancer. *Nat. Rev. Drug Discov.* **2006,** 5, 219-234.

Szakacs, G.; Varadi, A.; Ozvegy-Laczka, C.; Sarkadi, B. The role of ABC transporters in drug absorption, distribution, metabolism, excretion and toxicity (ADME-Tox). *Drug Discov. Today* **2008,** 13, 379-393.

Takahashi, M. *Farbatlas der onkologischen Zytologie*. Perimed Fachbuch Verlagsgesellschaft: Erlangen, 1987.

Ueno, N. T.; Bartholomeusz, C.; Herrmann, J. L.; Estrov, Z.; Shao, R.; Andreeff, M., et al. E1A-mediated paclitaxel sensitization in HER-2/neu-overexpressing ovarian cancer SKOV3.ip1 through apoptosis involving the caspase-3 pathway. *Clin. Cancer. Res.* **2000,** 6, 250-259.

Yu, D.; Liu, B.; Tan, M.; Li, J.; Wang, S. S.; Hung, M. C. Overexpression of c-erbB-2/neu in breast cancer cells confers increased resistance to Taxol via mdr-1-independent mechanisms. *Oncogene* **1996,** 13, 1359-1365.

Chapter 6

6 Studies on the efficacy of ABCB1 modulators by optical imaging of intra-cerebral tumor xenografts in nude mice

6.1 Introduction

The tremendous technological progress has facilitated a number of non-invasive methods for the monitoring of tumor growth and the detection of metastasis (Koo et al., 2006). The techniques with the highest significance in clinical use are Magnetic Resonance Imaging (MRI), Positron Emission Tomography (PET) and Computer Tomography (CT). Since these methods are technically elaborate as well as costly, optical imaging techniques are an attractive alternative in preclinical investigations. The two main forms, fluorescence imaging (FLI) and bioluminescence imaging (BLI), detect low levels of light (or photons) by means of extremely sensitive camera systems. The emission of light follows the excitation of fluorophores (see below) by an external light source (FLI) or originates from the enzymatic oxygenation of a substrate (BLI) (Day et al., 2004). Due to the correlation between light absorption and tissue depth, these imaging modalities are limited to small animal research (or to organs close to the surface of the skin). Since solely the amount of emitted light is quantified, the anatomic resolution of both methods is low.

6.1.1 Fluorescence imaging

As indicated above, the presence of a fluorophore, normally a fluorescent protein, in the investigated tissue is necessary. Nearly 20 years ago, the first protein of this type (GFP, green fluorescent protein) was identified and characterized (Prasher et al., 1992). In the following years, improved biomolecules were engineered with regard to fluorescence intensity (EGFP, enhanced GFP), emission wavelength (DsRed, red fluorescent protein)

and solubility (DsRed2) (Hoffman, 2009). Recently, a red fluorescent protein (termed Katushka) with favorable properties for in vivo imaging has been described (Shcherbo et al., 2007). Among other advantages, its emission maximum is shifted to 635 nm (better tissue penetration) and the extinction coefficient as well as the quantum yield (brighter fluorescence emission) has been substantially increased.
In preclinical oncology, so far especially GFP (Chishima et al., 1997; Peyruchaud et al., 2001) and DsRed2 (Bouvet et al., 2005; Yang et al., 2005) were utilized to monitor tumor growth and metastatic progression.

6.1.2 Bioluminescence imaging

The main advantage of BLI over FLI is the high sensitivity as there is no “light noise” (Koo et al., 2006), i.e. in contrast to FLI, no external light source generates background by auto-fluorescence of biomolecules (e.g. haemoglobin) in animal tissue. BLI becomes possible due to an enzyme-catalysed conversion of chemical energy into light (Wilson and Hastings, 1998). The oxidation of substrates (e.g. luciferin or coelenterazine) is mediated by a class of different enzymes (subsumed under the term luciferases) that can be found in a broad variety of species. Among the most prominent representatives are the North American firefly (*Photinus pyralis*) and the sea pansy (*Renilla reniformis*). Due to the described mechanisms, prior to BLI, the administration of the respective substrate is necessary.
In the literature, various applications of BLI for the monitoring of malignancies (resulting from luciferase expressing tumor cells) in the periphery are described (Jenkins et al., 2005; Pfost et al., 2009). Due to the high sensitivity, even the detection of small metastases in the region of the thorax and the intestine was reported (Scatena et al., 2004; Smakman et al., 2004). Furthermore, orthotopic xenograft models were developed, permitting the observation of tumor progression and the investigation of the efficiency of chemotherapy (Moriyama et al., 2004; Szentirmai et al., 2006).

The aim of this work was to investigate the therapeutic value of tariquidar and ME33-1 (the two ABCB1 modulators out of a small library of tariquidar analogs with the most pronounced effect on paclitaxel brain levels; cf. chapter 4) in the adjuvant therapy of malignant brain tumors. The in our laboratory established intracerebral human glioblastoma model in nude mice (Altenschöpfer, 1998; Fellner et al., 2002) had to be adopted to incorporate the aforementioned fluorescence- and bioluminescence-based methods. The refined model should enable optical in vivo imaging for the detection of a solid tumor at the beginning of the study and monitoring of tumor growth during therapy.

Prior to these studies in nude mice, the generated U-118 transfectants had to be characterized in vitro with regard to transfection efficiency, chemosensitivity and growth kinetics.

6.2 Materials and methods

6.2.1 Drugs and chemicals

Stock solutions of puromycin·2 HCl (Sigma, Deisenhofen, Germany) and geniticin disulfate (G418, Biochrom AG, Berlin, Germany) were prepared with Millipore filtered water and were stored at -20 °C until usage.

For the in vivo investigations, the potassium salt of D-luciferin (Molecular Imaging Products Company, Ann Arbor, MI and SYNCHEM OHG, Felsberg, Germany) was dissolved in PBS (8.0 g/L NaCl, 1.0 g/L $Na_2HPO_4 \cdot 2\ H_2O$, 0.20 g/L KCl, 0.20 g/L KH_2PO_4 and 0.15 g/L $NaH_2PO_4 \cdot H_2O$, pH 7.4) to achieve a concentration of 40 mg/mL. After sterile filtration the solution was aliquoted and stored at -78 °C.

Paclitaxel, doxorubicin as well as the cell culture media EMEM and DMEM were purchased from Sigma (Munich, Germany). For tariquidar and ME33-1 please refer to section 3.2.1. If not stated otherwise chemicals were obtained from Merck (Darmstadt, Germany) in p.a. quality.

6.2.2 Stable transfection of human U-118 MG glioblastoma cells

U-118 MG glioblastoma cells in passage 459 were transfected with the gene encoding the firefly luciferase2 codon optimized for the expression in mammals (pGl4.20 [luc2/Puro] vector; Promega, Mannheim, Germany). Additionally, the respective cells were co-transfected with the gene encoding the red fluorescent protein 2 (the pDsRed2-C1 vector (BD Bioscience Clontech, Heidelberg, Germany) was a gift from ACGT ProGenomics (Halle a. d. Saale, Germany)). In a third approach, transfection of U-118 MG cells (passage 453) was performed with the pTurboFP635-N vector (BioCat, Heidelberg, Germany) containing the gene for the far-red fluorescent protein Katushka. All experiments were performed using the transfection reagent FUGENE® HD (Roche Diagnostics, Mannheim, Germany) according to the following procedure.

U-118 MG cells were seeded into 12-well plates (BD Biosciences, Heidelberg, Germany) at a density of 180 000 cells/well. On the following day, 50 µL of serum-free DMEM containing 1 µg of the respective plasmid DNA in combination with 1.5, 3 or 4.5 µL FUGENE® HD were added drop-wise to each well. 36 hours after transfection, cells were

transferred to 12.5 cm^2 culture flasks (BD Biosciences) containing DMEM supplemented with the appropriate selection agent (cf. section 6.2.3).

After successful transfection was assured in the polyclonal cell populations, homogenous cell clones were isolated by the following procedure. Transfected cells were seeded at a low density (approximately 30 cells/cm^2) into petri dishes containing culture medium with suitable selection antibiotics. After several resistant colonies had reached a sufficient cell number, clones were picked via trypsinization and transferred into 12.5 cm^2 culture flasks. Subsequently, the various cell clones were characterized in vitro and in vivo.

6.2.3 Cell lines and culture conditions

The human glioblastoma cell lines U-87 MG and U-118 MG were grown in Eagle´s Minimum Essential Medium (EMEM, supplemented with 2.2 g/L $NaHCO_3$, 110 mg/L sodium pyruvate and 5 % FCS) and Dulbecco´s Minimum Essential Medium (DMEM, supplemented with 3.7 g/L $NaHCO_3$, 110 mg/L sodium pyruvate and 5 % FCS), respectively. The various transfectants were maintained in the aforementioned culture medium containing the following selection antibiotics (suitable concentrations were determined with wild type cells by means of the crystal violet chemosensitivity assay (data not shown)). Luciferase2 and DsRed2 co-transfected U-118 MG cells: 1.0 µg/L puromycin·2 HCl and 600 µg/L G418; luciferase2 mono-transfectants: 1.0 µg/L puromycin·2 HCl; Katushka mono-transfectants: 0.5 µg/L puromycin·2 HCl.

For further general information concerning the maintenance of cultured cells please refer to section 3.2.2.

6.2.4 Determination of chemosensitivity and in vitro growth characteristics

The assays were performed as described in sections 3.2.5 and 5.2.3.

6.2.5 Intracerebral and subcutaneous implantation of glioblastoma cells into nude mice

The subcutaneous tumor cell implantation is described in section 5.2.9. The intracerebral cell implantation was performed with slight modifications as described previously (Altenschöpfer, 1998; Hubensack, 2005). In brief: nude mice were anesthetized with ketamine/xylazine (cf. section 4.2.5) and the parietal bone was drilled through with a 1 mm diameter bit (3 mm on to the right-hand side of the sagittal line and 3 mm rostral of the coronal line). Subsequently, $5 \cdot 10^4$ transfected glioblastoma cells suspended in 10 µL of the

appropriate serum-free culture medium (prepared as described in section 5.2.9) were injected 3 mm deep into the brain tissue. Finally, the wound was closed with a surgical clamp and the pads of the animals were tattooed to make them individually identifiable.

6.2.6 Detection of Katushka- and DsRed2-mediated fluorescence

6.2.6.1 Fluorescence microscopy

Microscopic images of Katushka- and DsRed2-mediated fluorescence were acquired on a Carl Zeiss Cell Observer (excitation wavelength 545/25 nm, emission wavelength 605/70) and a Leica DM-IRB microscope (Texas Red filter cube; excitation wavelength 560/40 nm, emission wavelength 645/75), respectively.

6.2.6.2 Maestro™ imaging system

The U-118 MG transfectants were additionally investigated by means of fluorescence imaging. Cells were seeded at various densities (DMEM without phenolred) into black, flat-bottomed 96-well plates (Greiner, Frickenhausen, Germany). After an incubation period of at least one hour at 37 °C/5 % CO_2, Katushka- and DsRed2-mediated fluorescence was detected with the Maestro™ in vivo imaging system (500 FL system, Cambridge Research & Instrumentation, Woburn, MA). The selected filter settings enabled excitation in the range of 503 to 555 nm and detection of emitted light at wavelength higher than 580 nm. Data analysis was performed with the Maestro Software 2.6.0B.

6.2.7 Fluorescence imaging of subcutaneous glioblastoma in nude mice

For the in vivo investigations, mice were immobilized by ketamine/xylazine anesthesia (cf. section 4.2.5) and placed on the heated specimen stage (in order to stabilize body temperature during narcosis) of the aforementioned imaging system. For relevant instrument settings please refer to section 6.3.2.2.

6.2.8 Determination of luciferase2 activity

6.2.8.1 In cell lysates

The assays were essentially performed as described previously (Kühnle, 2010). In brief: cells were grown in 24-well plates to an approximate confluence of 80 - 100 %. After a washing step with PBS, cells were incubated with lysis buffer (25 mM Tricine™ (pH 7.8; Sigma, Munich, Germany), 10 % (v/v) glycerol, 2 mM EGTA, 1 % (v/v) Triton X-100

(Sigma), 5 mM $MgSO_4 \cdot 7\ H_2O$, 1 mM dithiotreitol (Sigma)) for 20 min under agitation. Aliquots of the lysates were transferred into polystyrene tubes, 100 µL of a 0.2 mg/mL D-luciferin solution in assay buffer (25 mM Tricine™ (pH 7.8), 5 mM $MgSO_4 \cdot 7\ H_2O$, 2 mM EGTA, 2 mM ATP (Boehringer, Mannheim, Germany), 100 µM coenzyme A (Sigma)) were added and the bioluminescence signal was determined over a period of 10 sec (as relative light units, RLU) on a Lumat LB 9501 (Berthold, Bad Wildbad, Germany).

For reasons of comparison, the obtained RLUs were normalized to the total protein content of each sample, which was determined by the method of Bradford (1976). 95 µL of lysis buffer were added to 5 µL of the various cell lysates and incubated with 1000 µL Bradford´s dye reagent (Bio Rad Laboratories, Munich, Germany) for 10 min. Subsequently, the absorbance at 595 nm was measured with an Uvikon 930 spectrophotometer (Kontron, Düsseldorf, Germany). The protein concentrations were calculated from a standard calibration curve using human serum albumin (Behringwerke, Marburg, Germany) in the range of 1 - 12 µg protein per sample. The normalized RLU values were expressed as $RLU/\mu g_{protein}$.

6.2.8.2 In whole cells

In analogy to the fluorescence based methods, U-118 MG glioblastoma cell transfectants were seeded in black 96-well microtiter plates (Greiner) at various densities (in 150 µL of phenolred-free culture medium). After an incubation period of at least one hour at 37 °C/5 % CO_2, 50 µL of a D-luciferin solution (680 µg/mL) in PBS was added to each well. Bioluminescence imaging was performed after 5 min of incubation by means of a back-illuminated Andor™ DV887 ECS-BV EMCCD camera installed in the housing of the Maestro™ in vivo imaging system. The device as well as additional modifications to reduce extraneous light to a minimum are described in detail in the PhD theses of Peter Jarzyna and Matthias Kühnle (Jarzyna, 2007; Kühnle, 2010). Data acquisition and analysis was performed with the Andor Solis imaging software 4.3.

6.2.9 Bioluminescence imaging of subcutaneous and intracerebral glioblastoma in nude mice

Ketamine/xylazine anesthetized (cf. section 4.2.5) mice received an intraperitoneal injection of freshly thawed solution of 40 mg/mL D-luciferin in PBS (100 µL for subcutaneous, 200 µL when orthotopic tumors were imaged). After a distribution period of 5 min, the mice were placed on the heated specimen stage of the imaging system and the bioluminescence signal was detected with an Andor™ DV887 ECS-BV EMCCD camera.

The relevant instrument settings are specified in the respective paragraphs of the results and discussion section.

6.2.10 Histology

The histological characterization of subcutaneous tumors is described in section 5.2.10. In order to detect intracerebral tumor xenografts, excised brains were fixed in Bouin´s solution and embedded in paraffin according to a standard procedure. In analogy to previous studies (Fellner et al., 2002), 15 serial coronal sections (6 µm) were cut every 200 µm starting and ending 1.5 mm rostral and caudal to the region of tumor cell injection. After deparaffinization and rehydration, samples were stained by the method of Masson-Goldner (Romeis, 1989).

6.2.11 Therapeutic in vivo studies

Compound preparation as well as the application of the ABCB1 modulators (tariquidar or ME33-1) and paclitaxel was performed essentially as described in section 4.2.5 and 5.2.11.

The first bioluminescence in vivo imaging of orthotopic glioblastomas was performed on days 14/15 post tumor cell implantation to assure the presence of a solid tumor. Subsequently, animals were assigned to the various treatment groups with respect to the bioluminescence signal in order to assure a homogeneous distribution of different sized brain tumors.

Mice treated with paclitaxel combined with an ABCB1 modulator (in the following designated as Pac/Mod group) received the modulators (50 mg/kg) by gavage into the stomach 2.5 hours prior to i.v. paclitaxel injection. Compounds were administered on days 16/17, 22/23 (4.0 mg/kg paclitaxel) and 29/30 (3.0 mg/kg paclitaxel) after tumor cell implantation. Mice of the control group were not treated whereas animals of a third group received the respective modulator. Furthermore, animals dosed with paclitaxel alone (the blank solvent of the ABCB1 modulators was additionally administered) were included in the study. Subsequently, tumor progression was monitored by means of BLI on days 27/28 and 34/35 post tumor cell implantation. The instrument settings in all therapeutic in vivo investigations were as follows: exposure time 900 s, EM gain 255, no binning, readout rate 1 MHz at 16 bit, stage height h2c.

At the end of the study (or earlier if the state of health required a preterm intervention (violation of no-go criteria)) animals were killed by cervical dislocation and brains were

dissected. The subsequent confirmation of tumorigenicity by histopathology is described in section 6.2.10.

6.3 Results and discussion

6.3.1 In vivo imaging using fluorescent and bioluminescent U-118 MG glioblastoma cells

In order to establish an intracerebral tumor model, which is accessible to in vivo imaging methods, human U-118 MG glioblastoma cells were transfected with the codon optimized firefly luciferase2. Additionally, the respective cells were co-transfected with gene encoding the red fluorescent protein 2. The generated mono- and co-transfectants were designated U-118 Luc2 and U-118 Luc2/DsRed2, respectively.

6.3.1.1 DsRed2-mediated fluorescence of U-118 transfectants

The success of the transfection procedure was assured in the polyclonal cell populations by means of fluorescence microscopy (see **Figure 6.1**).

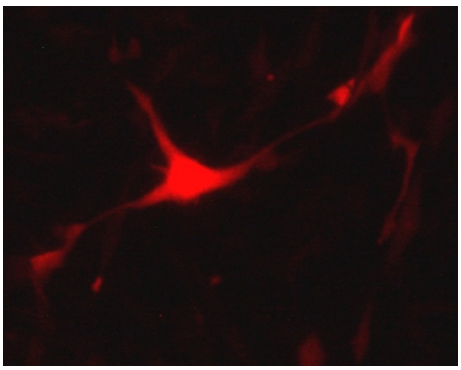

Figure 6.1: DsRed2 fluorescence of polyclonal U-118 Luc2/DsRed2 glioblastoma cells (Leica DM-IRB microscope; Texas Red filter cube: excitation wavelength 560/40 nm, emission wavelength 645/75 nm)

Since the resulting polyclonal U-118 transfectants showed low transfection efficiency as well as variable DsRed2-protein expression, cells were isolated in order to obtain clones with homogenous protein expression. The resulting cell populations were classified with respect to their fluorescence intensity with the Maestro^{TM} in vivo imaging system.

Figure 6.2 shows exemplarily the correlation between DsRed2-mediated light emission and the cell number of U-118Luc2/DsRed2 clones 3, 11 and 13.

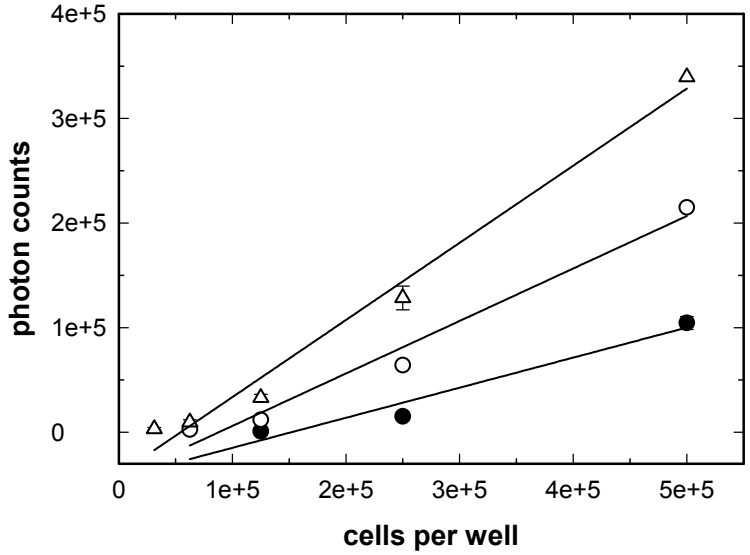

Figure 6.2: Fluorescence of U-118Luc2/DsRed2 clone 3 *(filled circles)*, clone 11 *(open circles)* and clone 13 cells *(open triangles)*; data acquisition with the Maestro™ imaging system; instrument settings: exposure time 5 s for 23 unmixed single images in the range from 580 - 800 nm (10 nm steps)

As becomes obvious, the expression level the DsRed2 protein differed between the investigated clones. Transfectants with a high expression of the red fluorescent protein 2 were selected for further in vitro investigations (see below).

6.3.1.2 Luciferase2-mediated bioluminescence of U-118 transfectants

In order to identify the cell clones with high luciferase activity, the bioluminescence light emission was measured after addition of D-luciferin to the lysates of the corresponding cell populations. Lysates of the wild type cells served as control (see **Figure 6.3**).

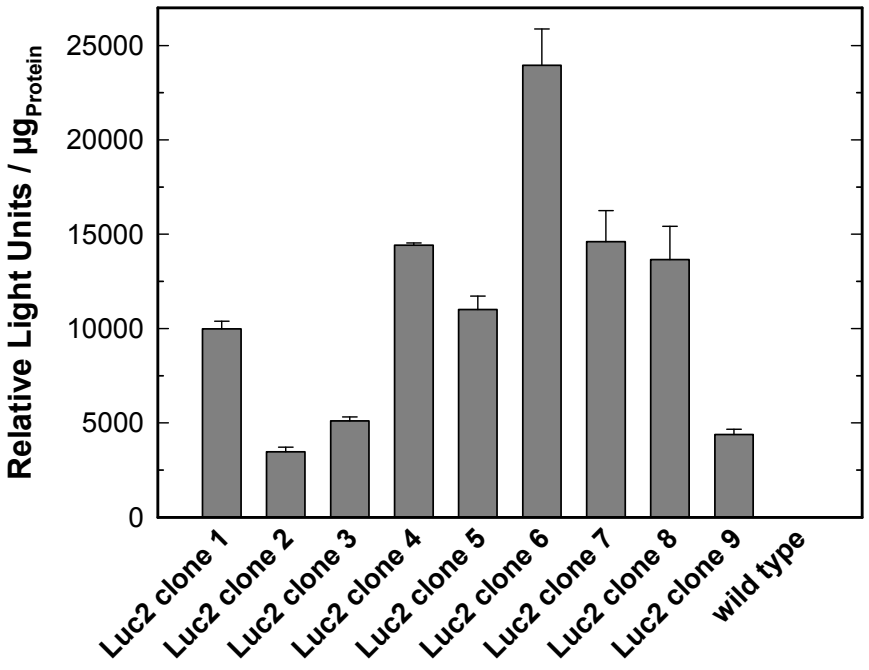

Figure 6.3: Specific luciferase2 activity determined in the lysates of various U-118 Luc2 clones 1 - 9; wild type cells served as negative control. Mean values ± SEM, n = 3

In contrast to the wild type U-118 MG cells, all resistant cell colonies and in particular the clones 4, 6, 7 and 8 showed substantial luciferase2 activity. The transfectants showing paramount bioluminescence were further characterized with the Andor™ EMCCD in vivo imaging system (see below).

By analogy with the mono-transfected cells, the cell lysates of U-118 Luc2/DsRed2 clones were investigated with regard to their luciferase2 activity (see **Figure 6.4**). Also the co-transfected cell populations exhibited sufficient luciferase2 activity. Nevertheless, compared to the mono-transfectants, the bioluminescence-mediated light emission was on average lower. Taking the fluorescence intensity into consideration, promising clones were selected and subsequently imaged.

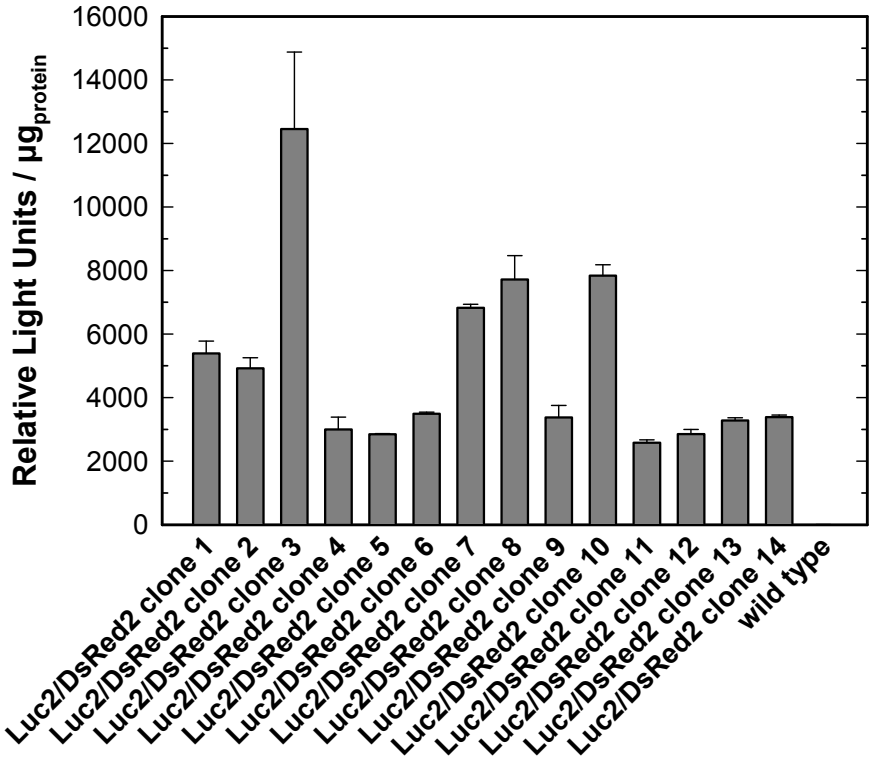

Figure 6.4: Specific luciferase2 activity determined in the lysates of various U-118 Luc2/DsRed2 clones; wild type cells served as negative control. Mean values ± SEM, n = 3

In order to investigate the luciferase2 activity in living cell, the selected transfectants were seeded in 96-well plates at various densities. Additionally, the minimal number of cells necessary for selective detection with the Andor™ EMCCD camera system should be elucidated.

Figure 6.5 shows exemplarily the bioluminescence-mediated light emission of U-118 Luc2 clones 5, 7 and 8. As becomes obvious, the extremely sensitive method allowed the detection of very low cell numbers. Whereas 8,000 – 16,000 cells of clone 5 yielded a passable signal-to-noise ratio, in the case of the clones 7 and 8 the limit of detection was lower than 4,000 cells. Wild type cells gave no signal at all investigated concentrations (up to 250,000 cells/well; data not shown).

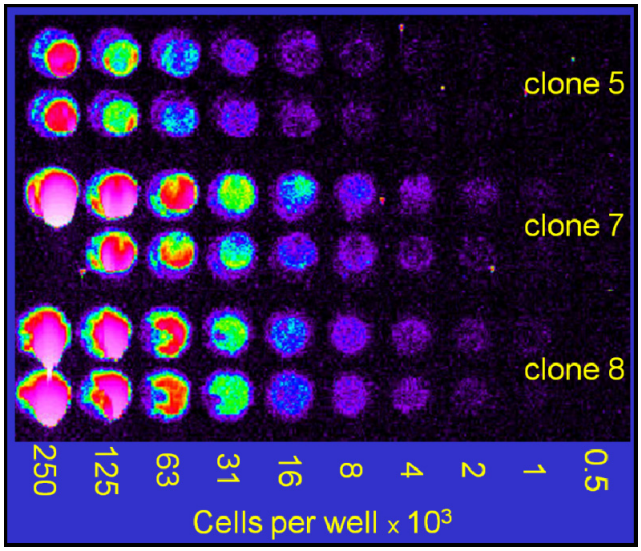

Figure 6.5: Specific luciferase2 activity of the U-118 Luc2 clones 5, 7 and 8 detected in living cells; image acquisition with an Andor™ DV887 ECS-BV EMCCD camera; instrument settings: exposure time 30 min, EM gain 255, no binning, readout rate 1 MHz at 16 bit

There were hints from the literature that the expression level of luciferase in tumor cells can retard growth kinetics of resulting tumors (Brutkiewicz et al., 2007). Consequently, clones with a detection limit ranging from 2,000 – 16,000 cells (U-118 Luc2 clones 5, 7, and 8 as well as U-118 Luc2/DsRed2 clones 3 and 13) were selected for further in vitro and in vivo studies.

6.3.1.3 Chemosensitivity and in vitro growth characteristics of luciferase2 and luciferase2/DsRed2 transfected glioblastoma cells

For a predictive and clinically relevant tumor model it is crucial to exclude an influence of the transfection on both, chemosensitivity and growth behavior. Additionally, the procedure used to obtain different clones (due to the genetic instability and heterogeneity of tumor cells, cf. chapter 5), could promote the selection of a specific subpopulation with significantly altered characteristics. Consequently, both features of the transfectants were investigated and compared to the wild type cells.

Figure 6.6 and **Figure 6.7** show the chemosensitivity of U-118 MG transfectants and wild type cells against doxorubicin and paclitaxel, respectively. The sensitivity of all investigated clones against both chemotherapeutic agents was comparable to the wild type cells.

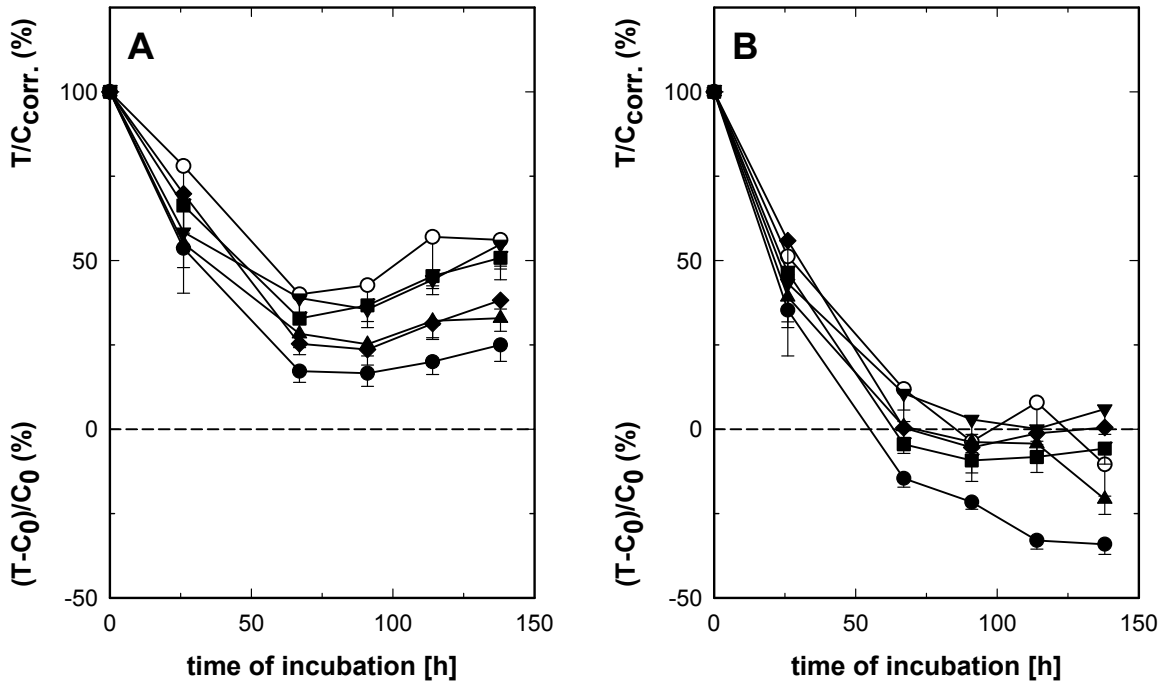

Figure 6.6: Chemosensitivity of U-118 MG cells *(open circles)* (passage 478) and transfectants (passage 16 - 18) against 500 nM **(A)** and 1000 nM **(B)** doxorubicin; U-118 Luc2 clone 5 *(filled inverted triangles)*, U-118 Luc2 clone 7 *(filled squares)*, U-118 Luc2 clone 8 *(filled triangles)*, U-118 Luc2/DsRed2 clone 3 *(filled circles)* and U-118 Luc2/DsRed2 clone 13 *(filled diamonds)*

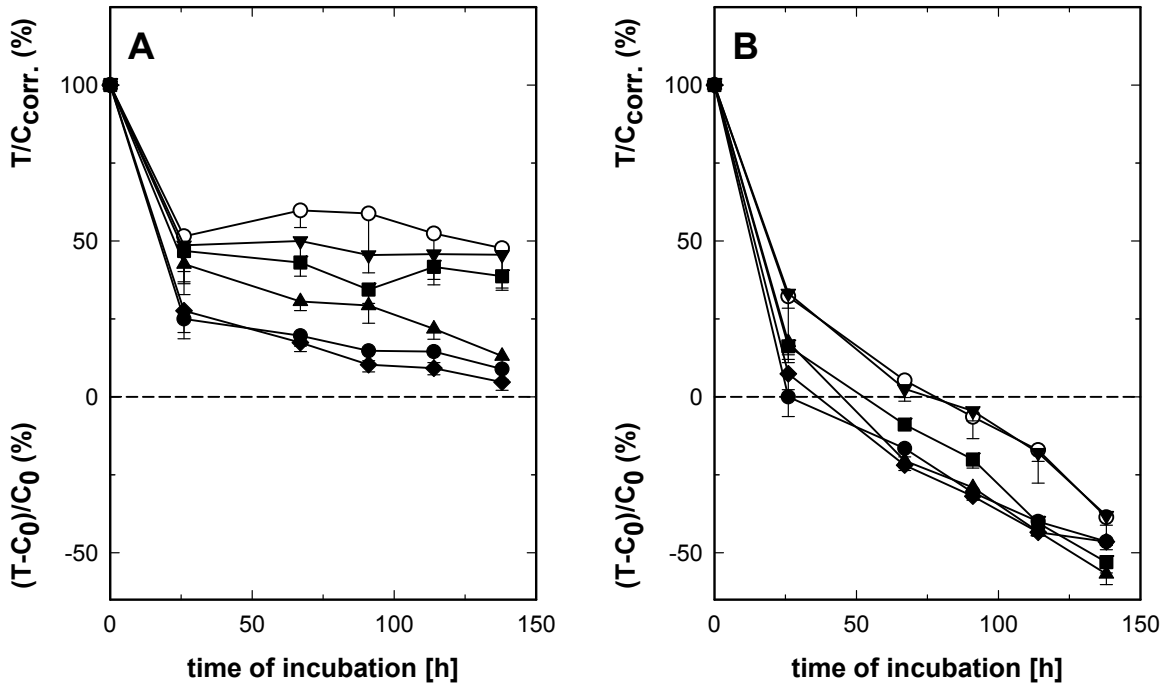

Figure 6.7: Chemosensitivity of U-118 MG cells *(open circles)* (passage 478) and transfectants against 10 nM **(A)** and 50 nM **(B)** paclitaxel; U-118 Luc2 clone 5 *(filled inverted triangles)*, U-118 Luc2 clone 7 *(filled squares)*, U-118 Luc2 clone 8 *(filled triangles)*, U-118 Luc2/DsRed2 clone 3 *(filled circles)* and U-118 Luc2/DsRed2 clone 13 *(filled diamonds)*

Additionally, the proliferation of mono- and co-transfected cells was investigated in vitro (see **Figure 6.8**). Similar to the results of the chemosensitivity investigations, within the range of experimental errors, there was no difference between wild type and luciferase expressing cells with respect to growth kinetics.

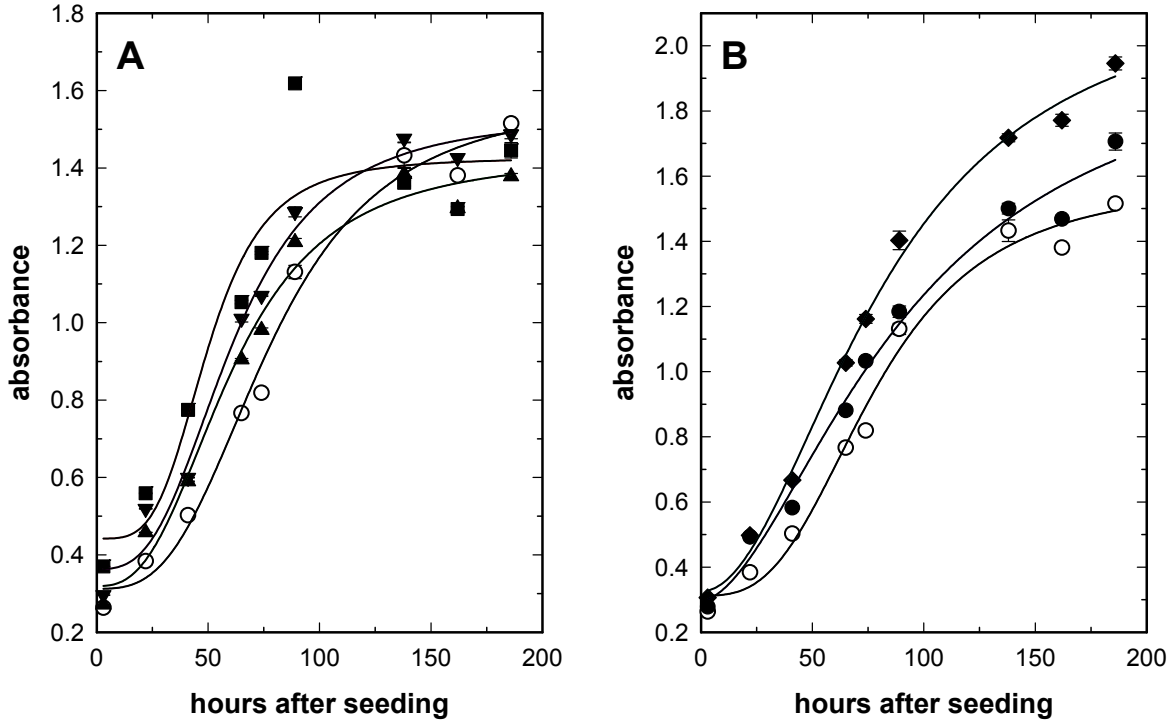

Figure 6.8: Growth kinetics of U-118 transfectants and wild type cells *(open circles)* (passage 480); **A)** U-118 Luc2 clone 5 *(filled inverted triangles)*, U-118 Luc2 clone 7 *(filled squares)* and U-118 Luc2 clone 8 *(filled triangles)*; **B)** U-118 Luc2/DsRed2 clone 3 *(filled circles)* and U-118 Luc2/DsRed2 clone 13 *(filled diamonds)*

6.3.1.4 Tumorigenicity and bioluminescence of subcutaneously implanted transfectants

In the next step, five clones selected during the in vitro investigations were implanted under the thoracic dermis of nude mice to assure stable expression of the transfected genes and detectability under in vivo conditions.

Figure 6.9 and **Figure 6.10** show the bright field as well as the bioluminescence images of nude mice bearing luciferase2 expressing glioblastomas resulting from U-118 Luc2 clone 7 and 8 cells. As becomes obvious, both tumors were identifiable by their specific light signal. For comparison, the tumor area (U-118 Luc2 clone 7: 5 x 5 mm^2, U-118 Luc2 clone 8: 5 x 5 mm^2) was measured with a sliding caliper.

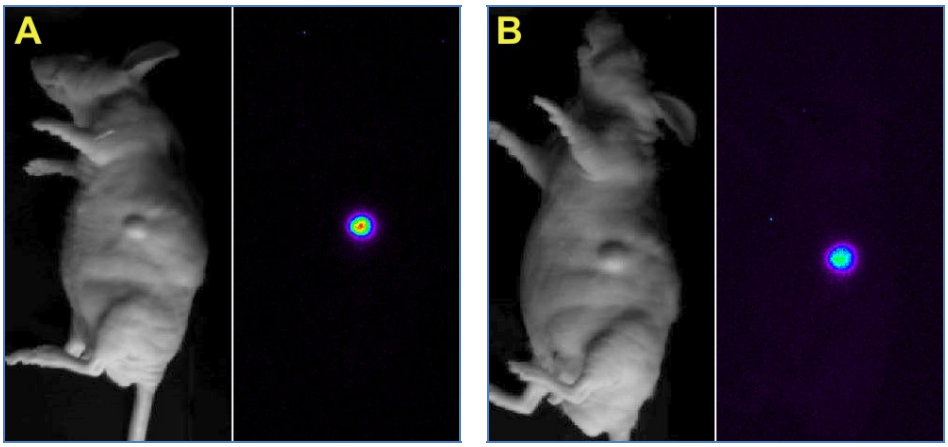

Figure 6.9: Bright field (left) and bioluminescence (right) in vivo images of a nude mouse bearing a subcutaneous U-118 Luc2 clone 7 xenograft 31 **(A)** and 38 days **(B)** after tumor cell implantation; image acquisition was performed 300 s after i.p. injection of D-luciferin. Instrument settings: exposure time 360 s, EM gain 100, no binning, readout rate 1 MHz at 16 bit

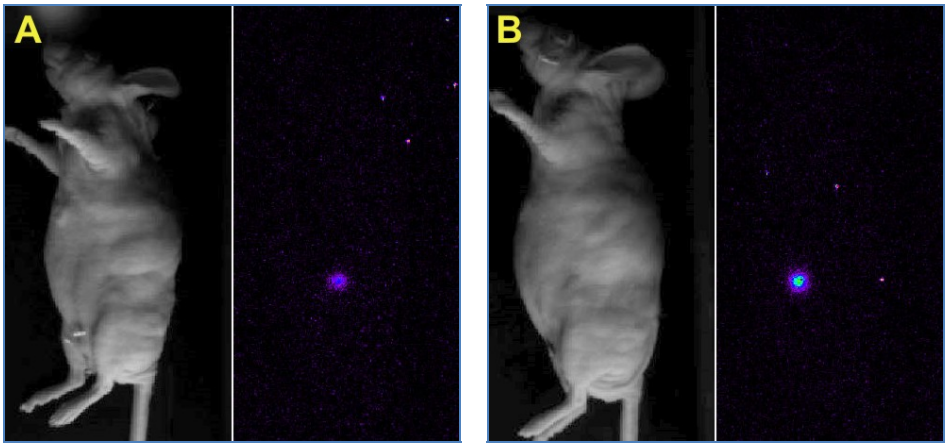

Figure 6.10: Bright field (left) and bioluminescence (right) in vivo images of a nude mouse bearing a subcutaneous U-118 Luc2 clone 8 xenograft 31 **(A)** and 38 days **(B)** after tumor cell implantation; image acquisition was performed 900 s after i.p. injection of D-luciferin. Instrument settings: exposure time 360 s, EM gain 255, no binning, readout rate 1 MHz at 16 bit

As expected due to the results of the in vitro investigations, xenografts resulting from U-118 Luc2 clone 5 cells showed a lower light intensity compared to clone 7 and 8. In contrast, U-118 Luc2/DsRed2 clone 3 tumors were not detectable by bioluminescence in vivo imaging (data not shown). In the case of clone 13 the tumors regressed before a first BLI could be performed (see below).

For grading of the transfectants, tissue samples were excised and histologically characterized. **Figure 6.11** shows exemplarily the histology of subcutaneous U-118 Luc2/DsRed2 clone 13 and U-118 Luc2 clone 7 xenografts, which did not differ from the wild type. Typical for subcutaneous, malignant U-118 MG glioblastoma is a rich stroma in which the anisomorphic cells, containing prominent nucleoli, are embedded.

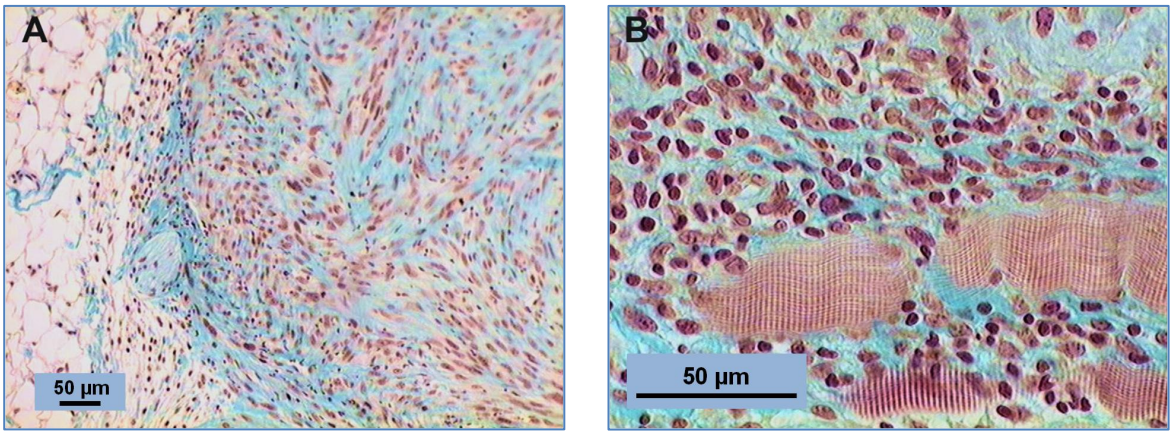

Figure 6.11: Masson-Goldner staining of luciferase2 expressing subcutaneous tumors; **A)** U-118 Luc2/DsRed2 clone 13 derived tumor located in the subepidermal adipose tissue (objective 10x); **B)** Detail view of a U-118 Luc2 clone 7 xenograft infiltrated by striated muscle (objective 40x)

In contrast to the encouraging results concerning transfection efficiency, chemosensitivity, growth kinetics and detectability, the tumorigenicity was variable and low (cf. **Figure 6.12**). None of the investigated glioblastoma variants showed stable and reproducible growth rates as required for the planned preclinical investigations. In general, after an initial phase of tumor formation (in ≥ 80 % of the animals), eventually the majority of tumors regressed. This behavior was especially pronounced for the co-transfectants (D, E). None of the U-118 Luc2 clone 5, 7 and 8 tumors (A - C) reached a tumor area ≥ 40 mm^2 within 80 days after subcutaneous cell implantation.

Nevertheless, it was speculated that the tumorigenicity of the glioblastoma cells might be higher when growing in their orthotopic localization. Consequently, the two most promising cell clones, U-118 Luc2 clone 7 and 8, were implanted into the brain of nude mice.

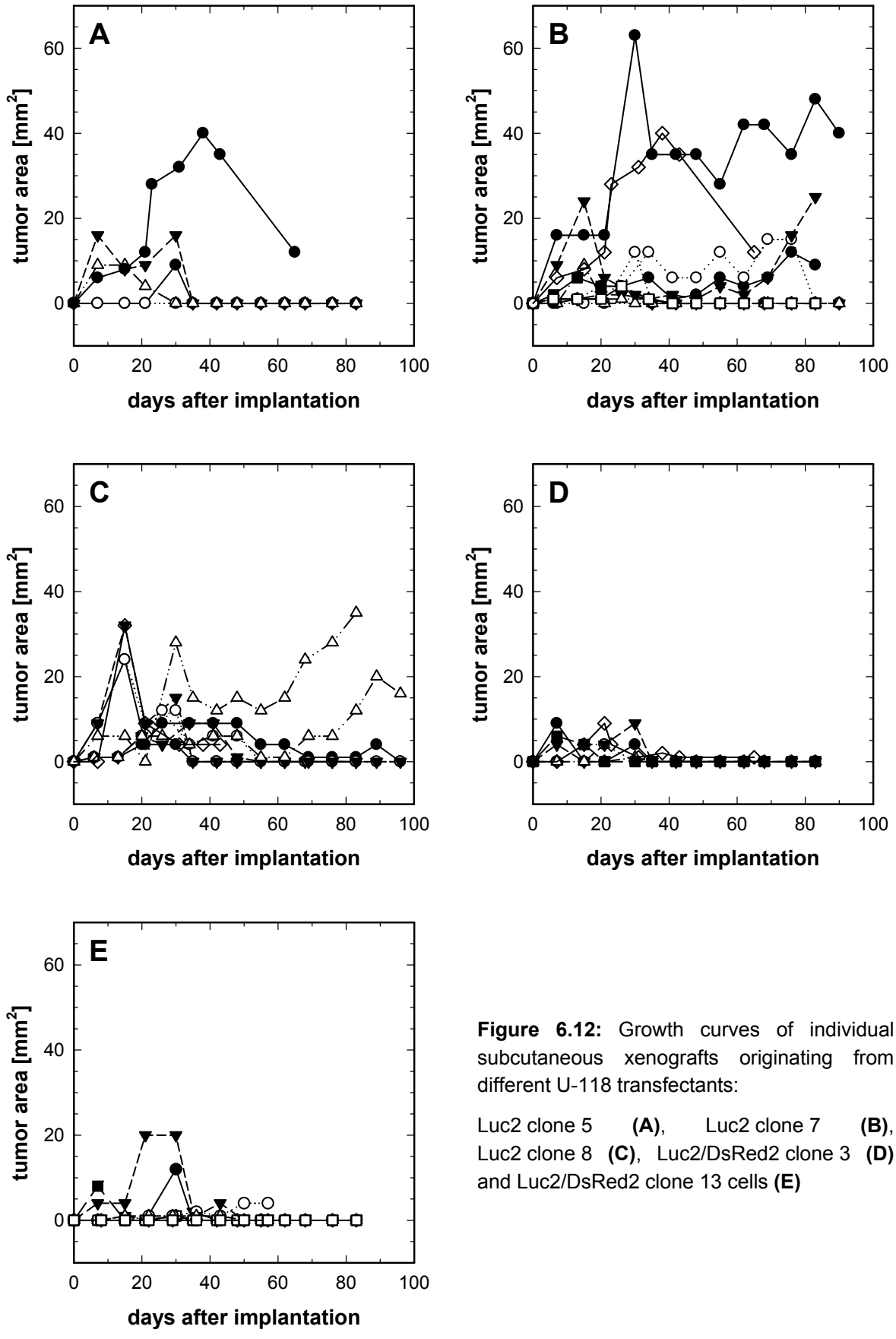

Figure 6.12: Growth curves of individual subcutaneous xenografts originating from different U-118 transfectants:

Luc2 clone 5 **(A)**, Luc2 clone 7 **(B)**, Luc2 clone 8 **(C)**, Luc2/DsRed2 clone 3 **(D)** and Luc2/DsRed2 clone 13 cells **(E)**

6.3.1.5 Tumorigenicity and bioluminescence of intracerebrally implanted transfectants

By analogy with the investigation of subcutaneous tumors, bioluminescence-mediated light emission was detected with the Andor™ EMCCD camera in the living animal.

Figure 6.13 and **Figure 6.14** show at one animal the results obtained with U-118 Luc2 clone 7 and 8 xenografts. The tumor "progression" was monitored over a period of 3 - 4 weeks. 9 days after orthotopic tumor cell injection, in 3 of 6 mice (both subgroups) intracerebral tumors were detectable by their specific light signals. In contrast to U-118 Luc2 clone 7 tumors (solely 2 tumors detectable at day 15), the signal emitted by clone 8 tumors slightly intensified until day 16 post cell implantation. Since no signal was observed in the group of animals transplanted with clone 7 at day 28, the ultimate tumor monitoring was brought forward to day 23 in the U-118 Luc2 clone 8 group. Similarly, only in one animal a reduced tumor-induced light signal (depicted in Figure 6.14 C) was observed.

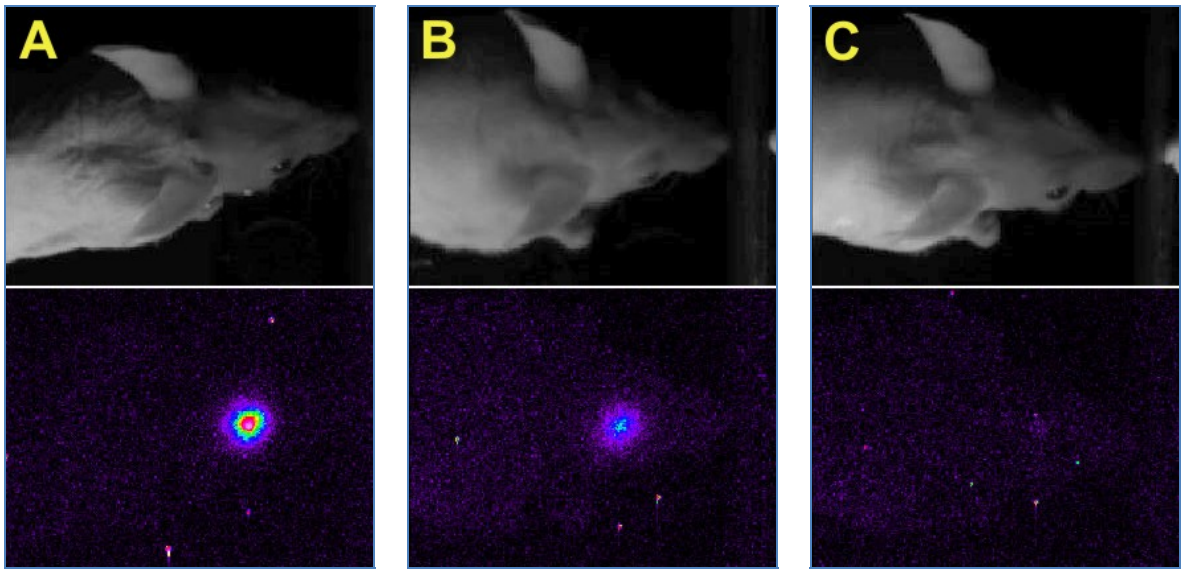

Figure 6.13: Bright field (top) and bioluminescence (bottom) in vivo images of a nude mouse bearing an intracerebral U-118 Luc2 clone 7 xenograft; image acquisition was performed 9 **(A)**, 15 **(B)** and 28 days **(C)** after tumor cell implantation. Instrument settings: exposure time 900 s, EM gain 255, no binning, readout rate 1 MHz at 16 bit

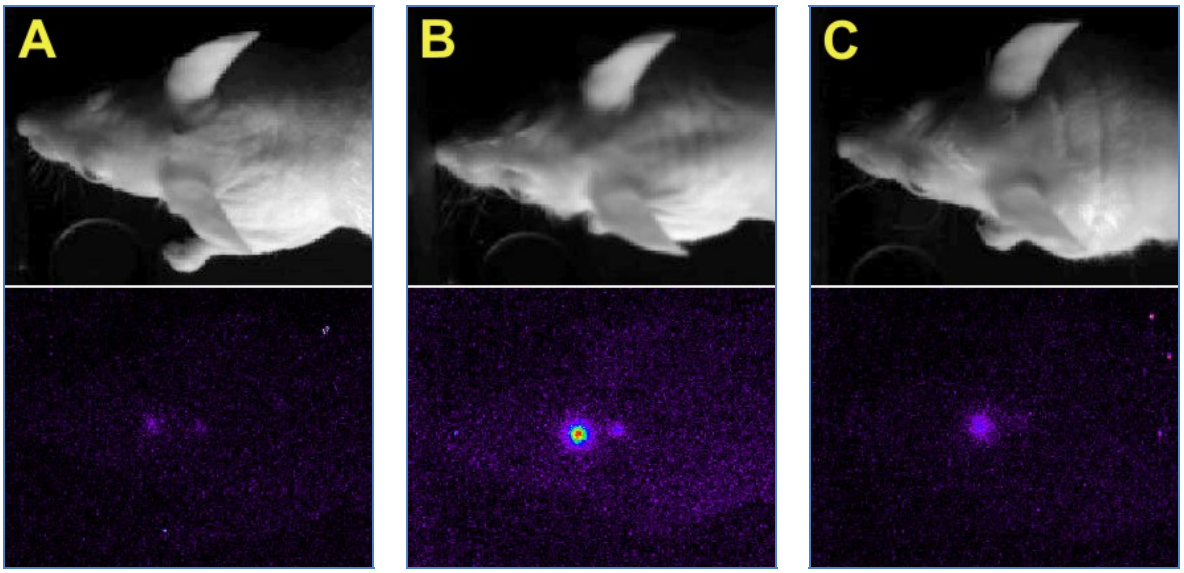

Figure 6.14: Bright field (top) and bioluminescence (bottom) in vivo images of a nude mouse bearing an intracerebral U-118 Luc2 clone 8 xenograft; image acquisition was performed 9 **(A)**, 16 **(B)** and 23 days **(C)** after tumor cell implantation. Instrument settings: Exposure time 900 s, EM gain 255, no binning, readout rate 1 MHz at 16 bit

To explore, if the reduced light signal resulted from tumor regression or the loss of luciferase2 expression in tumor tissue, the brains were dissected. Serial coronal sections (mean distance 200 µm; cf. section 6.2.10) of the brains were prepared and investigated by histology. No tumor tissue was found in the brains of nude mice when suspensions of U-118 Luc2 clone 7 cells had been injected. In contrast, malignant tissue was detected in one section of the brains of U-118 Luc2 clone 8 glioblastoma bearing animals (see **Figure 6.15**).

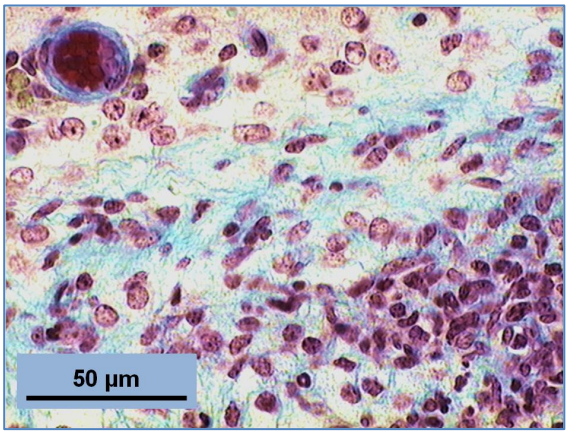

Figure 6.15: Masson-Goldner staining of luciferase2 expressing intracerebral U-118 Luc2 clone 8 xenograft; the transition between murine brain tissue and malignant human tumor tissue is depicted (objective 40x).

The findings are in agreement with the results of experiments performed with the subcutaneous tumors and confirm that the weak bioluminescence resulted from impaired tumor cell proliferation in vivo rather than from the loss of luciferase2 expression.

Since the luciferase2 and DsRed2 co-expressing U-118 tumors were not detectable in vivo (neither by bioluminescence nor by fluorescence imaging, data not shown), a third approach was pursued that is presented in the next section.

6.3.2 In vivo imaging of Katushka-mediated fluorescent U-118 MG glioblastoma cells

In a final approach, U-118 MG cells were transfected with the gene encoding the far-red fluorescent protein termed Katushka (the generated mono-transfectants were designated U-118 Katushka).

6.3.2.1 Katushka-mediated fluorescence of U-118 transfectants in vitro

In analogy to the DsRed2 expressing cells, resistant cell populations were isolated from the selection medium in order to obtain clones with a high protein expression. The subsequent characterization by means of fluorescence microscopy is presented in **Figure 6.16** with clone 6 as an example. Compared to the DsRed2 expressing transfectants, the resulting Katushka clones showed higher transfection efficiency as well as brighter fluorescence intensity.

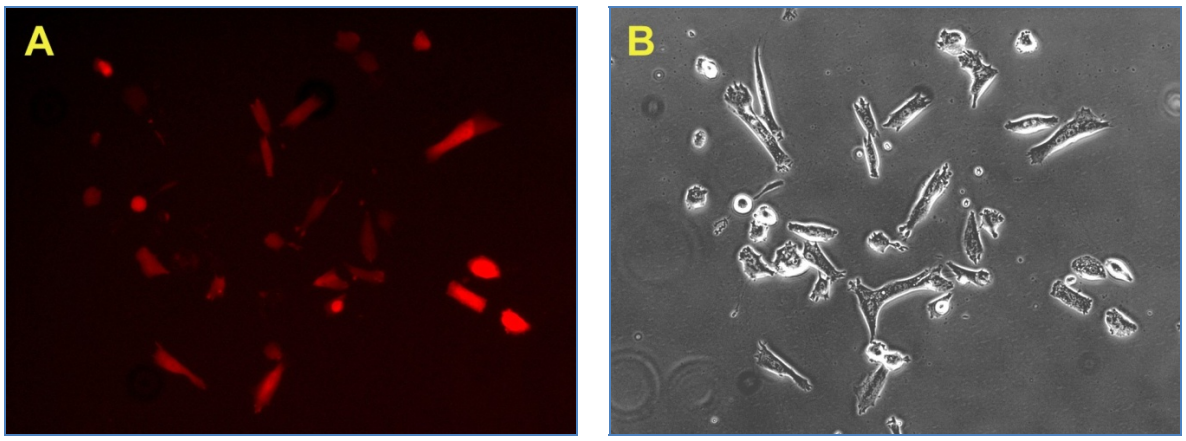

Figure 6.16: Katushka-mediated fluorescence **(A)** and phase contrast **(B)** image of U-118 Katushka clone 6 cells (Carl Zeiss Cell Observer; excitation wavelength 545/25 nm, emission wavelength 605/70 nm)

Subsequently, U-118 Katushka clones 1 - 9 were investigated with respect to their fluorescence intensity using the Maestro™ imaging system. As shown in **Figure 6.17**, the Katushka-mediated fluorescence emission correlated with the cell number in a linear manner. Especially U-118 Katushka clone 9 cells exhibited a supreme fluorescent intensity that was approximately 10-fold higher than observed in the DsRed2 transfectants (cf. **Figure 6.2**).

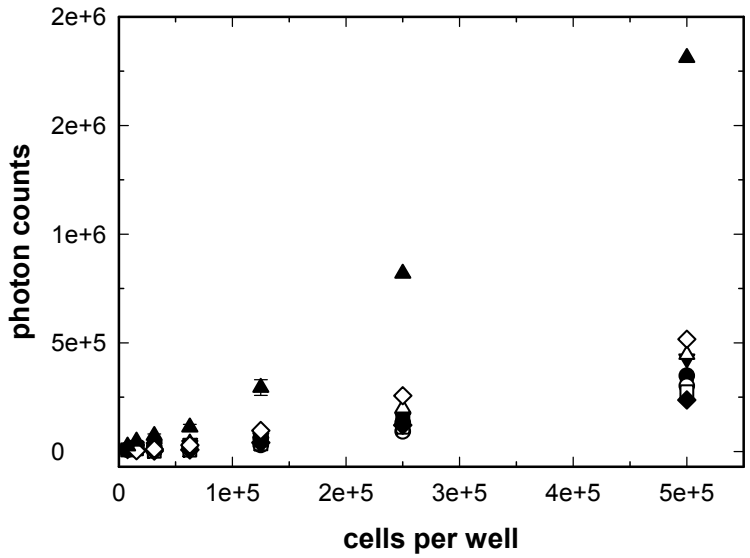

Figure 6.17: Fluorescence of U-118 Katushka cells; clone 9 *(filled triangles)* showed a pronounced higher expression of the Katushka protein compared to the other clones 1 - 8. Data acquisition with the Maestro™ imaging system; instrument settings: exposure time 5 s for 21 unmixed single images in the range from 600 - 800 nm (10 nm steps)

The U-118 Katushka clones 2, 6, 8 and 9 were selected for further in vivo studies.

6.3.2.2 In vivo imaging of subcutaneous tumors

After subcutaneous implantation of the genetically engineered glioblastoma cells into nude mice, only U-118 Katushka clone 2 and 6 cells were tumorigenic. As in the previous experiments, the malignant phenotype was confirmed by histopathology (see **Figure 6.18**).

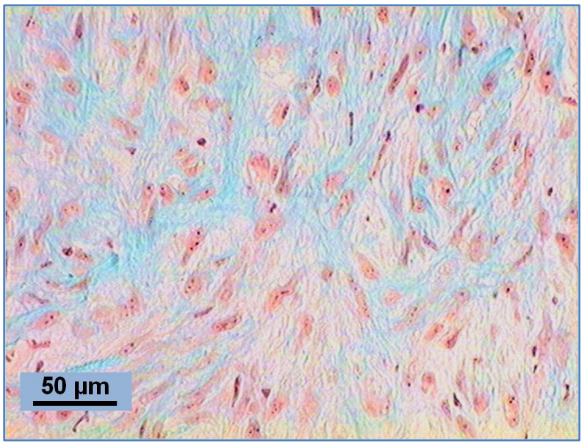

Figure 6.18: Masson-Goldner staining of a subcutaneous U-118 Katushka clone 2 tumor (objective 20x)

In contrast to the DsRed2 expressing tumors, U-118 Katushka clone 2 and 3 xenografts were detectable under in vivo conditions by means of the Maestro™ imaging device (see **Figure 6.19**). Although the fluorescence intensity was sufficient for subcutaneous investigations, the signal-to-noise ratio of these clones was too low for intracerebral studies. Unfortunately, clone 9 which was superior in terms of fluorescence intensity and thus most promising with respect to intracranial detection, was not tumorigenic.

Additionally, the irregular and discontinuous growth behavior (cf. **Figure 6.20**) did not favor elaborate orthotopic experiments.

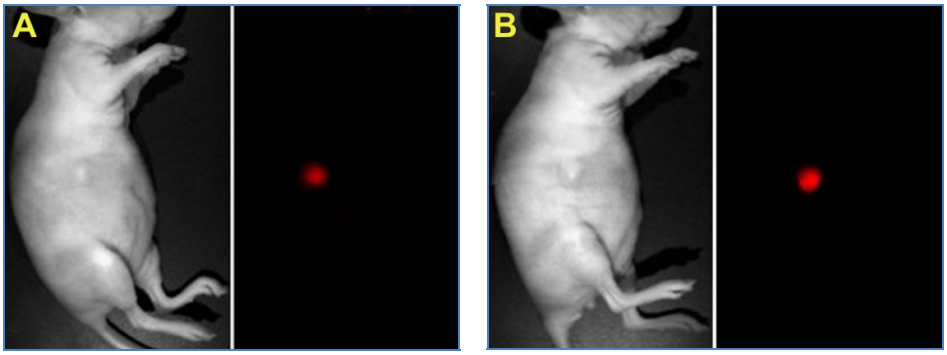

Figure 6.19: Bright field (left) and fluorescence (right) in vivo images of a nude mouse bearing a subcutaneous U-118 Katushka clone 2 xenograft; image acquisition was performed 16 **(A)** and 27 days **(B)** after tumor cell implantation. Instrument settings: exposure time 4 s for 23 unmixed single images in the range from 580 - 800 nm (10 nm steps)

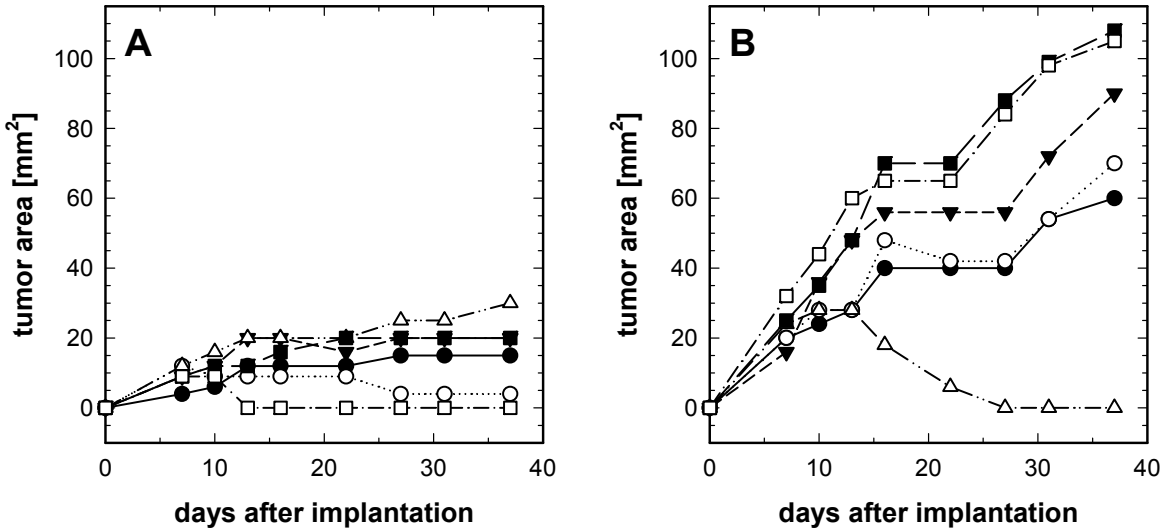

Figure 6.20: Growth curves of individual subcutaneous tumors originating from U-118 Katushka clone 2 **(A)** and clone 6 **(B)** cells

Since none of the nine U-118 MG transfectants (genetically engineered by 3 different approaches) showed sufficient tumorigenicity and persistent in vivo growth, the wild type glioblastoma cells were implanted subcutaneously (see **Figure 6.21**). Although the cell line was tumorigenic in previous studies (Altenschöpfer, 1998; Fellner et al., 2002), problematic growth characteristics were observed. Initially, in 6 of 7 mice a small tumor was formed. 4 xenografts regressed untimely and only two glioblastomas grew very slowly after a lag-period of approximately two months. It may be speculated that permanent subculturing (≥ 450 in vitro passages) or irregularities in the storage conditions (liquid nitrogen) may

have accounted for this outcome. In more recent investigations (Müller, 2007) similar problems concerning the in vivo growth behavior were reported with U-118 MG cells transfected with the gene encoding for EGFP.

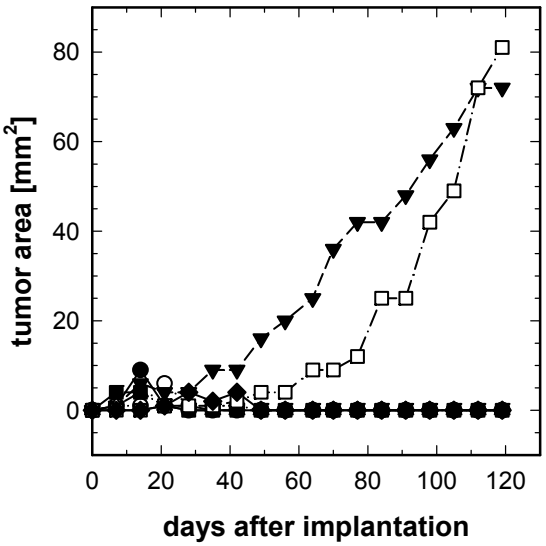

Figure 6.21: Growth curves of individual tumors originating from U-118 MG cells

6.3.3 Effect of concomitant application of paclitaxel and ABCB1 modulators on the growth of intracerebral human glioblastoma

The efforts to establish an intracerebral tumor model aimed at the evaluation of the therapeutic value of new ABCB1 modulators in combination with cytostatics in the treatment of malignant brain tumors. As presented above, these efforts failed due to insufficient tumorigenicity of the genetically engineered U-118 glioblastoma cells (the same holds for the wild type). Fortunately, Matthias Kühnle was successful in analogous attempts using highly tumorigenic U-87 MG cells (Kühnle, 2010). Subsequently, the U-87 Luc2 clone 3 xenografts (engineered and characterized as part of his PhD thesis) were utilized for treatment experiments investigating the effect of concomitant application of paclitaxel and ABCB1 modulators on intracerebral tumor growth. The extensive transplantation and in vivo imaging procedures were done in collaboration with Matthias Kühnle.

6.3.3.1 Chemosensitivity of luciferase2 expressing human U-87 MG glioblastoma cells

In a proof of principle study demonstrating the therapeutic value of ABCB1 inhibition at the BBB, it is crucial to exclude two possibilities. Firstly, increased paclitaxel toxicity due to inhibition of ABCB1 transporters in the cell membrane of glioblastoma cells (as seen for MDR Kb-V1 cells; cf. chapter 5); secondly, inherent toxicity of the P-gp modulator on the

utilized cells. **Figure 6.22** shows that tariquidar and ME33-1 neither increased the toxicity of paclitaxel (A - C) nor affected cell growth significantly when used alone (D).

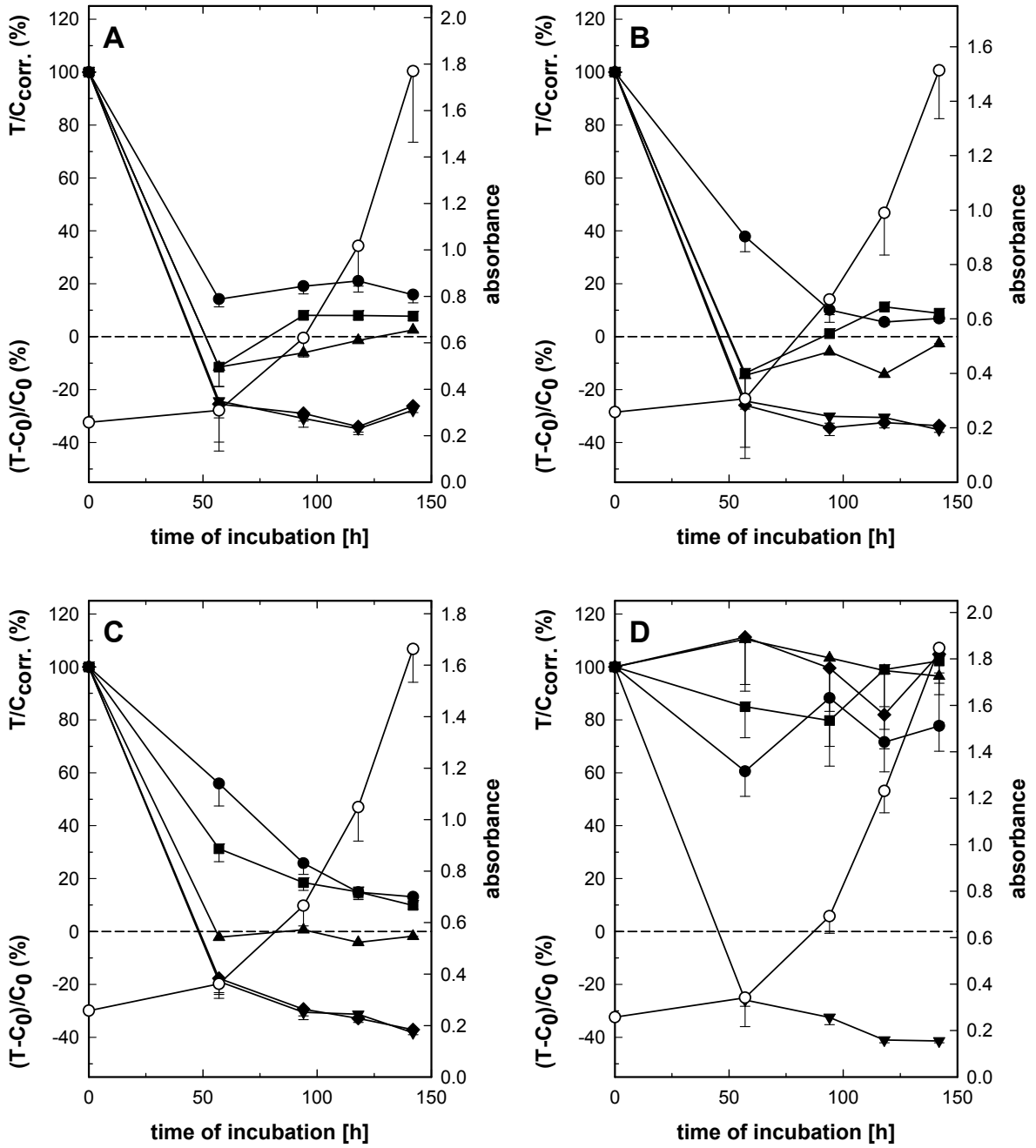

Figure 6.22: Chemosensitivity of U-87 Luc2 clone 3 (passage 5); vehicle *(open circles)*; **A)** Paclitaxel at various concentrations: 5 nM *(filled circles)*, 10 nM *(filled square)*, 50 nM *(filled triangles)*, 100 nM *(filled diamonds)* and 500 nM *(filled inverted triangles)*; respective concentrations of paclitaxel combined with 100 nM of ME33-1 **(B)** or tariquidar **(C)**; **D)** ABCB1 modulator alone: 100 nM *(filled circles)* and 500 nM *(filled squares)* of ME33-1; 100 nM *(filled triangles)* and 500 nM *(filled diamonds)* of tariquidar; 100 nM of vinblastine served as positive control *(filled inverted triangles)*.

6.3.3.2 Confirmation of tumorigenicity by bioluminescence imaging

A central objective of the new study design was to assure definitely the presence of a solid tumor at the beginning of treatment.

Figure 6.23 shows a characteristic example of the initial tumor monitoring. Up to 4 anesthetized mice (individually identifiable via tattooed pads) were placed on the specimen stage (segregated by a cross-shaped shield to eliminate falsification of the results by stray light) of the in vivo imaging system. In this case, the tumors were exemplarily classified into the categories small, medium and large (in the following order: upper left, lower right and lower left quadrant; the animal in the upper right corner was excluded due to the diffuse and undefined signal). Accordingly, the animals were assigned to the various treatment groups guaranteeing a homogeneous distribution with respect to the intensities of the tumor signal.

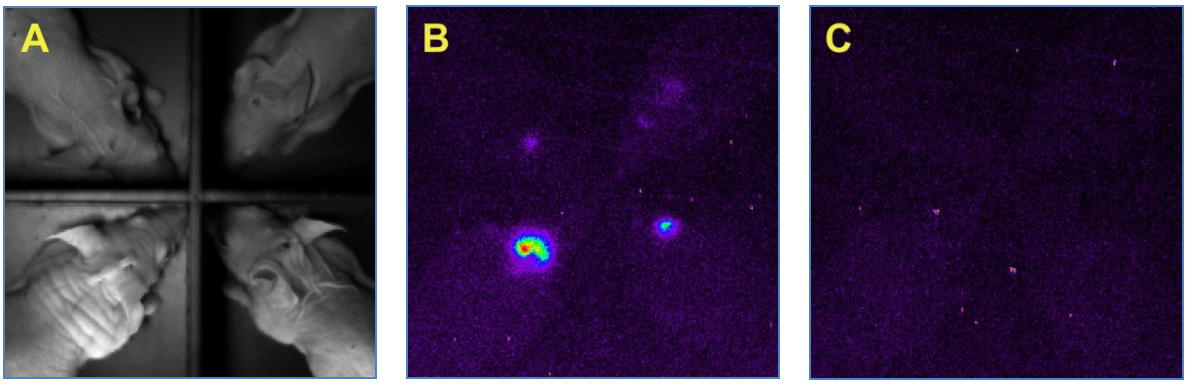

Figure 6.23: Confirmation of solid intracerebral U-87 Luc2 clone 3 tumors by means of bioluminescence in vivo imaging 14 days after cell implantation; bright field **(A)**, bioluminescence **(B)** and background image **(C)**; in all subsequent investigations, the instrument settings were kept constant: exposure time 900 s, EM gain 255, no binning, readout rate 1 MHz at 16 bit, stage height h2c

6.3.3.3 Observation of tumor growth by bioluminescence imaging

After the allocation to the respective treatment groups, the different test compounds were administered three times on a weekly schedule as described in detail in section 6.2.11. Untreated animals served as control.

Tumor progression was monitored by means of bioluminescence imaging on the days 27/28 and 34/35 after tumor cell implantation (see **Figure 6.24**). As becomes obvious, final image acquisition was impossible in the majority of the untreated mice. The rapid tumor progression resulted in a pronounced loss of body weight and required intervention (killing of the animals in order to avoid a violation of no-go criteria) in a number of animals. Additionally, debilitated animals were prone to demise during anesthesia. Since

intact blood circulation is necessary for the distribution of D-luciferin, the respective imaging data were useless. As expected, also the animals that received tariquidar, ME33-1 and paclitaxel showed strong luminescent signals already on days 27/28 after cell implantation. Consequently, an impact of these compounds on tumor progression is highly unlikely. In contrast, in the group treated with paclitaxel and tariquidar, final imaging was possible in 7 of 8 animals. Additionally, in three mice only a moderate light signal was detected that in turn indicates a retarded tumor progression. Similar results were observed when mice were dosed with paclitaxel and ME33-1. One tumor stagnated while in two animals a regression of the light signals was detected (cf. also section 6.3.3.4). In general, the mice in the Pac/Mod groups were in a better state of health compared to the other subgroups.

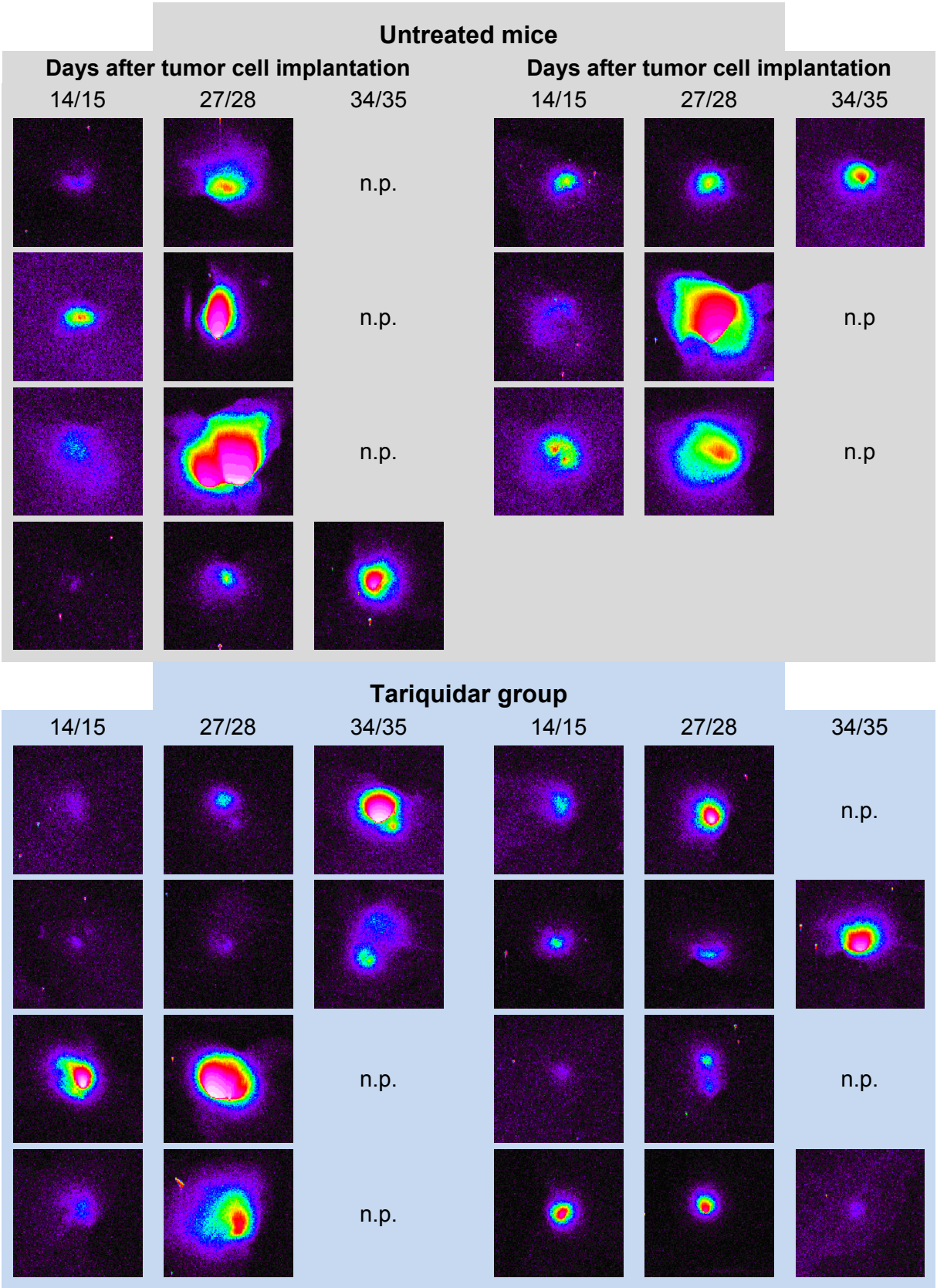
Untreated mice
Days after tumor cell implantation
14/15
27/28
34/35
n.p.
n.p.
n.p.
Days after tumor cell implantation
14/15
27/28
34/35
n.p
n.p
Tariquidar group
14/15
27/28
34/35
n.p.
n.p.
14/15
27/28
34/35
n.p.
n.p.

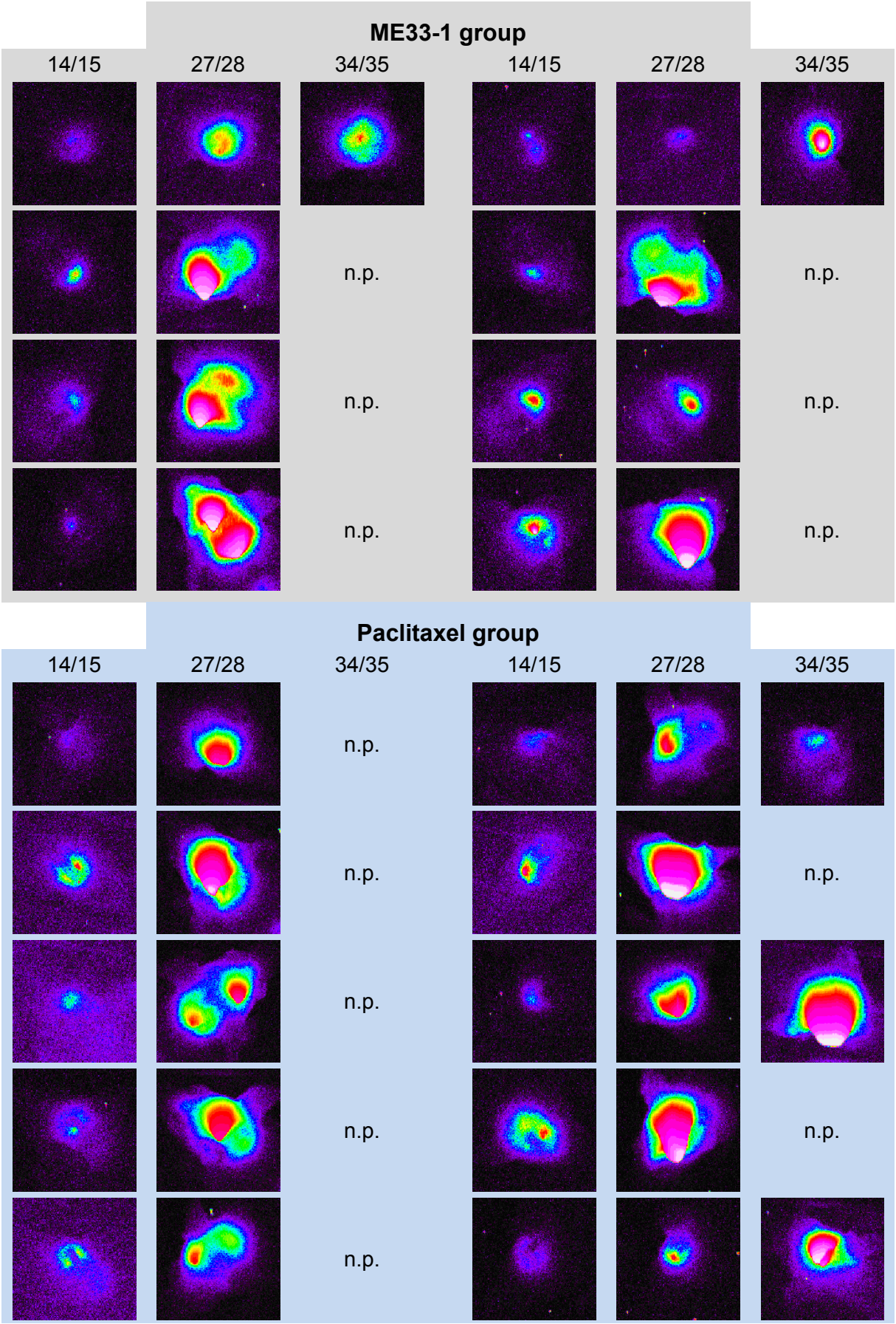
ME33-1 group
14/15
27/28
34/35
14/15
27/28
34/35
n.p.
n.p.
n.p.
n.p.
n.p.
n.p.
Paclitaxel group
14/15
27/28
34/35
14/15
27/28
34/35
n.p.
n.p.
n.p.
n.p.
n.p.
n.p.

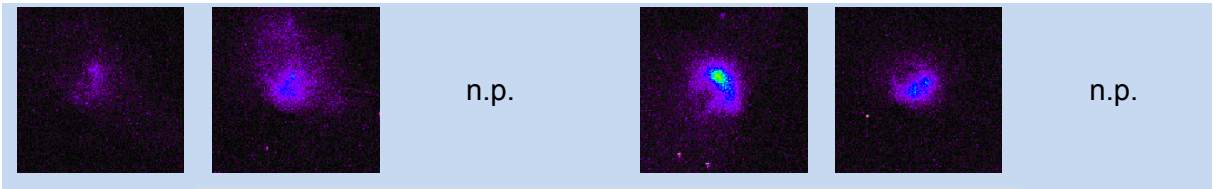

Paclitaxel + Tariquidar group

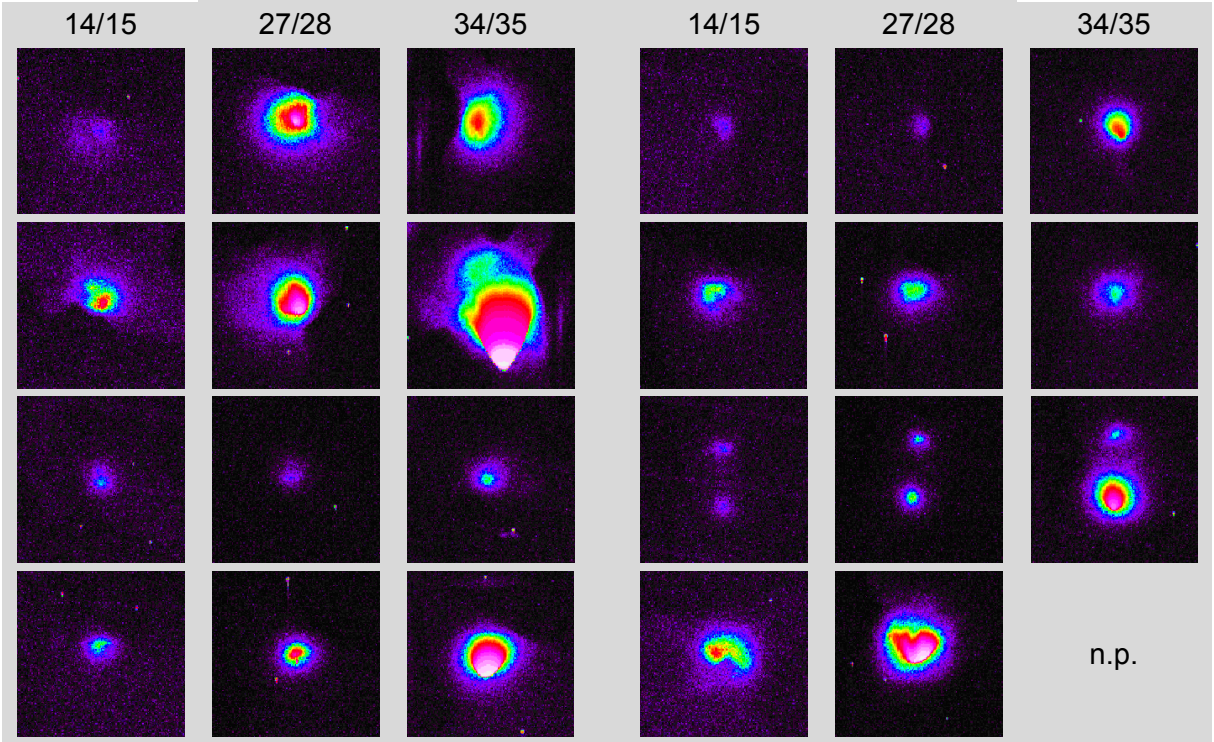

Paclitaxel + ME33-1 group

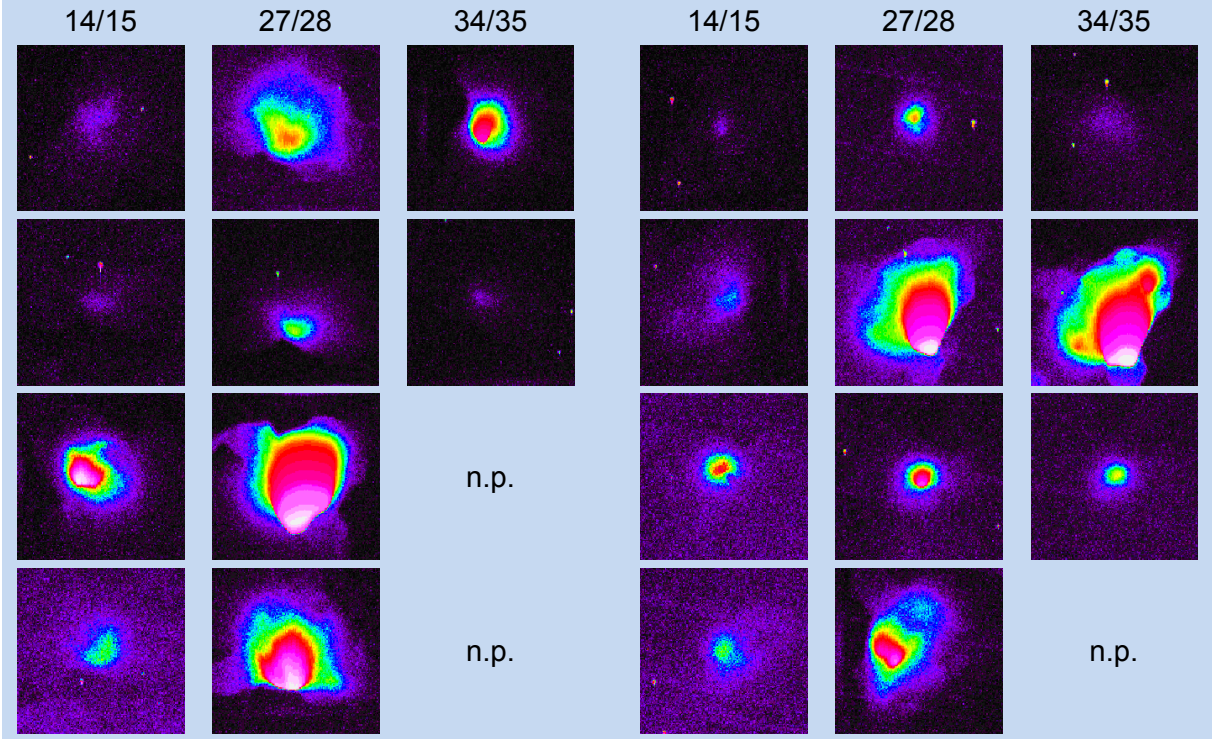

Figure 6.24: Specific light signals of intracerebral U-87 Luc2 clone 3 tumors in the various treatment groups detected by means of bioluminescence in vivo imaging; n.p.: it was not possible to perform the final image acquisition procedure successfully due to preterm death of an animal (e.g. during anesthesia or if the state of health (rapid tumor progression) required intervention (violation of no-go criteria)).

6.3.3.4 Comparison of bioluminescence signals with histological serial sections

Finally, serial coronal sections of the various brains were prepared and 10 selected samples were investigated histologically in order to verify tumorigenicity as well as to compare tumor area and the obtained specific light signals. Since the majority of tumors expanded beyond the prepared 15 serial sections, a quantitative determination was impossible. **Figure 6.25** shows the characteristic morphology of high grade human glioblastoma grown in mouse brain. Additionally, two excised brains are depicted in order to demonstrate that the resulting tumors were even macroscopically visible.

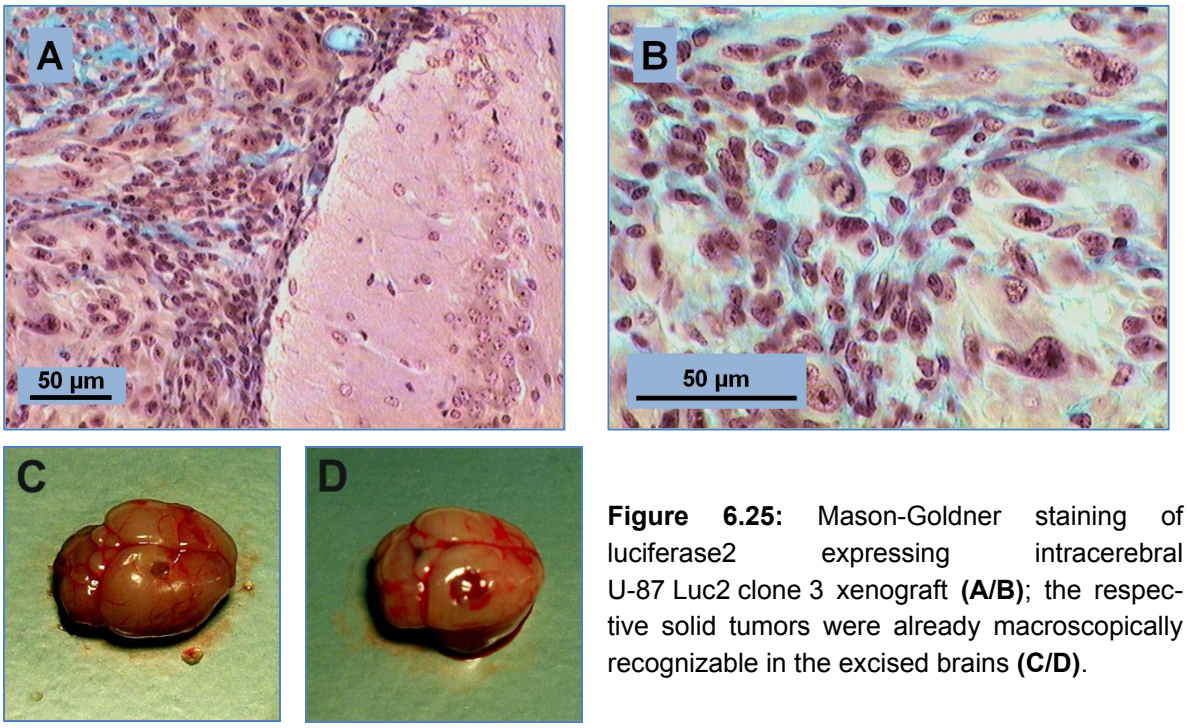

Figure 6.25: Mason-Goldner staining of luciferase2 expressing intracerebral U-87 Luc2 clone 3 xenograft **(A/B)**; the respective solid tumors were already macroscopically recognizable in the excised brains **(C/D)**.

As examples, **Figure 6.26** shows serial sections of two brains of nude mice and the respective bioluminescence image. A voluminous tumor (dark tissue) in the brain sections of an untreated control animal yielded a strong specific light signal. In contrast, the small tumor in brain sections of a mouse treated with paclitaxel combined with ME33-1 produced only a moderate signal.

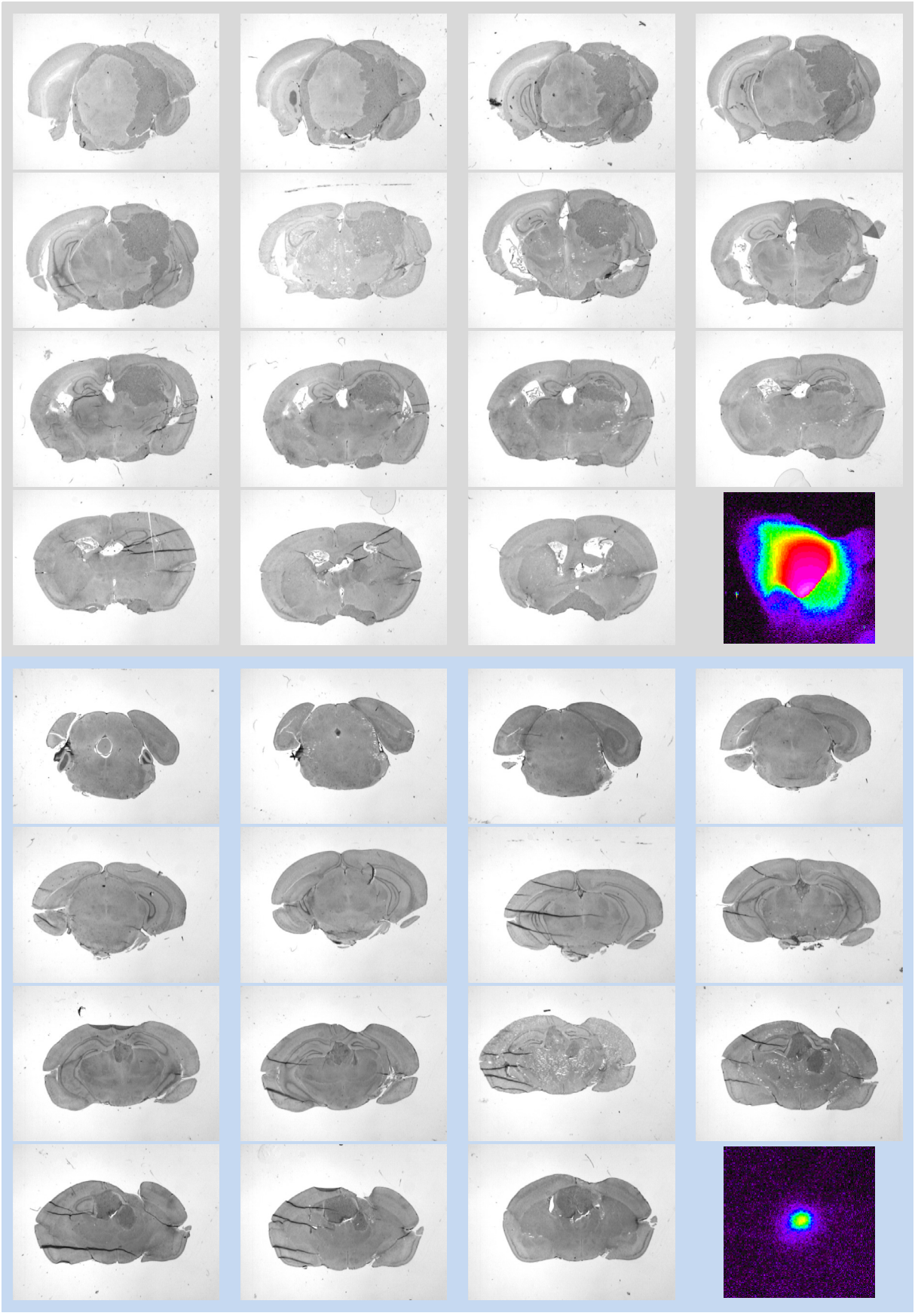

Figure 6.26: Serial coronal section of two representative brains of nude mice (mean distance 200 µm, starting and ending 1.5 mm rostral and caudal to the region of tumor cell injection) and the respective bioluminescence image; a tumor of substantial size is detected in the brain sections of an untreated control animal *(grey background)* whereas only little tumor tissue is visible in the serial brain sections of a mouse treated with paclitaxel combined with the ABCB1 modulator ME33-1 *(blue background)*.

In general, the bioluminescence signals correlated to the histologically detected tumor area. Nevertheless, in one of the two brains in which a regression of the light signal (paclitaxel + ME33-1 group) was observed, a tumor of extensive size was found (data not shown). As mentioned earlier, a supply of D-luciferin into the tumor tissue (via an intact blood circulation) is a prerequisite for successful detection by means of BLI. Additionally, the light signal correlates with the amount of the substrate present in the respective tissue. It may be speculated that inadequate distribution of D-luciferin may have caused the poor signal intensity.

6.4 Summary and conclusions

The present study aimed at the evaluation of the therapeutic value of new ABCB1 modulators in the chemotherapy of malignant brain tumors. Therefore, an existing intracerebral model in nude mice was modified to facilitate non-invasive determination of tumor burden and progression by means of optical in vivo imaging.

Consequently, human U-118 MG glioblastoma cells were transfected with the genes encoding for fluorescent proteins (DsRed2 and Katushka) or the luciferase2 enzyme. The in vitro characterization of the obtained transfectants revealed a low detection limit of both methods, BLI and FLI. Additionally, the chemosensitivity and the growth kinetics were similar to those of the wild type cells.

In subsequent in vivo investigations, the resulting luciferase2 expressing tumors were detectable subcutaneously as well as in the brain of the living animal. Additionally, the respective bioluminescence signal allowed a semi-quantitative evaluation of tumor size. In contrast to the encouraging results so far, none of the engineered U-118 glioblastoma variants proved to be suitable for preclinical investigations due to dissatisfying in vivo growth.

Since the efforts to establish an intracerebral U-118 glioblastoma model failed owing to inadequate tumorigenicity, highly tumorigenic U-87 Luc2 clone 3 xenografts were utilized for subsequent treatment experiments. The aim of these investigations was to elucidate, if the potential of tariquidar and ME33-1 in increasing the concentration of paclitaxel in the CNS (cf. chapter 4) is sufficient to improve brain cancer chemotherapy. Subsequent BLI

studies revealed a modest retardation of tumor progression with respect to the specific light signals. Additionally, a moderate survival benefit by co-administration of paclitaxel and ABCB1 modulators compared to the other treatment groups was observed.

Finally, selected brains were subjected to histopathological investigations and compared to the light signals obtained by in vivo imaging. In general, the bioluminescence signals were in good agreement with the histologically determined tumor area. Nevertheless, inconsistencies between the results obtained with both methods were observed as well. For example it may be difficult to quantitate very small tumors or xenografts located in the extramenigeal space by histological serial section. Additionally, the timely BLI process (approximately 40 min, background images included) requires a comparatively long immobilization of the tumor bearing mouse by anesthesia. This increases the risk that the animal awakes or eventually dies during anesthesia leading to false negative results. Additionally, the exact location of the tumor (deep in the brain tissue or at the surface) as well as the positioning of the scull may to some extent influence the detected light signal.

In summary, the accuracy of optical in vivo imaging was sufficient for a semi-quantitative evaluation of tumor progression. That enabled the confirmation of both, the existence as well as the homogeneous distribution of solid brain tumors at the beginning of the treatment experiments. Moreover, the combination of paclitaxel with tariquidar or ME33-1 revealed a moderate retardation of tumor progression combined with a modest survival benefit. With slight modifications in the study design (earlier onset of chemotherapy, increased concentration of the cytotoxic agent, no background acquisition) future trials may reveal the full potential of ABCB1 modulators in the adjuvant therapy of malignant brain tumors.

6.5 References

Altenschöpfer, P. Tumorpharmakologische und analytische Untersuchungen zur Optimierung neuer Zytostatika-beladener bioabbaubarer Implantate für die interstitielle Chemotherapie maligner Hirntumore. PhD thesis, University of Regensburg, Regensburg, Germany, 1998.

Bouvet, M.; Spernyak, J.; Katz, M. H.; Mazurchuk, R. V.; Takimoto, S.; Bernacki, R., et al. High correlation of whole-body red fluorescent protein imaging and magnetic resonance imaging on an orthotopic model of pancreatic cancer. *Cancer Res.* **2005,** 65, 9829-9833.

Bradford, M. M. A rapid and sensitive method for the quantitation of microgram quantities of protein utilizing the principle of protein-dye binding. *Anal. Biochem.* **1976,** 72, 248-254.

Brutkiewicz, S.; Mendonca, M.; Stantz, K.; Comerford, K.; Bigsby, R.; Hutchins, G., et al. The expression level of luciferase within tumour cells can alter tumour growth upon in vivo bioluminescence imaging. *Luminescence* **2007,** 22, 221-228.

Chishima, T.; Miyagi, Y.; Wang, X.; Yamaoka, H.; Shimada, H.; Moossa, A. R., et al. Cancer invasion and micrometastasis visualized in live tissue by green fluorescent protein expression. *Cancer Res.* **1997,** 57, 2042-2047.

Day, J. C.; Tisi, L. C.; Bailey, M. J. Evolution of beetle bioluminescence: the origin of beetle luciferin. *Luminescence* **2004,** 19, 8-20.

Fellner, S.; Bauer, B.; Miller, D. S.; Schaffrik, M.; Fankhänel, M.; Spruss, T., et al. Transport of paclitaxel (Taxol) across the blood-brain barrier in vitro and in vivo. *J. Clin. Invest.* **2002,** 110, 1309-1318.

Hoffman, R. M. Imaging cancer dynamics in vivo at the tumor and cellular level with fluorescent proteins. *Clin. Exp. Metastasis* **2009,** 26, 345-355.

Hubensack, M. Approaches to overcome the blood brain barrier in the chemotherapy of primary and secondary brain tumors: modulation of P-glycoprotein 170 and targeting of the transferrin receptor. PhD thesis, University of Regensburg, Regensburg, Germany, 2005.

Jarzyna, P. Preclinical investigations on the effect of the human hyaluronidase Hyal-1 on growth and metastasis of human colon carcinoma. PhD thesis, University of Regensburg, Regensburg, Germany, 2007.

Jenkins, D. E.; Hornig, Y. S.; Oei, Y.; Dusich, J.; Purchio, T. Bioluminescent human breast cancer cell lines that permit rapid and sensitive in vivo detection of mammary tumors and multiple metastases in immune deficient mice. *Breast Cancer Res.* **2005,** 7, R444-454.

Koo, V.; Hamilton, P. W.; Williamson, K. Non-invasive in vivo imaging in small animal research. *Cell. Oncol.* **2006,** 28, 127-139.

Kühnle, M. Experimental therapy and detection of glioblastoma: investigation of nanoparticles, ABCG2 modulators and optical imaging of intracerebral xenografts. PhD thesis, University of Regensburg, Regensburg, Germany, 2010.

Moriyama, E. H.; Bisland, S. K.; Lilge, L.; Wilson, B. C. Bioluminescence imaging of the response of rat gliosarcoma to ALA-PpIX-mediated photodynamic therapy. *Photochem. Photobiol.* **2004,** 80, 242-249.

Müller, C. New approaches to the therapy of glioblastoma: investigations on RNA interference, kinesin Eg5 and ABCB1/ABCG2 inhibition. PhD thesis, University of Regensburg, Regensburg, Germany, 2007.

Peyruchaud, O.; Winding, B.; Pecheur, I.; Serre, C. M.; Delmas, P.; Clezardin, P. Early detection of bone metastases in a murine model using fluorescent human breast cancer cells: application to the use of the bisphosphonate zoledronic acid in the treatment of osteolytic lesions. *J. Bone Miner. Res.* **2001,** 16, 2027-2034.

Pfost, B.; Seidl, C.; Autenrieth, M.; Saur, D.; Bruchertseifer, F.; Morgenstern, A., et al. Intravesical alpha-radioimmunotherapy with 213Bi-anti-EGFR-mAb defeats human bladder carcinoma in xenografted nude mice. *J. Nucl. Med.* **2009,** 50, 1700-1708.

Prasher, D. C.; Eckenrode, V. K.; Ward, W. W.; Prendergast, F. G.; Cormier, M. J. Primary structure of the Aequorea victoria green-fluorescent protein. *Gene* **1992,** 111, 229-233.

Romeis, B. *Mikroskopische Technik*. Urban & Schwarzenberg: Munich, Germany, 1989.

Scatena, C. D.; Hepner, M. A.; Oei, Y. A.; Dusich, J. M.; Yu, S. F.; Purchio, T., et al. Imaging of bioluminescent LNCaP-luc-M6 tumors: a new animal model for the study of metastatic human prostate cancer. *Prostate* **2004,** 59, 292-303.

Shcherbo, D.; Merzlyak, E. M.; Chepurnykh, T. V.; Fradkov, A. F.; Ermakova, G. V.; Solovieva, E. A., et al. Bright far-red fluorescent protein for whole-body imaging. *Nat. Methods* **2007,** 4, 741-746.

Smakman, N.; Martens, A.; Kranenburg, O.; Borel Rinkes, I. H. Validation of bioluminescence imaging of colorectal liver metastases in the mouse. *J. Surg. Res.* **2004,** 122, 225-230.

Szentirmai, O.; Baker, C. H.; Lin, N.; Szucs, S.; Takahashi, M.; Kiryu, S., et al. Noninvasive bioluminescence imaging of luciferase expressing intracranial U87 xenografts: correlation with magnetic resonance imaging determined tumor volume and longitudinal use in assessing tumor growth and antiangiogenic treatment effect. *Neurosurgery* **2006,** 58, 365-372; discussion 365-372.

Wilson, T.; Hastings, J. W. Bioluminescence. *Annu. Rev. Cell Dev. Biol.* **1998,** 14, 197-230.

Yang, M.; Jiang, P.; Yamamoto, N.; Li, L.; Geller, J.; Moossa, A. R., et al. Real-time whole-body imaging of an orthotopic metastatic prostate cancer model expressing red fluorescent protein. *Prostate* **2005,** 62, 374-379.

Chapter 7

7 Identification of putative binding modes of tariquidar-like modulators at P-glycoprotein

7.1 Introduction

34 years ago it was discovered that a glycosylated 170 kDa surface protein is responsible for reduced drug permeation (therefore designated P-glycoprotein) in colchicine resistant chinese hamster ovary cells (Juliano and Ling, 1976). Due to its relevance in MDR tumors, substantial efforts have been made to investigate the nature of this protein so that P-gp became the first cloned human ABC transporter (Chen et al., 1986). However, until recently there was a lack of structural information concerning mammalian ABC transporters at the atomic level, and structures obtained by electron microscopy, albeit at a low resolution of approximately 8 Å, were the best data available (Lee et al., 2008; Rosenberg et al., 2005). With a resolution of up to 3.8 Å, the recently published x-ray data of the murine Abcb1a transporter (Aller et al., 2009) allow detailed insights into the morphology of the protein (see **Figure 7.1**), thereby facilitating structure-based approaches.

In order to enable crystallization and improve resolution, the authors had to perform some structural modifications. Among others, three glycosylation sites in the first extracellular loop were removed and six cysteines were labeled with a mercury(II) complex. Crystals were grown using detergent solubilized protein in a nucleotide and magnesium free medium. Due to high flexibility, the N-terminus (amino acids 1-33) and the linker region (amino acids 627-683) connecting the first nucleotide binding domain with the second transmembrane domain (TMD2) could not be visualized. Importantly, the modified protein

showed almost full functionality and only minor differences between the structures obtained from the three different crystals were observed.

Among the essential topological features is the pseudo two-fold symmetry of the transporter, which becomes obvious by the front and back views presented in **Figure 7.1**. Furthermore, each topological half of the protein comprises TMs from the C- and the N-terminal side of the polypeptide chain to stabilize the Λ-shaped topology (the interlacing TMs are 4/5 and 10/11, respectively). Inside the transporter, at the interface of the two TMDs, an internal cavity is formed where the co-crystallized cyclic inhibitors QZ59-RRR and QZ59-SSS bind to the protein. Both QZ59-isomers inhibited calcein-AM efflux in the low micromolar range and decrease ATP hydrolysis, indicating that they (as tariquidar) are not transported by P-glycoprotein. At the intracellular face of Abcb1a, two nucleotide binding domains, NBD1 and NBD2, are separated by a distance of ~30 Å. NBD1 follows TM6 and is linked to the second TMD. NBD2 begins after TM12 and extends to the C-terminus of the protein.

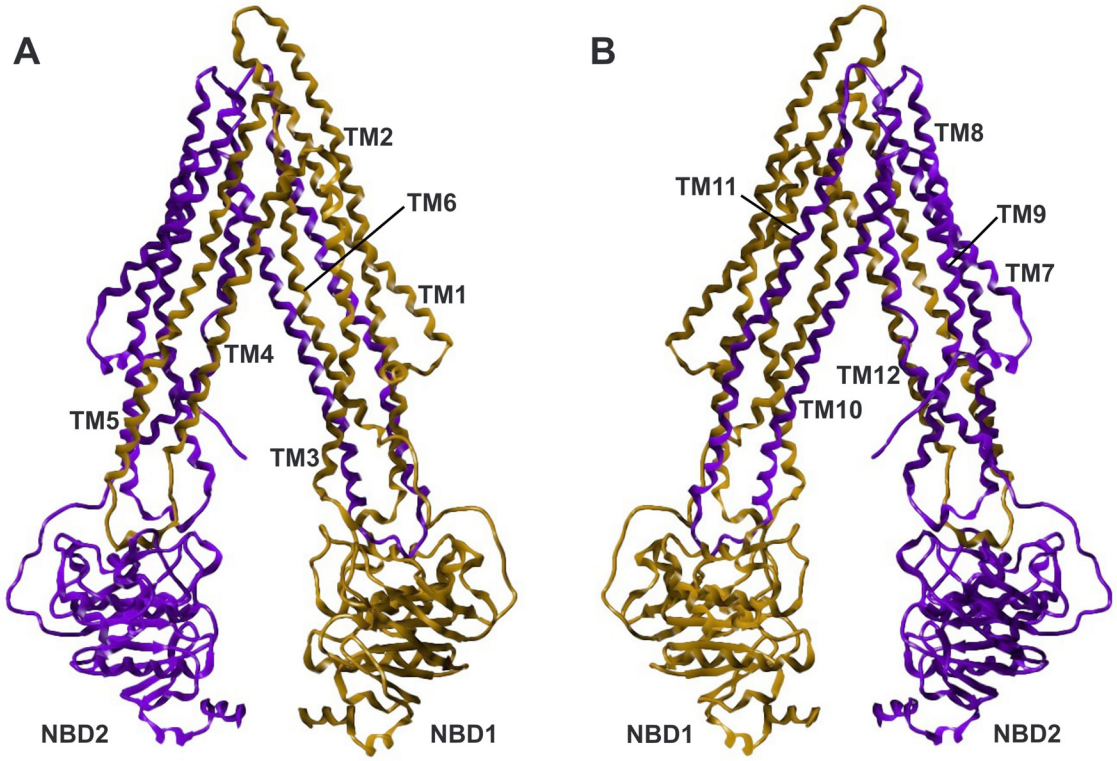

Figure 7.1: Ribbon-tube model of the murine Abcb1a transporter (multidrug resistance protein 3) on the basis of the 3.8 angstrom resolution x-ray structure (PDB ID 3g5u) (Aller et al., 2009) after energy minimization; transmembrane and nucleotide binding domains are labeled and colored in yellow (TM1 - TM6 (=TMD1); NBD1) and violet (TM7 - TM12 (=TMD2); NBD2), respectively. **A)** Front and **B)** back view of the protein backbone; as becomes obvious, TMs4 and 5 as well as TMs10 and 11 cross over to the diametrical bundle of TMs. This topology is crucial to stabilize the Λ-shaped conformation and to enable the large motional ranges required for substrate transport.

The detailed information provided by the x-ray structure served as basis for the docking studies presented in this chapter.

7.1.1 Mechanism of transport

A growing number of results from the literature coincide with the “hydrophobic vacuum cleaner”-model of substrate transport first described by Raviv et al. (1990). This model suggests that hydrophobic substrates enter the binding site directly from the plasma membrane and are exported by P-glycoprotein without reaching the cytosol. Moreover, there is substantial evidence that substrates are preferentially extracted from the cytoplasmic leaflet of the plasma membrane (Chen et al., 2001; Gatlik-Landwojtowicz et al., 2006; Shapiro and Ling, 1997).

The highly lipophilic character of substrates and inhibitors indicates accumulation within the bilayer. If there is direct access from the membrane (with a higher ligand concentration compared to the cytoplasm), inhibitory activity should, among other things, depend on the lipophilicity of the modulators. A correlation between lipophilicity and inhibitory activity was shown for propafenone-type modulators of P-glycoprotein (Schmid et al., 1999). Moreover, it could also be shown that the affinity of vinblastine, daunorubicin and verapamil to purified protein increased in the presence of more lipophilic phospholipids (Romsicki and Sharom, 1999).

Further evidence in favor of this transport mechanism is provided by the recently published x-ray structure of murine P-gp (Aller et al., 2009). Considering the approximate location of the plasma membrane, the Λ-shaped inward facing conformation forms a gate, which allows entry of lipophilic compounds directly from the inner (cytoplasmatic) leaflet of the bilayer (see **Figure 7.2**). This up to 9 Å wide gate is formed by TMs 4/6 on one and TMs 10/12 on the other side, respectively. After passing the portals, the compounds are located in the internal cavity of the transporter. This cavity with a volume of approximately 6000 $Å^3$ contains the binding site for substrates and inhibitors.

The subsequent mechanism of transport is assumed to resemble that described for the bacterial ABC transporter MsbA (Ward et al., 2007). ATP binding induces a packing rearrangement of the TMs and results in the dimerization of the NBDs. The concomitant twisting motion opens the protein to the extracellular space (associated with a decrease in substrate binding affinity) and enables unidirectional transport of the substrate. After nucleotide hydrolysis and release, the transporter returns to the inactive, inward-facing conformation. This transport mechanism is in accord with the influence of lipophilicity on the inhibitory activity of modulators and reasonable also with respect to evolutionary aspects (Higgins, 2007). Since many substrates of P-gp are toxic secondary metabolites of

plants (e.g. taxanes, vinca alkaloids and colchicine) or microorganisms (e.g. anthracyclines and cyclosporines), the ability of an organism to extrude those toxins, before they reach their intracellular targets, is a major evolutionary advantage.

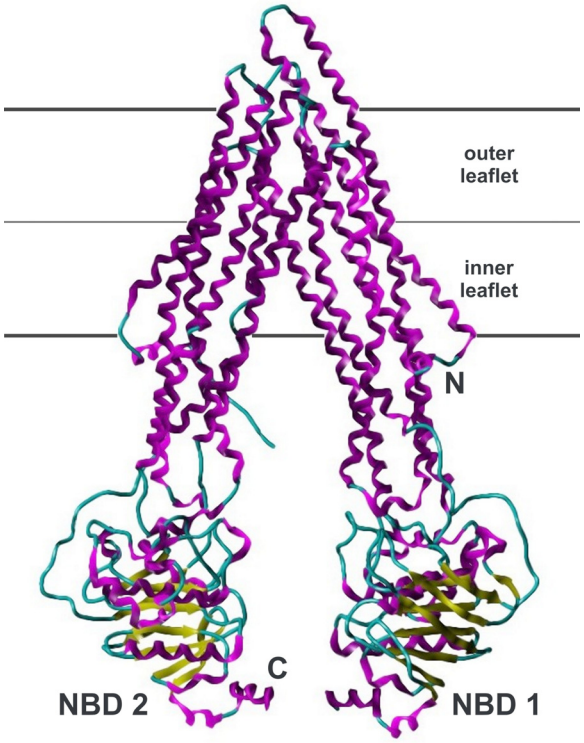

Figure 7.2: Approximate position of P-glycoprotein within the lipid bilayer; after entering the cell membrane, substrates accumulate dependent on their lipophilicity and are able to reach the internal cavity via an open gate in the inner leaflet.

7.1.2 Location of the binding region

The identification of the binding site of P-glycoprotein is a crucial step in understanding the mechanisms of drug transport (Globisch et al., 2008). Additionally, information about the interacting residues could facilitate structure-based design of inhibitors as well as structural optimization of drugs with respect to impeded efflux (Perego et al., 2001; Szakacs et al., 2006).

According to the probable transport mechanism (cf. section 7.1.1), it is reasonable to suppose that the binding site(s) is (are) located in the internal cavity within the plasma membrane (Higgins, 2007). Indeed, numerous experimental studies using diverse biochemical methods provided evidence that substrates and inhibitors bind in this region and helped to specify interaction sites (McDevitt and Callaghan, 2007).

Cross-linking experiments with the thiol-reactive substrate tris-(2-maleimidoethyl)amine (TMEA) on the human P-glycoprotein identified L339 (L335 in murine P-glycoprotein) and V982 (V978) to be important for substrate binding (Loo and Clarke, 2001a). ATPase activity of mutants containing cysteine in the respective amino acid positions was significantly decreased by cross-linking with TMEA. Additionally, cross-linking was reduced

by pre-incubation with P-gp substrates such as colchicine, vinblastine or verapamil. The importance of L339 for inhibiting transport function is also documented by studies with other thiol-reactive substrates. The covalent attachment of coumarin-maleimide to L339C significantly decreased ATP hydrolysis by P-glycoprotein (Rothnie et al., 2005). The mutant L339C was protected from covalent modification with thiol-reactive methanethiosulfonate-verapamil (MTS-verapamil) by pre-incubation with verapamil (Loo and Clarke, 2001b). In contrast, MTS-rhodamine (a derivative of another P-gp substrate) labeled F343C (murine F339) increased ATPase activity 5.8-fold (Loo et al., 2003a). Furthermore, addition of verapamil to the MTS-rhodamine labeled mutant further enhanced ATP hydrolysis (not observed with substrates like colchicine or calcein-AM). Therefore, the binding site of MTS-rhodamine seems to overlap with that of colchicines and calcein-AM, but not with that of verapamil. Among findings from other studies (Loo et al., 2003b), this indicates that various substrates bind to different sites within the same common drug-binding region.

In a different study (Loo et al., 2006), F728C mutation of the human protein (murine F724) resulted in a 4-fold decrease in the apparent verapamil affinity. Moreover, labeling of F728C with MTS-verapamil elevated ATPase activity 11.5-fold. In addition to verapamil, other ABCB1 substrates and inhibitors as cyclosporine A protected F728C from labeling with MTS-verapamil. All these experiments with verapamil and its derivatives are of special interest due to their similarity to tariquidar (see **Figure 7.3**).

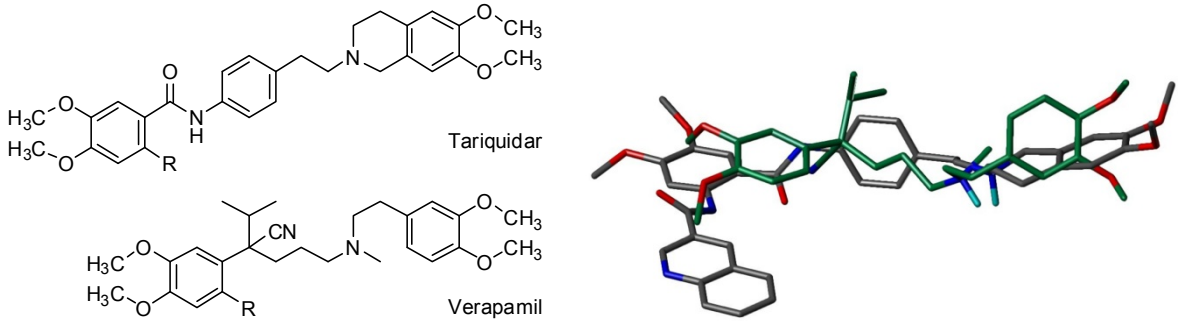

Figure 7.3: Similarity between the structures of tariquidar *(dark gray)* and verapamil *(green)* visualized by superposition; the structural formulas (left panel) indicate the common structural features (two dimethoxyphenyl moieties, the tertiary amine and the hydrophobic linker).

The recently disclosed crystal structures of the murine Abcb1a transporter, co-crystallized with two stereoisomers of a cyclic hexapeptide inhibitor (Aller et al., 2009), confirmed the participation of the above mentioned amino acids in binding. The two stereoisomers (QZ59-RRR and QZ59-SSS) bind in three (the SSS-isomer can occupy two sites) different locations and orientations to P-glycoprotein, showing that P-gp is able to interact with

different ligands via various and partially overlapping binding sites (Sheps, 2009). These findings are in agreement with the observed multispecifity of P-gp and other multidrug resistance transporters (Higgins, 2007). That the binding sites partially overlap may also explain inconsistent data in the literature about their number (Neyfakh, 2002). Additionally, the three polar amino acids Q721, Q986 and S989 are of particular importance in the "lower" binding site of the QZ59-SSS inhibitor (Aller et al., 2009) and were considered in the initial steps of the docking investigations (see below).

7.1.3 Genetic docking algorithm of FlexiDock™

The following explanations outline the main features of the applied genetic docking algorithm of FlexiDock™ and can be found in detail in the manual provided from Tripos™ (Tripos, 2006). All calculations were performed with the Molecular Modeling suite Sybyl 7.3 (Tripos, L.P., St. Louis, MO) on an SGI Octane Workstation.

Methodology and terminology of genetic docking algorithms are based on Darwinian evolution. Each member of a population is represented by a chromosome (potential solution) consisting of a collection of genes. Genes encode defined torsion angles (rotatable bonds) of the ligand and amino acid side chains as well as rigid body rotations and translations of the ligand in x-, y- and z-direction. In each generation, evolution occurs by mutation of genes (e.g. for a torsional gene: rotation about a specific bond) and crossover between chromosomes (exchange of genes).

For every chromosome, a fitness (or scoring) function (energy of all moving atoms in the protein-ligand complex, an additional term optionally weights H-bonds) based on a subset of the Tripos force field is calculated. Chromosomes with a high fitness function (well fitting ligand orientations and conformations) have a higher probability (selection pressure) of surviving to the next generation. Due to this "elitism", these solutions have the best chance to propagate into future generations and the quality of the solutions will increase with time. Additionally, checking for duplicates ensures the solution´s diversity over various generations.

The evolution process can be influenced by customizing the FlexiDock™ parameters. Among the most important ones are the number of seeds (population size), the definition of putative H-bond sites (corresponding solutions have a higher scoring function), the probability level (and the allowed range) of mutations and the number of generations to run. The last parameter is highly dependent on the number of rotatable bonds in both, the ligand and the binding site. Selecting the number of generations too small can result in no plausible solution. In contrast, choosing a too high number of generations will result in low diversity of the results since all genes have converged.

Additionally, it should be kept in mind that FlexiDock™ operates only in the torsional, rotational and transformational space. As a consequence, during the optimization process, bond lengths and angles remain constant.

7.2 Materials and methods

7.2.1 Selected ABCB1 modulators

In order to investigate the putative binding mode of tariquidar-like modulators at P-glycoprotein, five compounds were chosen for docking experiments (see **Figure 7.4**). Tariquidar, ME30-1 and ME5-7 have a common basic structure. Modifications in positions 4 and 5 of the benzamide moiety lead to substantial differences of the in vitro activity. Additionally, ME25-3, an inhibitor with a relative selectivity for the ABCG2 transporter (due to a shift of the quinoline-3-carbonylamino moiety to position 3 (meta)) was considered. Furthermore, the dual ABCB1/ABCG2 inhibitor elacridar with the benzamide moiety as part of an acridine ring was included in the docking experiments.

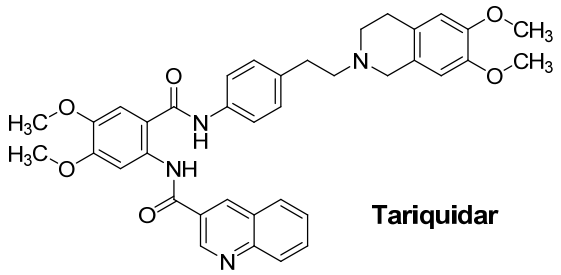

Tariquidar

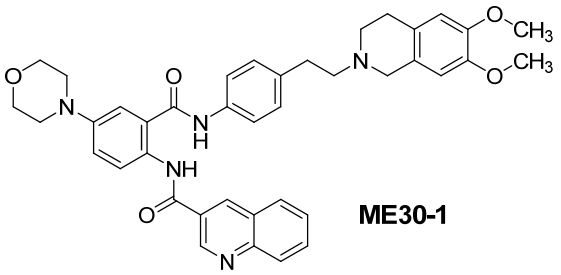

ME30-1

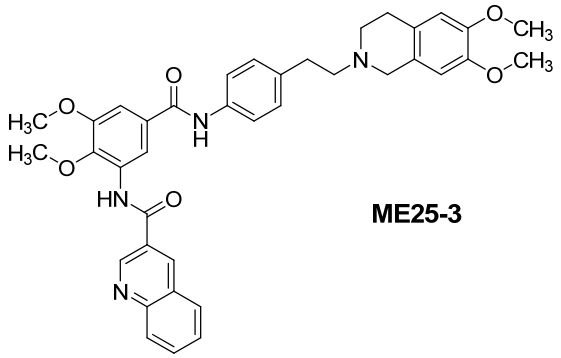

ME25-3

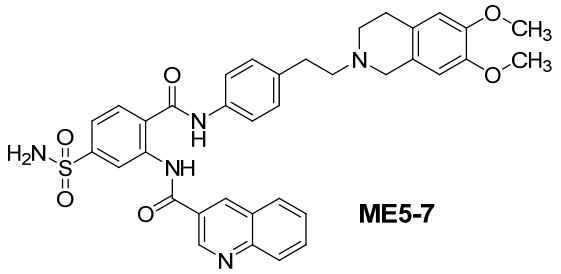

ME5-7

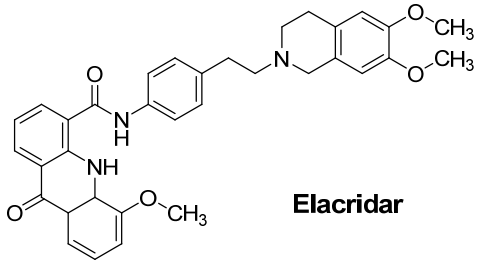

Elacridar

Compound IC_{50}-value [µM]	
Tariquidar	0.223
ME30-1	0.798
ME25-3	17.95
ME5-7	> 100
Elacridar	0.193

Figure 7.4: Chemical structures of compounds selected for docking experiments; ABCB1 inhibitory activity at human P-gp was determined on Kb-V1 cells with the calcein efflux assay by flow cytometry.

Under physiological conditions, the protonated species of tariquidar-like modulators predominates (> 73 %, calculated by ACD/Labs 12). Consequently, in all further investigations, the nitrogen in the tetrahydroisoquinoline moiety was regarded as being protonated.

7.2.2 Determination of IC_{50}- and log D-values

All tariquidar analogs were provided by the laboratory of Prof. Dr. König (University of Regensburg, Germany) and ABCB1 inhibitory activity was determined by means of the calcein efflux assay on the flow cytometer and in the micro-plate format. The assays on human Kb-V1 cells were performed according to Müller et al. (2007) and as described in chapter 3, respectively. Log D-values at pH 7.4 were calculated with ACD/Labs 12 software (Toronto, Canada).

7.2.3 Conformational analysis

Due to the high degree of flexibility inherent in the tariquidar-like modulators, the number of possible solutions had to be constrained by conformational analyses. Compound ME30-1 was split into two fragments (see **Figure 7.5**) which were separately analyzed by grid searches.

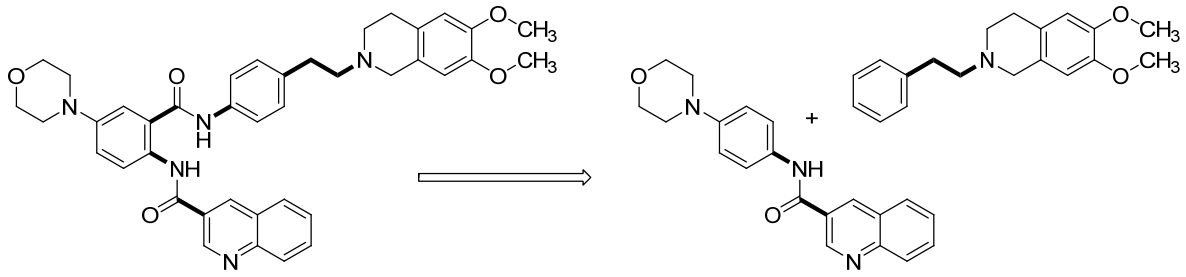

Figure 7.5: Flexible bonds of ME30-1 included in the conformational analysis are indicated in bold. In a first attempt the molecule was split and a grid search was performed for each moiety. Only preferred torsion angles were incorporated into subsequent conformational analyses of the whole structure.

A subsequent systematic search of the whole structure was restricted to energetically favored torsion angles resulting from the previous step. All conformations obtained by the systematic search were minimized. Every structure with an RMS distance to all other conformations of > 0.5 Å was regarded as individual local minimum. The energetically most favored extended conformer was used as starting conformation for docking experiments.

7.2.4 Preparation of the transporter

The 3.8 Å resolution x-ray structure (Aller et al., 2009) of the murine Abcb1a transporter (PDB ID Code: 3G5U) was obtained from the Protein Data Bank (Research Collaboratory for Structural Bioinformatics (RCSB), Rutgers University, NJ) and processed with the structure preparation tool implemented in Sybyl 7.3. The main modifications in brief: removal of mercury atoms; addition of hydrogens; addition of acetyl (N-termini of the polypeptide chain) and methylamino (C-termini of the polypeptide chain) groups; addition of AMBER7 FF99 charges; if necessary, correction of side chain conformations (with rotamer states from the Lovell library (Lovell et al., 2000)) to remove steric bumps. Subsequently, the protein was minimized with the AMBER7 FF99 force field (dielectric constant 4). This first minimization steps were performed by the steepest descent method. In a second minimization approach with the Powell conjugation gradient method, the transporter was allowed to relax to a total energy of approximately -4000 kcal mol^{-1}.

7.2.5 Docking of ABCB1 modulators

Results from labeling (Loo and Clarke, 2001b), cross-linking (Loo and Clarke, 2001a) and mutational experiments (Loo et al., 2006) as well as the location of the co-crystallized, cyclic inhibitors (Aller et al., 2009) were considered to localize the binding region. In a first attempt, the energetically favored conformations of the modulators were manually docked in this region, suggesting interactions with the essential amino acids described in section 7.1.2. In a second step, the FlexiDock™ module implemented in Sybyl 7.3 was used for refinement. All flexible bonds of the modulators and all side chains of amino acids in proximity to the pre-positioned ligand were defined as rotatable. In general, several runs using different starting seeds and a minimum of 750 generations per rotatable bond were performed. The obtained docking results were analyzed by visual inspection and used for further FlexiDock™ runs with marked H-bond donor and acceptor sites in the protein and the ligand.

In the resulting docking solutions, the modulators and amino acids within a radius of 6 Å around them were minimized with the Tripos force field (dielectric constant 1; ligand: Gasteiger-Hückel charges, protein: AMBER FF99 charges; range constraints of detected H-bonds: 1.7 Å to 2.2 Å) using the steepest descent method. Afterwards, the ligand was fixed, and the protein was minimized with the AMBER FF99 force field (dielectric constant 4; minimization method: Powell) until an RMS gradient of < 0.05 kcal mol^{-1} $Å^{-1}$ was achieved.

7.2.6 Sequence alignment

The primary amino acid sequences of the Abcb1a (P21447), the Abcb1b (P06795) and the ABCB1 transporters (P08183) were downloaded from the UniProt knowledgebase, and the sequence alignment was performed with CLUSTAL W2 (Larkin et al., 2007).

7.3 Results and discussion

7.3.1 Correlation between lipophilicity and inhibitory activity

Due to evolutionary aspects, the topology of the transporters and experimental evidence, substrates and modulators are most likely extracted directly from the lipid bilayer. The concentration of a particular compound in a lipophilic compartment is a function of its octanol-water partition coefficient. Thus, IC_{50}-values should not depend only on binding affinities, but also on the lipophilicity of the modulators.

In order to investigate this assumption, pIC_{50}-values of 23 selected tariquidar-like ABCB1 modulators (Müller, 2007) are correlated with their calculated log D-values. **Figure 7.6** shows a significant correlation between the inhibitory potency and lipophilicity. Tariquidar as well as the analogs investigated in more detail in the previous chapters appear above the regression line in the upper right corner of the graph. Accordingly, the "additional potency" of these compounds is caused by high affinity to the target and not only dependent on the concentration in the lipophilic compartment. However, hydrophobicity has a certain influence on activity due to membrane penetration and possibly hydrophobic interactions with the target.

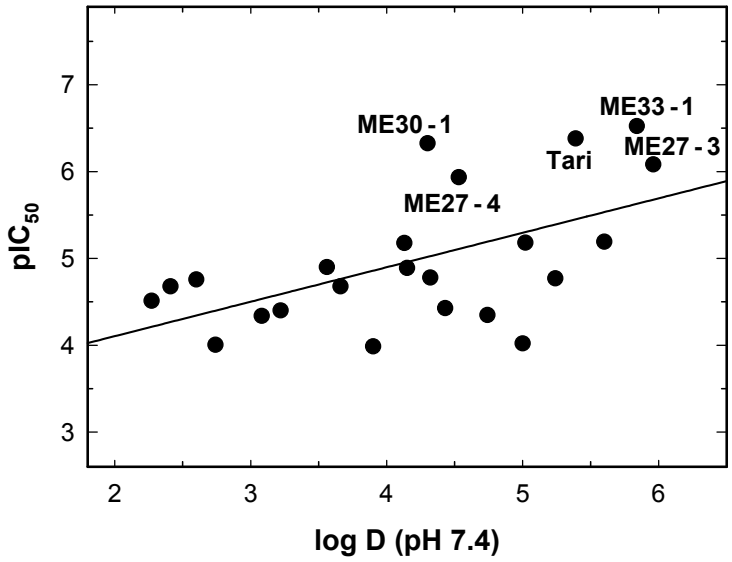

Figure 7.6: The pIC_{50}-values (determined with calcein efflux assay at the plate reader) of 23 selected tariquidar-like ABCB1 modulators are correlated with calculated log D-values.

Regression equation:

$pIC_{50} = 0.39 \log D + 3.31$

r = 0.56, s = 0.66, p = 0.005

r: coefficient of correlation
s: standard error of estimate
p: level of significance

By contrast, there are several compounds with poor affinity in spite of high hydrophobicity (lower right corner). The lack of hydrophilic compounds with high activity (upper left corner) may be due to low concentrations at the target. This complicates the design of potent hydrophilic, well soluble P-glycoprotein modulators with drug-like properties. Possibly, a prodrug concept could solve this problem (see section 7.4).

7.3.2 Conformational analysis of compound ME30-1

Since no crystallographic data of tariquidar or related structures were available from the Cambridge Structural Database (Cambridge Crystallographic Data Center, Cambridge, United Kingdom), representative conformational searches were performed for compound ME30-1 as described in section 7.2.3.

The resulting low-energy solutions were analyzed by visual inspection and could be grouped into two categories, "folded conformers" with a high contribution of intramolecular

interactions and “extended conformers”. **Figure 7.7** shows two distinctive representatives for the first category with low energy in consequence of intramolecular interactions.

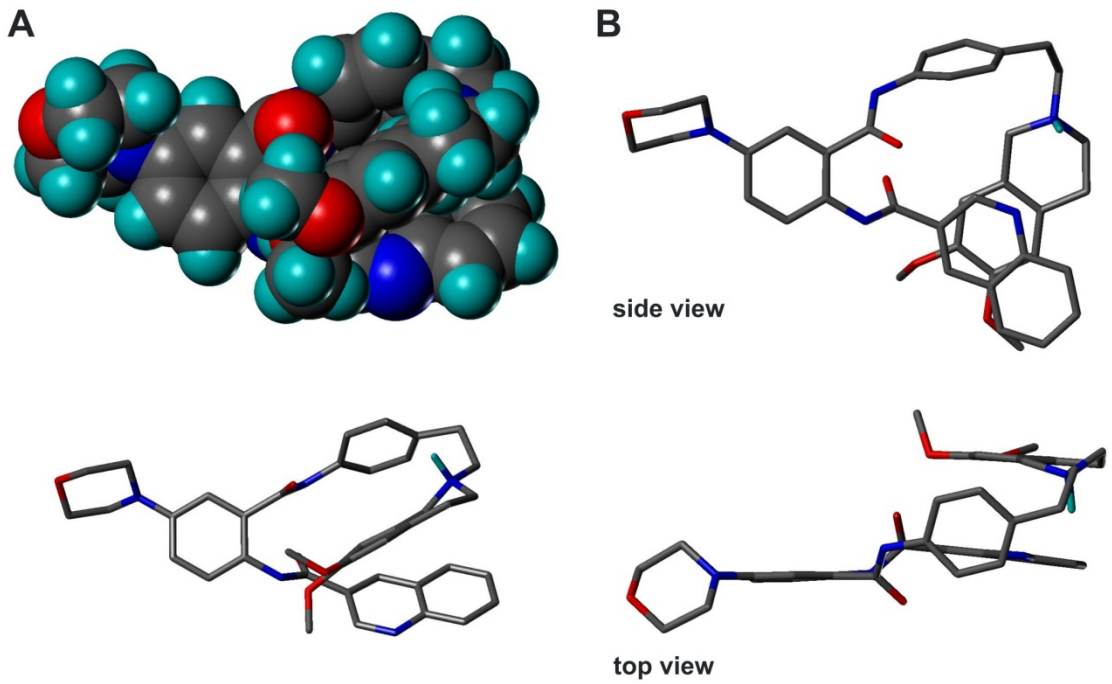

Figure 7.7: Two characteristic examples of energetically favored folded conformers of ME30-1. **A)** Spacefill and capped sticks illustration of a conformer stabilized by hydrophobic interactions. **B)** Side- and top view of a molecular conformation resulting from distinctive π-π stacking interactions

It is a common rule that minimization of the free, not target-bound compound overestimates intramolecular contacts as H-bonds and hydrophobic interactions which are probably not relevant for the conformation in the binding pocket (Klebe, 2009). Additionally, a molecular axis longer than 18 atoms appears to be favorable for effective inhibition of P-gp function (Wang et al., 2003).

Consequently, the energetically favored extended conformers were regarded to represent the receptor bound conformations. **Figure 7.8** shows low-energy conformers of compound ME30-1 from this group.

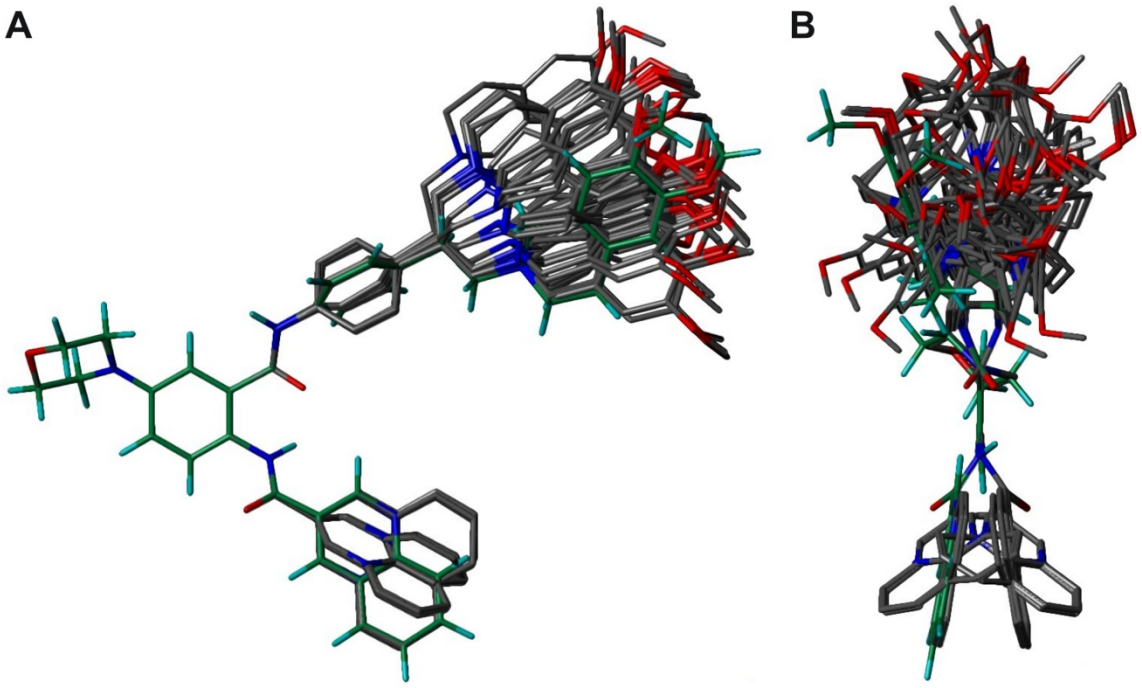

Figure 7.8: Superposition (side view) of 34 extended conformations of ME30-1 with calculated energies lower than 32 kcal/mol **(A)** and after rotation of 90° **(B)**; the lowest energy conformer, colored in green, was used for further docking experiments.

For all further docking experiments the energetically most favored extended conformer was used as starting conformation.

7.3.3 Analysis of binding modes of ABCB1 modulators

Five modulators with different structural features covering a sufficient range of IC_{50}-values (see section 7.2.1) were selected for docking experiments. All investigated modulators share a similar binding position (see **Figure 7.9** for ME30-1) in the C-terminal half of the transporter in the region of the plasma membrane. This location corresponds to the “lower” binding site of QZ59-SSS in the x-ray structure (Aller et al., 2009). Additionally, this location is in accordance with the suggested transport mechanism and with results from labeling, cross-linking and mutational experiments.

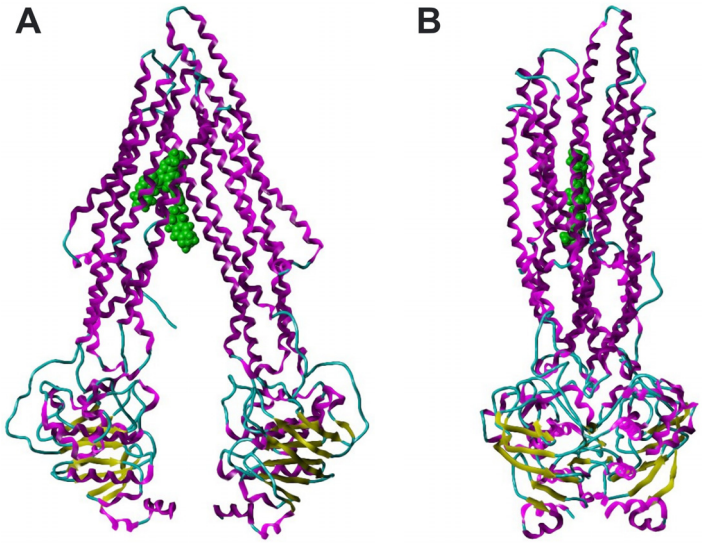

Figure 7.9: Overall front **(A)** and side view **(B)** of the ABCB1 transporter backbone with ME30-1 (in green) illustrating the approximate position of ligand binding; the modulator interacts at the level of the inner leaflet with residues in the C-terminal half (predominantly TM5, TM7 and TM12) of P-glycoprotein.

7.3.3.1 Binding modes of tariquidar and ME30-1

The binding mode of tariquidar, the best characterized and the most potent of the investigated modulators, is shown in **Figure 7.10**. The binding site consists of predominantly non-polar amino acids in TMs 5-9 and 12, which enable hydrophobic interactions. Additionally, polar amino acids in TM5 (Y303), TM7 (N717 and Q721) and TM12 (Q986 and S988) form hydrogen bonds with the molecule. An interaction found for all investigated modulators is the strong charge-assisted H-bond between the side chain of S988 and the protonated tertiary amine. As reported previously (Seelig and Landwojtowicz, 2000), a basic, tertiary amino group is an important structural feature of most ABCB1 inhibitors and substrates. Among other things (see section 7.4), the obvious steric freedom in the region around the tetrahydroisoquinoline moiety could be responsible for the broad variety of drugs interacting with P-gp.

In contrast, there is very limited space in position 3 (meta) and to some extent in position 4 (para) of the benzamide moiety. This fact is of special importance for the binding affinity of compounds with sterically discriminating moieties (e.g. ME25-3 and ME5-7) in these positions.

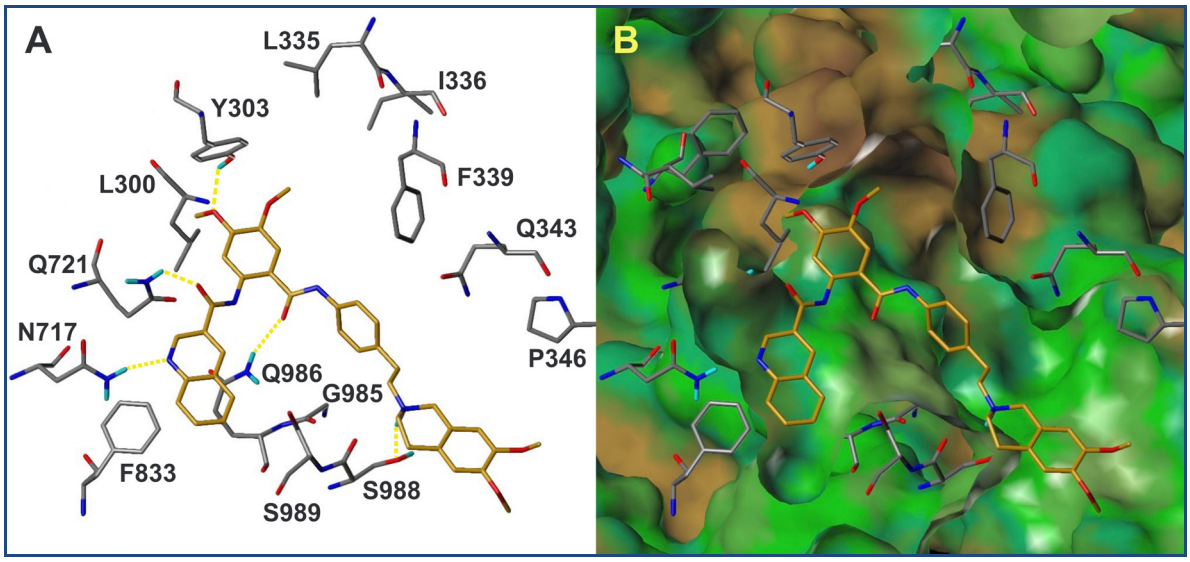

Figure 7.10: A) Model of the putative Abcb1a binding site for tariquidar; shown are residues within 3 Å around the ligand, except (for clarity) F724 (TM7), F766 (TM8), V978 and F990 (TM12). The orientation of tariquidar allows the formation of H-bonds (depicted as yellow dotted lines) with the side chains of Y303 (TM5), N717 (TM7), Q721 (TM7) and Q986 (TM12). Additionally, a strong charge-assisted H-bond between the hydroxy group of S988 (TM12) and the protonated tertiary amine is possible. **B)** Connolly surface (cross-sectional slice) of the binding site colored by the lipophilic potential (brown - lipophilic, green/blue - hydrophilic); in this representation, the limited space in position 3 and 4 of the benzamide moiety and, in contrast, a high degree of steric freedom around the dimethoxy-tetrahydroisoquinoline moiety becomes obvious.

The less potent analog ME30-1, bearing a morpholine substituent in position 5 of the benzamide moiety, showed a similar binding mode as tariquidar (see **Figure 7.11**). As a result of the lacking 4-methoxy group, the H-bond to Y303 in TM5 is not possible. Furthermore, the modulator is slightly shifted compared to tariquidar probably in order to fit the morpholine group to a hydrophobic pocket. This shift might also be responsible for the loss of the H-bond between the carbonyl oxygen of the benzamide moiety and Q986 in TM12. Nevertheless, the remaining H-bonds as well as the hydrophobic interactions may account for an effective inhibition of P-glycoprotein.

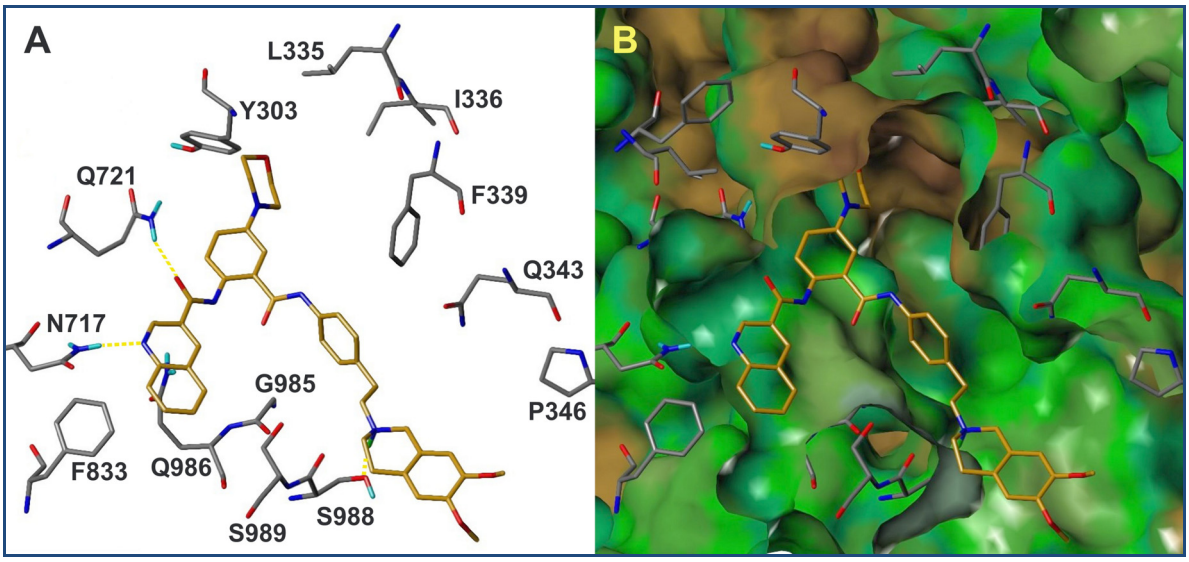

Figure 7.11: A) Model of the supposed Abcb1a binding site for ME30-1; shown are residues within 3 Å around the ligand, except (for clarity) F332 (TM6), F766 (TM8), V978 and M982 (TM12). As in the case of tariquidar, H-bonds with the side chains of N717 (TM7), Q721 (TM7) and S988 (TM12) are possible. In contrast, the interaction with Y303 (TM5) is lacking. The morpholine moiety fits to a hydrophobic pocket resulting in a slight shift of the molecule which possibly eliminates the H-bond to Q986 observed with tariquidar. **B)** Connolly surface (cross-sectional slice) of the binding site colored by the lipophilic potential (brown - lipophilic, green/blue - hydrophilic); also in the binding orientation of ME30-1, the limited space in meta- and para-position of the central aromatic ring is obvious.

7.3.3.2 Binding modes of ME25-3 and ME5-7

Compounds such as ME25-3, with the quinoline-3-carbonylamino substituent in position 3 of the benzamide moiety, are weak inhibitors of the ABCB1 transporter, but turned out to be ABCG2 selective modulators. This modification of the substitution pattern paved the way to discriminate between ABCB1 and ABCG2 modulators derived from tariquidar. The replacement of the methoxy group in position 4 with the sterically more demanding methoxycarbonyl moiety further reduced the affinity against P-gp and resulted in the most potent and selective ABCG2 modulators known so far (Kühnle et al., 2009).

Figure 7.10 A shows the orientation of ME25-3 in the binding pocket of P-gp in relation to tariquidar. As a consequence of the limited space for substituents in position 3 of the benzamide moiety (see above), the quinoline-3-carbonylamino substituent is suggested to fit to the hydrophobic pocket occupied by the morpholino group of ME30-1. This results in a loss of the H-bonds with N717 and Q721 (both in TM7). Since the interactions with Y303 in TM5 and S988 are still possible, at least low inhibitory activity at P-gp is retained.

In the case of ME5-7 a completely different binding mode compared to tariquidar must be assumed (**Figure 7.12 B**), although the quinoline-3-carbonylamino substituent is in the

“correct” position 2 of the benzamide moiety. In consequence of the steric bulk of the sulfonamide moiety, the entire molecule has to re-orientate. Apart from the H-bond of the tertiary amine with S988, all specific interactions observed for the other compounds are lost. Additionally, in this orientation only weak hydrophobic interactions of the quinoline moiety are possible. Probably, also the decrease in lipophilicity (poor accumulation in the membrane) due to the introduction of the sulfonamide moiety contributes to the total loss of apparent inhibitory activity at the ABCB1 transporter.

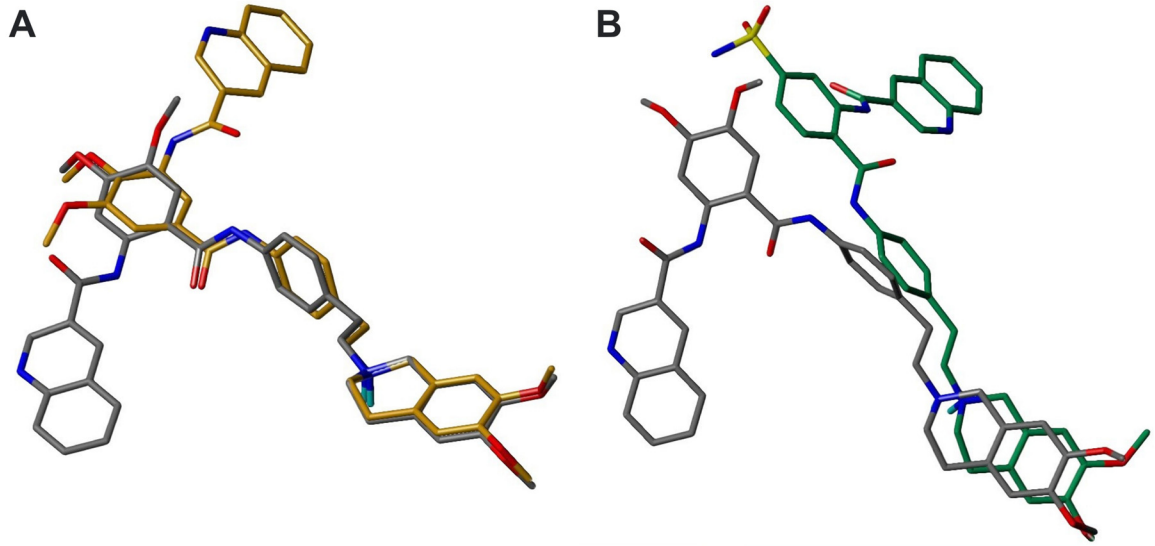

Figure 7.12: Orientation of ME25-3 (orange) and ME5-7 (green) in relation to tariquidar (dark grey) in the binding pocket of P-gp; **A)** The quinoline-3-carbonylamino moiety in meta-position is suggested to fit to the hydrophobic pocket (similarly like the morpholine moiety of ME30-1). Thus, the H-bonds of the quinoline-3-carbonylamino group with N717 and Q721 (seen with tariquidar and ME30-1) are impossible. Nevertheless, the H-bonds to Y303, S988 and potentially Q986 can still be formed and guarantee an at least low inhibitory activity. **B)** Due to the bulk of the sulfonamide group, the entire molecule has to re-orientate. At this position, all specific interactions (except for that of the tertiary amine) observed for tariquidar, ME30-1 and ME25-3 are lost. Combined with reduced hydrophobic interactions of the quinoline moiety in this orientation, the loss of affinity is comprehensible.

7.3.3.3 Binding mode of elacridar

Elacridar, a potent dual ABCB1/ABCG2 inhibitor with the benzamide moiety included in an acridine ring (mimicking a cyclic substitution in the ortho- and meta-position) was also investigated. Due to the lower bulk of the ring system compared to the meta-quinoline-3-carbonylamino group of ME25-3, an orientation of the benzamide moiety like in the case of tariquidar is still possible.

From **Figure 7.13** it becomes obvious that elacridar addresses the same binding region as the other modulators, but in a unique and slightly different manner. Y303 (TM5) interacts with the carbonyl group at the acridine ring (like the 4-methoxy group in tariquidar and ME25-3) and Q986 (TM12) contacts the 10-methoxy substituent instead of the carbonyl function in the benzamide moiety of tariquidar. This results in a shift of the molecular axis towards TM6 and fits the ring system in the narrow part of the binding pocket. Additionally, a dual charge-assisted hydrogen bond between the protonated tertiary amine and both, the backbone and the side chain oxygen of S988 is possible.

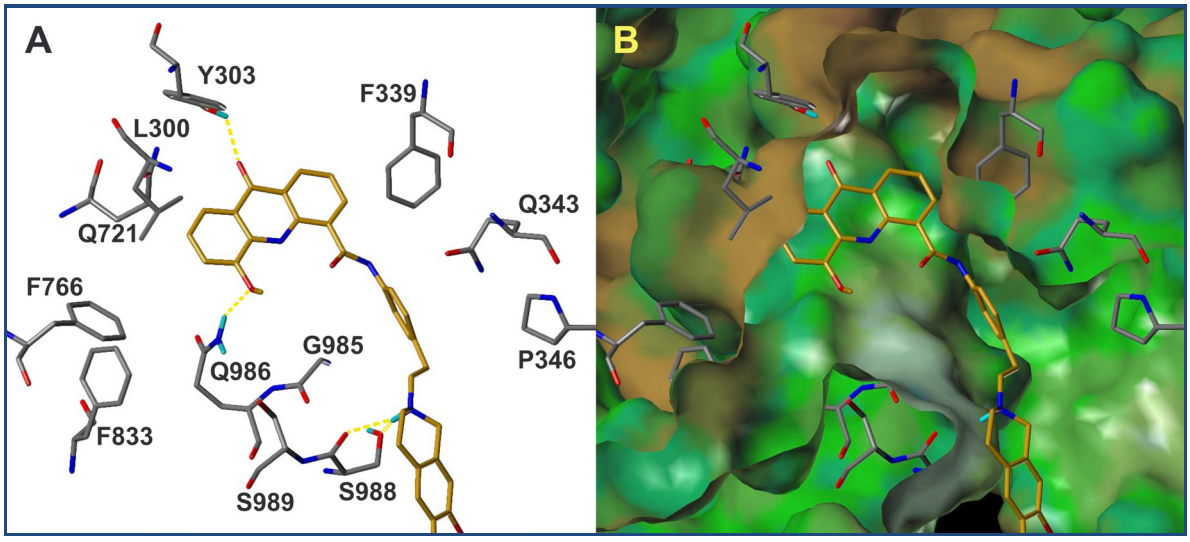

Figure 7.13: A) Model of the assumed Abcb1a binding site for elacridar; shown are residues within 3 Å around the ligand, except (for clarity) A981, V984 and D993 (TM12). Formation of H-bonds is possible with Y303 (TM5), Q986 (TM12) and both, the backbone and the side chain oxygen of S988 (TM12). **B)** Connolly surface (cross-sectional slice) of the binding site colored by the lipophilic potential (brown - lipophilic, green/blue - hydrophilic); a minor twist of the acridine ring enables the accommodation in the binding pocket and H-bonds with Y303 and Q986.

A further cause for the high activity of elacridar might be favored entropy driven binding due to the reduced flexibility in contrast to the tariquidar-like modulators.

7.4 Summary and conclusions

In the following, items associated with species differences of the transporters and conclusions with respect to the design of optimized modulators (regarding solubility, affinity and verification of binding modes) will be addressed.

Abcb1a and Abcb1b are results of a gene duplication in rodents (Dean and Annilo, 2005). Our docking studies were based on the x-ray structure of the murine Abcb1a transporter. The binding mode at human P-glycoprotein may be more or less different (Gottesman et

al., 2009). Indeed, substrate patterns and inhibitory potencies of modulators differ among the two murine isoforms themselves and the human transporter (Schwab et al., 2003; Tang-Wai et al., 1995). Nevertheless, the sequence identity between Abcb1a and the human transporter of 87.3 % is high (93.3 % similarity), even higher than the identity between the two murine isoforms (83.9 % identity, 92.1 % similarity). With regard to the proposed binding modes of tariquidar-like modulators, mainly residues in close proximity to the ligands are relevant. **Table 7.1** shows the high degree of conserved residues especially between the human and the murine Abcb1a transporter. Only F833 in TM9 is replaced by a threonin residue. With respect to the second rodent transporter, five amino acids are different. In this case, especially the replacement of Q986 by asparagine could affect the inhibitory potency.

Accordingly, all tariquidar-like modulators investigated in chapter 3 on murine P388D$_1$Doxo cells showed nearly the same affinity increase (IC_{50}-ratios) compared to the assay on human Kb-V1 cells. This can be explained with the specific experimental set-up and the utilized cell species. Valspodar with a unique structure (and a presumably distinct binding region) exhibited a significantly greater IC_{50}-ratio.

Table 7.1: Comparison of residues forming the binding pocket of tariquidar in docking studies on the murine transporter Abcb1a with the corresponding residues of the human (ABCB1) and the second murine analog (Abcb1b)[a,b]

Abcb1a	L 300	Y 303	Y 306	F 332	L 335	I 336	F 339	Q 343	P 346	N 717	Q 721	F 724	
ABCB1	*	*	*	*	*	*	*	*	*	*	*	*	
Abcb1b	*	*	*	*	*	L	*	H	*	*	*	*	
TM		5				6					7		
Abcb1a	L 758	S 762	F 766	A 830	F 833	F 974	V 978	A 981	M 982	G 985	Q 986	S 988	S 989
ABCB1	*	*	*	*	T	*	*	*	*	*	*	*	*
Abcb1b	M	*	*	*	T	*	*	*	*	*	N	*	*
TM		8		9					12				

[a] In order to consider different orientations of the various ligands, amino acids within 6 Å of the modulator are listed.

[b] Stars indicate sequence identity of the corresponding residue with the murine Abcb1a transporter.

Our results might be helpful in the design of P-gp modulators. Structural modifications increasing solubility are not appropriate due to the influence of lipophilicity on inhibitory activity. The modulators require a certain amount of hydrophobicity to accumulate in the membrane and approach the binding site. A prodrug concept could help to solve this problem.

Structural modifications of tariquidar with probably positive influence on the P-gp affinity of the modulators are summarized in **Figure 7.14**. Targeting Q343 in TM6 with an H-bond

donor or acceptor group could stimulate binding by an additional specific interaction. Rigidisations of the ligand could increase inhibitory activity due to enhanced entropy driven binding. Considering the substantial size of the binding pocket, also bivalent compounds are conceivable. The second pharmacophore could bind to residues in the upper region of the internal cavity (occupied by the QZ59-isomers).

Addressing of Gln 343

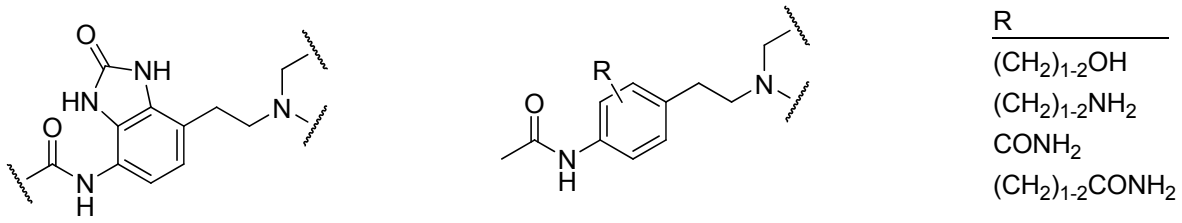

Rigidisations

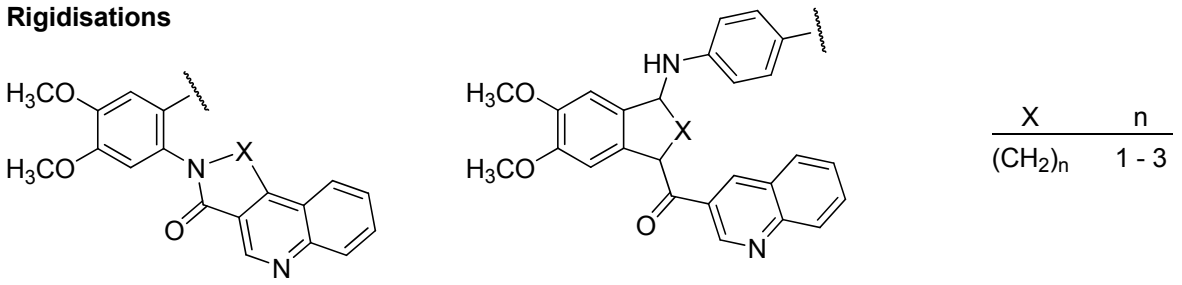

Bivalent Compounds

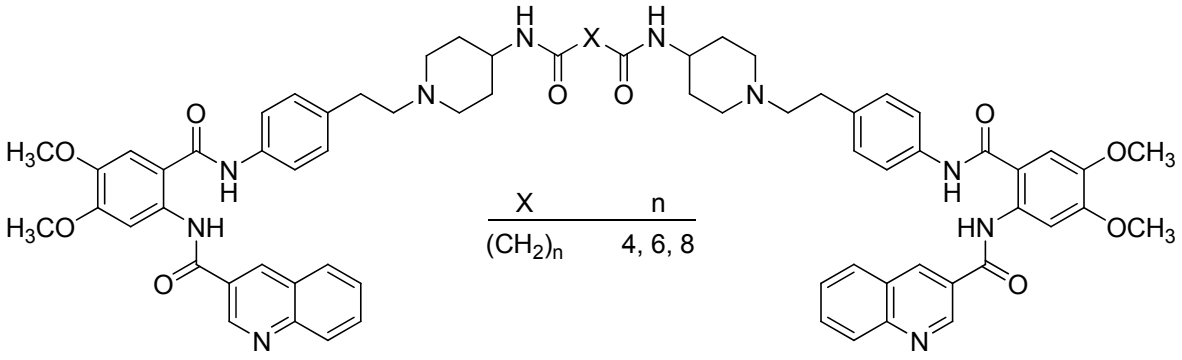

Figure 7.14: Suggested structural modifications of tariquidar to increase affinity to the ABCB1 transporter.

Furthermore, it would be helpful to verify the "lipophilicity hypothesis" and the proposed binding modes with a series of structurally altered compounds.

Table 7.2 summarizes possible modifications, the anticipated effect and the rationale based on the proposed binding modes. In particular, alkylation of the tertiary amine should be probed, because the interaction with S988 is suggested to be crucial for all investigated

modulators. Nevertheless, due to multispecifity of P-gp, it is also conceivable, that such compounds are able to bind with an altered binding mode at a different binding site.

Table 7.2: Overview about recommended structural modifications to verify the suggested binding modes; additionally, the predicted effects on the inhibitory potency and the underlying mechanisms are listed.

Recommended structural modification	Predicted effect on potency	Rationale
mono- and dichlorinated derivatives at the central aromatic ring system	increase	higher lipophilicity increases concentration in membrane
replacement of dimethoxy-tetrahydroisoquinoline moiety with piperidine	unaltered	no distinct interactions of the dimethoxybenzyl moiety
alkylation of the tertiary amine	pronounced decrease	loss of charge-assisted H-bond(s) with S988
replacement of isoquinoline moiety with 2-naphthyl moiety	decrease	loss of specific interaction with N717
removal of the 4,5-dimethoxy groups of the benzamide moiety	decrease	loss of H-bond with Y303

Additionally, the limited sterical freedom in meta- and para-position of the benzamide moiety is in agreement with the observed selectivity of meta- and para-substituted tariquidar analogs for the ABCG2 transporter. The exact knowledge of the binding region at P-gp can also facilitate an anti-target based design of selective ABCG2 modulators.

In summary, the molecular modeling investigations facilitate a unique insight into the structure and function of P-glycoprotein. The location of the proposed binding region is in accordance with the suggested transport mechanism and with results from labeling, cross-linking, mutational and x-ray crystallographic experiments. The proposed binding modes largely agree with the inhibitory potencies of tariquidar-like modulators and can explain the selectivity of the meta- and para-substituted analogs for the ABCG2 transporter. Furthermore, the putative binding site with six polar residues distributed over 4 TMs in a highly lipophilic environment provides the necessary selectivity, flexibility and multispecificity P-glycoprotein is notorious for.

7.5 References

Aller, S. G.; Yu, J.; Ward, A.; Weng, Y.; Chittaboina, S.; Zhuo, R., et al. Structure of P-glycoprotein reveals a molecular basis for poly-specific drug binding. *Science* **2009,** 323, 1718-1722.

Chen, C. J.; Chin, J. E.; Ueda, K.; Clark, D. P.; Pastan, I.; Gottesman, M. M., et al. Internal duplication and homology with bacterial transport proteins in the mdr1 (P-glycoprotein) gene from multidrug-resistant human cells. *Cell* **1986,** 47, 381-389.

Chen, Y.; Pant, A. C.; Simon, S. M. P-glycoprotein does not reduce substrate concentration from the extracellular leaflet of the plasma membrane in living cells. *Cancer Res.* **2001,** 61, 7763-7769.

Dean, M.; Annilo, T. Evolution of the ATP-binding cassette (ABC) transporter superfamily in vertebrates. *Annu. Rev. Genomics Hum. Genet.* **2005,** 6, 123-142.

Gatlik-Landwojtowicz, E.; Aanismaa, P.; Seelig, A. Quantification and characterization of P-glycoprotein-substrate interactions. *Biochemistry* **2006,** 45, 3020-3032.

Globisch, C.; Pajeva, I. K.; Wiese, M. Identification of putative binding sites of P-glycoprotein based on its homology model. *ChemMedChem.* **2008,** 3, 280-295.

Gottesman, M. M.; Ambudkar, S. V.; Xia, D. Structure of a multidrug transporter. *Nat. Biotechnol.* **2009,** 27, 546-547.

Higgins, C. F. Multiple molecular mechanisms for multidrug resistance transporters. *Nature* **2007,** 446, 749-757.

Juliano, R. L.; Ling, V. A surface glycoprotein modulating drug permeability in Chinese hamster ovary cell mutants. *Biochim. Biophys. Acta* **1976,** 455, 152-162.

Klebe, G. Konformationsanalyse. In *Wirkstoffdesign Entwurf und Wirkung von Arzneistoffen*, 2009; Vol. 2.

Kühnle, M.; Egger, M.; Müller, C.; Mahringer, A.; Bernhardt, G.; Fricker, G., et al. Potent and selective inhibitors of breast cancer resistance protein (ABCG2) derived from the p-glycoprotein (ABCB1) modulator tariquidar. *J. Med. Chem.* **2009,** 52, 1190-1197.

Larkin, M. A.; Blackshields, G.; Brown, N. P.; Chenna, R.; McGettigan, P. A.; McWilliam, H., et al. Clustal W and Clustal X version 2.0. *Bioinformatics* **2007,** 23, 2947-2948.

Lee, J. Y.; Urbatsch, I. L.; Senior, A. E.; Wilkens, S. Nucleotide-induced structural changes in P-glycoprotein observed by electron microscopy. *J. Biol. Chem.* **2008,** 283, 5769-5779.

Loo, T. W.; Bartlett, M. C.; Clarke, D. M. Methanethiosulfonate derivatives of rhodamine and verapamil activate human P-glycoprotein at different sites. *J. Biol. Chem.* **2003a,** 278, 50136-50141.

Loo, T. W.; Bartlett, M. C.; Clarke, D. M. Simultaneous binding of two different drugs in the binding pocket of the human multidrug resistance P-glycoprotein. *J. Biol. Chem.* **2003b,** 278, 39706-39710.

Loo, T. W.; Bartlett, M. C.; Clarke, D. M. Transmembrane segment 7 of human P-glycoprotein forms part of the drug-binding pocket. *Biochem. J.* **2006,** 399, 351-359.

Loo, T. W.; Clarke, D. M. Cross-linking of human multidrug resistance P-glycoprotein by the substrate, tris-(2-maleimidoethyl)amine, is altered by ATP hydrolysis. Evidence for rotation of a transmembrane helix. *J. Biol. Chem.* **2001a,** 276, 31800-31805.

Loo, T. W.; Clarke, D. M. Defining the drug-binding site in the human multidrug resistance P-glycoprotein using a methanethiosulfonate analog of verapamil, MTS-verapamil. *J. Biol. Chem.* **2001b,** 276, 14972-14979.

Lovell, S. C.; Word, J. M.; Richardson, J. S.; Richardson, D. C. The penultimate rotamer library. *Proteins* **2000,** 40, 389-408.

McDevitt, C. A.; Callaghan, R. How can we best use structural information on P-glycoprotein to design inhibitors? *Pharmacol. Ther.* **2007,** 113, 429-441.

Müller, C. New approaches to the therapy of glioblastoma: investigations on RNA interference, kinesin Eg5 and ABCB1/ABCG2 inhibition. PhD thesis, University of Regensburg, Regensburg, Germany, 2007.

Müller, C.; Gross, D.; Sarli, V.; Gartner, M.; Giannis, A.; Bernhardt, G., et al. Inhibitors of kinesin Eg5: antiproliferative activity of monastrol analogues against human glioblastoma cells. *Cancer Chemother. Pharmacol.* **2007,** 59, 157-164.

Neyfakh, A. A. Mystery of multidrug transporters: the answer can be simple. *Mol. Microbiol.* **2002,** 44, 1123-1130.

Perego, P.; De Cesare, M.; De Isabella, P.; Carenini, N.; Beggiolin, G.; Pezzoni, G., et al. A novel 7-modified camptothecin analog overcomes breast cancer resistance protein-associated resistance in a mitoxantrone-selected colon carcinoma cell line. *Cancer Res.* **2001,** 61, 6034-6037.

Raviv, Y.; Pollard, H. B.; Bruggemann, E. P.; Pastan, I.; Gottesman, M. M. Photosensitized labeling of a functional multidrug transporter in living drug-resistant tumor cells. *J. Biol. Chem.* **1990,** 265, 3975-3980.

Romsicki, Y.; Sharom, F. J. The membrane lipid environment modulates drug interactions with the P-glycoprotein multidrug transporter. *Biochemistry* **1999,** 38, 6887-6896.

Rosenberg, M. F.; Callaghan, R.; Modok, S.; Higgins, C. F.; Ford, R. C. Three-dimensional structure of P-glycoprotein: the transmembrane regions adopt an asymmetric configuration in the nucleotide-bound state. *J. Biol. Chem.* **2005,** 280, 2857-2862.

Rothnie, A.; Storm, J.; McMahon, R.; Taylor, A.; Kerr, I. D.; Callaghan, R. The coupling mechanism of P-glycoprotein involves residue L339 in the sixth membrane spanning segment. *FEBS Lett.* **2005,** 579, 3984-3990.

Schmid, D.; Ecker, G.; Kopp, S.; Hitzler, M.; Chiba, P. Structure-activity relationship studies of propafenone analogs based on P-glycoprotein ATPase activity measurements. *Biochem. Pharmacol.* **1999,** 58, 1447-1456.

Schwab, D.; Fischer, H.; Tabatabaei, A.; Poli, S.; Huwyler, J. Comparison of in vitro P-glycoprotein screening assays: recommendations for their use in drug discovery. *J. Med. Chem.* **2003,** 46, 1716-1725.

Seelig, A.; Landwojtowicz, E. Structure-activity relationship of P-glycoprotein substrates and modifiers. *Eur. J. Pharm. Sci.* **2000,** 12, 31-40.

Shapiro, A. B.; Ling, V. Extraction of Hoechst 33342 from the cytoplasmic leaflet of the plasma membrane by P-glycoprotein. *Eur. J. Biochem.* **1997,** 250, 122-129.

Sheps, J. A. Biochemistry. Through a mirror, differently. *Science* **2009,** 323, 1679-1680.

Szakacs, G.; Paterson, J. K.; Ludwig, J. A.; Booth-Genthe, C.; Gottesman, M. M. Targeting multidrug resistance in cancer. *Nat. Rev. Drug Discov.* **2006,** 5, 219-234.

Tang-Wai, D. F.; Kajiji, S.; DiCapua, F.; de Graaf, D.; Roninson, I. B.; Gros, P. Human (MDR1) and mouse (mdr1, mdr3) P-glycoproteins can be distinguished by their respective drug resistance profiles and sensitivity to modulators. *Biochemistry* **1995,** 34, 32-39.

Tripos. *FlexiDock™ Manual*. 2006.

Wang, R. B.; Kuo, C. L.; Lien, L. L.; Lien, E. J. Structure-activity relationship: analyses of p-glycoprotein substrates and inhibitors. *J. Clin. Pharm. Ther.* **2003,** 28, 203-228.

Ward, A.; Reyes, C. L.; Yu, J.; Roth, C. B.; Chang, G. Flexibility in the ABC transporter MsbA: Alternating access with a twist. *Proc. Natl. Acad. Sci. U. S. A.* **2007,** 104, 19005-19010.

Chapter 8

8 Summary

The ABCB1 transporter (P-glycoprotein), an ATP-driven efflux protein, strongly influences the absorption, distribution and excretion of various drugs. As an essential component of the blood-brain barrier, P-glycoprotein limits the penetration of potent cytostatic agents (e.g. paclitaxel) into the central nervous system (CNS). Furthermore, over-expression of ABCB1 transporters in tumor cells is one of the major mechanisms of classical multidrug resistance (MDR) in cancer. Hence, inhibition of P-glycoprotein is an attractive strategy to improve the therapy of both, tumors in the CNS and MDR malignancies in the periphery.

Accordingly, a series of potent inhibitors derived from the 3rd generation P-glycoprotein modulator tariquidar was investigated in vitro. A fluorescence-based efflux-assay using human Kb-V1 cells was established at the microtiter plate format. The obtained data were in good agreement with the validated flow cytometric method while throughput was substantially increased. Additionally, cells expressing the murine transporter were generated to assure activity at rodent P-glycoprotein. Further biopharmaceutical investigations (concerning toxicity, stability, plasma albumin binding and inhibition of cytochrome P450 isoenzymes) confirmed the suitability of tariquidar and the three most promising derivatives (bearing polar residues such as a methoxyethoxyethylamino (ME27-4), a morpholino (ME30-1) or an ethoxyethyloxy (ME33-1) moiety) for further in vivo studies.

In order to determine the concentration of the selected modulators in brain and plasma samples, a solid-phase extraction procedure followed by RP-HPLC analysis was validated. The method yielded reproducible high recoveries, a low limit of quantification as well as high accuracy and precision. The concomitant administration of paclitaxel in successive bio-distribution studies in NMRI mice revealed favorable bioavailability and high metabolic stability of the tariquidar-like compounds. As desired, the modulators significantly increased the brain AUC of paclitaxel. The observed increase by a factor of two to four

correlated with the previously determined in vitro potency of the various inhibitors. In contrast to the co-administration of the 2nd generation modulator valspodar, the plasma AUC of paclitaxel was unaffected, indicating lower systemic toxicity.

To investigate if the increased paclitaxel brain concentration is of relevance for the therapy of malignant brain tumors, an intracerebral xenograft model in nude mice was refined. Human U-118 MG glioblastoma cells were transfected with the genes encoding for the far-red fluorescent protein or the luciferase2 (Luc2) enzyme to facilitate non-invasive determination of tumor burden by means of fluorescence or bioluminescence imaging (BLI). Tumors originating from intracranial injection of luciferase2 expressing cells were detectable in the living animal. Unfortunately, the growth behavior was unsuitable for the intended in vivo investigations. Alternatively, highly tumorigenic U-87 Luc2 xenografts were utilized for subsequent treatment experiments evaluating the combination of paclitaxel with the most potent modulators ME33-1 or tariquidar. Since the obtained light signals largely correlated with the histological determined tumor burden, BLI revealed a moderate retardation of tumor progression when paclitaxel was combined with an ABCB1 modulator.

Furthermore, the therapeutic value of the co-administration of ABCB1 modulators with paclitaxel in the treatment of MDR tumors was investigated. For this purpose, ABCB1 transporter over-expressing Kb-V1 cells were extensively characterized in vitro followed by subcutaneous implantation into nude mice. The resulting malignancies showed high tumorigenicity, reproducible growth kinetics and maintained transporter expression in vivo. In subsequent treatment experiments ME30-1, ME33-1 and tariquidar were investigated. In contrast to the other modulators, only the combination of ME30-1 with paclitaxel significantly slowed down the growth of Kb-V1 tumors compared to paclitaxel mono-therapy.

Additionally, molecular modeling investigations were performed based on the very recently published x-ray structure of the murine Abcb1a transporter. Conformational analysis of the tariquidar-like modulators provided the starting conformation for successive docking experiments. The location of the subsequently identified binding region is in accordance with the suggested transport mechanism and experimental data from the literature. The proposed binding modes largely agree with the inhibitory potencies of the investigated ABCB1 modulators and explain the negligible ABCB1 activity of tariquidar-derived, selective ABCG2 modulators. The findings facilitate the structure based design of optimized ABCB1 modulators and may contribute to improve the adjuvant cancer chemotherapy of glioblastomas and MDR tumors.

Appendices

A Appendix 1: In vitro activity of epothilones against human glioblastoma cells and interaction with ABC transporters

A.1 Introduction

Due to the crucial role of microtubules in cell transport, signaling and mitosis, drugs which destabilize (e.g. vinca alkaloids) or stabilize (e.g. taxanes) microtubules are among the most commonly prescribed anticancer agents (Goodin et al., 2004). Although taxanes are active against a broad range of solid malignancies, their clinical use is limited. The most important issues are the risk of hypersensitivity reactions, toxicity (first and foremost on hematopoiesis (dose limiting) and the nervous system (cumulative)) and tumor resistance (Morris and Fornier, 2008).

The epothilones, a new class of microtubule-stabilizing agents (Bollag et al., 1995) are naturally occurring 16-membered macrocyclic polyketides with no structural relation to the taxanes (see **Figure A.1**).

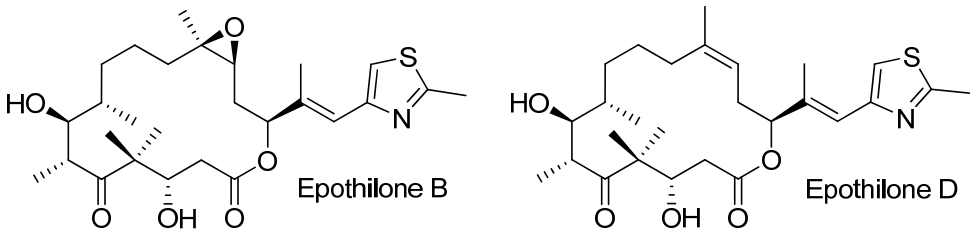

Figure A.1: Chemical structures of the two investigated epothilones. This compound class was initially discovered as cytotoxic metabolites from the myxobacterium *Sorangium cellulosum.*

Beside their impressive intracellular accumulation (Wartmann and Altmann, 2002), the epothilones are of special interest because of their activity against both, multidrug resistant

cancer cells (Kowalski et al., 1997) and tumors (Altmann et al., 2000). Since the expression of P-glycoprotein is one of the major mechanisms of MDR in cancer (Szakacs et al., 2006), the epothilones are considered to be not or at least less susceptible to ABC transporter mediated chemoresistance and hence superior to established cytostatic drugs such as vinblastine and paclitaxel (Aghajanian et al., 2007).

Due to the fact that epothilones are able to displace [^{3}H]-paclitaxel from microtubules, an overlapping or even identical binding site was postulated (Bollag et al., 1995; Wartmann and Altmann, 2002). The proposed common binding pocket on β-tubulin has (despite the above mentioned poor structural similarity to paclitaxel) encouraged speculations about a common pharmacophore (Giannakakou et al., 2000).

The publication of the structure of epothilone A (Epo A) bound to tubulin determined by electron crystallography and nuclear magnetic resonance spectroscopy (Nettles et al., 2004) revealed that Epo A and paclitaxel indeed occupy a rather expansive common binding site (see **Figure A.2**). However, since side chains and all functional groups (except C7-OH) exploit distinctly different regions of the binding pocket, the speculations about a common pharmacophore turned out to be wrong.

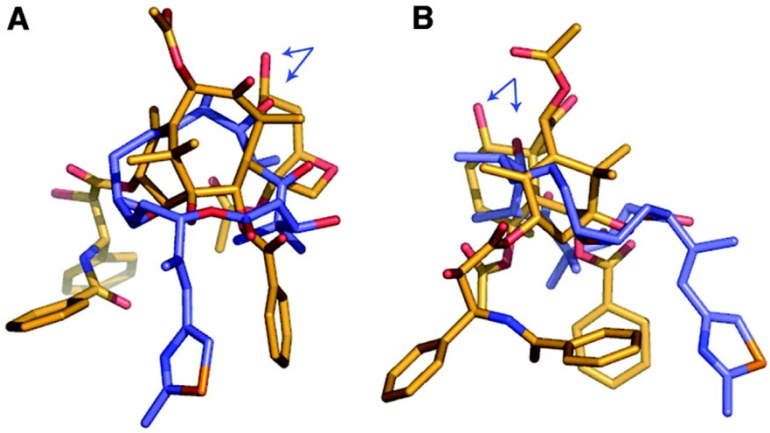

Figure A.2: Superposition of Epo A (*blue*) and paclitaxel (*gold*) in ß-tubulin. The single common center (C7-OH) is indicated by blue arrows. The image in **(A)** relates to a 90° rotation of the image in **(B)**. Reprinted from Nettles et al. (2004) with permission from The American Association for the Advancement of Science.

Nevertheless, the fact that such structurally diverse compounds[1] (Kar et al., 2003) bind with low nanomolar affinity to the same promiscuous binding pocket in totally different orientations by interacting with an optimal subset of residues raises the question whether this is also possible for the multispecific binding region of P-glycoprotein. And indeed, there is evidence that epothilones have a certain susceptibility for the ABCB1 transporter and that there are differences in affinity depending on the structure of the particular epothilones (Chou et al., 1998; Goodin et al., 2004; Wartmann and Altmann, 2002).

[1] In all probability the endogenous neuronal tau protein also interacts with the same binding site at β-tubulin

Consequently, the major aim of this investigation was the further elucidation of interactions between epothilones and ABC transporters as well as their activity against different human glioblastoma cell lines.

A.2 Materials and methods

A.2.1 Drugs and chemicals

Epothilone B and epothilone D were kindly provided by the Helmholtz Zentrum für Infektionsforschung (Braunschweig, Germany). Mitoxantrone stocks were obtained by diluting Novantron® (Wyeth Pharma, Münster, Germany) in 70 % ethanol. A 10 mM stock solution of Ko143 in DMSO was a gift from Dr. A. H. Schinkel (Netherlands Cancer Institute). Rotenone and mitoxantrone were purchased from Sigma (Munich, Germany). Tariquidar and the tariquidar-like modulators were synthesized according to the literature (Egger et al., 2007; Hubensack, 2005). Murine serum was isolated from mature CD-1 mice and stored at -78 °C until usage.

A.2.2 Cell lines and culture conditions

Cells were maintained as described in section 3.2.2.

A.2.3 Chemosensitivity assay

The assays were performed as described in section 3.2.5.

A.2.4 Calcein-AM efflux assay

The assays were performed as described in section 3.2.3.1.1.

A.2.5 Confocal laser-scanning microscopy

The assays were performed as described in section 3.2.7.

A.3 Results and discussion

A.3.1 Antiproliferative activity against human glioblastoma cells

The susceptibility of the tumor to the selected cytostatic drug is a major prerequisite for the co-administration of anticancer agents and ABCB1 modulators in brain cancer chemotherapy. Consequently, in a first step the sensitivity of U-87 MG, U-118 MG and U-373 MG glioblastoma cells against epothilone B (Epo B) and epothilone D (Epo D) was investigated by means of the crystal violet chemosensitivity assay.

A.3.1.1 Effect of permanent exposure

The impact of permanent incubation with Epo B and D on proliferating U-87 MG and U-118 MG cells is presented in **Figure A.3** and **Figure A.4**. Epo B shows cytostatic effects at a concentration of 0.5 nM and no cytocidal effects up to 10 nM. In the case of Epo D approximately 10-fold higher concentrations were required for equal drug action.

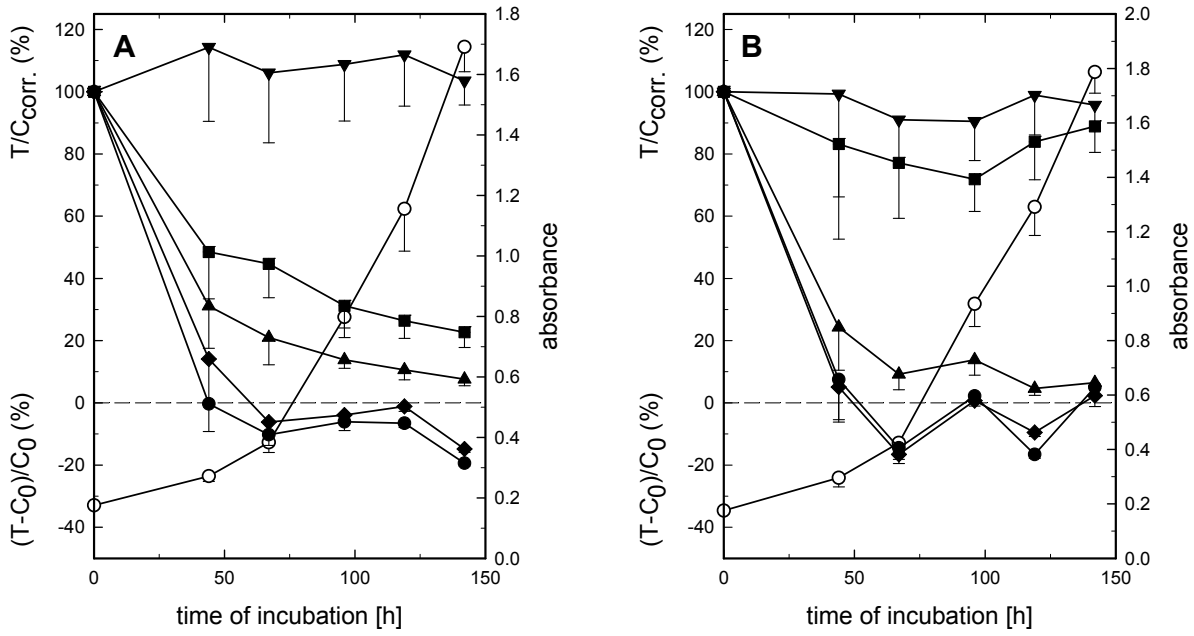

Figure A.3: Effect of Epo B and Epo D on proliferating U-87 MG cells (passage 180) during permanent incubation; vehicle *(open circles)*; **A)** Epo B at different concentrations: 0.1 nM *(filled inverted triangles)*, 0.5 nM *(filled squares)*, 1 nM *(filled triangles)*, 5 nM *(filled circles)* and 10 nM *(filled diamonds)*; **B)** Epo D at different concentrations: 0.5 nM *(filled inverted triangles)*, 1 nM *(filled squares)*, 5 nM *(filled triangles)*, 10 nM *(filled circle)* and 50 nM *(filled diamonds)*

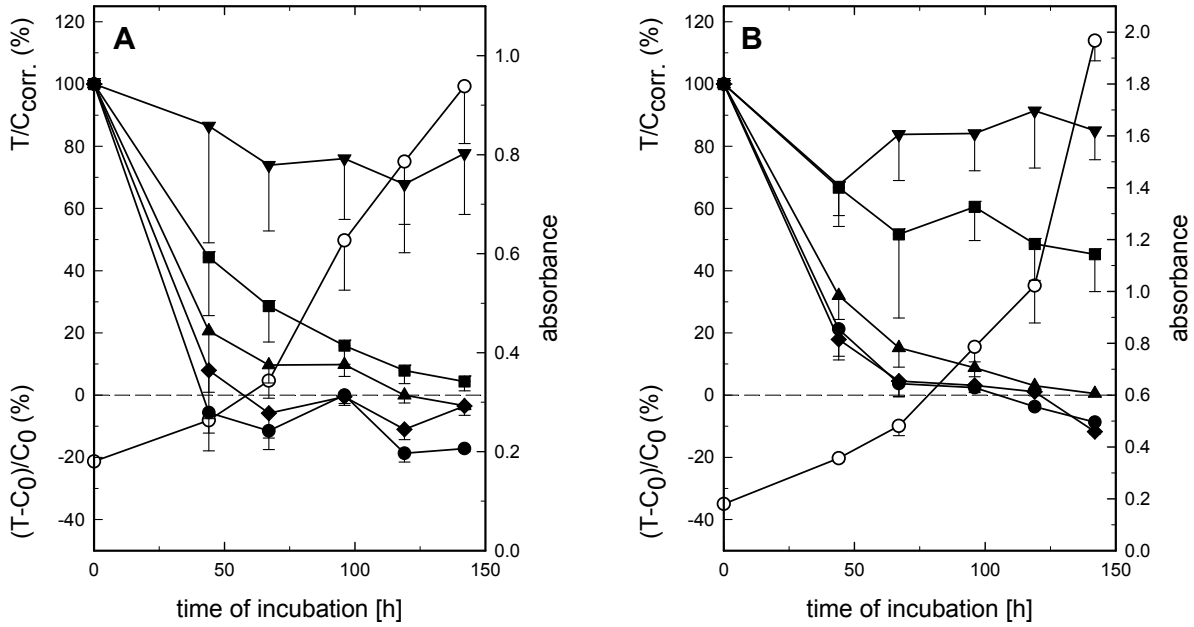

Figure A.4: Effect of Epo B and Epo D on proliferating U-118 MG cells (passage 495) during permanent incubation; vehicle *(open circles)*; **A)** Epo B at different concentrations: 0.1 nM *(filled inverted triangles)*, 0.5 nM *(filled squares)*, 1 nM *(filled triangles)*, 5 nM *(filled circles)* and 10 nM *(filled diamonds)*; **B)** Epo D at different concentrations: 0.5 nM *(filled inverted triangles)*, 1 nM *(filled squares)*, 5 nM *(filled triangles)*, 10 nM *(filled circle)* and 50 nM *(filled diamonds)*

When results obtained with U-373 MG cells (data not shown) are considered, the sensitivity of the selected glioblastoma cells against Epo B and D decreases according to the following order: U-373 MG cells > U-118 MG > U-87 MG. Taken together, impact on the growth of glioblastoma cells was already achieved at very low (sub-nanomolar to single digit nanomolar) concentrations.

A.3.1.2 Effect of short-term exposure

In order to investigate the cytotoxic activity at conditions (concerning exposure time and concentration) achievable in vivo, Epo B and D were removed from the culture medium after different exposure times.

Figure A.5 illustrates that a concentration of 20 nM Epo B for one hour was sufficient to reach a cytostatic drug effect. The prolongation of the exposure period did not enhance activity. This indicates that an initial damage is responsible for the antiproliferative activity. The same correlation was observed for Epo D (at a higher concentration of 100 nM).

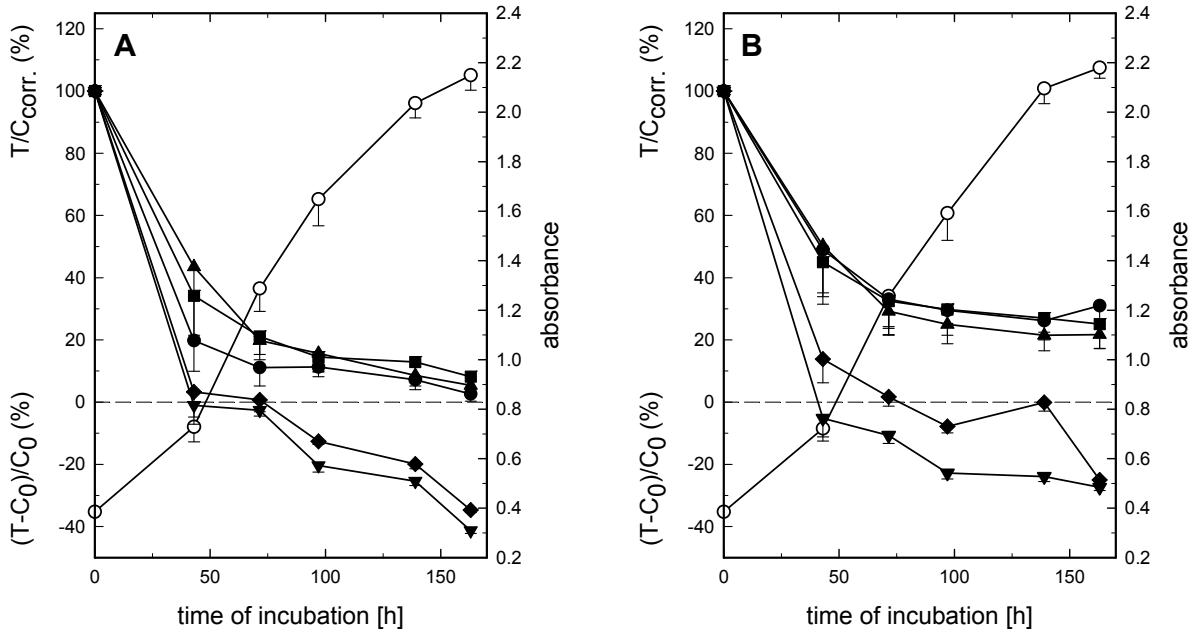

Figure A.5: Effect of Epo B and Epo D on proliferating U-118 MG cells (passage 499) during short term exposure; vehicle *(open circles)*; 100 nM VBL, permanent exposure *(filled inverted triangles)*; **A)** Epo B, 20 nM with different exposure times: 1 h *(filled squares)*, 3 h *(filled triangles)*, 5 h *(filled circles)* and permanent *(filled diamonds)*; **B)** Epo D, 100 nM with different exposure times: 1 h *(filled squares)*, 3 h *(filled triangles)*, 5 h *(filled circles)* and permanent *(filled diamonds)*

A.3.2 Influence of murine serum on stability and activity of epothilones

The previous results showed that the investigated epothilones are active in vitro. However, these experiments do not consider problems such as plasma protein binding and enzymatic degradation. Consequently, Epo B and D were incubated in murine serum prior to the experiment.

As becomes obvious from **Figure A.6**, pre-incubation of Epo B decreased its activity five to ten-fold (this effect was also observed with U-87 MG and U-373 MG cells; data not shown). Since the decrease in activity did not correlate with the pre-incubation period, a high plasma protein binding may be assumed.

In contrast, exposure of Epo D to murine serum resulted in total loss of activity regardless of pre-incubation period and concentration (results confirmed by analogous experiments with U-87 MG and U-373 MG cells; data not shown).

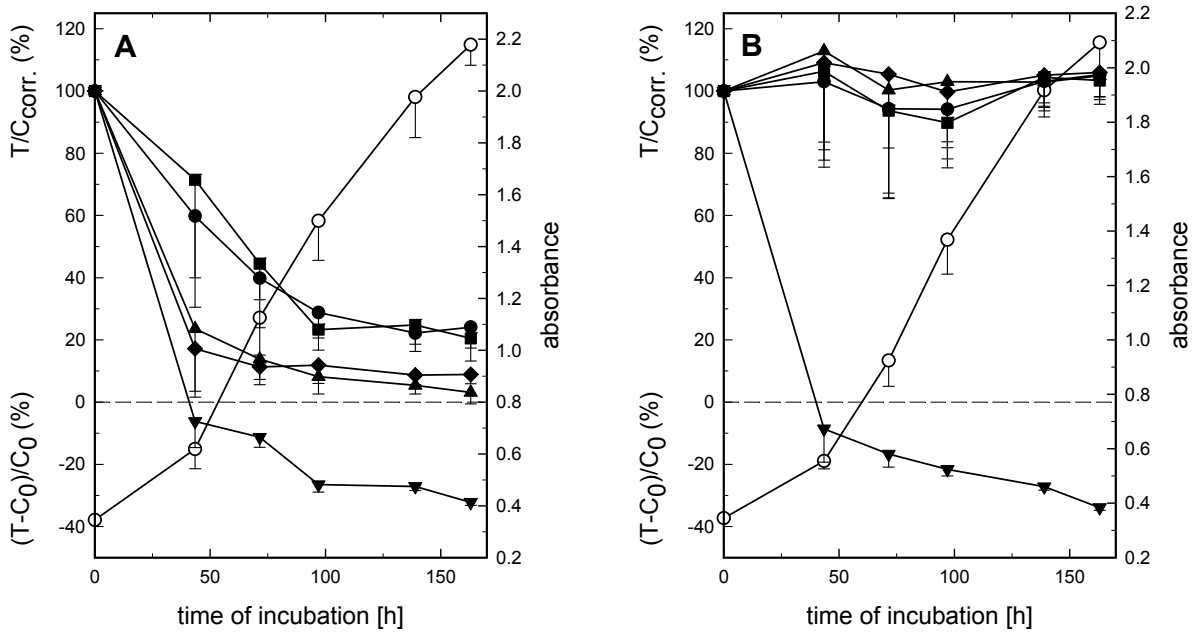

Figure A.6: Effect of Epo B and Epo D (pre-incubated with murine serum) on proliferating U-118 MG cells (passage 499); vehicle *(open circles)*, 100 nM VBL without pre-incubation period *(filled inverted triangles)*; **A)** Epo B at different concentrations and pre-incubation periods: 2 nM and 1 h *(filled squares)*, 5 nM and 1 h *(filled triangles)*, 2 nM and 3 h *(filled circles)*, 5 nM and 3 h *(filled diamonds)*; **B)** Epo D at different concentrations and pre-incubation periods: 5 nM and 1 h *(filled squares)*, 20 nM and 1 h *(filled triangles)*, 5 nM and 3 h *(filled circles)*, 20 nM and 3 h *(filled diamonds)*

The observed instability in murine serum is in agreement with hints from the literature and is probably caused by serum esterases (Chou et al., 2001). A lower susceptibility to murine enzymes is also described for Epo B (Blum et al., 2001). In all three main metabolites, the macrocyclic lactone ring was opened to the acid.

A.3.3 Effect on quiescent U-373 MG cells

In order to study whether the antiproliferative effect of the compounds is caused by specific interference during cell cycle, confluent U-373 MG glioblastoma cells were incubated with Epo B and D at high concentrations (see **Figure A.7**). Rotenone, an inhibitor of NADH ubiquinone oxidoreductase served as positive control for unspecific toxicity.

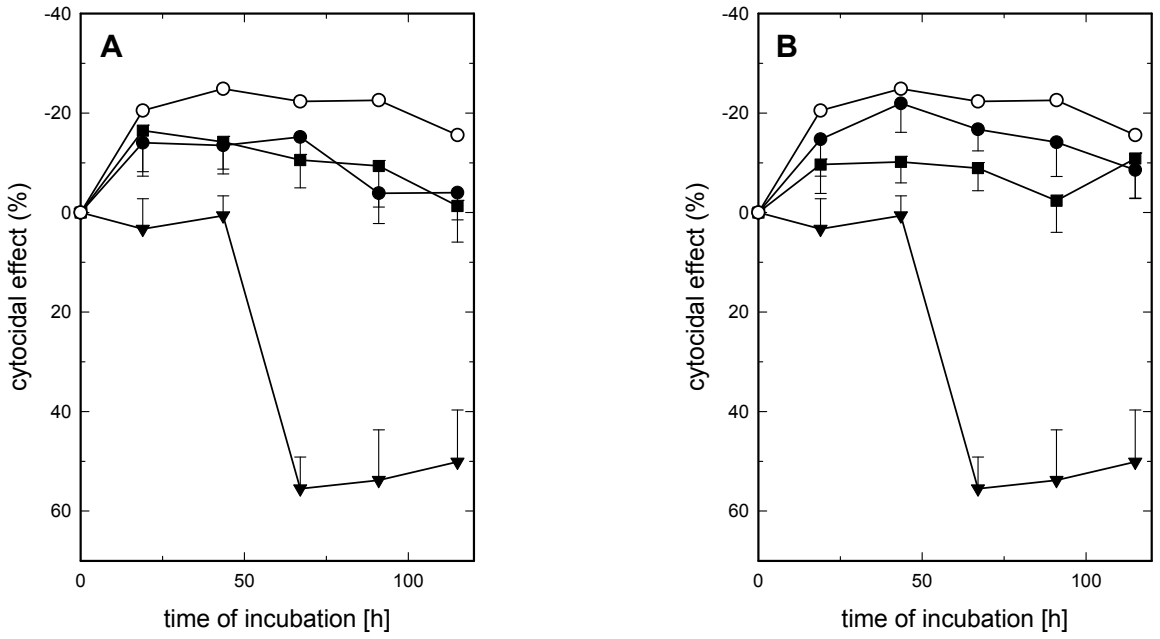

Figure A.7: Effect of Epo B and Epo D on resting U-373 MG cells (passage 240) during permanent incubation; vehicle *(open circles)*, rotenone 1 µM *(filled inverted triangles)*; **A)** Epo B at different concentrations: 5 nM *(filled circles)* and 50 nM *(filled squares)*; **B)** Epo D at different concentrations: 10 nM *(filled circles)* and 100 nM *(filled squares)*

As becomes obvious from the depicted results, Epo B as well as Epo D exerted (beyond their specific interference during cell cycle) no additional, unspecific cytocidal effect on quiescent cells.

A.3.4 Interactions with the ABCB1 transporter

For the applicability in the chemotherapy of malignant brain tumors it is important that the cytostatic drug is no substrate of transporters expressed at the BBB (in particular ABCB1 and ABCG2). Consequently, ABCB1 transporter (over)expressing Kb-V1 cells were incubated with various concentrations of Epo B and D. Additionally, cells were exposed to 100 nM of the selective P-gp modulator ME33-1. In the investigated concentration, the modulator alone had no impact on the growth of Kb-V1 cells (data not shown). The results of the chemosensitivity assays are illustrated in **Figure A.8** and **Figure A.9**.

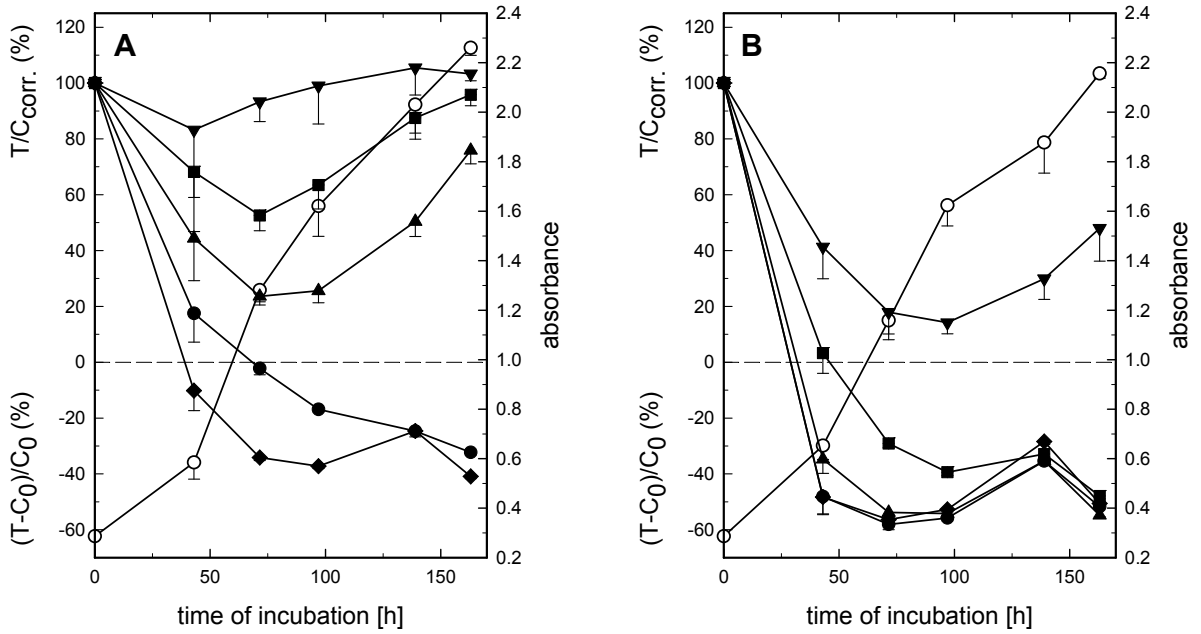

Figure A.8: A) Effect of Epo B on proliferating Kb-V1 cells (passage 61) during permanent incubation; **B)** Epo B in combination with 100 nM ME33-1; vehicle *(open circles)*, Epo D at different concentrations: 0.1 nM *(filled inverted triangles)*, 0.5 nM *(filled squares)*, 1 nM *(filled triangles)*, 5 nM *(filled circles)* and 10 nM *(filled diamonds)*

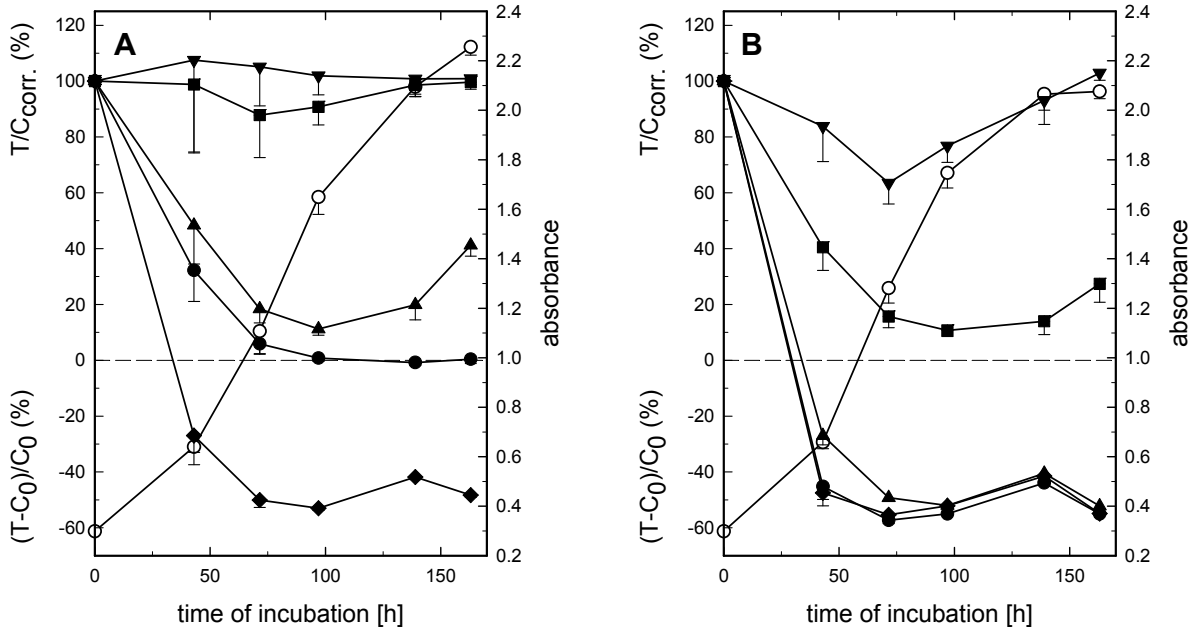

Figure A.9: A) Effect of Epo D on proliferating Kb-V1 cells (passage 61) during permanent incubation; **B)** Epo D in combination with 100 nM ME33-1; vehicle *(open circles)*, Epo D at different concentrations: 0.5 nM *(filled inverted triangles)*, 1 nM *(filled squares)*, 5 nM *(filled triangles)*, 10 nM *(filled circles)* and 50 nM *(filled diamonds)*

The chemosensitivity of Kb-V1 cells against Epo B as well as Epo D was increased 5 to 10 times by addition of ME33-1. These results militate in favor of a week interaction of the respective epothilones with the ABCB1 transporter.

Since inhibitors of P-gp are often poorly transported substrates, Epo B and Epo D were further investigated by means of the calcein-AM efflux assay (see **Figure A.10**).

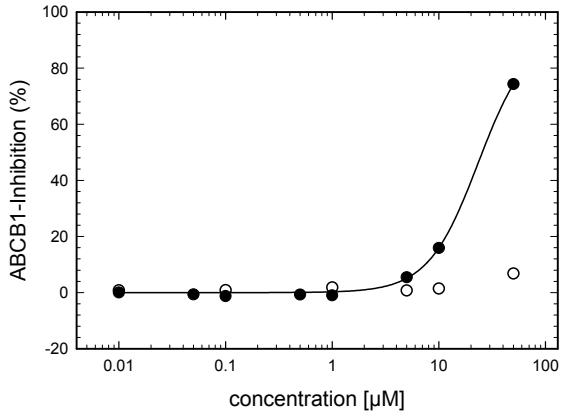

Figure A.10: ABCB1 inhibition by Epo B *(open circles)* and Epo D *(filled circles)* in dependence of their concentration determined with the calcein-AM efflux assay at the flow cytometer

Indeed, Epo D showed in concentrations ≥ 10 µM inhibition of ABCB1 transporter activity.

A.3.5 Interactions with the ABCG2 transporter

For selectivity reasons, Epo B and D were also investigated (in cooperation with Matthias Kühnle) concerning the affinity to BCRP. By analogy to the investigations described in section A.3.4, ABCG2 transporter (over)expressing MCF-7/Topo cells were used. Instead of ME33-1 the selective BCRP modulator Ko143 was chosen for the co-incubation experiments.

Figure A.11 shows that the sensitivity of MCF-7/Topo cells against Epo D was not increased by addition of Ko143. The results of analogous experiments with Epo B were identical (data not shown). In addition, no inhibition of the ABCG2 transporter at concentrations up to 50 µM was detected by means of the flow cytometric mitoxantrone efflux assay (data not shown).

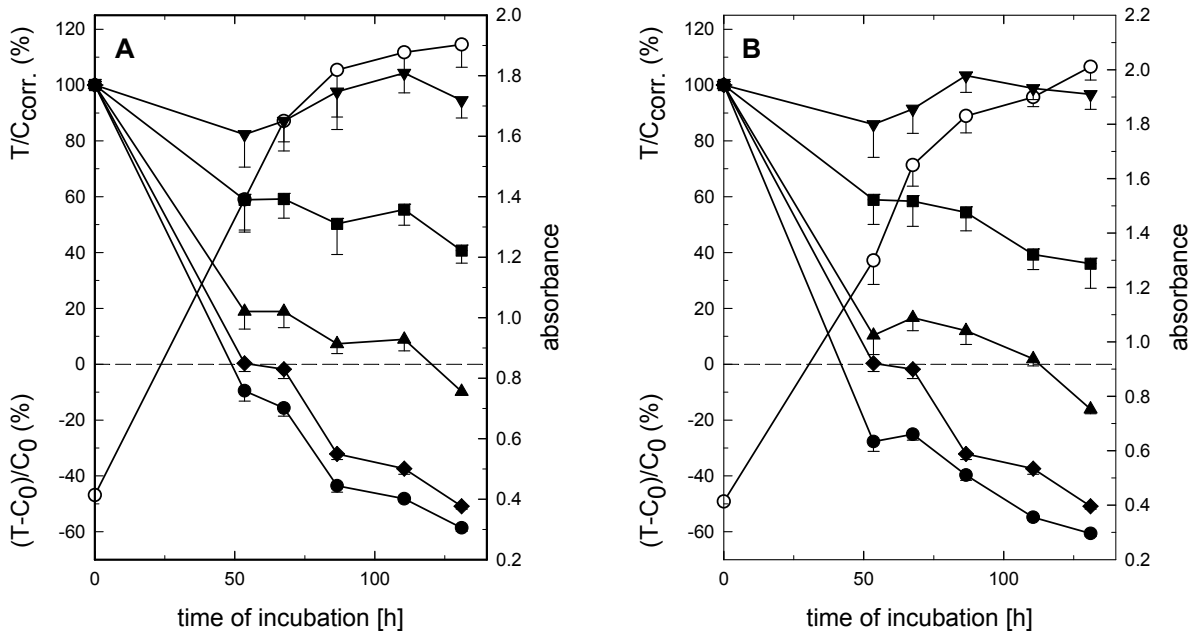

Figure A.11: A) Effect of Epo D on proliferating MCF-7/Topo cells (passage 150) during permanent incubation; **B)** Epo D in combination with 100 nM Ko143; Vehicle *(open circles)*, 10 nM VBL *(filled diamonds)* and Epo D at different concentrations: 0.5 nM *(filled inverted triangles)*, 1.0 nM *(filled squares)*, 5.0 nM *(filled triangles)* and 10 nM *(filled circles)*

A.3.6 Effect of epothilones on the tubulin architecture of Kb-V1 cells

Confocal laser-scanning microscopy was performed to investigate the effect of Epo B and D on the tubulin architecture. It can be seen from **Figure A.12** that Kb-V1 cells incubated with Epo B or D showed no abnormalities in the morphology of the cytoskeleton.

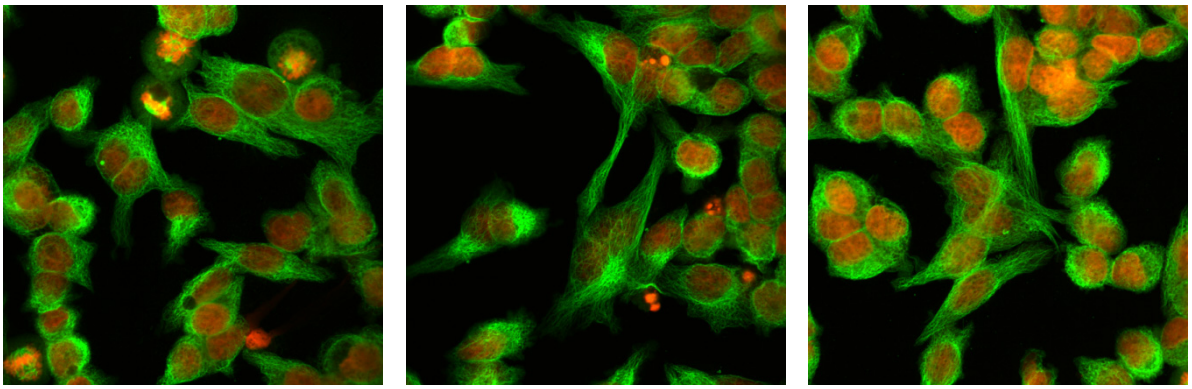

Figure A.12: Kb-V1 cells were incubated with 0.5 nM Epo B and 1 nM Epo D for 3 hours. The tubulin architecture was not visibly changed.

A.4 Summary

Epo B and D inhibited the growth of different glioblastoma cells at very low (sub-nanomolar to single digit nanomolar) concentrations. At higher concentrations (20 nM of Epo B or 100 nM of Epo D, respectively) even an exposure time of one hour was sufficient for cytostatic drug effects.

Issues associated with plasma protein binding and enzymatic degradation were investigated by pre-incubation of epothilones with murine serum. These experiments showed that only Epo B is sufficiently stable for further in vivo studies in rodents. Moreover, investigations on quiescent glioblastoma cells revealed no unspecific toxicity in the investigated concentration range.

Taken together, the experiments showed that Epo B and D were active against human glioblastoma cells under conditions mimicking the situation in vivo. In addition, the calcein-AM efflux assay disclosed a certain impact on ABCB1 transporters. The results were confirmed by co-incubation experiments with P-gp expressing cells that revealed an increased chemosensitivity of Kb-V1 cells when combined with an ABCB1 modulator.

In summary, epothilone B is a candidate for further preclinical tumor-pharmacological studies in combination with ABCB1 modulators.

A.5 References

Aghajanian, C.; Burris, H. A., 3rd; Jones, S.; Spriggs, D. R.; Cohen, M. B.; Peck, R., et al. Phase I study of the novel epothilone analog ixabepilone (BMS-247550) in patients with advanced solid tumors and lymphomas. *J. Clin. Oncol.* **2007,** 25, 1082-1088.

Altmann, K. H.; Wartmann, M.; O'Reilly, T. Epothilones and related structures - a new class of microtubule inhibitors with potent in vivo antitumor activity. *Biochim. Biophys. Acta* **2000,** 1470, M79-91.

Blum, W.; Aichholz, R.; Ramstein, P.; Kuhnol, J.; Bruggen, J.; O'Reilly, T., et al. In vivo metabolism of epothilone B in tumor-bearing nude mice: identification of three new epothilone B metabolites by capillary high-pressure liquid chromatography/mass spectrometry/tandem mass spectrometry. *Rapid Commun. Mass Spectrom.* **2001,** 15, 41-49.

Bollag, D. M.; McQueney, P. A.; Zhu, J.; Hensens, O.; Koupal, L.; Liesch, J., et al. Epothilones, a New Class of Microtubule-stabilizing Agents with a Taxol-like Mechanism of Action. *Cancer Res.* **1995,** 55, 2325-2333.

Chou, T. C.; O'Connor, O. A.; Tong, W. P.; Guan, Y.; Zhang, Z. G.; Stachel, S. J., et al. The synthesis, discovery, and development of a highly promising class of microtubule stabilization agents: curative effects of desoxyepothilones B and F against human tumor xenografts in nude mice. *Proc. Natl. Acad. Sci. U. S. A.* **2001,** 98, 8113-8118.

Chou, T. C.; Zhang, X. G.; Balog, A.; Su, D. S.; Meng, D.; Savin, K., et al. Desoxyepothilone B: an efficacious microtubule-targeted antitumor agent with a promising in vivo profile relative to epothilone B. *Proc. Natl. Acad. Sci. U. S. A.* **1998,** 95, 9642-9647.

Egger, M.; Li, X. Q.; Müller, C.; Bernhardt, G.; Buschauer, A.; König, B. Tariquidar analogues: Synthesis by Cu-^{I}-catlyzed N/O-aryl coupling and inhibitory activity against the ABCB1 transporter. *Eur. J. Org. Chem.* **2007**, 2643-2649.

Giannakakou, P.; Gussio, R.; Nogales, E.; Downing, K. H.; Zaharevitz, D.; Bollbuck, B., et al. A common pharmacophore for epothilone and taxanes: molecular basis for drug resistance conferred by tubulin mutations in human cancer cells. *Proc. Natl. Acad. Sci. U. S. A.* **2000,** 97, 2904-2909.

Goodin, S.; Kane, M. P.; Rubin, E. H. Epothilones: Mechanism of Action and Biologic Activity. *J. Clin. Oncol.* **2004,** 22, 2015-2025.

Hubensack, M. Approaches to overcome the blood brain barrier in the chemotherapy of primary and secondary brain tumors: modulation of P-glycoprotein 170 and targeting of the transferrin receptor. PhD thesis, University of Regensburg, Regensburg, Germany, 2005.

Kar, S.; Fan, J.; Smith, M. J.; Goedert, M.; Amos, L. A. Repeat motifs of tau bind to the insides of microtubules in the absence of taxol. *EMBO J.* **2003,** 22, 70-77.

Kowalski, R. J.; Giannakakou, P.; Hamel, E. Activities of the microtubule-stabilizing agents epothilones A and B with purified tubulin and in cells resistant to paclitaxel (Taxol(R)). *J. Biol. Chem.* **1997,** 272, 2534-2541.

Kühnle, M. Experimental therapy and detection of glioblastoma: investigation of nanoparticles, ABCG2 modulators and optical imaging of intracerebral xenografts. PhD thesis, University of Regensburg, Regensburg, Germany, 2010.

Morris, P. G.; Fornier, M. N. Microtubule active agents: beyond the taxane frontier. *Clin. Cancer Res.* **2008,** 14, 7167-7172.

Nettles, J. H.; Li, H.; Cornett, B.; Krahn, J. M.; Snyder, J. P.; Downing, K. H. The binding mode of epothilone A on alpha, beta-tubulin by electron crystallography. *Science* **2004,** 305, 866-869.

Szakacs, G.; Paterson, J. K.; Ludwig, J. A.; Booth-Genthe, C.; Gottesman, M. M. Targeting multidrug resistance in cancer. *Nat. Rev. Drug Discov.* **2006,** 5, 219-234.

Wartmann, M.; Altmann, K. H. The biology and medicinal chemistry of epothilones. *Curr. Med. Chem. Anticancer Agents* **2002,** 2, 123-148.

B Appendix 2: Development of an automated cryopreservation procedure for solid tumors

B.1 Introduction

This work focused on the development of a standardized and automated freezing procedure for the cryopreservation of human cancer xenografts and was done in collaboration with Matthias Kühnle. For further information concerning the technical assembly of the freezing device and other applications of the developed cryopreservation procedure please refer to his PhD thesis (Kühnle, 2010). Additionally, the tumorigenicity and the growth kinetics of re-thawed tumor tissue were investigated.

B.2 Materials and methods

B.2.1 Chemicals, culture media and technical devices

All chemicals were purchased from Merck (Darmstadt, Germany). Eagle`s Minimum Essential Medium (Sigma, Deisenhofen, Germany) was supplemented with 110 mg/L sodium pyruvate (Serva, Heidelberg, Germany) and 2.2 g/L sodium hydrogen carbonate. A computer controlled rate freezer IceCube 14S from SYLAB Geräte GmbH (Neupurkersdorf, Austria) was used for the experiments.

B.2.2 Freezing and procedure

DMSO was added to Eagle´s Minimum Essential Medium to reach a final concentration of 10 % and was subsequently sterile filtered into cryo-tubes (Greiner Bio-One, Frickenhausen, Germany). 6-10 tumor samples, generated as described in (section 5.2.9), were transferred into the cryo-tubes and stored on ice for transport.

Approximately 10 minutes before microprocessor controlled freezing according to the previously optimized protocol, samples were taken from ice. This protocol guaranteed that the increase in temperature at the point of crystallization was counteracted by extensive and rapid cooling of the freezing chamber (see **Figure B.1**). Therefore, a constant cooling

rate of the sample was regained approximately 50 % earlier what in turn minimized tissue damage (due to reduced ice crystal growth and crystallization heat).

Chamber temp. [°C]	Δ Temp. per minute [°C/min]	Runtime current step [min]	Runtime total [min]
20.0	0	0	0
0	-2.0	10.0	10.0
0	0	5.0	15.0
-14.5	-1.0	14.5	29.5
-70.0	-59.5	0.9	30.4
-70.0	0	0.5	30.9
-27.0	20.0	2.2	33.1
-22.0	2.0	2.5	35.6
-40.0	-1.0	18.0	53.6
-140.0	-2.0	50	103.6

Table B.1: Parameters of the optimized cryopreservation protocol. After 30.4 minutes (at the lowest chamber temperature of -70 °C) the crystallization was additionally triggered by controlled autoseeding for 25 seconds.

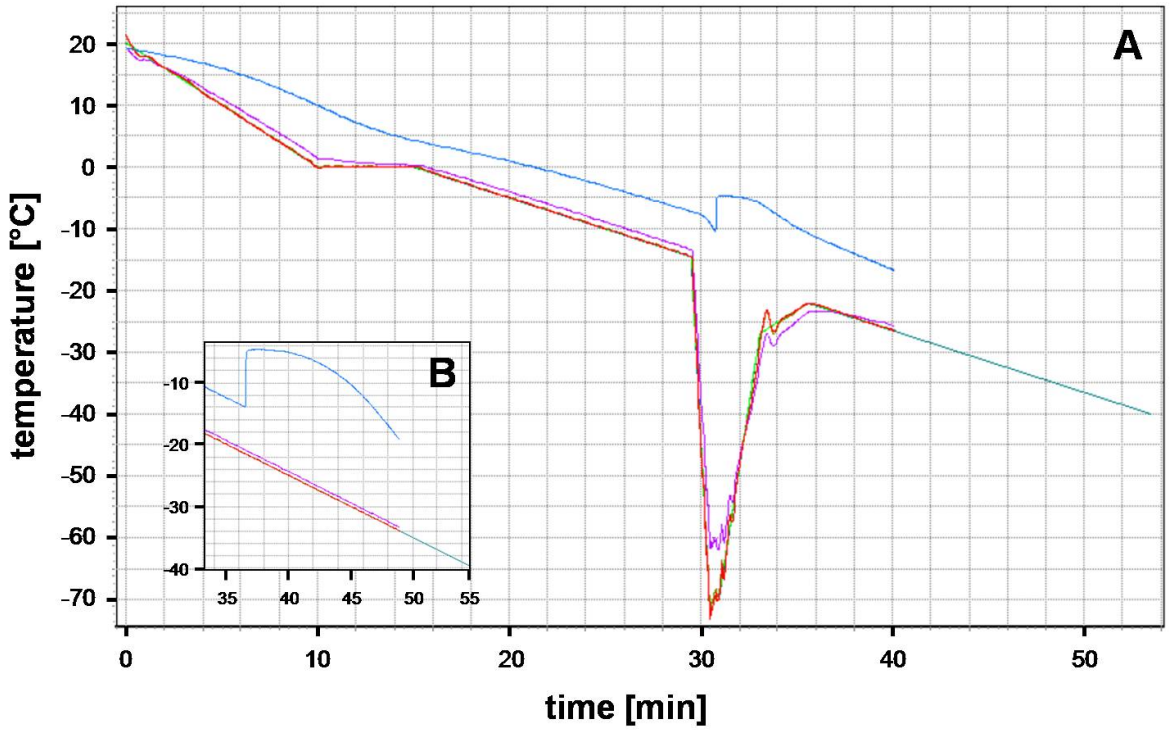

Figure B.1: A) Details of the temperature gradient of the optimized freezing protocol at different positions of the freezing chamber. The turquoise curve represents the programmed temperature profile whereas the blue curve shows the actual temperature of the sample in the cryo-tubes. In comparison to the starting protocol (with a linear cooling rate of 1 °C/min, depicted in **B**), the observed rise in temperature at the time of crystallization is considerably lower and shorter (approximately 50 % each).

After 104 minutes, the samples had reached a final, uncritical temperature of -140 °C and a constant cooling rate was no longer necessary. Subsequently, the cryo-tubes were transferred into a Dewar container for long range storing over liquid nitrogen.

B.2.3 Thawing procedure and subcutaneous xenograft implantation

Immediately before transplantation, cryopreserved tumor tissue samples were thawed rapidly by swiveling the cryo-tubes in 37 °C warm water. Afterwards, the samples were washed with sterile PBS. The subsequent tissue implantation procedure was performed as described in section 5.2.9.

B.3 Results and discussion

B.3.1 Effect of freezing and thawing on tumorigenicity and growth kinetics of Kb-V1 tumors

After approximately 3 month of storage over liquid nitrogen, Kb-V1 tissue samples maintained tumorigenicity and generated solid tumors in nude mice. Growth kinetics were determined and compared to the growth characteristics of non-frozen control tumors of the respective in vivo passage (see **Figure B.2**).

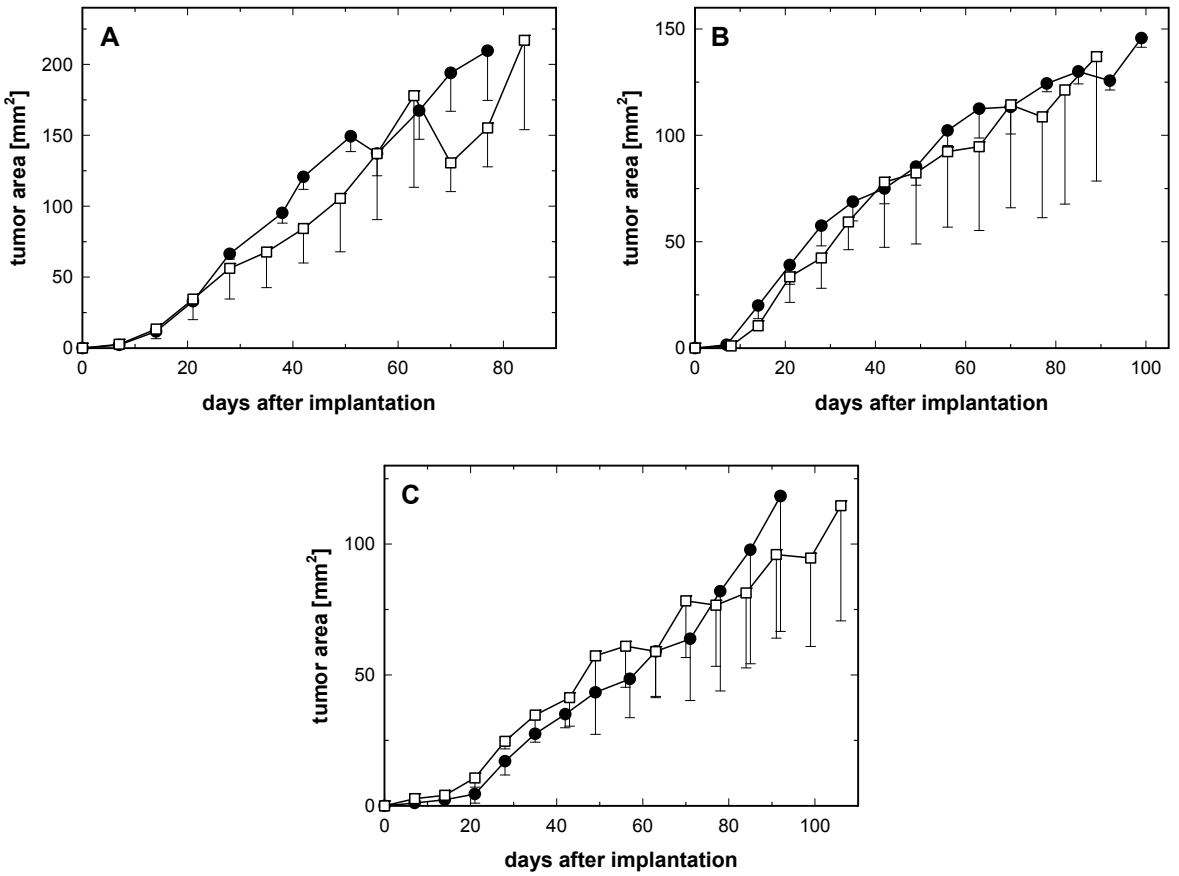

Figure B.2: The in vivo growth curves of subcutaneously growing Kb-V1 tumors are depicted (mean values ± SEM). Growth kinetics of tumors obtained by implantation of frozen and re-thawed tumor pieces *(filled circles)* are compared to serially transplanted control tumors *(open squares)* over various passages. **A)** In vivo passage 1; take rate investigational group 78 %, control mice 88 %; **B)** In vivo passage 2; take rate investigational group 100 %, control mice 75 %; **C)** In vivo passage 3; take rate investigational group 71 %, control mice 50 %

Tumors originating from frozen tissue samples showed growth characteristics and take rates comparable to serially transplanted xenografts. In **Figure B.3**, a retardation of tumor growth in higher passages (cf. section 5.3.2.1) is obvious.

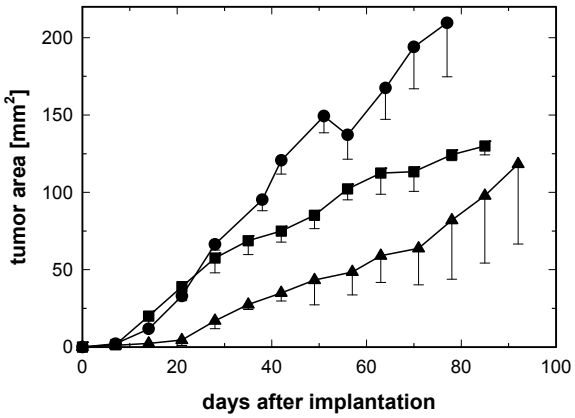

Figure B.3: Comparison of the growth kinetics (mean values ± SEM) of malignancies obtained by implantation of frozen and re-thawed tumor pieces over various in vivo passages: first *(filled circles)*, second *(filled squares)* and third passage *(filled triangles)*

In summary, an automated cryopreservation protocol was established and refined. The optimized procedure minimizes heat-related tissue damage and enables long-term storage of solid tumor samples. Since further investigations with Kb-V1 tumors revealed sustained tumorigenicity as well as comparable growth kinetics, cryopreserved tissue samples can replace serial transplantation of the respective tumor. Consequently, the established procedures can reduce the number of animals required to establish tumor-pharmacological models in nude mice and will be of high benefit for future preclinical studies.

Ich erkläre hiermit an Eides statt, dass ich die vorliegende Arbeit ohne unzulässige Hilfe Dritter und ohne Benutzung anderer als der angegebenen Hilfsmittel angefertigt habe; die aus anderen Quellen direkt oder indirekt übernommenen Daten und Konzepte sind unter Angabe des Literaturzitats gekennzeichnet.

Regensburg, ……..

Peter Höcherl